

OKINAWA INSTITUTE OF SCIENCE AND TECHNOLOGY
GRADUATE UNIVERSITY

Thesis submitted for the degree

Doctor of Philosophy

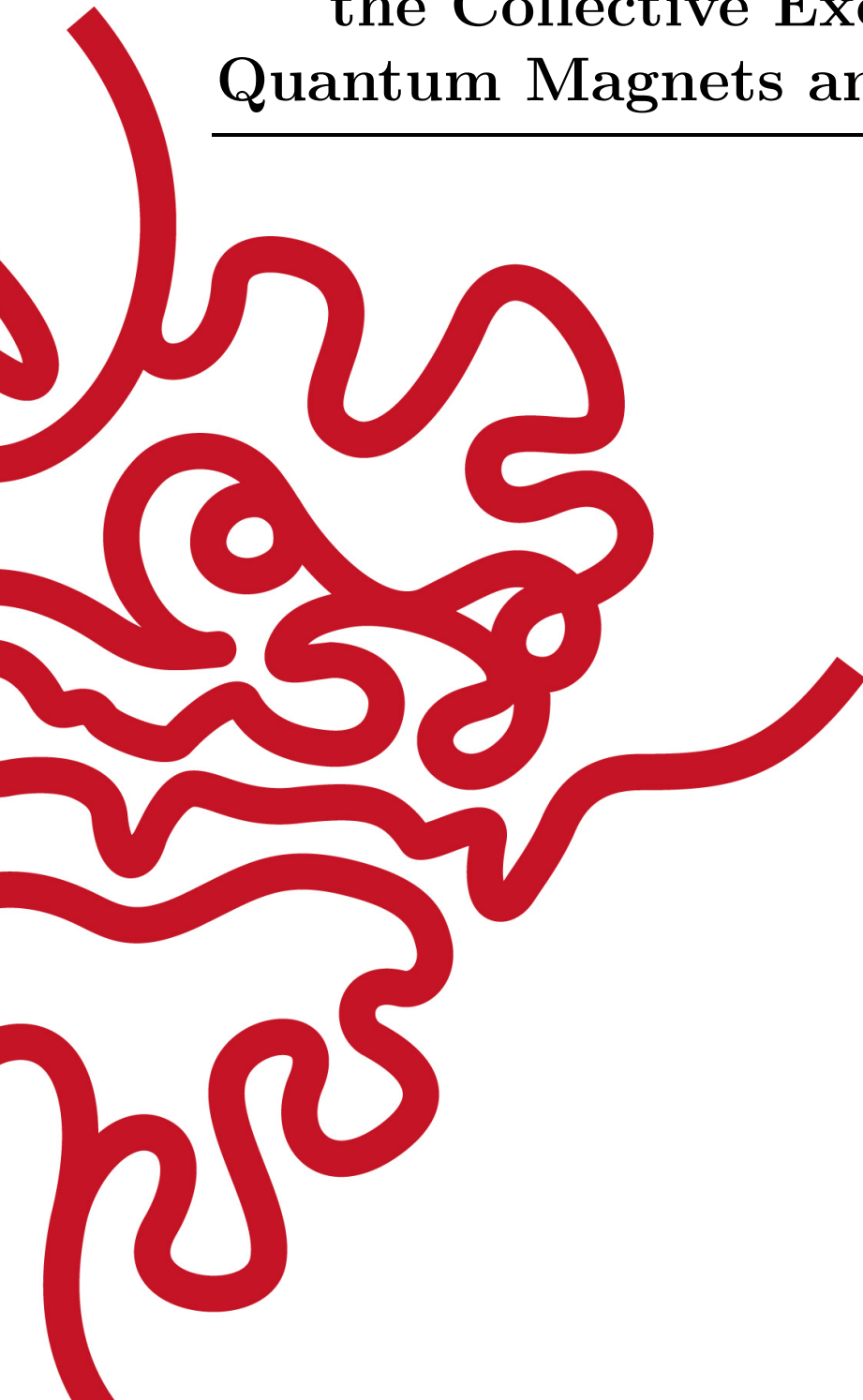
**Analogues of Light and Gravity in
the Collective Excitations of
Quantum Magnets and Cold Atoms**

by

Leilee Chojnacki

Supervisor: **Nic Shannon**

June, 2024



Declaration of Original and Sole Authorship

I, Leilee Chojnacki, declare that this thesis entitled *Analogues of Light and Gravity in the Collective Excitations of Quantum Magnets and Cold Atoms* and the data presented in it are original and my own work.

I confirm that:

- No part of this work has previously been submitted for a degree at this or any other university.
- References to the work of others have been clearly acknowledged. Quotations from the work of others have been clearly indicated, and attributed to them.
- In cases where others have contributed to part of this work, such contribution has been clearly acknowledged and distinguished from my own work.
- None of this work has been previously published elsewhere, with the exception of the following manuscript: L. Chojnacki, R. Pohle, H. Yan, Y. Akagi and N. Shannon, *Gravitational wave analogues in spin nematics and cold atoms*, Phys. Rev. B **109**, L220407 – Published 14 June 2024.

Manuscript contributions: N. Shannon conceived of and supervised the project, building on earlier work with A. Smerald. R. Pohle and Y. Akagi originally noted behaviour in spin nematics analogous to merging black holes. L. Chojnacki carried out analytic calculations establishing the connection between spin nematic excitations and gravitational waves. H. Yan provided critical review and helped improve formulation of the analytic results. L. Chojnacki and R. Pohle carried out independent numerical simulations of vortex annihilation processes. L. Chojnacki made estimates of timescales relevant to cold atom and magnetic insulators. All figures in the main text were prepared by L. Chojnacki. L. Chojnacki wrote the original draft of the manuscript, H. Yan and N. Shannon edited, and all authors contributed to revisions of the manuscript.

Date: June, 2024

Abstract

Analogies are fundamental for human reasoning. In condensed matter, analogies with high-energy phenomenology have led to new insights, as exemplified by the Anderson-Higgs mechanism, which led to the electroweak unification. Other extreme-scale phenomena beyond the realm of experiment or observation can nevertheless be embodied by condensed matter analogues, at least in part. These analogues, such as the Hawking radiation emitted from the horizons of classical flowing fluids, can provide new avenues for empirically-driven inquiry.

In this Thesis, I identify connections between two of nature’s fundamental force carrying Bosons and the Goldstone modes found in ordered phases of quantum magnets and cold atoms. Specifically, I show how the long-wavelength spin waves in a collinear antiferromagnet—known to be massless, spin-1 excitations—correspond to photons. Building on this framework, I then establish that the long-wavelength excitations of a ferroquadrupolar, quantum spin-nematic are massless, spin-2 excitations, which correspond to gravitons, i.e. quantized gravitational waves, in flat spacetime. Since quantum spin nematics can be realized in spinor condensates, I argue that these results offer an avenue for realizing a one-to-one analogue of gravitational waves in experiment. This connection is further illustrated through simulation of a ferroquadrupolar spin-nematic phase, as realized in the spin-1 Bilinear-Biquadratic model on a triangular lattice. Working in a $U(3)$ representation which captures both dipolar and quadrupolar degrees of freedom, I simulate both the thermodynamic and dynamical properties of this model. Within Classical Monte Carlo simulation, I find results consistent with a topological phase transition into the spin nematic phase, mediated by the unbinding of vortices. Using Molecular Dynamics simulations, I then elaborate on the dynamical properties of these vortices, and demonstrate how the annihilation of pairs of vortices could be used to generate analogue gravitational waves in spin nematics, suggesting a route to realization in spinor condensates. I qualitatively extend the analogue to the profile of waves emitted by vortex pairs in the spin nematic, as compared to the characteristic profile measured by LIGO originating from binary mergers of massive objects.

Acknowledgments

“Anything and anyone can fail, but brave good friends help.” Frank Herbert

If memory is a finite resource, then one possible measure of the age of a computer becomes not how much information it has accumulated but rather how much it has deleted, erased, lost, or discarded. Of course, people are much more than computers, and science is ultimately a very human endeavour.

Besides the question of age, there is also the question of maturity. And if age were measured by how much information has been forgotten, then perhaps maturity can be measured by how much we are successful in remembering and holding on to, to apply again later in life.

With that in mind, I wish to acknowledge the people which have been critical to the development of this Thesis.

First I would like to thank my supervisor Nic Shannon for being a unique source of inspiration and motivation, and for supporting me to make the most of my time at OIST and to do my best work. For showing me how to make the time available count. For years of guidance, and ultimately being one of the most human people I know.

Many thanks to Dr. Rico Pohle for supervising the development of my numerical toolbox, for remorselessly going after all the flaws in my arguments and always helping to keep my reasoning on point. Thank you for many years of friendly and helpful support.

To Prof. Han Yan for sharing your insight over the course of our discussions, for cooking up a concise way to re-express the coordinate transformation needed for the gravitational wave analogue in terms of Gell-Mann matrices, and teaching me how to bring out the underlying structure in equations with more compact notation.

To Prof. Yutaka Akagi and Prof. Yukiotoshi Motome for kindly hosting me over the course of many visits to the University of Tokyo.

To Prof. Ludovic Jaubert, Prof. Roser Valentí, Prof. Monika Aidelsburger and Prof. Johannes Reuther who also kindly hosted me during respective visits to the University of Bordeaux, the Goethe Universitaat Frankfurt, Ludwig-Maximilian University of Munich, and the Freie Universitaat Berlin.

Thanks to my fellow TQM members Jonas, Geet, Tokuro, Kim, Ananya, Matthias, Snigdha, Jiahui for good company, friendship and many fun and interesting discussions. Special thanks to Geet for a really solid first introduction to HPC and Monte Carlo simulation.

And to those who made up my network of support over the years: to Sahar and Rike for many great culinary and hiking adventures across Okinawa. To Yazmin Zurita for reminding me how to see the world with childlike spirit. To Lakshmi Priya for your

wholehearted devotion to learning martial arts with me, and self-sacrifice alongside me on the Student Council for the long haul. To Przemek for holding space. To Bogna for many deeply insightful discussions about life, the world of science, and everything. To Nicolas for mentoring me with tough questions and great insight, and showing me that what I thought impossible is possible.

I also wish to thank the institution that is the Student Council, which served as a necessary way for me to direct the frustrations of the pandemic in a constructive way. Through it, I transformed all the unexpressed thoughts into positive actions. I learned so much about people, and I grew more understanding and forgiving of others and myself. To my peers Lorena, Sonia, Izabela, and Lakshmi, thanks for helping sail the ship through 2021. And to the brave souls who stepped up with me in 2022 Lakshmi, Miles, Gaston, Theo, Stash, Charlotte, Emily, Jan, Julian and Josie, thank you all. It has been a remarkable journey (and a big thank you also to the remaining associates who I did not work so closely with). In particular thanks to Stash for taking up the flag so I could retire, safe in the knowledge that the ship sails on! May the things we stood for become one day facts of life, and thus utterly unremarkable.

Big thanks to Simon Hall, for plenty of good humour and many interesting conversations, and to Kozue Higashionna for taking care of so much. Thanks to Prof. Thomas Busch, Dean of the Graduate School, for providing opportunities and reminding me the importance of planting seeds early and often. A final special thanks to former Acting President Albrecht Wagner, for imparting on me invaluable wisdom, and teaching me by example how to lead with humility. And finally to Okinawa, for presenting many opportunities to overcome fear and adversity, and to OIST, for supplying me many lessons that I will no doubt still unpackage for a lifetime.

Dedication

To Okinawa, for even in the moments when one might feel utterly alone, the forces of life are strong here. And to the people of Japan and Okinawa, who funded my education. Always remember your connection to the natural world.

Table of Contents

Declaration of Original and Sole Authorship	ii
Abstract	iii
Acknowledgments	iv
Dedication	vi
Table of Contents	vii
List of Figures	x
List of Tables	xv
1 Introduction	1
1.1 The role of analogy in physics and this Thesis	2
1.2 Microscopic origins of models of magnetism	4
1.2.1 Spin algebra and the Heisenberg Hamiltonian	7
1.2.2 A model for spin-1 magnets	9
1.2.3 Landau paradigm of phase transitions, symmetry breaking and order parameters	10
1.2.4 Topological phase transitions: The XY model	13
1.2.5 Detecting and simulating magnetic order	14
1.2.6 Magnetism in cold atoms	16
1.3 A brief review of light	17
1.4 On the quadrupolar nature of gravitational waves	20
1.5 Thesis outline	24
2 Massless Bosons: Magnetic Goldstone modes, Photons and Gravi- tons	26
2.1 Goldstone's theorem and spontaneous symmetry breaking	27
2.1.1 Coleman and Hohenberg-Mermin-Wagner theorems	30
2.2 (3+1)D electromagnetism in vacuum	30
2.2.1 Lorentz covariance of the gauge field A^μ implies the existence of transverse and gauge modes	32
2.2.2 Poynting vector, energy conservation and visualization of the spin-1 field	35

2.2.3	Canonical quantization of photons	37
2.2.4	Masslessness from symmetry breaking	37
2.3	Linearized gravity as a spin-2 field theory	38
2.3.1	From General Relativity to Linearized gravity	39
2.3.2	Gravity as a gauge theory	42
2.3.3	An intuitive look at gauge fixing linearized gravity	45
2.3.4	Gravitational waves in Linearized Gravity	46
2.3.5	Quantized spin-2 excitations	49
2.4	Chapter summary	51
3	Analogues of electromagnetism in magnetic phases	52
3.1	The XY model as a toy model for electromagnetism on a lattice	53
3.1.1	Goldstone modes of the O(2) XY ferromagnet	53
3.1.2	Hydrodynamic model of planar rotors: a sigma model for the XY ferromagnet	54
3.1.3	A mapping to (2+1)D electromagnetism, its photon and charges	54
3.2	Emergent electromagnetism in spin ice	58
3.3	Low energy excitations of the Heisenberg model and the collinear Néel Antiferromagnet	59
3.3.1	Lorentz covariance from semiclassical treatment of the equations of motion	59
3.3.2	SU(2) $S = \frac{1}{2}$ spin coherent states for spin path integrals	63
3.3.3	Quantum non-linear sigma model for a Heisenberg antiferromagnet	65
3.4	Light, magnons, action! A dictionary for spin-1 excitations	71
3.5	Analogue photons in experiment	74
3.5.1	Analogue photons in magnetic insulators	74
3.5.2	Analogue photons in cold atoms	75
3.6	Chapter summary	76
4	Analogue of linearized gravity in spin nematics and spinor condensates	78
4.1	Quadrupolar order and spin nematics	79
4.2	Representation of nematic order and nematic Goldstone modes in spin-1 magnets	81
4.3	The $s = 1$ spin coherent states	85
4.4	Quantum non-linear sigma model for a spin-1 nematic	88
4.4.1	The minimal spin-1 model: the Bilinear Biquadratic model	88
4.4.2	Effective low-energy field theory of the ferroquadrupolar spin nematic	89
4.5	What starts with action ends with action: a dictionary for spin-2 excitations	94
4.5.1	Mapping linearized gravity gauge constraints onto the physical constraints of ferroquadrupolar order	94
4.5.2	Quadrupolar nature of excitations in linearized gravity and spin nematics	97
4.5.3	Homotopy and defects of the spin nematic phase	99

4.6	Spin nematics in experiment	100
4.6.1	Spin nematics in magnetic insulators	100
4.6.2	Spin nematics in spinor condensates	102
4.7	Chapter summary	103
5	Numerical investigation of gravitational wave analogues	105
5.1	Classical Monte Carlo methods	105
5.1.1	Equilibrium measurements, estimators and block averaging . . .	107
5.1.2	Simulated Annealing	110
5.1.3	Overrelaxation	111
5.1.4	Marsaglia method	112
5.1.5	U(3) representation for spin-1 in simulation	112
5.2	Molecular Dynamics	115
5.2.1	Runge-Kutta methods	115
5.2.2	Dynamical structure factors from simulation	117
5.3	Connecting it all: nematic gravitational waves in simulation	122
5.3.1	Possible topologically mediated transition in 2D spin nematics .	122
5.3.2	Attractive interactions between vortex pairs	126
5.3.3	The “chirp” of nematic gravitational waves	127
5.4	A proposal to realize nematic gravitational waves in spinor condensates	131
5.4.1	Experimental protocol	132
5.4.2	Timescales for gravitational wave analogues	132
5.5	Chapter summary	133
6	Conclusions and outlook	134
	Bibliography	137
	Appendices	156
A	Comparing the strength of electromagnetism to gravity	156
B	Gravitational-wave-induced deformation on an object of known shape	157
C	Semiclassical intuitions: from classical spins to Dirac strings	158
C.1	Building a semiclassical low-energy field theory: the hydrodynamic limit of the Heisenberg model	161
D	Singlet, triplet and quintuplet for $s = 1$	167
E	Spin probability density	170
F	Enter the A-matrix	171
F.1	U(3) representation of the FQ phase and its excitations	171
F.2	Equations of motion	174
G	Discrete Fourier transform methods	175

List of Figures

1.1	(a) The unassuming lodestone, capable of aligning itself to the Earth’s magnetic field and attracting objects made e.g. of steel and iron. This rare magnetized form of the mineral magnetite has been induced into a permanent magnet by naturally occurring fields in excess of 0.1T, suspected to occur by lightning strike [1, 2]. (b) Sketch of a ferromagnetic spin configuration. (c) Sketch of an antiferromagnetic spin configuration. (d) Sketch of a ferrimagnetic spin configuration. For the antiferromagnet and ferrimagnet, the different sublattices are coloured distinctly in blue and red respectively. Fig. 1.1(a) reproduced from [3], Public Domain.	4
1.2	(a) The low temperature phase diagram for the Bilinear, Biquadratic model [Eq. (1.19)] on the triangular lattice, obtained via mean-field analysis [4–6]. Notice the appearance of quadrupolar orderings, dominant in the limits where the biquadratic term is dominant. (b) Ground state of the triangular lattice Bilinear-Biquadratic model, exhibiting on-site quadrupolar order [Eq. (4.23)]. Fig. 1.2(a) reproduced from [5, 6] with permission, and Fig. 1.2(b) from [7] with permission.	12
1.3	Correlations obtained from simulation at low temperatures in O(3) antiferromagnets on the cubic and pyrochlore lattices. (a) Equal-time structure factor for an O(3) antiferromagnet on a cubic lattice, showing a slice in the [001] plane. Clearly visible Bragg peaks at (π, π, π) signal antiferromagnetic order. (b) Equivalent results for an O(3) antiferromagnet on the pyrochlore lattice, showing pinch points associated with algebraic spin correlations.	15
1.4	Magnetic excitations of two-dimensional antiferromagnets in experiment and simulation, showing linearly-dispersing excitations approaching the ordering vector. (a) Inelastic neutron scattering measurements for the square lattice antiferromagnet La_2CuO_4 . (b) $S(\mathbf{q}, \omega)$ obtained by Molecular Dynamics simulation, discussed in Chapter 5, for the square lattice Heisenberg antiferromagnet. Fig. 1.4(a) reproduced from [8] with permission.	16

1.5	Different polarizations of light. (a) Dipole oscillations resulting from a shifting centre of mass along the z -direction result in linearly polarized excitations of the electromagnetic field. (b) Dipole oscillations resulting from a shifting centre of mass along the y -direction result in linearly polarized excitations of the electromagnetic field. (c) A rotating dipole in the yz -plane result in circularly polarized excitations of the electromagnetic field. (d) A rotating dipole in the yz -plane result in circularly polarized excitations of the electromagnetic field.	18
1.6	Quadrupolar oscillations of a source correspond to deviations from spherical symmetry. The corresponding wave induces spatial deformation shown on the yellow ring due to a linearly polarized gravitational wave as seen by the observer in the figure.	21
1.7	Data from the first LIGO observation of the gravitational wave event GW150914, a binary black-hole merger, depicting the characteristic chirp of the event. The signal from the event 1.4 ± 0.6 billion light-years away is only perceptible above the background for the short period of time during which the merger produces a large burst of gravitational wave output. Figure reproduced from [9], available under the terms of the Creative Commons Attribution 3.0 License.	23
1.8	Spectrogram showcasing the time-frequency decomposition of the waves emitted by defect pairs in a spin nematic. Full description of this result in Chapter 5.	25
3.1	Spin configurations in an XY magnet, showing the connection with electric charges. Colour bars represent the angle $\theta \in [-\pi, \pi]$ associated to the spins. (a) Charges with opposite winding number generate a field configuration whose energy can be minimized by bringing the charges closer together. (b) Charges with both positive winding number generate a field configuration whose energy can be minimized by moving charges further apart.	57
3.2	Illustration of the origin of the Berry phase arising in quantum magnets. (a) Sketch of the Berry phase swept out between times τ_j and τ_{j+1} . (b) An arbitrary closed trajectory in the space of spin coherent states delineates two patches of the sphere, showing the ambiguity in defining areas of closed loops on the sphere.	69
3.3	Analogue E and B fields arising in the continuum field description of the antiferromagnetic Goldstone modes of the Heisenberg antiferromagnet. The field $\vec{\phi}_A$ represents the non-trivial transverse components of the staggered magnon field ϕ^μ and equivalently of the gauge field A^μ	72

-
- 4.1 **(a)** The magnetic state with quantum number $m = 1$ can be represented by an $O(3)$ vector pointing along the positive z direction. **(b)** The spin probability surface of the $|0\rangle$ state is characterized by absence of favoured dipolar orientation, and showcases inversion symmetry reflective of the preserved time-reversal symmetry. This state is clearly quadrupolar. **(c)** The magnetic state with quantum number $m = -1$ can be represented by an $O(3)$ vector pointing along the negative z direction. See e.g. [10] or Appendix E for descriptions of how to define these surfaces. 82
- 4.2 The three time-reversal invariant states defined in Eq. 4.17, with orientations along the respective coordinate axes. States in this basis are described by the complex vector \mathbf{d} defined in Eq. 4.18. 83
- 4.3 Equipotential surfaces demonstrating the equivalent quadrupolar breathing behaviour of the modes of both gravity [cf. Eq. 4.105] and the spin nematic [cf. Eq. (4.107)]. Figure reproduced from [7] with permission. 99
- 4.4 The manifold \mathbb{RP}^2 , the order parameter space of both the nematic liquid crystal and the ferroquadrupolar liquid crystal, its symmetry restoring excitations, and topological defects in order parameter space and real-space. All antipodal points on the boundary of the hemisphere are identified. **(a)** For a ground state ordered along the x -direction, the two transverse Goldstone modes are indicated by the blue arrows, denotes Q_{xy} and Q_{yz} respectively. **(b)** The π_1 point defects on this manifold correspond to topologically non-trivial loops such as shown in the blue dashed line, where the red antipodal points are identified. Such loops are not oriented, as loops of two distinct orientations can always be smoothly deformed into one another on this manifold, leading to the \mathbb{Z}^2 nature of the defects. **(c)** Topological point defects of a spin nematic on a two dimensional lattice as observed in the two-dimensional projection of the director field, obtained by Monte Carlo simulation. 101
- 5.1 Benchmarks for the blocking procedure for error estimation of derived quantities. **(a)** Heat capacity as a function of temperature in the $O(3)$ square lattice Heisenberg model at $J = 1$, calculated with and without the blocking strategy, both results overlaid. The results are in agreement within statistical uncertainty. **(b)** Energy E and order parameter M autocorrelations as a function of simulation time allow determination of an appropriate choice of N_B , valid to the lowest temperatures of interest in the system. The autocorrelation decays rapidly, such that N_B on the order of 100 is more than sufficient. 109
- 5.2 Convergence of the second moments of the derived components x_m at large sampling number, revealing firstly that the statistical errors in all components respect the central-limit theorem and secondly that the expressions Eq. (5.33) components are not biased or correlated. 114

-
- 5.3 Sample benchmark plots for classical Monte Carlo simulation of the spin-1 Bilinear-Biquadratic model Eq. 5.28 on the triangular lattice, showing agreement with results Fig. 15 in [11]. **(a)** Equal-time structure factor measuring correlations of the \mathcal{A} degrees of freedom, evaluated at $T = 0.030J$ for the triangular lattice Bilinear-Biquadratic model, for $J_1 = 0$ and $J_2 = -1$. **(b)** Equal-time structure factor for \mathcal{Q} degrees of freedom, evaluated for the same parameters. The Brillouin zone boundary is depicted in white dashed line, and the blue dashed line delineates the irreducible wedge. **(c)** Corresponding slice of $S_{\mathcal{A}}(\mathbf{q})$ along the irreducible wedge, evaluated at $T = 0.030J$ for the triangular lattice Bilinear-Biquadratic model, for $J_1 = 0$ and $J_2 = -1$. **(d)** Corresponding slice of $S_{\mathcal{Q}}(\mathbf{q})$ along the irreducible wedge, evaluated at $T = 0.030J$ for the triangular lattice Bilinear-Biquadratic model, for $J_1 = 0$ and $J_2 = -1$ 116
- 5.4 Benchmark plots for fourth-order Runge-Kutta simulation of the U(3) equations of motion Eq. 5.46. **(a)** Conserved quantities related to the spin length, such as $\text{Tr}(\mathcal{A})$ shown here, are useful diagnostics for correct implementation of the simulation. For all states simulated $\text{Tr}(\mathcal{A}) = 1$, and it remains so to machine precision for the duration of simulation. **(b)** Deviation of the energy from the initial configuration for a U(3) ferroquadrupolar state as the system is time evolved with a fourth-order Runge-Kutta method. Small errors are accrued and can be further reduced in magnitude by decreasing the simulation stepsize h 118
- 5.5 $S(\mathbf{q}, \omega)$ evaluated from Molecular Dynamics simulations for different models on the square lattice, showcasing the different character of the low-energy excitations. **(a)** $S(\mathbf{q}, \omega)$ on the irreducible wedge for the square lattice XY ferromagnet at $T = 0.010J$, showing the linearly dispersing Goldstone mode. **(b)** $S(\mathbf{q}, \omega)$ on the irreducible wedge for the square lattice O(3) antiferromagnet at $T = 0.010$, showing the linearly dispersing Goldstone modes. **(c)** $S(\mathbf{q}, \omega)$ on the irreducible wedge for the square lattice O(3) ferromagnet at $T = 0.010J$, showing the quadratically dispersing Goldstone mode. 120
- 5.6 Molecular dynamics simulations showing the excitation spectra of a ferroquadrupolar spin nematic, on the triangular lattice Bilinear-Biquadratic model at $J_1 = 0$ and $J_2 = -1$, at $T = 0.050$. These results are in agreement with Fig. 16 in [11]. **(a)** $S_{\mathcal{A}}(\mathbf{q}, \omega)$, **(b)** $S_{\mathcal{Q}}(\mathbf{q}, \omega)$ and **(c)** $S(\mathbf{q}, \omega)$ on the irreducible wedge for the specified parameters. 121
- 5.7 Exploration of topological phase transition into the ferroquadrupolar phase. **(a)** Heat capacity as a function of temperature in the U(3) triangular lattice Bilinear-Biquadratic model at $J_1 = 0$ and $J_2 = -1$, exhibiting a peak in the heat capacity. **(b)** Order parameter susceptibility as a function of temperature in the U(3) triangular lattice Bilinear-Biquadratic model at $J_1 = 0$ and $J_2 = -1$, exhibiting as scaling behaviour in good agreement with the scaling analytically predicted for the BKT transition. This is consistent with the onset of a topologically mediated phase transition into the ferroquadrupolar phase. 123

5.8	Sequence of images showing the total quadrupolar operator $\sum_{\alpha\beta} \mathcal{Q}^{\alpha\beta}$ in real-space, obtained by time-evolution acting on a single configuration extracted from Monte Carlo simulation. The image is riddled with \mathbb{Z}^2 vortices, which experience attractive interactions and generate analogue gravitational waves during the in-spiral leading up to, during and after annihilation events, see also Fig 5.9.	127
5.9	Sequence of close-up images showing the total quadrupolar operator $\sum_{\alpha\beta} \mathcal{Q}^{\alpha\beta}$ in real-space, obtained by time-evolution of an initialized pair of defects. The emission of analogue gravitational waves leading up to and after the annihilation event is shown.	128
5.10	Sequence of images showing the total quadrupolar operator $\sum_{\alpha\beta} \mathcal{Q}^{\alpha\beta}$ in real-space, obtained by time-evolution of an initialized pair of defects. The distinct wave trains corresponding to events identified in Fig. 5.11 are marked by arrows.	129
5.11	(a) Spectrogram of the time-resolved signal corresponding to the total quadrupolar operator $\sum_{\alpha\beta} \mathcal{Q}^{\alpha\beta}$, as “measured” by a line of “detectors” placed on the triangular lattice orthogonal to the passing wavefront. The line of “detectors” is placed at a positions marked in blue in Fig. 5.10. (b) A zoom-in on the chirp emitted by the vortex annihilation, characterized by the upturn in the frequency composition of the wavefronts towards late times. Windowing artifacts are present in the signal, due to the large size of the time window relative to the duration of the merger event.	130
C.1	Sketch of the gauge field A , with Dirac string at South pole	160
C.2	(a) If the mode of excitation is assumed to locally move spins from both lattices away from the ground state rigidly as shown here, then the resulting restoring force that counteracts the fluctuation \vec{l} leads to torques τ_1 and τ_2 whose actions oppose each other and the spins cannot move. This means such fluctuating modes are in fact dynamically disallowed. (b) The allowed modes of the antiferromagnet result from the two sublattices canting towards one another away from the aligned state.	162
G.1	Colour map of the matrix elements of F_{256}	176

List of Tables

3.1	Summary of the two dual formulations of electromagnetism in (2+1)D.	56
3.2	Dictionary connecting AFM and EM excitations	73

Chapter 1

Introduction

“Analogy is the core of cognition.” - Douglas Hofstadter

Life as we know it exists because of light. 3.4 billion years ago, the first organisms capable of extracting energy from light evolved. Their use of ambient light—a deep sea precursor of photosynthesis—marked the first of many biological innovations involving light. The abundant presence of geothermal and astrophysical light sources was fundamental to this, but so too was the curious fact that the fine structure constant is in the right range of values for chemistry as we know it to exist. Human civilization too has shared a long history in making use of light in even the most primitive forms of technology, from fire all the way to our modern communication infrastructure.

It was not until much more recently when, in 2016, a wave of excitement passed through the physics community with the confirmed detection of another of nature’s cosmic messengers. In that year, the LIGO collaboration announced confirmation of the first observation of gravitational waves, originating from a distant binary black hole merger [9]. Many decades of pioneering efforts were required to overcome the observational difficulties involved, which arise from another curious fact of nature, namely, that gravitational excitations are much weaker than electromagnetic ones. The successful confirmation of their existence, and the scale of hierarchies separating us from natural sources, motivate the search for gravitational waves, or at least their analogues, in a lab.

In this Thesis, I chart a path to a novel experimentally viable analogue of gravitational waves, which—to the best of our knowledge—is the first of its kind to be in one-to-one correspondence with the gravity of (3+1)D flat spacetime. The approach presented in this Thesis allows us to start off by making clean identifications of relevant physics which we can then identify appropriate condensed matter realizations for. Starting from the low-energy effective continuum field theory, we will discover clean realizations of the excitations of electromagnetism and gravity in magnetic systems, and support these results with numerical simulation.

In this Chapter, I start by setting the tool of analogy in physics on the historical stage, and in more recent context of the dialogue between high and low-energy physics, in order to exemplify how it can serve in the context of magnetism. I then successively provide a broad overview of magnetic order, photons in electromagnetism, and gravitational waves in linearized gravity, laying the basic conceptual framework that later Chapters will rest upon.

1.1 The role of analogy in physics and this Thesis

The study of physics, indeed of nature, was described in 1976 by Sir Charles Frank as the discipline

“[...] *not just concerning the Nature of Things, but concerning the Inter-connectedness of all the Natures of Things*” [12].

Indeed, science proceeds by the construction of insightful models to explain experiments and observations, often drawing upon analogies with known phenomena. Every model of nature is an approximation, but within their operating limits and their contemporary scientific context, analogies can be extremely powerful and predictive. The mathematical similarities which existed between electrodynamics and hydrodynamics were of great insight to J.C. Maxwell, who coined the phrase “*method of physical analogy*” to refer to this process of reasoning. Indeed, countless formal or observed similarities have long played a critical role in the development of human understanding, across all domains of physics.

For example, during a time when little was known about the heavenly bodies beyond their trajectories across the sky, Galileo famously reasoned about them by analogy. Following development of his own telescope in 1609, he first observed changing patterns of bright and dark spots on the lunar surface. By analogy with the Earth’s surface, he was able to infer that these patterns moving across the Moon’s surface were shadows cast by mountains and valley walls, the position and size of which depended on the relative orientation of the Moon and Sun. He was later able to further infer, again in analogy to the Earth, that the bodies he observed orbiting Jupiter were also moons.

More recently, the wide range of striking parallels between high-energy phenomenology and properties of condensed matter systems have led to many fruitful insights and key advances in the development of the Standard Model and beyond. The Anderson-Higgs mechanism, as first put forward by Anderson [13] within the context of superconductivity, set the stage for the later development of a fully covariant generalization of the mechanism by which Nambu-Goldstone modes acquire mass [14–16], and provided the framework necessary for the unification of electrodynamics and the weak force. It was later suggested that the symmetry breaking phase transition undergone by liquid Helium when cooled to the superfluid phase mimics the symmetry breaking phase transition undergone by the early universe [17], showcasing the potential for low energy experiments to inform physics relevant to the high-energy domain.

Presently, there is a major question which confronts modern high-energy physics, namely, how to reconcile the Standard Model with Gravitation, as described by General Relativity. One difficulty is that observing a regime in nature where strong gravitational phenomena and quantum effects are simultaneously important is beyond our current technological grasp. This motivates the search for analogue platforms in which field theories can be tested in regimes which combine gravitational and quantum effects.

Several promising candidate platforms have been the subject of the last 40 years of investigation, and analogies with experimental realization have gained much traction within the classical and quantum fluids communities and beyond [18]. Prominent early work was carried out in the context of superfluid ^3He , establishing that its rich

phenomenological structure can be thought of as analogous to a condensed matter universe with its own version of gravity [17, 19, 20].

In parallel, while studying the problem of black hole evaporation, Unruh used an analogue with classical fluid flow into a “dumb hole” to estimate the contribution to thermal emission from the horizon in the high-frequency regime, providing evidence in support of black hole evaporation via Hawking radiation and suggesting use of a sonic analogues as accessible testbeds [21, 22]. This stimulated a wide variety of experimental work to probe this scalar form of Hawking radiation in classical fluids [23, 24], in cold atoms [25], in quantum Hall systems [26], in optics [27, 28] and with further proposals in semimetals [29, 30].

Independently, it was pointed out by Kleinert [31] that the topological structure of defects in crystals can be used to define curvature and torsion as necessary to describe curved spacetimes, establishing a key analogy between the tensor structure of elasticity theory and gravity. This idea was further developed in the search for a quantum theory for spacetime which at the fundamental level is a Planck scale quantum crystal [32–36]. The duality between elasticity theory and aspects of fracton physics [37] is also connected to emergent gravitational properties in models with fractonic excitations [38].

Further experimental work aiming to reproduce curved spacetimes has been recently underway, in which dynamical excitations play some role akin to an effective spacetime geometry [39, 40]. The phononic density waves investigated in this context then play the role of scalar gravitational waves [41, 42]. However, modified theories of gravity aside, the gravitational waves in (3+1)D gravity are tensorial in nature, consistent in the linearized limit with the excitations of a spin-2 field theory [43, 44].

In the context of magnetic insulators, gravitational analogues are relatively unexplored. There are however many established analogues with electromagnetism, arising as early as the 1970’s with the identification of the 2D XY model with reduced dimensional electrostatics [45]. These insights were informed following greater understanding of how vortices can drive phase transitions topologically, otherwise forbidden in low dimensional systems [46, 47], a mechanism referred to as the Berezinskii-Kosterlitz-Thouless transition. More recently a fully dynamical effective (2+1)D theory of electromagnetism has also been made explicit [48].

The development of a magnetic analogue of the proton disorder in water ice [49, 50] within pyrochlore oxides [51] led to the term spin ice [52]. It was prominently established in quantum spin ice that features of (3+1)D electromagnetism emerge, such as magnetic monopoles [53, 54], photons [55, 56], and an effective fine structure constant [57]. A strong case has been made for the existence of emergent electrodynamics in candidate materials such as $\text{Yb}_2\text{Ti}_2\text{O}_7$ [58], $\text{Pr}_2\text{Hf}_2\text{O}_7$ [59], and $\text{Ce}_2\text{Zr}_2\text{O}_7$ [60, 61], $\text{Ce}_2\text{Hf}_2\text{O}_7$ [62] and $\text{Ce}_2\text{Sn}_2\text{O}_7$ [63]. Moiré engineering has also been proposed as an independent route to generate emergent electromagnetism [64], outside of the spin ice context.

The key point is that in each of these analogue realizations, the effective fine structure constant (when it exists) is different than that of the Universe, and opens a door to regimes which are otherwise beyond our experimental reach in this Universe. In this Thesis I begin the search for gravitational wave analogues of measurable impact in magnetic insulating phases called spin nematics.

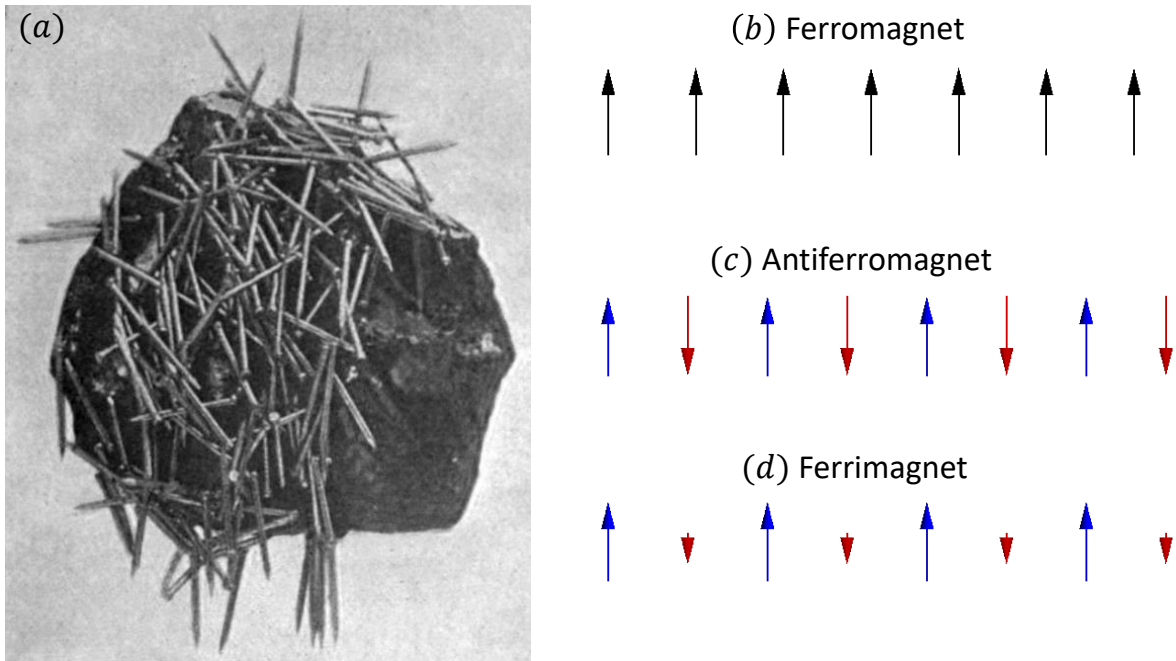


Figure 1.1: (a) The unassuming lodestone, capable of aligning itself to the Earth’s magnetic field and attracting objects made e.g. of steel and iron. This rare magnetized form of the mineral magnetite has been induced into a permanent magnet by naturally occurring fields in excess of 0.1T, suspected to occur by lightning strike [1, 2]. (b) Sketch of a ferromagnetic spin configuration. (c) Sketch of an antiferromagnetic spin configuration. (d) Sketch of a ferrimagnetic spin configuration. For the antiferromagnet and ferrimagnet, the different sublattices are coloured distinctly in blue and red respectively. Fig. 1.1(a) reproduced from [3], Public Domain.

Starting first from electromagnetism analogues to develop a recipe for identifying the relevant physics in gravity, I proceed in this Thesis to the development of a tensor analogue of gravitational waves, in direct and one-to-one correspondence with the gravitational waves in the flat (3+1)D Universe. In this Chapter, I next proceed to introduce some key points about magnetic insulators, and present the effective magnetic models which we will be concerned with in this Thesis.

1.2 Microscopic origins of models of magnetism

The earliest documented observations of macroscopic magnetism date back to the 6th century B.C in Ancient Greece and the 4th century B.C in China, following the discovery of lodestone [65], a rare permanently magnetized form of the mineral magnetite which awed the ancient world, see Fig. 1.1. On the microscopic scale, the relevant ingredient leading to this property is called a magnetic dipole moment. The term magnetic dipole moment references the oriented dipole field produced by e.g. a current loop. Such fields are produced by charged particles with non-trivial angular momentum \mathbf{J} in proportion to

$$\mathbf{m} = g\mu_B\mathbf{J} , \quad (1.1)$$

where g is a factor that depends on the species of particle and μ_B is the Bohr magneton, defined as

$$\mu_B = \frac{e\hbar}{2m_e}. \quad (1.2)$$

The intrinsic angular momentum—conventionally denoted \mathbf{S} —of an elementary particle is a relativistic property and receives the name spin. Spin is quantized in half-integer units of \hbar , a fact discussed further in Appendix C. Since all elementary particles possess an intrinsic spin, but not all elementary particles are charged, not all spins possess a magnetic moment. However, electrons and protons in nuclei will generate magnetic moments. For further reading, see e.g. [66]. Ultimately, macroscopic magnetism arises from the collective interactions of microscopic magnetic moments in materials.

Naively, one may attribute the origin of macroscopic magnetic phenomena to the interaction of atomic or electronic magnetic moments within a material via long-ranged magnetic dipole-dipole interaction. However, a back-of-the-envelope estimate of the energy scale of the intrinsic dipole-dipole interaction is on the order $E \sim 10^{-5}eV$, equivalent to a temperature scale of $T = \frac{E}{k_B} \sim 0.1K$. Given that typical Curie temperatures for transition metal and rare earth compounds are on the order $T_C \sim 10^2 - 10^3K$ [67], this indicates that the dipole-dipole interaction is in fact several orders of magnitude too weak to account for observed magnetic ordering in these materials. In general, magnetism in solids cannot be accounted for if we only consider the classical magnetic dipole interactions. Instead, the primary contributions arise from the strong interactions between electrons (in particular unpaired electrons), and interactions between nuclear spins can also play a role [66].

The full quantum-mechanical many-body problem with a complete description of the interactions between particles is an intractable problem for large particle numbers, making a complete description of a magnetic material by brute force enumeration unreasonable. However, use of reasonable approximations to construct effective models, such as the observation that magnets exist in the solid state, allow us to construct a wealth of both tractable and predictive problems, many of which are introduced in e.g. [68]. This field of study is far from exhausted, as complete understanding of even long known magnetic materials such as magnetite is still the subject of investigation, e.g. [69, 70], in addition to the host of novel materials and phenomena that are still being uncovered, some characterizable by novel symmetry breaking properties, such as the recently discovered altermagnetism e.g. [71].

In metals, the electrons near the top of the conduction band are only weakly bound to the ion. In this case, interactions between the delocalized electrons have a very weak effect on collective properties of the material. On the other hand, transition metal and rare earth elements supply electrons mostly localized in d and f orbitals around their parent ion, and interactions effects between neighbouring electrons in the crystal are relevant.

One major simplification we can make is to narrow attention to the low-energy subspace, as many questions regarding the material properties can be answered with knowledge of the ground state and low-lying excitations. In this case, the simplest

effective models are those which capture the energy splitting arising from ground state degeneracies lifted by interactions. To briefly see this, let's consider the effect of interactions on two neighbouring electrons, leaning on more extensive treatments in [67, 72].

In the absence of interaction, the wavefunction of a single electron can be decomposed into

$$\Psi(x, \sigma) = \psi(x)\chi(\sigma) , \quad (1.3)$$

where $\psi(x)$ describes the spatial dependence of the orbital and $\chi(\sigma)$ describes the electron spin state.

For two electrons, the composite spin states can be described by the basis

$$|s = 1, m = 1\rangle = |\uparrow\uparrow\rangle , \quad (1.4a)$$

$$|s = 1, m = 0\rangle = \frac{1}{\sqrt{2}} (|\uparrow\downarrow\rangle + |\downarrow\uparrow\rangle) , \quad (1.4b)$$

$$|s = 1, m = -1\rangle = |\downarrow\downarrow\rangle , \quad (1.4c)$$

$$|s = 0, m = 0\rangle = \frac{1}{\sqrt{2}} (|\uparrow\downarrow\rangle - |\downarrow\uparrow\rangle) , \quad (1.4d)$$

where the two spin- $\frac{1}{2}$ moments can possess a total spin moment of either $s = 1$ or $s = 0$, depending respectively on the symmetric or antisymmetric alignment of the spin moments. The symmetric spin-1 states define a triplet of states, while the antisymmetric spin-0 state is called the singlet state. In the absence of any interactions, the singlet and triplet energy levels are degenerate. However, the introduction of a Coulomb interaction between electrons splits the energy levels between the singlet and triplet states according to the exchange character of the full wavefunction, assuming the orbital character is not allowed to change.

Given that the electron is a fermion, the total wavefunction must have antisymmetric character under exchange with another electron. In this way, if the orbital wavefunction is symmetric, then the spin wavefunction must be antisymmetric and viceversa.

In ferromagnetic materials, the electrons populate orthogonal orbitals in the ground state. In this case, the antisymmetric orbital wavefunction is favoured, such that the singlet energy is increased by Coulomb repulsion, by an amount we shall parametrize by J , while the triplet energy is lowered by J . The origin of this behaviour is the same as that governing Hund's rule for atomic spin distribution, namely, that electrons populate orbitals in such a way as to maximize their total spin.

In the more common antiferromagnetic materials, the electrons populate overlapping orbitals such that the orbital part of the wavefunction is expected to be symmetric, and therefore the antisymmetric spin wavefunction is favoured, leading to a singlet ground state and triplet excited state, also separated by an energy difference on the order $2J$.

We see that we can expect two types of magnetic behaviours already from joint consideration of the Coulomb interaction and Pauli exclusion. It is instructive here to introduce the spin algebra before presenting the effective exchange model which captures this process.

1.2.1 Spin algebra and the Heisenberg Hamiltonian

Before returning to the two-body exchange described in the last section, let us explicitly define the spin operators

$$\mathbf{S} = (S^x, S^y, S^z), \quad (1.5)$$

with dimensions of angular momentum, measured in units of \hbar , and which satisfy the canonical commutation relations

$$[S^\alpha, S^\beta] = i\hbar\epsilon_{\alpha\beta\gamma}S^\gamma. \quad (1.6)$$

where \hbar is the Plank constant

$$\hbar \approx 1.05 \cdot 10^{-34} \frac{J}{s}. \quad (1.7)$$

As done here, I will implicitly use the Einstein summation convention over repeated indices throughout this Thesis. In addition, I will work throughout this Chapter in natural units, where $\hbar = 1$, since the appropriate factors of \hbar can be conveniently restored by dimensional analysis where required.

By conventionally choosing an eigenbasis of S^z for description of spin problems, the spin algebra also permits the definition of ladder operators

$$S^+ = S^x + iS^y, \quad (1.8a)$$

$$S^- = S^x - iS^y, \quad (1.8b)$$

which act on elements of the eigenbasis to raise and lower the spin angular momentum by factors of \hbar respectively. With the S^z component singled out, we cannot independently determine the remaining components due to the commutation structure. However, another good quantum number can be defined in terms of the eigenvalues of the operator

$$\mathbf{S} \cdot \mathbf{S} = (S^z)^2 + \frac{1}{2}(S^+S^- + S^-S^+). \quad (1.9)$$

Therefore, taken collectively, this all leads to the curious property that

$$\langle \mathbf{S}^2 \rangle = s(s+1), \quad (1.10)$$

contrary to what would be expected for a classical vector, for which instead

$$\mathbf{S}^2 = s^2. \quad (1.11)$$

Classical vectors are nevertheless useful to good approximation in the context of numerical simulation and can faithfully reproduce much of the key relevant physics, as elaborated on in Chapter 5.

Each of the S^α operators are related to the elements of the appropriate representation of $SU(2)$, with the dimension of representation fixed by the intrinsic angular

momentum quantum number s . The electron has intrinsic angular momentum characterized by the quantum number

$$s = \pm \frac{1}{2}, \quad (1.12)$$

and the appropriate spin operators are in correspondence with the Pauli operators

$$S^\alpha = \frac{1}{2}\sigma^\alpha. \quad (1.13)$$

Now we return to the two-body problem described in the previous section. We can define an operator P_{12} which exchanges the spin component of the wavefunction between sites 1 and 2

$$P_{12} = 2\mathbf{S}_1 \cdot \mathbf{S}_2 + \frac{1}{2} \quad (1.14)$$

$$= 2 \left(S_1^z S_2^z + \frac{1}{2}(S_1^+ S_2^- + S_1^- S_2^+) \right) + \frac{1}{2}, \quad (1.15)$$

normalized such that the triplet and singlet states are respectively the $+1$ and -1 eigenvalue states of this operator. The difference between the expectation values of the exchange operator P_{12} is then proportional to the energy splitting in both the ferromagnetic and antiferromagnetic cases. Remarkably, such two-body short range interactions turn out to be enormously effective to leading order [67, 72], and therefore effective models for the interaction terms can be derived from the two body Coulomb problem with due consideration of Pauli exclusion, as first pointed out by Dirac [73]. To capture the relevant effect in a many-body system, it is therefore enough to focus on an effective model of locally pairwise exchange interactions, namely, the Heisenberg model [74]

$$\mathcal{H} = J \sum_{\langle ij \rangle} \mathbf{S}_i \cdot \mathbf{S}_j, \quad (1.16)$$

which to leading order describes the exchange interaction between spin- $\frac{1}{2}$ degrees of freedom.

As a closing remark, it is worth noting that the first example of magnetite is in fact neither a ferromagnet nor an antiferromagnet. It is in fact a combination of both, with alternating antialigned and aligned magnetic moments in one to three ratio such that macroscopically the magnetization is finite. This is an example of ferrimagnetism—see Fig. 1.1(d)—a common property of several magnetic oxides besides magnetite known collectively as ferrites. These materials have more complicated ordering that is still the subject of investigation e.g. [69, 70], and will not be further discussed in this Thesis.

While the microscopic underpinnings described here are therefore oversimplified relative to the ferrites, the Heisenberg model nevertheless captures the essence of macroscopic ferromagnetic and antiferromagnetic behaviour. In Chapter 3, we will be concerned primarily with the antiferromagnetic phase of the Heisenberg model, which we will see supports an analogue of photons.

Next, we will review a closely related spin model for spin-1 magnets, which we will

see in Chapter 4 supports an analogue of gravitational waves.

1.2.2 A model for spin-1 magnets

Having explored some of the possibilities that exist for spin- $\frac{1}{2}$ magnets, next let us consider what fundamental differences arise in the case of larger spin, since we will be concerned with the physics of spin-1 magnets in Chapters 4 and 5 of this Thesis, in relation to an analogue of gravitational waves. The relevant details reviewed here are documented in e.g. [10, 72].

In the case of spin-1 magnets, there are five $s = 2$ states, three $s = 1$ states, and one $s = 0$ state, see Appendix D. It would be reasonable to assume that there may be more relevant physics to describe the ground state than captured by the Heisenberg Hamiltonian [Eq. (1.16)]. In fact, generically for $s > \frac{1}{2}$, the action of the operator

$$(S_1^+ S_2^- + S_1^- S_2^+) |\alpha, \beta\rangle \neq C |\beta, \alpha\rangle, \quad (1.17)$$

with appropriate normalization C , indicates that the exchange operator P_{12} defined in the $s = \frac{1}{2}$ case will no longer exchange spins. With the introduction of pairwise Coulomb interaction and examination of the higher order contributions, the energy splitting between the three groupings can no longer be described by the bilinear Heisenberg term alone. This means the previous permutation operator P_{12} is no longer enough to describe the interaction between spin-1 moments.

By introduction of a second projection operator

$$P_{s=0} = \frac{1}{3} [(\mathbf{S}_1 \cdot \mathbf{S}_2)^2 - 1], \quad (1.18)$$

which only acts on the singlet subspace to adjust its relative energy level, one arrives at the Bilinear, Biquadratic exchange model [72]

$$\mathcal{H}_{\text{BBQ}} = J_1 \sum_{\langle ij \rangle} \mathbf{S}_i \cdot \mathbf{S}_j + J_2 \sum_{\langle ij \rangle} (\mathbf{S}_i \cdot \mathbf{S}_j)^2. \quad (1.19)$$

The biquadratic term is in fact trivial for $s = \frac{1}{2}$. It can be shown [72] that generally there are only relevant exchange interactions for spin S which take the form of $(\mathbf{S}_i \cdot \mathbf{S}_j)^p$, up to powers $p \leq S$.

Further details on alternative microscopic origins of the biquadratic term specific to materials described by the Hubbard model can be found in e.g. [75–77].

The important distinction with the spin- $\frac{1}{2}$ case is the following: for spin- $\frac{1}{2}$ there are no non-trivial tensor operators composed from angular momentum that could hide further symmetries of the Hilbert space. In the spin-1 case however, there are subspaces of the Hilbert space which cannot be rotated between with angular momentum generators alone [78, 79]. Instead, the state space is spanned by the generators of a larger algebra, such as $SU(3)$ [5, 10, 80, 81] or $U(3)$ [11, 82]. We will return to this fact in Chapter 4.

1.2.3 Landau paradigm of phase transitions, symmetry breaking and order parameters

The previously discussed models possess distinct states with macroscopic behaviours, such as ferromagnetism, that arise from a particular ordering of the microscopic magnetic moments. Each state with specific macroscopic properties is called a phase of the model, or material, that it describes. The importance of microscopic components in realizing such behaviour was argued for by Maxwell in 1875 [83], who argued that phases, and in particular phase transitions, were evidence of the atomic and molecular basis of matter. Later, Landau introduced the perspective that to understand any symmetry breaking phase transition we only require knowledge of the symmetries involved [84]. Depending on the external conditions that determine the thermodynamic environment of the material, the same microscopic constituents will result in different phases, and changes to those conditions can drive transitions between phases. This dependence is something we encounter regularly through water, a substance whose solid, liquid and gaseous phases exist naturally within the temperature and pressure ranges available naturally on Earth. In the context of magnetism [66], at temperatures above a threshold called the Curie temperature, the magnetic moments fluctuate wildly due to the thermal energy in the system, and this destroys any energy-minimizing correlations that would result in ordering. However, at temperatures below the Curie temperature, the thermal fluctuations are more tame, and correlated domains can persist leading the system to enter an ordered phase.

Quantitatively, we can see how such behaviour arises by considering the free energy [85]

$$F = E - TS . \tag{1.20}$$

In equilibrium, a system minimizes its free energy. At temperatures above a characteristic threshold of the system (e.g. the Curie temperature), the entropic term TS dominates. Minimization of the free energy is achieved by maximizing the entropy. As a result, the degrees of freedom of the system will arrange themselves on average in the most disorderly fashion possible. In the context of magnetism, the high temperature phase is known as paramagnetic and has no long-range correlations. At temperatures below the critical threshold, the free energy is instead minimized by decreasing the internal energy of the system. This contribution is described by the model Hamiltonian.

The internal conditions that determine the strength and sign of different interactions also play a fundamental role in determining the ordering behaviour that emerges. The cartoon image of magnetic moments \mathbf{m} as axial vectors which align (ferromagnetic ordering for $J < 0$) and antialign (antiferromagnetic ordering for $J > 0$) define the semiclassical ground states of the Heisenberg Hamiltonian on an unfrustrated lattice. In each of these two distinct phases, we can write down a macroscopic quantity which will be non-zero in the corresponding low-temperature phase, and vanishes in the high-temperature phase. For the ferromagnetic phase with all on-site magnetic moments

\mathbf{m}_i aligned, the magnetization defined by

$$\mathbf{m} = \frac{1}{N} \sum_i^N \mathbf{m}_i \quad (1.21)$$

is non-zero. The same quantity is zero in the antiferromagnetic phase, so we can define instead the staggered magnetization

$$\mathbf{m}_s = \frac{1}{N} \sum_i^N (-1)^i \mathbf{m}_i, \quad (1.22)$$

which is non-zero in the antiferromagnetic phase, and vanishing in the ferromagnetic phase.

Such quantities receive the name order parameter, and as was first formulated by Landau [84], arise in systems whose low-energy phase spontaneously breaks at least one symmetry present in the free energy (or in Lagrangian formalism, the action) of the system. The order parameter in the paradigm defined by Landau is therefore a quantity which encodes information about how the system has spontaneously broken a discrete or continuous symmetry. As we will see in the next Chapter, if the symmetry broken is continuous, then there will exist linearly dispersing excitations that introduce deviations away from the ordered ground state, the nature of which is predicted by broken symmetries and the order parameter.

The other key insight put forward by Landau [84] regarding such symmetry breaking phase transitions is that in their vicinity we can effectively describe the free energy as a sum over symmetry allowed powers of the order parameter, without needing to know any microscopic details of the system. Therefore, detailed description of the entire partition function is not required to approximate the critical behaviour around the phase transition, and the associated insensitivity to microscopic details is behind the existence of Universality classes into which we can lump systems based on their critical behaviour.

Let's consider an example. In the case of the Heisenberg model 1.16, the free energy can be expressed in terms of the magnetization [86]

$$f_{Heis} = \frac{1}{N} F_{Heis} = \alpha(T) |\mathbf{m}|^2 + \gamma(T) |\mathbf{m}|^4 + \mathcal{O}(|\mathbf{m}|^6), \quad (1.23)$$

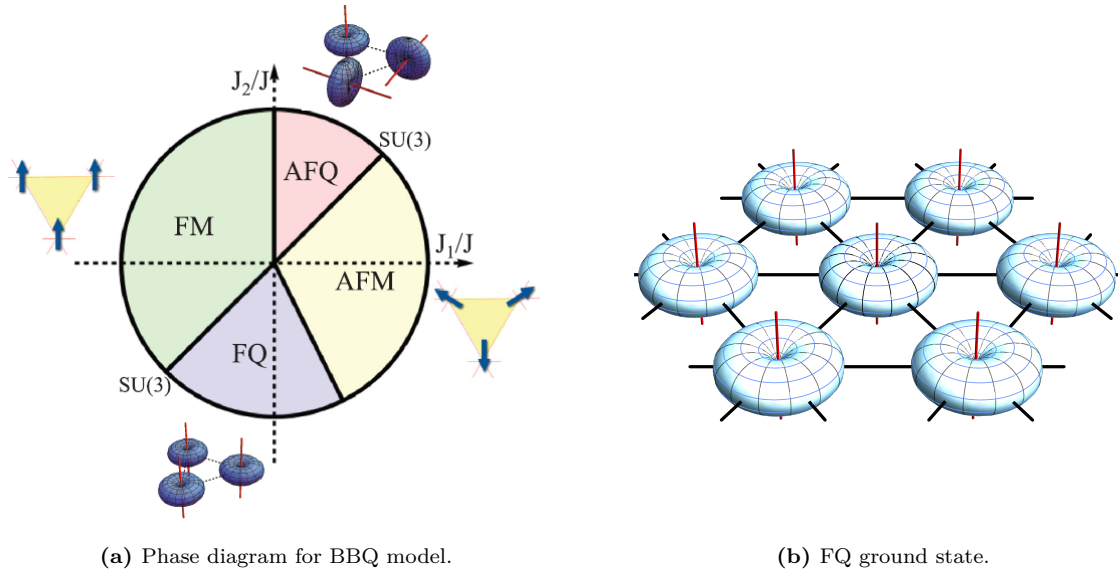
where odd terms are not invariant under the symmetry of the Hamiltonian under rotations, and thus do not feature. We assume that the leading temperature dependence can be described by the coefficient α of the lowest order term, such that

$$\alpha(T) = a(T - T_c), \quad (1.24)$$

$$\gamma(T) = c. \quad (1.25)$$

The equilibrium condition minimizing the free energy then gives

$$\frac{\partial f}{\partial m} = 0, \quad (1.26)$$



(a) Phase diagram for BBQ model.

(b) FQ ground state.

Figure 1.2: (a) The low temperature phase diagram for the Bilinear, Biquadratic model [Eq. (1.19)] on the triangular lattice, obtained via mean-field analysis [4–6]. Notice the appearance of quadrupolar orderings, dominant in the limits where the biquadratic term is dominant. (b) Ground state of the triangular lattice Bilinear-Biquadratic model, exhibiting on-site quadrupolar order [Eq. (4.23)]. Fig. 1.2(a) reproduced from [5, 6] with permission, and Fig. 1.2(b) from [7] with permission.

$$\implies |\mathbf{m}| = \pm \sqrt{\frac{a(T_c - T)}{c}}, \quad T \leq T_c, \quad (1.27)$$

and by definition

$$|\mathbf{m}| = 0, \quad T \geq T_c. \quad (1.28)$$

The expression for \mathbf{m} is a smooth function of temperature, albeit with a discontinuous slope at T_c . This is the defining characteristic of a second-order phase transition.

In general, Landau’s paradigm for expressing the behaviour of the free energy around the critical temperature makes explicit non-analyticities induced in the free energy and its derivatives by the change of phase, and allows classification of the order of phase transitions based on the order of derivative in which discontinuities arise. For further reading, see e.g. [85].

Whereas on simple lattices the Heisenberg model [Eq. (1.16)] leads to either ferromagnetic or antiferromagnetic order, the Bilinear-Biquadratic model [Eq. (1.19)] offers new possibilities, see e.g. Fig. 1.2. Of particular interest for this Thesis is the ferroquadrupolar ordered phase. This is a type of spin nematic which, as will be presented in Chapter 4, in fact bears mathematical similarity in the low-energy limit to linearized gravity.

On-site quadrupolar order with a biquadratic term in the Hamiltonian was first discussed by Blume and Hseieh [87], independent of lattice geometry. Chen and Levy studied the appearance of quadrupolar order in systems with spin greater than 1, motivated by pnictide materials where the effective spin is larger than $\frac{3}{2}$ [88]. Andreev and Grischuk later provided a more detailed discussion of quadrupolar order, including

the possibility of formation of effective spin-1 moments across bonds in spin- $\frac{1}{2}$ magnets [89–91]. In the time since, our understanding of where to expect spin nematic phases has improved in both magnetic insulators [4, 90–98], with triangular lattice candidate materials NiGa₂S₄ [99, 100] and FeGa₂S₄ [101], and spinor condensates [102–109].

The ferroquadrupolar phase is characterized by the absence of magnetic dipole ordering

$$\langle \mathbf{S} \rangle = 0 , \quad (1.29)$$

but still possesses a non-trivial quadrupole ordering in which there is a favoured plane, e.g.

$$\langle (S^x)^2 \rangle = \langle (S^y)^2 \rangle \neq \langle (S^z)^2 \rangle . \quad (1.30)$$

This leads to a natural choice for order parameter in terms of the symmetric, traceless, tensor

$$Q^{\alpha\beta} = \frac{1}{2} (S^\alpha S^\beta + S^\beta S^\alpha) - \frac{1}{3} \delta^{\alpha\beta} S^\gamma S^\gamma . \quad (1.31)$$

This spin nematic order will play a key role in this Thesis, and we will return to it in connection to analogue gravitational waves in Chapter 4. Note that by construction

$$\text{Tr}(Q) = 0 , \quad (1.32)$$

and therefore, the non-trivial scalar invariants one can construct in this case take the form

$$\text{Tr}(Q^n) \neq 0 , \quad n \geq 2 . \quad (1.33)$$

Symmetry arguments can then be applied in this case to predict the relevant form of the free energy

$$F_{FQ} = a(T - T_c) \text{Tr}(Q^2) + b \text{Tr}(Q^3) + c \text{Tr}(Q^4) , \quad (1.34)$$

where note that odd terms are in this case allowed since they remain invariant under rotations, and the presence of the third-order term leads to the paramagnetic-nematic transition being first order [110, 111].

The insight of Landau that symmetry alone plays the driving role in determining the behaviour of phase transitions laid the groundwork for further critical insights into the nature of the dynamics in symmetry broken phases, such as the description of Goldstone modes, which we will return to in Chapter 2.

1.2.4 Topological phase transitions: The XY model

Condensed matter systems are host to a wide variety of interesting phases of matter, especially at low temperatures. As a system is cooled, it is not uncommon for the low-energy phase to have reduced symmetry relative to the high-energy phase, as we

have just seen to be described by the Landau paradigm. However, as we will see in Chapter 2, such phase transitions in which the order is characterized by continuous symmetry breaking cannot take place in reduced dimensional systems. This does not exclude the possibility of phase transitions which do not exhibit genuine spontaneous symmetry breaking and instead are characterized by the emergence of a different kind of collective structure, namely topological structures or defects. This alternative type of transition was first proposed by Berezinskii [46] and later by Kosterlitz and Thouless [47], and receives the name BKT-transition.

The canonical example of a model exhibiting this kind of phase transition is the 2D XY model

$$\mathcal{H} = J \sum_{\langle ij \rangle} \mathbf{S}_i \cdot \mathbf{S}_j = JS^2 \sum_{\langle ij \rangle} \cos(\theta_i - \theta_j) , \quad (1.35)$$

defined for (classical) $O(2)$ spins

$$\mathbf{S} = S \begin{pmatrix} \cos \theta \\ \sin \theta \end{pmatrix} , \quad (1.36)$$

motivated as the paradigmatic effective model describing the universality class of two-dimensional superconductors [112–114], observed also in liquid crystals [110] and Bose-Einstein Condensates (BECs) [115].

At high temperatures, the model possesses exponentially decaying spin correlations, with correlation length described by

$$\xi_{BKT} \sim e^{\frac{b}{\sqrt{T-T_c}}} , \quad (1.37)$$

with critical temperature T_c . However, below the critical temperature, the correlations instead decay algebraically, behaviour mediated by the presence at low energies of bound vortex pairs. At high-energies, the vortex pairs unbind and proliferate freely. We will see examples of similar behaviour in spin nematics in Chapter 5.

1.2.5 Detecting and simulating magnetic order

After having discussed magnetic orders and phase transitions, it is now worth a few remarks about the relevant measurable quantities that signal magnetic order in experiment.

As previously discussed, the distinguishing feature of the ferromagnet is a finite macroscopic magnetization

$$\langle \mathbf{S} \rangle \neq 0 , \quad (1.38)$$

and this therefore serves as an appropriate order parameter. This could already be detected long ago in lodestone due to the interaction with e.g. the Earth's magnetic field. Precise measurements of magnetization can be carried out at the level of entire samples using magnetic resonance techniques [116]. Magnetization can nowadays be probed even down to molecular resolution, e.g. [117].

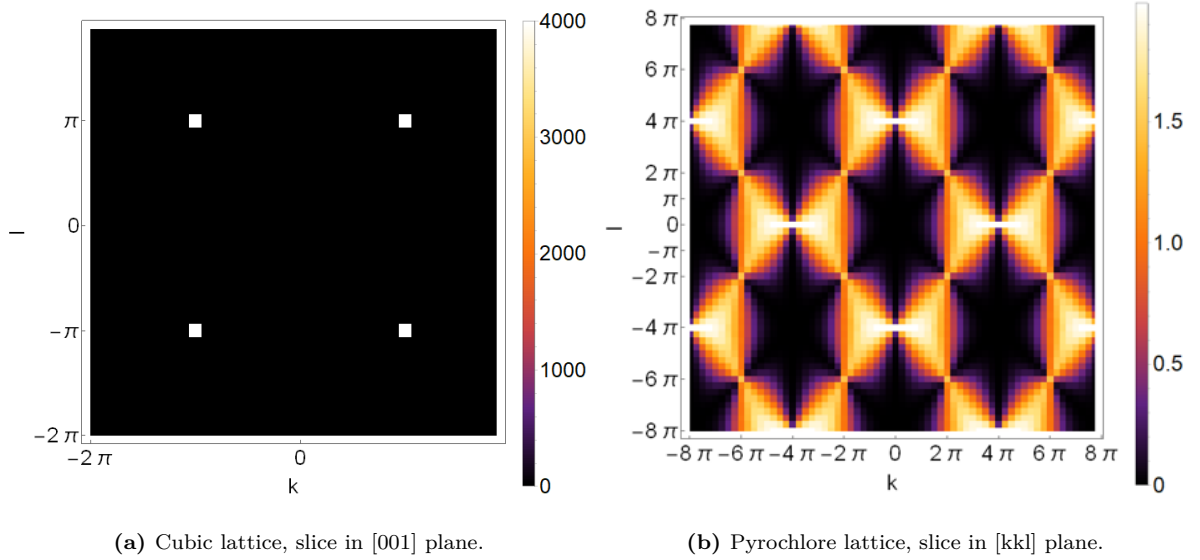


Figure 1.3: Correlations obtained from simulation at low temperatures in O(3) antiferromagnets on the cubic and pyrochlore lattices. **(a)** Equal-time structure factor for an O(3) antiferromagnet on a cubic lattice, showing a slice in the [001] plane. Clearly visible Bragg peaks at (π, π, π) signal antiferromagnetic order. **(b)** Equivalent results for an O(3) antiferromagnet on the pyrochlore lattice, showing pinch points associated with algebraic spin correlations.

However, for the antiferromagnet,

$$\langle \mathbf{S} \rangle = 0 . \quad (1.39)$$

Therefore, we need to be more creative about how we measure its presence by taking a closer look at the structure of correlations. Specifically in the antiferromagnetic case, there is a crystalline structure within which neighbouring spins are antialigned. This pattern is detectable in the structure of the spatial two-spin correlation function, whose Fourier transform can be measured typically in solid state via neutron scattering leading to the momentum space distribution, see e.g. [118],

$$S(\mathbf{q}) = \frac{1}{N} \sum_{i,j} \langle \mathbf{S}(\mathbf{r}_i) \mathbf{S}(\mathbf{r}_j) \rangle e^{-\mathbf{q} \cdot (\mathbf{r}_i - \mathbf{r}_j)} . \quad (1.40)$$

In the broader condensed matter context, such two-point functions receive the name static or equal-time structure factor, see Fig. 1.3.

In addition, since these measurements do not destroy the sample under examination, it is also possible to study correlations over time, as this reveals information about the dynamics and excitations in the material. The relevant quantity we evaluate in theory and experiment is the dynamical structure factor

$$S(\mathbf{q}, \omega) = \frac{1}{N} \int dt e^{i\omega(t-t_0)} \sum_{i,j} \langle \mathbf{S}(\mathbf{r}_i, t) \mathbf{S}(\mathbf{r}_j, t_0) \rangle e^{-\mathbf{q} \cdot (\mathbf{r}_i - \mathbf{r}_j)} . \quad (1.41)$$

From the dynamical measurements, we can extract information about the dispersion

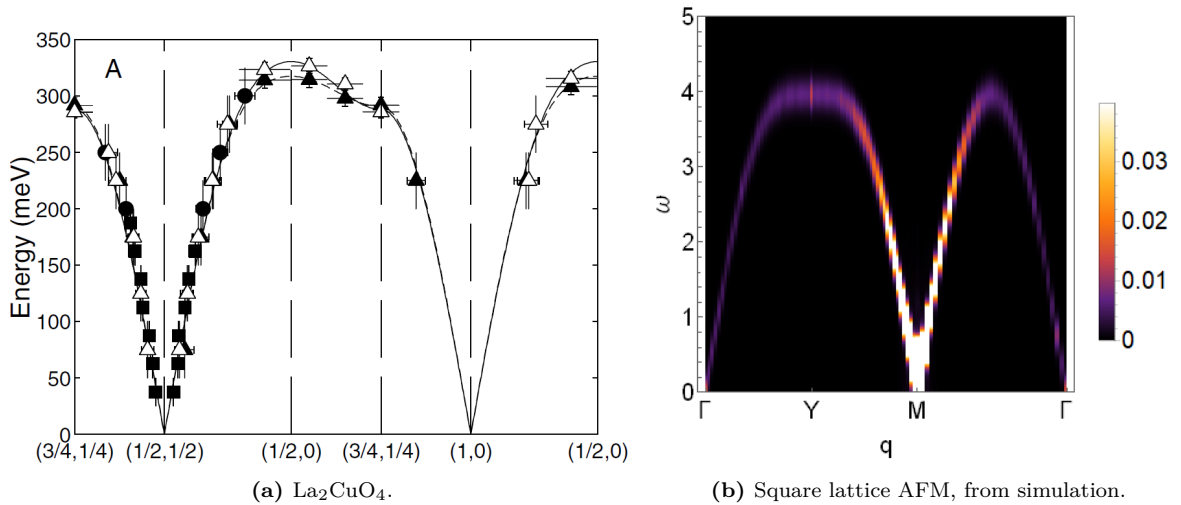


Figure 1.4: Magnetic excitations of two-dimensional antiferromagnets in experiment and simulation, showing linearly-dispersing excitations approaching the ordering vector. **(a)** Inelastic neutron scattering measurements for the square lattice antiferromagnet La_2CuO_4 . **(b)** $S(\mathbf{q}, \omega)$ obtained by Molecular Dynamics simulation, discussed in Chapter 5, for the square lattice Heisenberg antiferromagnet. Fig. 1.4(a) reproduced from [8] with permission.

of excitations in a variety of materials and models, see Fig. 1.4a]. The nature of the low-energy dispersion of excitations will play a recurring role in this Thesis for both the identification of analogues of photons and gravitational waves, and we will return to the measurement of the relevant dynamical structure factors in Chapter 5.

1.2.6 Magnetism in cold atoms

While our historical contact with magnetism came by means of crystalline materials, there are novel possibilities to use quantum fluids with a manifold of internal spin states to exhibit magnetic phenomena. Superfluids, such as ^3He , are a natural example of candidate quantum fluids that meet this criteria [119, 120]. Most recently, there is renewed excitement focused on the study of the so-called “spinor condensates”, cold atom condensates typically of effective spin-1 or spin-2 atoms, such as ^{23}Na or ^{87}Rb , whose effective spin arises depending on the hyperfine manifold populated [121].

Two developments have extended the reach of ultracold gases enormously in the last few decades [122]. Firstly, the use of Feshbach resonances provided the ability to tune interaction strengths beyond the weakly interacting regime [123, 124]. Secondly, the ability to trap atoms in optical lattices now allows access to a wide variety of periodic geometries and low dimensional physics [125]. The micrometer sized lattice constants in such systems additionally allow single-site resolution and addressing [126, 127].

These advances have paved the way for further exploration of many-body physics in the ultracold regime, leading to a rapid explosion of new accessible physics, including e.g. $\text{SU}(N)$ models as accessible versions of strongly-interacting gauge theories [128], a subject which has engaged the attention of many theoretical works e.g. [129, 130].

As mentioned in the Introduction, scalar analogues of gravitational waves and curvature have already been realized in the cold atom context [39–42, 131]. A natural next

step would be to extend the exploration to systems with internal degrees of freedom. This Thesis proposes that nematic phases realized in spinor condensates could provide a full tensor analogue, see Chapters 4-6.

In summary, we have seen how magnetism can arise in natural materials, what phases can manifest, and what interactions must be realizable in artificial platforms for quantum simulation of magnetic models. In the remainder of this Chapter, we briefly turn attention to the phenomena this Thesis will show analogues for in magnetism, namely, electromagnetism and photons and linearized gravity and gravitational waves.

1.3 A brief review of light

In Chapter 3, I will explicitly introduce analogues of photons in the context of magnetic systems, making use of parallels in their respective field theories. Here I remind the interested reader of the historical development of ideas leading to the currently standard notion of a photon.

The independent notions of light, electrostatics and Coloumb's law, and magnetic phenomenology were known to exist since at least the 18th century. However, it was not until the beginning of the 19th century that the interconnectedness of these three phenomena started becoming clearer, finally crystallizing with the comprehensive presentations of electrodynamics that were spearheaded by J.C. Maxwell from the 1850's onwards [132, 133].

The main shift in perspective came with the introduction of the concept of fields. In this view electric charges generate radial electric field lines \mathbf{E} , and electric charges in constant motion generate solenoidal magnetic field lines \mathbf{B} , both of which decay in strength with distance but nevertheless in principle reach out to infinity. Importantly, changes in charge distribution or charge acceleration are not communicated instantaneously to points arbitrarily far away but instead must be propagated as disturbances of the field lines.

The equations describing the dynamics of these fields were presented then by Maxwell, and were later grouped by Heaviside [134] into the set of four vector equations now known as Maxwell's equations, which in differential form can be written as follows

$$\nabla \cdot \mathbf{B} = 0 , \quad (1.42a)$$

$$\nabla \cdot \mathbf{E} = \frac{\rho_e}{\epsilon_0} , \quad (1.42b)$$

$$\nabla \times \mathbf{E} + \partial_t \mathbf{B} = 0 , \quad (1.42c)$$

$$\nabla \times \mathbf{B} - \frac{1}{c^2} \partial_t \mathbf{E} = \mu_0 \mathbf{J} , \quad (1.42d)$$

where c is the speed at which field disturbances propagate. These electromagnetic oscillations were later confirmed by Hertz to be responsible for light [135].

Notice that the right-hand-sides of all equations Eq. (1.42) are vanishing in vacuum. Taking the time derivative of equations Eq. (1.42c-1.42d) and substituting Eq. (1.42a-

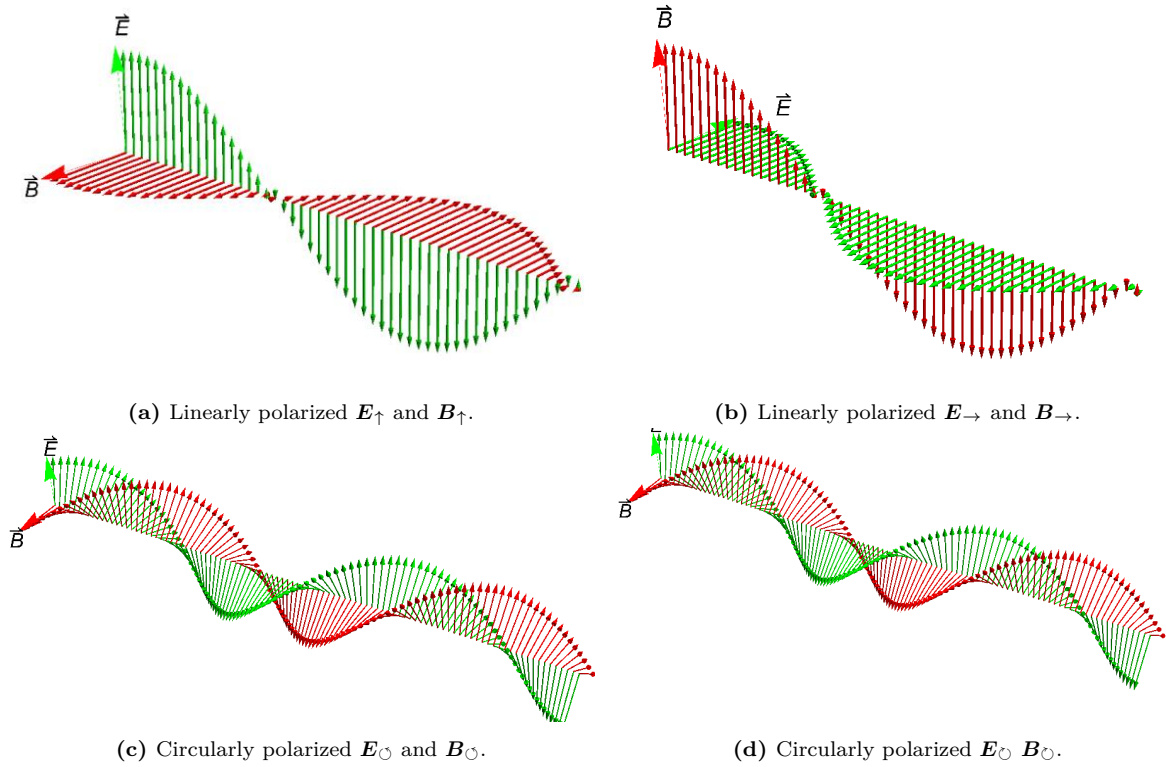


Figure 1.5: Different polarizations of light. (a) Dipole oscillations resulting from a shifting centre of mass along the z -direction result in linearly polarized excitations of the electromagnetic field. (b) Dipole oscillations resulting from a shifting centre of mass along the y -direction result in linearly polarized excitations of the electromagnetic field. (c) A rotating dipole in the yz -plane result in circularly polarized excitations of the electromagnetic field. (d) A rotating dipole in the yz -plane result in circularly polarized excitations of the electromagnetic field.

1.42b) leads to the wave equations

$$\frac{1}{c^2} \partial_t^2 \mathbf{E} = \nabla^2 \mathbf{E} , \quad (1.43a)$$

$$\frac{1}{c^2} \partial_t^2 \mathbf{B} = \nabla^2 \mathbf{B} , \quad (1.43b)$$

which possess self-propagating massless wave solutions in terms of the coupled oscillating electric and magnetic fields, which can propagate far from any sources, see Fig. 1.5.

The generation of such oscillating solutions is generally tied to the motion of charges (real or virtual), allowing one to motivate description of the angular momentum character of electromagnetic radiation in terms of the multipole expansion of the source, whose terms capture progressively higher order angular features [136]. The zeroth order moment is the monopole moment, which respects spherical symmetry. Due to charge conservation, the monopole moment

$$Q = \int dx^d \rho_e , \quad (1.44)$$

is conserved, and therefore has trivial time derivative and generates a field only elec-

trostatically. The monopole moment cannot change in time and therefore cannot lead to electromagnetic waves. However, the dipole moment

$$\mathbf{d} = \int dx^d \rho_e \mathbf{r} , \quad (1.45)$$

is generically non-trivial, and dominates the expansion. Therefore, electromagnetic waves are produced by either rotating or oscillating dipoles and will transform under rotation as vectors, namely, they have spin $s = 1$.

Oscillating dipoles lead to the linearly polarized radiation modes, which can be decomposed into the basis $\mathbf{E}_{\rightarrow}^{(x)}$ and $\mathbf{E}_{\uparrow}^{(x)}$, shown in Fig. 1.5,

$$\mathbf{E}_{\rightarrow}^{(x)} = |\mathbf{E}| \begin{pmatrix} 0 \\ \cos(\mathbf{k}\mathbf{x} - \omega t) \\ 0 \end{pmatrix} , \quad \mathbf{B}_{\rightarrow}^{(x)} = |\mathbf{B}| \begin{pmatrix} 0 \\ 0 \\ \cos(\mathbf{k}\mathbf{x} - \omega t) \end{pmatrix} , \quad (1.46a)$$

$$\mathbf{E}_{\uparrow}^{(x)} = |\mathbf{E}| \begin{pmatrix} 0 \\ 0 \\ \cos(\mathbf{k}\mathbf{x} - \omega t) \end{pmatrix} , \quad \mathbf{B}_{\uparrow}^{(x)} = |\mathbf{B}| \begin{pmatrix} 0 \\ -\cos(\mathbf{k}\mathbf{x} - \omega t) \\ 0 \end{pmatrix} , \quad (1.46b)$$

A rotating dipole is described by a superposition of oscillating motion in the plane perpendicular to radiation. The resulting circularly polarized radiation can be decomposed into a linear superposition of the the two linear polarizations

$$\mathbf{E}_{\circlearrowleft}^{(x)} = \frac{1}{\sqrt{2}}(\mathbf{E}_{\rightarrow}^{(x)} + i\mathbf{E}_{\uparrow}^{(x)}) , \quad \mathbf{B}_{\circlearrowleft}^{(x)} = \frac{1}{\sqrt{2}}(\mathbf{B}_{\rightarrow}^{(x)} + i\mathbf{B}_{\uparrow}^{(x)}) , \quad (1.47a)$$

$$\mathbf{E}_{\circlearrowright}^{(x)} = \frac{1}{\sqrt{2}}(\mathbf{E}_{\rightarrow}^{(x)} - i\mathbf{E}_{\uparrow}^{(x)}) , \quad \mathbf{B}_{\circlearrowright}^{(x)} = \frac{1}{\sqrt{2}}(\mathbf{B}_{\rightarrow}^{(x)} - i\mathbf{B}_{\uparrow}^{(x)}) . \quad (1.47b)$$

This dynamical framework then clearly supported the idea that forces do not act spontaneously at a distance, and rather in the electromagnetic case propagate through the corresponding fields. It was initially assumed that there was a background medium which represented the field at rest called the aether. However, after the Michelson-Morley experiment ruled out the possibility of a fixed universal frame of reference for such an aether [137], it became clear that there is no privileged inertial reference frame. This context led Einstein to postulate that electromagnetic fields propagate at a constant speed, namely the speed of light c , and that the laws of physics must remain invariant for every inertial observer, leading to Special Relativity [138]. These two realizations impose the constraint that fundamental fields in spacetime must transform reversibly under elements of the Poincaré group, and that the actions associated to any such field must be invariant under Poincaré transformation.

To make the relativistic symmetries of electromagnetism manifest, it is usual to work in terms of the vector potential

$$A^\mu = (A^t, \mathbf{A}) , \quad (1.48a)$$

$$A_\mu = (-A_t, \mathbf{A}) , \quad (1.48b)$$

which is a gauge field possessing redundant degrees of freedom, defined in terms of the

electric and magnetic fields

$$E_i = -\frac{1}{c^2}\partial_t A_i - \partial_i A_t, \quad (1.49a)$$

$$B_i = \epsilon^{ijk}\partial_j A_k. \quad (1.49b)$$

The wave equation describing propagating modes of electromagnetism can then be written as follows

$$\frac{1}{c^2}\partial_t^2 A^\mu = \partial_i^2 A^\mu, \quad (1.50)$$

still consistent with electromagnetic waves—or photons—as massless spin-1 bosons. In Chapter 2, I will review the description of photons in terms of the gauge field A^μ .

1.4 On the quadrupolar nature of gravitational waves

In this section, I briefly recount the key principles leading to the geometrization of gravity and how it predicts spin-2 (quadrupolar) gravitational waves.

A curious feature of the natural world that was noted already in the works of Galileo, Kepler and Newton is the proportionality of gravitational mass and inertial mass. This empirically established observation arose from the fact—known in Ancient Greece and to Aristotle—that two unequal weights accelerate under the action of gravity with the same acceleration. This idea is what Einstein later termed the Weak Equivalence Principle, with the refined statement that there is no way for any isolated observer to determine if any perceived acceleration is due to the presence of a gravitating body or acceleration of the observer.

This key fact led Einstein to conclude non-trivially that gravity must be a geometric theory in which, as stated by John Wheeler

“space acts on matter and tells it where to move, while matter acts on space and tells it how to curve” [139],

collected in the Einstein equations

$$G_{\mu\nu} = \frac{8\pi G}{c^4}T_{\mu\nu}, \quad (1.51)$$

where the tensor $G_{\mu\nu}$ describes the curvature of spacetime, and the stress-energy tensor $T_{\mu\nu}$ describes the distribution of mass-energy density.

The free space Einstein equations permit self-propagating wave solutions, in a similar way to electromagnetism. We will revisit this in Chapter 2. However, from consideration of the leading terms in the multipole expansion, we find that these waves are necessarily rank-2 tensors which transform under rotation with angular momentum $s = 2$. The monopole moment

$$M = \int d^d x \rho_m \quad (1.52)$$

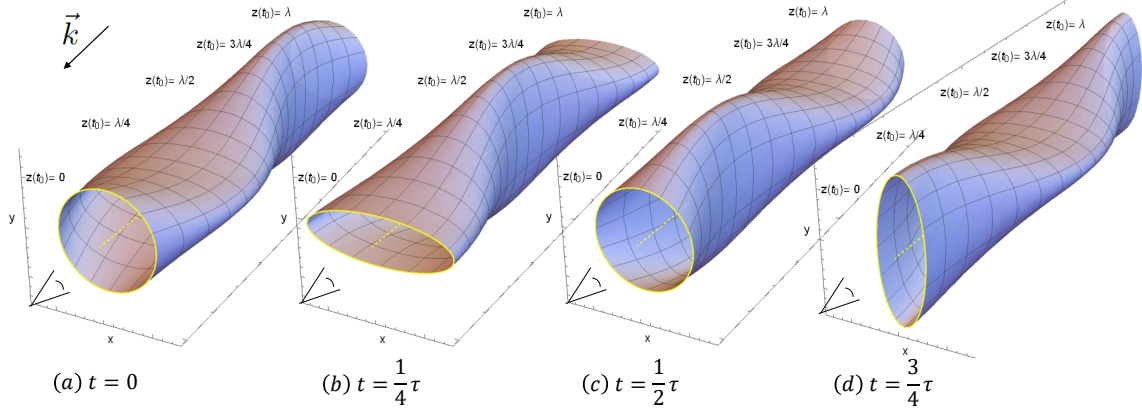


Figure 1.6: Quadrupolar oscillations of a source correspond to deviations from spherical symmetry. The corresponding wave induces spatial deformation shown on the yellow ring due to a linearly polarized gravitational wave as seen by the observer in the figure.

is conserved due to energy-momentum conservation. The dipole moment

$$\mathbf{d} = \int d^d x \rho_m \mathbf{r} \quad (1.53)$$

is also necessarily conserved due to conservation of momentum. Therefore, is it only the quadrupole moment

$$Q^{ij} = \int d^d x \rho_m (x^i x^j - \frac{2}{3} \delta^{ij} r^2), \quad (1.54)$$

which can contribute to leading order to gravitational waves, under the unmodified theory of general relativity.

As in the case of electromagnetic waves, we can decompose the independent modes of gravitational waves into linear polarizations generated by an oscillating quadrupole moment, which for a wave propagating in the z -direction take the form

$$h_{\mu\nu}^+ = e^{ik^\mu x_\mu} \begin{pmatrix} 0 & 0 & 0 & 0 \\ 0 & h_+ & 0 & 0 \\ 0 & 0 & -h_+ & 0 \\ 0 & 0 & 0 & 0 \end{pmatrix}, \quad (1.55a)$$

$$h_{\mu\nu}^\times = e^{ik^\mu x_\mu} \begin{pmatrix} 0 & 0 & 0 & 0 \\ 0 & 0 & h_\times & 0 \\ 0 & h_\times & 0 & 0 \\ 0 & 0 & 0 & 0 \end{pmatrix}. \quad (1.55b)$$

An example of the deformation induced by such a linearly polarized wave is shown in Fig. 1.6.

Rotating quadrupole moments generate waves of non-trivial helicity. There are two independent modes of helicity $\gamma = \pm s = \pm 2$ describing gravitational waves, which without loss of generality can be described classically for a wave propagating along the z -direction as

$$h_{\mu\nu}^{\circlearrowleft} = e^{ik^\mu x_\mu} \begin{pmatrix} 0 & 0 & 0 & 0 \\ 0 & h_+ & ih_\times & 0 \\ 0 & ih_\times & -h_+ & 0 \\ 0 & 0 & 0 & 0 \end{pmatrix}, \quad (1.56a)$$

$$h_{\mu\nu}^{\circlearrowright} = e^{ik^\mu x_\mu} \begin{pmatrix} 0 & 0 & 0 & 0 \\ 0 & h_+ & -ih_\times & 0 \\ 0 & -ih_\times & h_+ & 0 \\ 0 & 0 & 0 & 0 \end{pmatrix}, \quad (1.56b)$$

where in terms of the linear polarizations, we define

$$h_{\mu\nu}^{\circlearrowleft} = h_{\mu\nu}^+ + ih_{\mu\nu}^\times, \quad (1.57a)$$

$$h_{\mu\nu}^{\circlearrowright} = h_{\mu\nu}^+ - ih_{\mu\nu}^\times. \quad (1.57b)$$

In Fig. 1.6, the effect of such a wave on distances separating events in spacetime is visualized. These forms make explicit that a gravitational wave is characterized by the presence of non-trivial spatial components of the metric only. That is, the temporal components of the metric are not affected by the passage of the wave. These modes correspond to strain modes that are transverse to the direction of propagation. However, in our day to day experience we do not encounter such deformations due to the relative weakness of gravity and, consequently, of its excitations.

The amount of power radiated into a gravitational wave is related to the source properties in the following power law[139]

$$P_{GW} = \frac{2}{45} \frac{G}{c^4} M^2 l^4 \omega^6. \quad (1.58)$$

Given that the factor

$$\frac{G}{c^4} \approx 8 * 10^{-45} \frac{s^2}{kg m}, \quad (1.59)$$

what realistic output could we ever hope to achieve in a laboratory setting? Even if we consider a steel beam of length $l = 20m$, rotating at $\omega = 28rad/s$, then the power output is around $10^{-30}J/s$. This is ridiculously small to hope to ever generate gravitational waves ourselves for any useful purpose in ordinary laboratories. By contrast, the amount of power radiated by astrophysical sources during e.g. the collapse of a supernovae into a neutron star is expected to generate a burst lasting around $0.1s$ with power output the order of $10^{60}J/s$ [139].

In summary, gravitational waves themselves are fundamentally distinct from light,

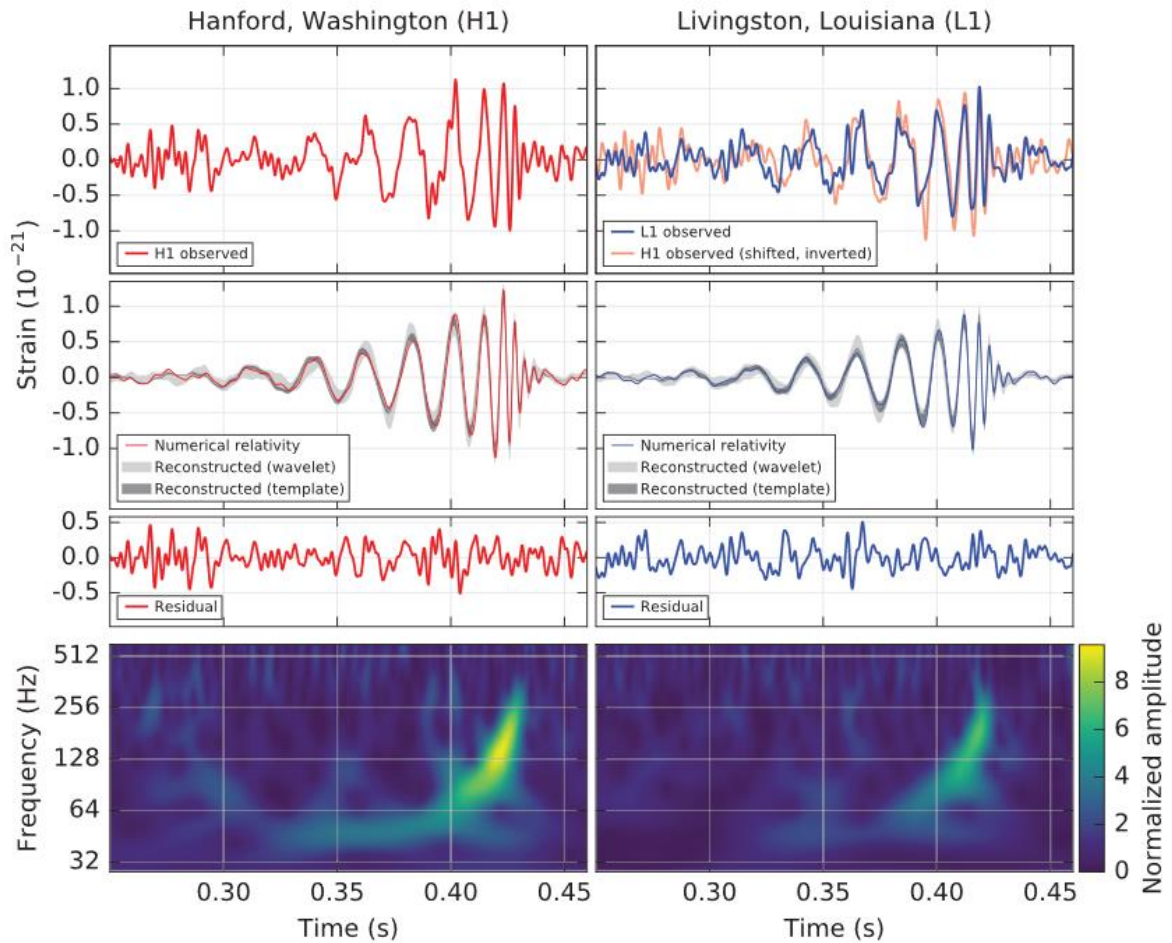


Figure 1.7: Data from the first LIGO observation of the gravitational wave event GW150914, a binary black-hole merger, depicting the characteristic chirp of the event. The signal from the event 1.4 ± 0.6 billion light-years away is only perceptible above the background for the short period of time during which the merger produces a large burst of gravitational wave output. Figure reproduced from [9], available under the terms of the Creative Commons Attribution 3.0 License.

not only due to the hierarchy of scales separating their relevant observational ranges, but as spin-2 excitations which mediate an attractive force. Unlike their photonic counterparts, gravitational radiation strong enough to be detectable is not experimentally reproducible, therefore the laboratory use of spin-2 (quadrupolar) waves has not been explored. It is therefore of interest to access an analogue counterpart in the lab.

1.5 Thesis outline

In this Chapter, we have learned about analogues which realize parts of electromagnetism or gravity, magnetism and magnetic order, and electromagnetic radiation and gravitational waves. Building on ideas introduced in this Chapter, in this I Thesis establish a novel connection between gravitational waves and spin nematic excitations. In particular, I will develop the connection between the Goldstone modes of a ferroquadrupolar spin nematic and gravitational waves as described by linearized gravity first by analytic considerations. The critical result is that the action for a ferroquadrupolar spin nematic has the same form as that of linearized gravity, and this allows the construction of a dictionary relating the excitations of the spin nematic to gravitational waves.

I will then expand upon this finding with numerical simulations, showcasing that spin nematics exhibit topological point defects which experience attractive interactions, leading to in-spiral and eventually annihilation. I simulate that the pattern of wave emission for such an annihilation event generates a characteristic chirp of its own, see Fig. 1.8, resembling the wave emission of binary mergers of astrophysical objects which trigger gravitational waves significant enough to be detected on Earth.

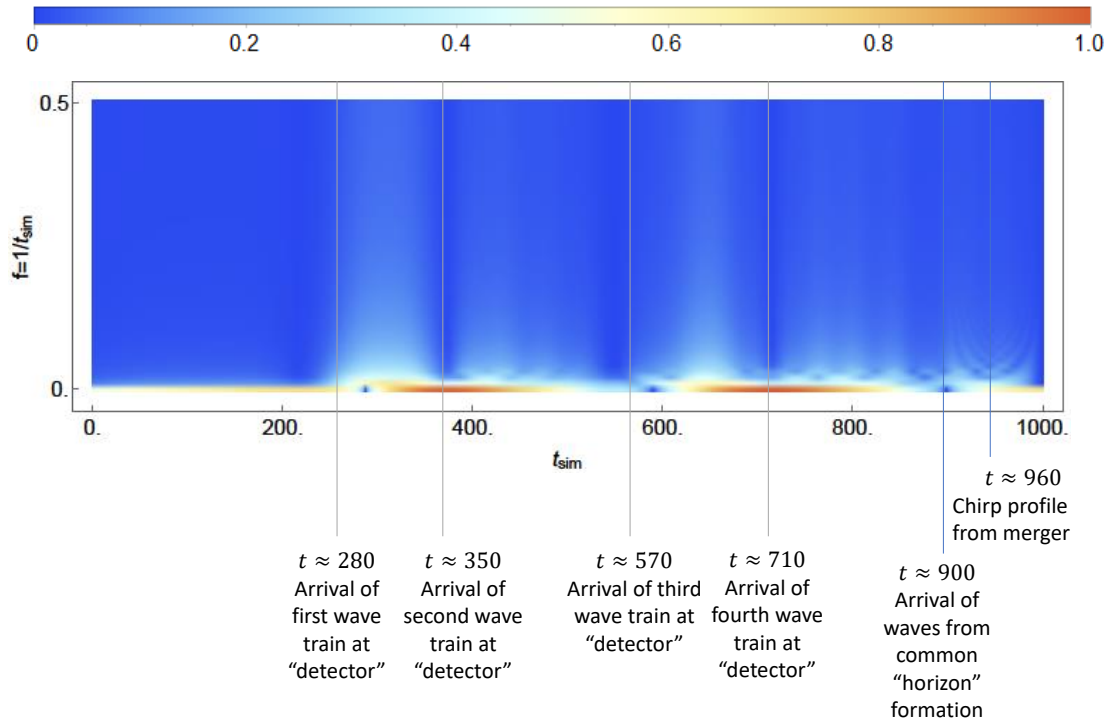
To provide the detailed fundamental background required, Chapter 2 discusses spontaneous symmetry breaking, and how it leads to Goldstone modes in the magnetic phases of interest in this thesis. Chapter 2 will also work in detail through the relevant background on the field theory for electromagnetism and linearized gravity in vacuum.

The purpose of Chapter 3 is to lay out what analogues have already been discussed in the context of magnetism, starting with the XY ferromagnet and spin ice, and to explicitly motivate a connection between photons and the Heisenberg antiferromagnet by way of providing a recipe that can be generalized to an analogue of gravitational waves for a spin nematic.

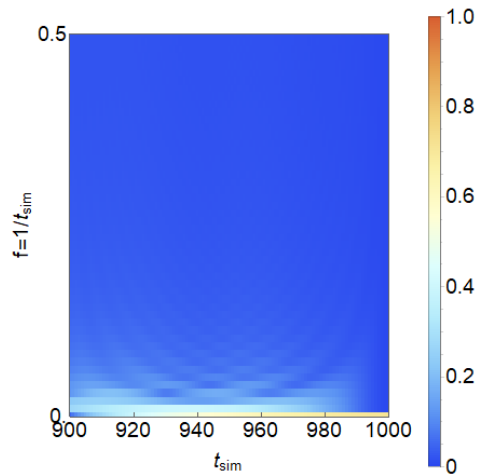
In Chapter 4, I will present a quantum spin nematic analogue to linearized gravity, in which self-propagating dynamical modes are naturally supported, and furthermore in the low-energy limit correspond to massless, spin-2 bosons in one-to-one correspondence with gravitational waves in vacuum.

Chapter 5 focuses on numerical simulation of the discussed analogues, and showcases how analogue gravitational waves can be generated in 2D realizations of the ferroquadrupolar spin nematic phase of the microscopic Bilinear-Biquadratic model by the annihilation of \mathcal{Z}_2 vortices. Building on this, I outline an experimental protocol that would allow such waves to be observed in spinor condensates.

In Chapter 6, I provide an outlook on this work and suggested directions for further inquiry.



(a) Spectrogram from simulated gravitational wave emission.



(b) Chirp signal corresponding to vortex annihilation.

Figure 1.8: Spectrogram showcasing the time-frequency decomposition of the waves emitted by defect pairs in a spin nematic. Full description of this result in Chapter 5.

Chapter 2

Massless Bosons: Magnetic Goldstone modes, Photons and Gravitons

“The most incomprehensible thing about the world is that it is comprehensible.” - Albert Einstein, as quoted by P.A. Schilpp (1949).

Vacuum states, whether they be a condensed matter ground state or the ground state of the Universe, can possess two categories of excitation, one of which are excitations that cost a finite amount of energy to generate and are therefore referred to as gapped or massive excitations, e.g. massive elementary particles, or topological excitations of the kind present in the XY model.

A second kind of excitation are those which have a vanishing dispersion at long wavelength, such that at infinitely long wavelength the perturbation of the ground state in fact has no energy cost. These are called massless or gapless excitations. In this Thesis, we will be concerned primarily with massless excitations of vacuum and they are therefore the subject of this Chapter.

The existence of gapped excitations in a given system does not preclude the existence of gapless excitations, and vice versa¹. There is no unique way to determine if a system is necessarily gapped or gapless, though one can conclude that gapless Bosonic modes should exist in the context of systems with spontaneously broken continuous symmetries. This is a consequence of Goldstone’s theorem.

This Chapter provides technical background material for the remainder of the Thesis. I begin by introducing Goldstone’s theorem, and how spontaneously broken continuous symmetries lead to massless excitations termed Goldstone Bosons. I also review the counting procedures for these Goldstone modes, essential material for the development of analogues of photons and gravitational waves.

I then revisit the massless, spin-1 Boson of electromagnetism, the photon, providing a more technical overview of electromagnetism, in order to equip the reader with enough background to understand magnetic analogues that will be presented in Chapter 3.

¹In Chapter 4, we will revisit the idea of topological excitations in a spin nematic, which provide an example of this.

I finally review the construction of the linearized limit of gravity with its associated massless spin-2 Bosonic modes i.e. gravitational waves, for which I will present a magnetic analogue in Chapter 4.

2.1 Goldstone's theorem and spontaneous symmetry breaking

It was famously established by Emmy Noether that for every continuous symmetry of an action, there exists a corresponding conserved charge [140]. That said, the individual states of a system are not required to respect all the symmetries of the action. This is typical of the difference between high-temperature, high-symmetry phases and low-temperature, reduced-symmetry phases, characteristic of all phase transitions that fall within the Landau paradigm [84]. In the context of magnetism, we have already seen an example of this. For the Heisenberg model [Eq. (1.16)], an active global rotation of the spin basis does not change the inner product between neighbouring spin dipole operators, and therefore leaves the Hamiltonian—and equivalently the action—unchanged. However for a particular ferromagnetic ground state, the spins are all aligned along a particular direction e.g. $\langle S^z \rangle \neq 0$, and therefore the same active transformation that leaves the Hamiltonian invariant will now transform the ground state to another equivalent ground state. The selection of one of many possible ground states is an example of what is meant by a spontaneously broken symmetry.

Now let us generically suppose the action is a functional of a given quantum field ϕ , where the symmetry group of the action is G and corresponding conserved charge is Q . Given that the charge Q is the generator of transformations of the given symmetry group G , we can define a unitary operator $U(Q)$ that induces a symmetry transformation. Consider then the fluctuations of the field, which result from an infinitesimal symmetry transformation

$$\delta^{(Q)}\phi = -i[\phi, U(Q)] . \quad (2.1)$$

In a state of the system preserving the full symmetry group, the vacuum expectation value of the fluctuations of the field should vanish, and correspondingly so should the associated commutator

$$\langle i[U(Q), \phi] \rangle = 0 . \quad (2.2)$$

Now suppose some subset of symmetries are broken by the ground state of the system. Then, the ground state of the system is symmetric under some $H \in G$, where $\dim(G/H) = m$. In this case, the vacuum expectation value of fluctuations are non-vanishing

$$\langle i[U(Q), \phi] \rangle \neq 0 , \quad (2.3)$$

and can be used to define an order parameter. As was originally observed by Nambu and Goldstone [141–143] from studying gauge theory in the context of superconductivity, the non-vanishing fluctuations are gapless modes corresponding to long wavelength

excitations in the manifold of the broken symmetry generators, since these correspond to directions in which the free energy landscape around the ordered state is flat. There has been much subsequent work to generalize the original theorem of Goldstone [144] to a wider class of systems in both high-energy physics and condensed matter, including applicability to systems which do not exhibit Lorentz invariant actions [145]—such as the Heisenberg ferromagnet—or with higher form symmetries [146]—such as photons in electromagnetism, as comprehensively reviewed in [147].

The correspondence of the number of gapless modes to broken symmetry generators is not always one-to-one [148], and depends on the form of the dispersion relation

$$\omega = c|\mathbf{k}|^p . \quad (2.4)$$

The power p in the dispersion relation depends in turn on whether or not the action of the system is Lorentz invariant [145]. For systems with odd power p , the number of Goldstone modes n_{odd} is in correspondence with the number of broken symmetry generators, called type-I. However, for systems whose dispersion relation is of even power p , there is an internal coupling of degrees of freedom leading to a reduced number of Goldstone modes n_{even} , called type-II. With these definitions in place, the total number of Goldstone modes is related to the number of broken symmetries by the relation [148, 149]

$$n_{odd} + 2n_{even} = m . \quad (2.5)$$

In summary, the dimension of the flat free energy manifold only corresponds to the number of independent zero energy modes if the system is relativistically invariant. Otherwise, the zero energy modes couple pairwise.

A simple classical example exhibits how modes can couple to reduce the number of Goldstone modes corresponding to the broken symmetry generators [150]. Consider a pendulum of length l suspended from the ceiling, hanging such that it is oriented along the z -direction. The direction of gravity can be thought to break the $O(3)$ symmetry of the pendulum, confining it to dangle along z rather than any other direction on the sphere. There are two independent modes of the pendulum: it is free to oscillate independently along x or y directions with arbitrarily low-energy. Each of the two modes will carry a non-trivial angular momentum

$$L_x = l \hat{x} \times \mathbf{p}_x , \quad (2.6a)$$

$$L_y = l \hat{y} \times \mathbf{p}_y . \quad (2.6b)$$

Now suppose that the pendulum is not simply hanging from the ceiling, but it is also rotating; that is, it carries an intrinsic angular momentum $L_z \neq 0$.

In this case, the angular momentum Poisson Bracket places constraints on the independence of components of angular momentum

$$\{L_a, L_b\} = \epsilon^{abc} L_c , \quad (2.7)$$

such that if L_z is now fixed, L_x and L_y can no longer be independent modes and are instead coupled into one precessing mode. The sign of L_z fixes the orientation of the precession, and breaks the discrete time-reversal symmetry: for a given orientation of

L_z , the precession looks different when viewed forwards or backwards in time. With broken time-reversal symmetry, the action describing this system will not be Lorentz invariant.

Let's consider next the quantum mechanical version of this example. Instead of a pendulum, consider a spin moment with intrinsic angular momentum \mathbf{S} . In the absence of any interactions, the spin moment is free to point anywhere on a sphere. However, if constrained to point, for example, along the z-direction, then the $O(3)$ symmetry is broken, with resulting expectation value

$$\langle 0 | S_z | 0 \rangle \neq 0 . \quad (2.8)$$

This breaks the two rotational symmetries with unitary transformations

$$R_x(\theta_1) = e^{i\theta_1 S_x} , \quad R_y(\theta_2) = e^{i\theta_2 S_y} , \quad (2.9)$$

such that

$$\langle 0 | [R_1, S_z] | 0 \rangle \neq 0 , \quad (2.10)$$

$$\langle 0 | [R_2, S_z] | 0 \rangle \neq 0 , \quad (2.11)$$

and we therefore expect two Goldstone modes. However, the angular momentum commutation relations

$$[S_a, S_b] = i\epsilon^{abc} S_c , \quad (2.12)$$

will not allow for two independent Goldstone modes, given that the expectation value of S_z is fixed. This would seem to suggest that all magnetic systems are doomed to behave in a way that violates Lorentz invariance; however this example only captures the exceptional case of the Heisenberg ferromagnet, in which the finite macroscopic magnetization $\mathbf{m} \neq 0$ explicitly breaks time-reversal symmetry, and therefore is subject to the counting for type-II modes. In this case

$$\omega \propto |k|^2 \quad \implies \quad n_{\text{even}} = 1 . \quad (2.13)$$

On the other hand, intuitively we can see that time-reversal symmetry is restored for the Heisenberg antiferromagnet by considering the full unit cell in which

$$\mathbf{m}_A + \mathbf{m}_B = 0 , \quad (2.14)$$

such that

$$\omega \propto |k| \quad \implies \quad n_{\text{odd}} = 2 . \quad (2.15)$$

In Chapter 3, we will see in more detail why this is the case, and how this allows the system to be effectively described by the Lorentz invariant non-linear sigma model with two independent Goldstone modes.

2.1.1 Coleman and Hohenberg-Mermin-Wagner theorems

Relevant to Chapter 5 of this Thesis, there are conditions under which spontaneous symmetry breaking is not allowed. This is true in particular in systems of dimension less than three, as was already suggested in the 1930's by Bloch [151], Peierls [152] and Landau [84], and this importantly motivates the existence of topological phase transitions in a variety of low-dimensional models [46, 47].

Indeed, the tendency to order plays out differently in low dimensional systems, as introduced by Hohenberg [153], Mermin and Wagner [154] and Coleman [155] independently.

Hohenberg first proposed [153] a rigorous demonstration of the absence of long-range order in two-dimensional systems. However, the precedence of this article is often omitted or unknown, due to the prior appearance in print of the Letter by Mermin and Wagner [156]. The range of interactions is important for these results. In the context of quantum spin models, with short-range interactions that obey

$$\frac{1}{2N} \sum_{\langle ij \rangle} J_{ij} |\mathbf{r}_i - \mathbf{r}_j| < \infty, \quad (2.16)$$

the statement holds that there can be no true long-range order at finite temperatures in dimensions $d \leq 2$. Coleman later showed that in the case of (1+1)D field theories the vacuum expectation value of the fluctuation $\delta\phi$ of a scalar field ϕ must be vanishing to avoid singularities [155]. This implies that in (1+1)D all symmetries must remain manifest. However, importantly for this Thesis, the inability of the long wavelength Goldstone modes to stabilize an ordered phase does not exclude the existence of other types of excitation which can induce and stabilize a broken symmetry phase. We can reconcile the latter possibility in low dimensional systems which exhibit topologically mediated transitions, as was first proposed by Berezinskii [46] and later Kosterlitz and Thouless [47] in the context of the 2D XY model.

2.2 (3+1)D electromagnetism in vacuum

In this Section, I provide technical background on electromagnetism in vacuum and its massless, spin-1 bosons (photons), which is needed to understand the analogues of electromagnetism reviewed and presented in Chapter 3. The treatment which follows adopts conventional notations established in e.g. [157, 158]. Electromagnetism is a gauge theory of a spin-1 field, described by a 4-vector A_μ with a $U(1)$ symmetry, and which is compatible with both special relativity and can be canonically quantized.

Maxwell's equations in vacuum can be cast in terms of the field A_μ

$$\frac{1}{2} \partial_\mu (\partial^\mu A^\nu - \partial^\nu A^\mu) = 0, \quad (2.17)$$

where from here on I use the notation for the components of an arbitrary four-vector $a^\mu = (a^0, a^1, a^2, a^3)$, instead of $a^\mu = (ca^t, a^x, a^y, a^z)$. I also use the convention

$$A^\mu = (A^0, \mathbf{A}), \quad (2.18a)$$

$$A_\mu = \eta_{\mu\nu} A^\nu = (-A^0, \mathbf{A}) , \quad (2.18b)$$

with $\eta_{\mu\nu} = \text{diag}(-1, 1, 1, 1)$.

Suppose that a solution to Eq. (2.17) admits a Fourier decomposition

$$A^\nu(x^\mu) = \sum_{k_\mu} \tilde{A}^\nu(k_\mu) e^{ik_\mu x^\mu} , \quad (2.19)$$

such that

$$\left(\partial^\mu \partial_\mu \delta_\mu^\nu - \partial^\mu \partial_\nu \right) A^\mu = 0 , \quad (2.20a)$$

$$\implies \left(k^\mu k_\mu \delta_\mu^\nu - k_\mu k^\nu \right) \tilde{A}^\mu = 0 , \quad (2.20b)$$

$$(2.20c)$$

where we can define the sparse matrix $K_{\mu\nu}$

$$K_{\mu\nu} = \left(k^\mu k_\mu \delta_\mu^\nu - k_\mu k^\nu \right) . \quad (2.21)$$

This matrix has the property that $\det(K) = 0$ for any k_μ, k_ν . This is clear since for non-trivial \tilde{A}^μ , K must be singular. Furthermore, K has one eigenvector with zero eigenvalue

$$K_{\mu\nu} \tilde{A}^\mu = \lambda \tilde{A}^\mu , \quad \lambda = 0 , \quad (2.22a)$$

$$\implies \tilde{A}^\mu = k^\mu , \quad (2.22b)$$

from which

$$K \tilde{A}^\mu = K k^\mu = 0 , \quad (2.23a)$$

$$\implies K \left(\tilde{A}^\mu - i\epsilon k^\mu \right) = 0 , \quad (2.23b)$$

$$\implies \tilde{A}^\mu = \tilde{A}^\mu - i\epsilon k^\mu , \quad (2.23c)$$

$$\implies A^\mu = A^\mu + \partial^\mu \epsilon . \quad (2.23d)$$

where A^μ is therefore also a valid solution of Maxwell's equations. We can therefore see the gauge symmetry explicitly appear.

Armed with this, we can work backwards to identify the explicit form of the electromagnetism Lagrangian. Compatibility with special relativity assumes that the equations of motion must be Lorentz covariant, and therefore the Lagrangian must have Lorentz covariant form with terms like

$$\mathcal{L} = c_1 \partial_\mu A_\nu \partial^\mu A^\nu + c_2 \partial_\mu A_\nu \partial^\nu A^\mu + c_3 \partial_\mu \partial^\mu (A_\nu A^\nu) . \quad (2.24)$$

Invariance of the Lagrangian under the $u(1)$ symmetry

$$A^\mu = A^\mu + \partial^\mu \epsilon , \quad (2.25)$$

implies that $c_1 = -c_2$ and $c_3 = 0$. The Lagrangian can then be factorized leading to

the following action describing electromagnetism in flat vacuum, which is quadratic in the vector field A_μ

$$\mathcal{S}_{EM} = -\frac{1}{2} \int dx^4 \eta_{\alpha\nu} (\partial_\mu A^\alpha \partial^\mu A^\nu - \partial_\mu A^\alpha \partial^\nu A^\mu) , \quad (2.26)$$

equivalent to

$$\begin{aligned} \mathcal{S}_{EM} &= -\frac{1}{4} \int dx^4 (\partial_\mu A_\nu - \partial_\nu A_\mu) (\partial^\mu A^\nu - \partial^\nu A^\mu) , \\ &\equiv \frac{1}{4} \int dx^4 F_{\mu\nu} F^{\mu\nu} . \end{aligned} \quad (2.27)$$

The action Eq. (2.27) and corresponding equations of motion Eq. (2.17) are invariant under the gauge transformation Eq. (2.25). We will next see how gauge transformation can be used to make explicit the transverse nature of the propagating modes allowed by Maxwell's equations.

2.2.1 Lorentz covariance of the gauge field A^μ implies the existence of transverse and gauge modes

In this Section we will learn that the Lorentz covariance of the gauge field A^μ leads to a distinction between the physically dynamical components of the gauge field which are necessarily transverse to the propagation, and the non-dynamical components which can be gauged away. The transverse nature of the dynamical components will be a key property to keep in mind when visiting magnetic analogues in Chapter 3.

It turns out that the nature of the gauge freedom Eq. (2.25) will already determine the minimal set of non-trivial components, reducing the number of components of A^μ that are dynamically non-trivial.

Under the right conditions on A^μ , namely

$$\partial_\mu A^\mu = 0 , \quad (2.28)$$

Eq. (2.17) contains the wave equation

$$\partial^\mu \partial_\mu A^\nu = 0 , \quad (2.29)$$

which we will review here to be consistent with the minimal expression of non-trivial components. Without loss of generality, consider specifically $k^\mu = (k^0, 0, 0, k^3)$

$$\tilde{A}^0 = \tilde{A}^0 - k^0 \epsilon , \quad (2.30a)$$

$$\tilde{A}^1 = \tilde{A}^1 , \quad (2.30b)$$

$$\tilde{A}^2 = \tilde{A}^2 , \quad (2.30c)$$

$$\tilde{A}^3 = \tilde{A}^3 - k^3 \epsilon . \quad (2.30d)$$

It is clear that at least one component of \tilde{A}^μ , and A^μ can be eliminated by appropriate choice of the scalar field ϵ , while the transverse degrees of freedom will remain

unchanged by gauge transformation.

For propagating modes which are massless, these must obey the null condition

$$k^\mu k_\mu = 0, \quad (2.31)$$

which in turn implies that if we choose

$$\partial_\mu A^\mu \rightarrow \partial_\mu A^\mu + \partial_\mu \partial^\mu \epsilon = 0, \quad (2.32a)$$

$$\implies \partial_\mu A^\mu = -\partial_\mu \partial^\mu \epsilon, \quad (2.32b)$$

$$\implies k_\mu \tilde{A}^\mu = k_\mu k^\mu \epsilon, \quad (2.32c)$$

$$\implies k_\mu \tilde{A}^\mu = 0, \quad (2.32d)$$

then \tilde{A}^μ is orthogonal to the four-momentum, independent of the selection of ϵ .

For the specific case of propagation along the z -axis, it must hold that $k_0 = -k_3$. Lightlike propagation in combination with the condition $k_\mu \tilde{A}^\mu = 0$ (known as the Lorenz gauge condition) in turn implies

$$A^0 = A^3. \quad (2.33)$$

The scalar degree of freedom ϵ can then be used to set

$$A^0 = A^3 = 0. \quad (2.34)$$

In addition, under this condition, it is straightforward to see that Maxwell's equations Eq. (2.17) do indeed reduce to the wave equation Eq. (2.29). This makes explicit the transverse nature of the excitations of electromagnetism in vacuum (photons). In Chapter 3, we will connect this notion of transverse excitations to the Heisenberg antiferromagnet, which also has two massless dynamically non-trivial degrees of freedom that are expressed transverse to the order parameter.

To understand why the non-transverse degrees of freedom are in fact unphysical, I next review how the distinction between the transverse and gauge modes follows from relativistic transformations of the gauge field, as first indicated by Kim and Wigner [159–161]. Consider Lorentz transformations $\Lambda = \{R, B\}$, where R is the set of $O(3)$ rotations generated by J_i and B is the set of boosts generated by K_i , for $i = x, y, z$

$$J_x = \begin{pmatrix} 0 & 0 & 0 & 0 \\ 0 & 0 & 0 & 0 \\ 0 & 0 & 0 & -i \\ 0 & 0 & i & 0 \end{pmatrix}, \quad K_x = \begin{pmatrix} 0 & -i & 0 & 0 \\ -i & 0 & 0 & 0 \\ 0 & 0 & 0 & 0 \\ 0 & 0 & 0 & 0 \end{pmatrix}, \quad (2.35a)$$

$$J_y = \begin{pmatrix} 0 & 0 & 0 & 0 \\ 0 & 0 & 0 & i \\ 0 & 0 & 0 & 0 \\ 0 & -i & 0 & 0 \end{pmatrix}, \quad K_y = \begin{pmatrix} 0 & 0 & -i & 0 \\ 0 & 0 & 0 & 0 \\ -i & 0 & 0 & 0 \\ 0 & 0 & 0 & 0 \end{pmatrix}, \quad (2.35b)$$

$$J_z = \begin{pmatrix} 0 & 0 & 0 & 0 \\ 0 & 0 & -i & 0 \\ 0 & i & 0 & 0 \\ 0 & 0 & 0 & 0 \end{pmatrix}, \quad K_z = \begin{pmatrix} 0 & 0 & 0 & -i \\ 0 & 0 & 0 & 0 \\ 0 & 0 & 0 & 0 \\ -i & 0 & 0 & 0 \end{pmatrix}, \quad (2.35c)$$

which satisfy the following commutation relations

$$[J_i, J_j] = i\epsilon_{ijk}J_k, \quad (2.36a)$$

$$[K_i, K_j] = -i\epsilon_{ijk}J_k, \quad (2.36b)$$

$$[J_i, K_j] = -i\epsilon_{ijk}K_k. \quad (2.36c)$$

When elements of the Lorentz group act on a massless particle, they either alter the 4-momentum or leave it intact. For the case considered in the previous section, where $k_\mu = (-k_3, 0, 0, k_3)$, we see that

$$R_z k_\mu = k_\mu, \quad (2.37a)$$

$$R_i k_\mu \neq k_\mu, \quad i = 1, 2, \quad (2.37b)$$

$$B_i k_\mu \neq k_\mu, \quad i = 1, 2, 3, \quad (2.37c)$$

where the generator that leaves the 4-momentum intact must effect a transformation instead on the internal degrees of freedom of the field.

It is well known that there are two further generators that leave the 4-momentum intact [159–161]

$$N_1 = K_x - J_y = \begin{pmatrix} 0 & -i & 0 & 0 \\ -i & 0 & 0 & -i \\ 0 & 0 & 0 & 0 \\ 0 & i & 0 & 0 \end{pmatrix}, \quad (2.38a)$$

$$N_2 = K_y + J_x = \begin{pmatrix} 0 & 0 & -i & 0 \\ 0 & 0 & 0 & 0 \\ -i & 0 & 0 & i \\ 0 & 0 & i & 0 \end{pmatrix}. \quad (2.38b)$$

Together, these generators which affect the internal degrees of freedom are called the Little Group. The available internal degrees of freedom are spanned by action of the group elements

$$G(u, v, \theta) = e^{-i(uN_1 + vN_2 + \theta R_z)}, \quad (2.39)$$

such that the field A_μ transforms as

$$G(u, v, \theta)A_\mu = \begin{pmatrix} A_0 \\ A_1 \cos(\theta) - A_2 \sin(\theta) \\ A_2 \cos(\theta) + A_1 \sin(\theta) \\ A_3 \end{pmatrix} + \begin{pmatrix} A_1 u + A_2 v \\ 0 \\ 0 \\ A_1 u + A_2 v \end{pmatrix}$$

$$+ \begin{pmatrix} \frac{1}{2}(A_3 - A_0)(u^2 + v^2) \\ (A_0 - A_3)u \\ (A_0 - A_3)v \\ \frac{1}{2}(A_0 - A_3)(u^2 + v^2) \end{pmatrix}. \quad (2.40)$$

The first term corresponds to physical rotations of the transverse degrees of freedom, and the remaining two terms affect the gauge. Note that the series expansion for $G(u, v) = e^{-i(uN_1 + vN_2)}$ is trivial beyond order $\mathcal{O}(N_i^3)$, such that in contrast to $G(\theta)$, $G(u, v)$ is not a compact function of u or v . These elements act on the gauge redundant degrees of freedom, leading to effective linear rescaling of components A_0 and A_3 . The components of the field A_μ can therefore be thought of as living on a $4D$ cylinder of infinite extent in the A_0 and A_3 directions, and fixed radius in the transverse plane. The transverse components correspond to the photon degrees of freedom, which in Chapter 3, I will show to be in explicit correspondence with the magnons of the Heisenberg antiferromagnet.

In summary, the action of the Lorentz group on the electromagnetic vector field corresponds to transverse rotations, acting on the photon degrees of freedom, and gauge transformations which mix in the longitudinal and temporal degrees of freedom.

2.2.2 Poynting vector, energy conservation and visualization of the spin-1 field

We have seen how it is always possible to choose Lorenz gauge such that all components of A_μ satisfy the wave equation Eq. (2.29). To show this is consistent with energy-momentum conservation, let's examine the stress-energy tensor components for EM in terms of the gauge invariant tensor $F^{\mu\nu}$

$$T^{\mu\nu} = \frac{1}{4\pi} \left(F^{\mu\alpha} F_\alpha^\nu - \frac{1}{4} \eta^{\mu\nu} F^{\alpha\beta} F_{\alpha\beta} \right), \quad (2.41)$$

which has scalar component corresponding to the relativistic energy density

$$T^{00} = \frac{1}{4\pi} \left[\left(\partial^0 A^\alpha - \partial^\alpha A^0 \right) \left(\partial^0 A_\alpha - \partial_\alpha A^0 \right) + \frac{1}{4} \eta^{00} \left(\partial_\alpha A_\beta - \partial_\beta A_\alpha \right) \left(\partial^\alpha A^\beta - \partial^\beta A^\alpha \right) \right], \quad (2.42)$$

vector components corresponding to the flux of energy density through a surface orthogonal to the vector

$$T^{0j} = \frac{1}{4\pi} \left(F^{0\alpha} F_\alpha^j \right) \quad (2.43)$$

$$= \frac{1}{4\pi} \left(\partial^0 A^\alpha - \partial^\alpha A^0 \right) \left(\partial^j A_\alpha - \partial_\alpha A^j \right), \quad (2.44)$$

and tensor components

$$T^{ij} = \frac{1}{4\pi} \left(F^{i\alpha} F_{\alpha}^j - \frac{1}{4} \delta^{ij} F^{\alpha\beta} F_{\alpha\beta} \right), \quad (2.45)$$

which obey the conservation law

$$\partial_{\mu} T^{\mu\nu} = 0. \quad (2.46)$$

This implies that the scalar and vector components are unchanging in time. Using the definition of electric and magnetic fields, we can reduce these components to the following expressions

$$T^{00} = \frac{1}{4\pi} \left(\epsilon_0 E^{\alpha} E_{\alpha} + \frac{1}{\mu_0} B^{\alpha} B_{\alpha} \right), \quad (2.47a)$$

$$T^{0j} = \frac{1}{4\pi} E_m B_n \epsilon^{mnj}, \quad (2.47b)$$

$$T^{ij} = \frac{1}{4\pi} \left(\epsilon_0 E^i E^j + \frac{1}{\mu_0} B^i B^j - \delta^{ij} T^{00} \right). \quad (2.47c)$$

The components T^{0j} define the Poynting vector. The condition for energy conservation on the fields \mathbf{E} and \mathbf{B} therefore follows from the definition of the Poynting vector, in terms of the spatial (and not Lorentz invariant) fields \mathbf{E} and \mathbf{B}

$$|\mathbf{S}| = |\mathbf{E} \times \mathbf{B}| = \text{const}, \quad (2.48)$$

where

$$\mathbf{E} = -\partial_t \mathbf{A}, \quad (2.49a)$$

$$\mathbf{B} = \nabla \times \mathbf{A}. \quad (2.49b)$$

By definition as the flux of momentum density, the Poynting vector is parallel to the direction of travel of the wave

$$\mathbf{S} \cdot \mathbf{k} = 0. \quad (2.50)$$

Next, let's define explicitly the circular polarizations of respective helicity $\gamma = \pm 1$

$$\mathbf{A}_{\circ}, \mathbf{A}_{\ominus}, \quad (2.51)$$

which define a pair under time reversal symmetry.

Taking the case of $\mathbf{k} = k\hat{z}$, we find that consistency with energy momentum conservation leads to the explicit components

$$\mathbf{A}_{\circ} = |\mathbf{A}| \begin{pmatrix} \cos(kz - \omega t) \\ \sin(kz - \omega t) \\ 0 \end{pmatrix}, \quad \mathbf{A}_{\ominus} = |\mathbf{A}| \begin{pmatrix} \cos(kz - \omega t) \\ -\sin(kz - \omega t) \\ 0 \end{pmatrix}, \quad (2.52)$$

with fields

$$\mathbf{E}_\circ = |\mathbf{A}|\omega \begin{pmatrix} -\sin(kz - \omega t) \\ \cos(kz - \omega t) \\ 0 \end{pmatrix}, \quad \mathbf{E}_\circ = |\mathbf{A}|\omega \begin{pmatrix} \sin(kz - \omega t) \\ \cos(kz - \omega t) \\ 0 \end{pmatrix}, \quad (2.53a)$$

$$\mathbf{B}_\circ = |\mathbf{A}|k \begin{pmatrix} \cos(kz - \omega t) \\ \sin(kz - \omega t) \\ 0 \end{pmatrix}, \quad \mathbf{B}_\circ = |\mathbf{A}|k \begin{pmatrix} -\cos(kz - \omega t) \\ \sin(kz - \omega t) \\ 0 \end{pmatrix}, \quad (2.53b)$$

where

$$|\mathbf{A}| = \frac{|\mathbf{E}|}{\omega} = \frac{|\mathbf{B}|}{k}, \quad (2.54)$$

$$\implies |\mathbf{E}| = c|\mathbf{B}|, \quad (2.55)$$

with

$$\omega = ck. \quad (2.56)$$

In conclusion, conservation of energy-momentum determines the relationship between the electric and magnetic fields. The self-propagating electromagnetic fields of a photon are visualized in Fig. 1.5 in Chapter 1.

2.2.3 Canonical quantization of photons

The previous treatments were valid for not only a classical relativistic spin-1 field, but are also valid for a quantized spin-1 field. We can write the second quantized decomposition of the photon excitations as [162]

$$A^\mu(\mathbf{x}) = (2\pi)^{\frac{3}{2}} \int \frac{d^3\mathbf{p}}{\sqrt{2\omega}} (a^\mu(\mathbf{p})e^{-i\mathbf{p}\cdot\mathbf{x}} + a^{\dagger\mu}(\mathbf{p})e^{i\mathbf{p}\cdot\mathbf{x}}), \quad (2.57)$$

where the field operators a^μ and $a^{\dagger\mu}$ satisfy the Bosonic commutation relations

$$[a^\mu(x), a^{\dagger\nu}(x')] = \delta(x' - x)\delta^{\mu\nu}. \quad (2.58)$$

In conclusion, photons are massless, spin-1 Bosons. In addition, as shown in previous sections, the non-trivial components of the photon are always transverse. These facts are critical for the identification of photon analogues in the condensed matter context, and in Chapter 3, I will explicitly introduce a one-to-one analogue of photons in the excitations of the Heisenberg antiferromagnet.

2.2.4 Masslessness from symmetry breaking

Massless vector field theories are known to have non-regularizable singularities unless a gauge degree of freedom is introduced [44]. Here I briefly review an alternative perspective on the relationship between the gauge freedom and the masslessness of the photon.

In Section 2.2.1, I described photons as transverse gauge bosons by assuming they must be massless, which automatically fixes of residual gauge degree of freedom.

There is a fundamental reason to expect the masslessness of the photon beyond the need to regularize the vector field theory, namely, that it was long suspected that photons could be described as the Goldstone mode of a spontaneously broken symmetry and therefore must be massless [146].

Consider again the U(1) symmetry of Eq. (2.25). If we take Lorentz gauge as before, we find

$$\partial_\mu A^\mu = 0 , \quad (2.59a)$$

$$\partial_\mu A^\mu = -\partial_\mu \partial^\mu \epsilon , \quad (2.59b)$$

$$\implies \partial_\mu \partial^\mu \epsilon = 0 , \quad (2.59c)$$

$$\implies \epsilon(x^\nu) = a + \omega_\nu x^\nu . \quad (2.59d)$$

That is, if not imposing automatically the masslessness of the photon leading to the null condition, there is a residual gauge degree of freedom.

If we now consider the differential associated to a continuous gauge transformation

$$\delta^{(\epsilon)} A^\mu \equiv \partial_\mu A'^\mu - \partial_\mu A^\mu = \partial^\mu \epsilon = \omega_\nu \delta_\mu^\nu = \omega_\mu , \quad (2.60)$$

which in turn is related to the generator of continuous residual gauge transformations

$$\delta^{(\epsilon)} A^\mu = -i[A^\mu, Q^\nu] \neq 0 . \quad (2.61)$$

This in turn suggests we should be able to think of the photon degrees of freedom as Goldstone modes related to a broken symmetry, in closer analogy to the Goldstone modes of e.g. magnetic insulators.

A more formal way to describe the symmetry breaking undergone by electromagnetism invokes higher form symmetries [147, 163]. Recent extension of Goldstone's theorem to higher form symmetries therefore offers a concrete perspective on the masslessness of photons and its relation to broken symmetries [164], though a deeper discussion goes beyond the scope of this Thesis.

In conclusion, this suggests that it is reasonable to look for analogues of photons in the Goldstone modes of condensed matter systems.

2.3 Linearized gravity as a spin-2 field theory

In the Thesis' quest for analogues, including analogue gravitational waves, it is natural to ask what is the simplest theory which describes the effects of gravitation, and in our case, gravitational waves. The first and simplest theory of gravity was developed by Newton, in which the Newtonian force law is related to the potential

$$\mathbf{F} = -\nabla\phi , \quad (2.62)$$

Newtonian physics does not predict waves, since within this framework, the gravitational potential generated is assumed to respond instantaneously in a global way to

local changes of density

$$\nabla^2 \phi = 4\pi G \rho_m . \quad (2.63)$$

This would of course violate causality.

At first glance, a scalar field theory such as

$$\mathcal{L} = -\frac{1}{2}(\partial_\mu \phi \partial^\mu \phi + g\phi T_\mu^\mu) , \quad (2.64)$$

might seem to be enough. However, a problem arises if we consider that the only scalar available to couple to the scalar field ϕ is the trace of the energy-momentum tensor T_μ^μ . For electromagnetic fields, $T_{\mu EM}^\mu = 0$ and therefore such a theory of gravitation could not couple to photons [165]. However, observations of gravitational lensing and deflection of light indicates empirically that this coupling cannot be trivial.

A massless vector field, such as

$$\mathcal{L} = -\frac{1}{4}(\partial_\mu A_\nu - \partial_\nu A_\mu)(\partial^\mu A^\nu - \partial^\nu A^\mu) - j^\mu A_\mu , \quad (2.65)$$

will also not work since the sign of interactions mediated by a spin-1 vector field is opposite to that of gravitation. Namely, for spin-1 fields, like charges repel.

The only other possibility for a long-range force carrier is a spin-2 tensor field, since for higher orders one cannot identify a conserved field with 3 or more space-time indices to which the force carrier can couple [44]. The question then becomes, in what limit can one write down a spin-2 field theory which is consistent with general relativity?

2.3.1 From General Relativity to Linearized gravity

In this section and the following, I will review the linearized limit of gravity, following conventions laid out in e.g. [139, 158, 165, 166]. General Relativity is a geometric theory of gravity, in which the fundamental notion of geometry is contained in the metric tensor $g_{\mu\nu}(x^\rho)$. This provides the ruler for defining the inner product between 4-vectors defined on the spacetime manifold, and is defined as a symmetric tensor. The full Einstein action for gravity in vacuum has the form

$$\mathcal{S}_E = \frac{c^3}{16\pi G} \int d^4x \sqrt{-g} R . \quad (2.66)$$

This action is comprised of two contributing scalar terms. The first is the Jacobian term $\sqrt{-g}$, defined in terms of

$$g = \det(g_{\mu\nu}) , \quad (2.67)$$

where the metric $g_{\mu\nu}$ in this Universe has negative signature, such that the square root is well-defined in this form². The second is the Ricci scalar R , defined in terms of

²A more general way to express the Jacobian term is

$$J = \sqrt{|g|} \quad (2.68)$$

successive contractions of the Riemann tensor $R_{\rho\sigma\mu\nu}$, which can be expressed via the Ricci tensor $R_{\sigma\mu}$ as follows

$$\begin{aligned} R_{\sigma\nu} &= R^\lambda_{\sigma\lambda\nu} \\ &= g^{\mu\rho} R_{\rho\sigma\mu\nu} , \end{aligned} \quad (2.69a)$$

$$\begin{aligned} R &= g^{\sigma\nu} R_{\sigma\nu} \\ &= g^{\sigma\nu} g^{\mu\rho} R_{\rho\sigma\mu\nu} , \end{aligned} \quad (2.69b)$$

where the Riemann tensor is defined to first order in the metric tensor as follows

$$R_{\rho\sigma\mu\nu} = \frac{1}{2} (\partial_\mu \partial_\sigma g_{\rho\nu} + \partial_\rho \partial_\nu g_{\mu\sigma} - \partial_\rho \partial_\mu g_{\nu\sigma} - \partial_\nu \partial_\sigma g_{\rho\mu}) . \quad (2.70)$$

In the weak field limit, the metric can be written in terms of small perturbations on the flat spacetime background $\eta_{\mu\nu}$, that is

$$g_{\mu\nu} = \eta_{\mu\nu} + h_{\mu\nu} , \quad (2.71a)$$

$$g^{\mu\nu} = \eta^{\mu\nu} - h^{\mu\nu} , \quad (2.71b)$$

where we will use the following convention for the Minkowski metric $\eta_{\mu\nu}$

$$\eta^{\mu\nu} = \text{diag}(-1, 1, 1, 1) . \quad (2.72)$$

The linearized limit is valid where

$$|h_{\mu\nu}| \ll \eta_{\mu\nu} . \quad (2.73)$$

In this limit, the Riemann tensor becomes

$$R_{\rho\sigma\mu\nu} = \frac{1}{2} (\partial_\mu \partial_\sigma h_{\rho\nu} + \partial_\rho \partial_\nu h_{\mu\sigma} - \partial_\rho \partial_\mu h_{\nu\sigma} - \partial_\nu \partial_\sigma h_{\rho\mu}) . \quad (2.74)$$

such that to order $\mathcal{O}(h^2)$ the Ricci tensor and Ricci scalar take the forms

$$R_{\sigma\nu} = \frac{1}{2} (\eta^{\mu\rho} - h^{\mu\rho}) R_{\rho\sigma\mu\nu} , \quad (2.75a)$$

$$\eta^{\mu\rho} R_{\rho\sigma\mu\nu} = \frac{1}{2} (\partial^\rho \partial_\sigma h_{\rho\nu} + \partial^\mu \partial_\nu h_{\mu\sigma} - \partial^\mu \partial_\mu h_{\nu\sigma} - \partial_\nu \partial_\sigma h^\mu_\mu) , \quad (2.75b)$$

$$-h^{\mu\rho} R_{\rho\sigma\mu\nu} = \frac{1}{2} (\partial_\mu h^{\mu\rho} \partial_\sigma h_{\rho\nu} + \partial_\rho h^{\mu\rho} \partial_\nu h_{\mu\sigma} - \partial_\rho h^{\mu\rho} \partial_\mu h_{\nu\sigma} - \partial_\nu h^{\mu\rho} \partial_\sigma h_{\mu\rho}) , \quad (2.75c)$$

and

$$R = (\eta^{\nu\sigma} - h^{\nu\sigma}) R_{\sigma\nu} , \quad (2.76a)$$

$$\eta^{\nu\sigma} R_{\sigma\nu} = \frac{1}{2} (\partial^\rho \partial^\nu h_{\rho\nu} + \partial^\mu \partial^\sigma h_{\mu\sigma} - 2\partial^\mu \partial_\mu h$$

which describes geometries with positive signature, the simplest example of which is Euclidean spacetime.

$$+ \partial_\mu h^{\mu\rho} \partial_\sigma h_\rho^\sigma + \partial_\rho h^{\mu\rho} \partial_\nu h_\mu^\nu - \partial_\rho h^{\mu\rho} \partial_\mu h - \partial^\sigma h^{\mu\rho} \partial_\sigma h_{\mu\rho} \Big), \quad (2.76b)$$

$$-h^{\nu\sigma} R_{\sigma\nu} = \frac{1}{2} \left(h^{\nu\sigma} \partial^\rho \partial_\sigma h_{\rho\nu} + h^{\nu\sigma} \partial^\mu \partial_\nu h_{\mu\sigma} - h^{\nu\sigma} \partial^\mu \partial_\mu h_{\nu\sigma} - h^{\nu\sigma} \partial_\nu \partial_\sigma h_\mu^\mu + \mathcal{O}(h^3) \right), \quad (2.76c)$$

where the terms linear in h in the above are total derivatives and will not contribute to the action. Therefore, the relevant terms in the Ricci scalar can be collected below

$$R = - \left(2\partial^\mu h^{\sigma\nu} \partial_\mu h_{\sigma\nu} - 2\partial_\mu h \partial_\mu h - 2\partial_\mu h^{\mu\rho} \partial_\sigma h_\rho^\sigma + 2\partial^\mu h_{\sigma\nu} \partial^\nu h \right). \quad (2.77)$$

The Jacobian term in the Einstein action also admits a perturbative expansion around the background Minkowski spacetime in the weak field limit.

$$g = \det |g^{\mu\nu}| = - \det |\eta^{\mu\rho}| \det |g_\rho^\nu|, \quad (2.78)$$

and in the linearized limit,

$$\det |g_\rho^\nu| \approx \det |\delta_\rho^\nu + h_\rho^\nu|, \quad (2.79)$$

$$= e^{\ln(\det |\delta_\rho^\nu + h_\rho^\nu|)}, \quad (2.80)$$

$$= e^{\text{Tr}(\ln(\delta_\rho^\nu + h_\rho^\nu))}, \quad (2.81)$$

$$\approx 1 + h + \mathcal{O}(h^2). \quad (2.82)$$

Then the gravitational action takes the form ³

$$\mathcal{S}_{LGR} = - \frac{c^3}{16\pi G} \int d^4x \left(\partial^\nu h^{\alpha\beta} \partial_\nu h_{\alpha\beta} + \partial^\mu h \partial_\mu h - 2\partial_\mu h^{\alpha\mu} \partial_\rho h_\alpha^\rho - 2\partial^\alpha h_{\alpha\nu} \partial^\nu h \right), \quad (2.84)$$

where

$$\eta^{\mu\nu} \partial_\mu \partial_\nu \equiv \partial_\mu \partial^\mu. \quad (2.85)$$

In this limit, gravity can be explicitly expressed as a spin-2 field theory without non-renormalizable singularities arising from self-interaction [43]. This is called the linearized limit.

The free space Einstein equations resulting from the full action take the form

$$\begin{aligned} G_{\mu\nu} &= 0, \\ g^{\mu\nu} (R_{\mu\nu} - \frac{1}{2} g_{\mu\nu} R) &= 0, \\ R = 2R &\implies R = 0. \end{aligned}$$

³Note that including the terms to order $\mathcal{O}(h^2)$ in the Riemann tensor itself does not change the form of the final result for the action, though it does lead to additive contributions which reduce the size of the overall numerical prefactor [165], such that

$$\frac{c^3}{16\pi G} \rightarrow \frac{c^3}{64\pi G}. \quad (2.83)$$

Consistent with Eq. (2.84), in the linearized limit the Einstein equations become

$$R_{\mu\nu} = \frac{1}{2}(\partial_\mu\partial_\lambda h^\lambda{}_\nu - \partial^\lambda\partial_\lambda h^\mu{}_\nu - \partial_\mu\partial_\nu h^\lambda{}_\lambda - \partial^\nu\partial_\lambda h^\lambda{}_\mu) = 0. \quad (2.86)$$

As in the case of electromagnetism, it is clear in this form that with appropriate conditions on $h^\lambda{}_\nu$ the Einstein equations reduce to a wave equation. We will next justify the grounds on which such conditions apply and arrive from that to the explicit form for self-propagating gravitational wave solutions.

2.3.2 Gravity as a gauge theory

Despite the fact that the metric tensor of General Relativity, and particularly Linearized Gravity, has many components, it turns out that for propagations in vacuum only two are dynamically relevant. I review here first the counting argument leading to this for a general non-linearized metric, further discussed in e.g. [139, 158, 166]. I then review how in the case of Linearized Gravity, e.g. [165], these two are the transverse components of the tensor wave, and the remaining degrees of freedom can be gauged away from the symmetry of General Relativity, namely, the symmetry under coordinate transformations.

According to special relativity, physical law is invariant under the Poincaré group, such that the symmetry group under which all laws and physical observables remains invariant is the set of Lorentz transformations (rotations and boosts) between the frames of inertial observers.

General relativity has a much larger symmetry group: that of all possible coordinate transformations. This follows from the Strong Equivalence Principle, which is the statement that the laws of physics are the same in all arbitrary coordinate systems. This can be interpreted as symmetry under the following transformation

$$x^\mu \rightarrow f(x^\mu), \quad (2.87)$$

The symmetry of general relativity under such arbitrary coordinate transformation results in the following tensor transformation properties

$$dx'^\mu = dx^\alpha \frac{\partial x^\mu}{\partial x^\alpha}, \quad (2.88a)$$

$$g'_{\mu\nu} = g_{\alpha\beta} \frac{\partial x^\alpha}{\partial x^\mu} \frac{\partial x^\beta}{\partial x^\nu}. \quad (2.88b)$$

Any rank- n object that transforms with the appropriate Jacobian is called a tensor in General Relativity. Notice that the transformation is trivial for scalars. Objects that do not transform this way are non-tensorial.

The selection of an appropriate coordinate system can be thought of as equivalent to fixing a gauge. It follows that therefore a gauge choice can be imposed by a conditions that do not transform under coordinate transformation, i.e. they are non-tensorial. A

canonical example of this in General Relativity is the Christoffel connection

$$\Gamma_{\mu\nu}^{\lambda} = \left(\frac{1}{2} g^{\lambda\sigma} (-g_{\mu\nu,\sigma} + g_{\sigma\mu,\nu} + g_{\nu\sigma,\mu}) \right), \quad (2.89)$$

which is an object that is invoked to define the covariant derivative of a tensor v_{ν} on a curved spacetime

$$\nabla_{\mu} v_{\nu} = \partial_{\mu} v_{\nu} + \Gamma_{\mu\nu}^{\lambda} v_{\lambda}. \quad (2.90)$$

Therefore, for a scalar

$$\nabla_{\mu} \phi = \partial_{\mu} \phi. \quad (2.91)$$

Returning to the problem of determining the number of dynamical degrees of freedom of the metric tensor, the simplest combination of non-tensorial object is the following

$$g^{\mu\nu} \Gamma_{\mu\nu}^{\lambda} = 0. \quad (2.92)$$

This gives four constraint equations, and the choice is referred to as the harmonic gauge. To see what this implies, consider the fully covariant d'Alembertian of a scalar quantity

$$\square\phi = g^{\mu\nu} \nabla_{\mu} \nabla_{\nu} \phi = g^{\mu\nu} (\partial_{\mu} \partial_{\nu} \phi - \Gamma_{\mu\nu}^{\lambda} \partial_{\lambda} \phi). \quad (2.93)$$

In harmonic gauge, the second term vanishes such that

$$\square\phi = g^{\mu\nu} \partial_{\mu} \partial_{\nu} \phi. \quad (2.94)$$

Note that the arbitrary coordinate transformation $x'^{\mu} \rightarrow f(x^{\mu})$ can be expanded to first order in small changes. This amounts to the effective gauge transformation

$$x'^{\mu} = x^{\mu} + \xi^{\mu}(x), \quad (2.95)$$

where $\xi^{\mu}(x)$ is assumed small. This has 4 components.

Since each coordinate component x^{α} is a scalar quantity, then the harmonic gauge condition can be reexpressed as the following condition on the coordinates

$$\square x^{\alpha} = g^{\mu\nu} \partial_{\mu} \partial_{\nu} x^{\alpha} = g^{\mu\nu} \partial_{\mu} \delta_{\nu}^{\alpha} = 0. \quad (2.96)$$

We can see there is a residual gauge freedom for the form of ξ after choosing harmonic gauge. One choice that is consistent with harmonic gauge to fix these degrees of freedom is

$$\square \xi^{\alpha} = 0. \quad (2.97)$$

This gives a further 4 constraints, such that in total there remain

$$10 - 4 - 4 = 2 \quad (2.98)$$

independent field modes. In Chapter 4, we will see that this matches the number of independent Goldstone modes available to a quantum spin nematic.

Next, we would like to explicitly identify which two components of the metric tensor correspond to dynamical self-propagating modes, for which we can focus on the weak field limit, namely, in vacuum and with the linearized field equations [Eq. (2.86)].

Introduce the conventional notation

$$\partial_\nu \xi_\mu \equiv \xi_{\mu,\nu} . \quad (2.99)$$

and plugging the linearized metric [Eq. (2.71b)] into Eq. (2.88b), and using

$$\frac{\partial x'^\mu}{\partial x^\alpha} = \delta_\alpha^\mu - \xi^\mu_{,\alpha} , \quad (2.100)$$

the gauge transformation in linearized gravity takes the form

$$h'_{\mu\nu} = h_{\mu\nu} - \xi_{\mu,\nu} - \xi_{\nu,\mu} . \quad (2.101)$$

This incidentally defines the Lie derivative along ξ_μ (using the metricity property). Therefore, one can interpret the Lie derivative as the change in functional form of the metric (or other tensorial object) under a linearized coordinate transformation [139].

In linearized theory, harmonic gauge means

$$\eta^{\mu\nu} \Gamma_{\mu\nu}^\lambda = 0 , \quad (2.102)$$

Explicitly, using $\eta_{\mu\nu,\alpha} = 0$ and discarding all terms to $\mathcal{O}(h^2)$ we find

$$\eta^{\mu\nu} \left(\frac{1}{2} g^{\lambda\sigma} (-g_{\mu\nu,\sigma} + g_{\sigma\mu,\nu} + g_{\nu\sigma,\mu}) \right) = 0 , \quad (2.103a)$$

$$\eta^{\mu\nu} \left(\frac{1}{2} \eta^{\lambda\sigma} (-h_{\mu\nu,\sigma} + h_{\sigma\mu,\nu} + h_{\nu\sigma,\mu}) \right) = 0 , \quad (2.103b)$$

$$\frac{1}{2} \eta^{\mu\nu} (-h_{\mu\nu,}^\lambda + h^\lambda_{\mu,\nu} + h_\nu^\lambda_{,\mu}) = 0 , \quad (2.103c)$$

$$\frac{1}{2} (-h^\nu_{\nu,}^\lambda + h^{\lambda\nu}_{,\nu} + h^{\nu\lambda}_{,\nu}) = 0 , \quad (2.103d)$$

$$h^{\lambda\nu}_{,\nu} - \frac{1}{2} h^\nu_{\nu,}^\lambda = 0 , \quad (2.103e)$$

$$h^\nu_{\lambda,\nu} - \frac{1}{2} h^\nu_{\nu,\lambda} = 0 , \quad (2.103f)$$

$$\partial_\nu (h^\nu_{\lambda} - \frac{1}{2} h^\alpha_{\alpha} \delta^\nu_{\lambda}) = 0 , \quad (2.103g)$$

We can use this to motivate the form of the metric perturbation

$$\bar{h}^\mu_{\nu} = h^\mu_{\nu} - \frac{1}{2} h^\alpha_{\alpha} \delta^\mu_{\nu} , \quad (2.104)$$

which represents the **transverse, trace-reversed** form of the harmonic gauge. The origin of the name stems from the properties

1. Trace-reversed nature of $\bar{h}^\lambda{}_\nu$ is explicitly seen by contracting with $\eta_{\mu\lambda}$ and considering $\bar{h}_{\mu\nu} = h_{\mu\nu} - \frac{1}{2}h\eta_{\mu\nu}$ such that $\bar{h} = -h$.
2. The condition $\partial_\nu(h^\nu{}_\lambda - \frac{1}{2}h^\alpha{}_\alpha\delta^\nu{}_\lambda) = 0$ in linear theory can be Fourier transformed to give $\partial_\nu \leftrightarrow ik_\nu$. The condition $k^\nu\bar{h}^\alpha{}_\nu = 0$ implies that the field distortions are perpendicular to the direction of the momentum four-vector, ie. they are **transverse**.

After imposing, harmonic gauge, there is still a residual freedom which can be used to impose a further four constraints. One of these constraints can be used to remove the trace, such that $h_{\mu\nu}$ and $\bar{h}_{\mu\nu}$ are equivalent. It is then conventional to make the following set of choices complementary with harmonic gauge

$$h^\mu{}_\mu = 0, \text{ [traceless]} \quad (2.105a)$$

$$h_{0\mu} = 0, \text{ [no scalar or vector components]} \quad (2.105b)$$

$$\partial^n h_{nm} = 0, \text{ [no longitudinal dynamics]}. \quad (2.105c)$$

This explicit form is critical for the gravitational wave analogue we will explore in Chapter 4, based on the Goldstone modes of a spin nematic.

2.3.3 An intuitive look at gauge fixing linearized gravity

Here I present an alternative, and I hope intuitive, way to arrive at the reason for the transverse nature of gravitational waves.

Suppose we attempt a gauge transformation that is meant to “undo” the presence of propagating waves in $h_{\mu\nu}$, by assuming plane wave form for the gauge degrees of freedom

$$\xi^\mu(x) = \sum_k c_\mu(k)e^{ik^\rho x_\rho}, \quad (2.106)$$

where the c_μ are the Fourier transformed gauge degrees of freedom. The gauge transformation then alters the metric as follows

$$h'_{\mu\nu}(x) = h_{\mu\nu}(x) + \partial_\mu\xi_\nu + \partial_\nu\xi_\mu, \quad (2.107)$$

$$\implies h'_{\mu\nu}(k) = h_{\mu\nu}(k) + k_\mu c_\nu + k_\nu c_\mu. \quad (2.108)$$

We see explicitly in energy/frequency space that

$$h'_{00} = h_{00} + 2k_0 c_0, \quad (2.109a)$$

$$h'_{0n} = h_{0n} + k_0 c_n + k_n c_0, \quad (2.109b)$$

$$h'_{mn} = h_{mn} + k_m c_n + k_n c_m. \quad (2.109c)$$

A convenient gauge choice can then be seen to be one that minimizes all non-trivial components for a given wave-vector k^μ . Specifically from Eq. (2.109a-2.109c), we observe that whenever the gauge terms vanish, then the corresponding component of $h_{\mu\nu}$ cannot be trivialized.

Consider then the cases where the gauge terms make a non-trivial contribution to Eq. (2.109a-2.109c) for a given k^μ , considering all 16 component equations independently. Since $k_0 \neq 0$ for any wave (which must carry energy), we can always choose a frame/gauge such that $h_{00} = 0$, by fixing the coefficients c_0 .

Without loss of generality, let us assume that the wave propagates along a direction k_i . We can see that the components h_{0i} and h_{ii} can be chosen to be vanishing also by fixing c_i .

Since components of k_j for $j \neq i$ transverse to the direction of propagation vanish these do not provide any further constraint on the form of $h_{\mu\nu}$, and generically the components $h_{jk} \neq 0$ for $j, k \neq i$.

This leaves

$$16 - 1 - 6 - 5 = 4 \quad (2.110)$$

non-trivial components using the available constraints from setting the value for the c^μ . Therefore, not all components can be made trivial and one cannot gauge away the gravitational waves.

Of the 4 remaining non-trivial components, independence of one component is lost due to symmetry of the metric, and independence of another is lost to require tracelessness of the perturbation $h_{\mu\nu}$. This leaves two independent dynamical degrees of freedom which describe gravitational waves.

We therefore arrive at the conditions Eq. (2.105). Under these conditions, the action for linearized gravity on the Minkowski background takes the form

$$\mathcal{S}_{\text{LGR}} = -\frac{c^3}{16\pi G} \int dx^4 \eta_{\mu\nu} \left[\partial^\mu h^{\alpha\beta} \partial^\mu h_{\alpha\beta} \right], \quad (2.111)$$

for which the equations of motion become

$$R_{\mu\nu} = -\frac{1}{2} \square h_{\mu\nu} = 0, \quad (2.112)$$

where since we only keep terms to $\mathcal{O}(h)$, the d'Alembertian is Minkowski, i.e.

$$\square = \eta^{\mu\nu} \nabla_\mu \nabla_\nu. \quad (2.113)$$

In conclusion, we recover the conditions of the previous Section, which make explicit that the Einstein equations reduce to the wave equation, whose solutions in term are the transverse gravitational waves that will be explicitly described in the next Section.

2.3.4 Gravitational waves in Linearized Gravity

In this Section, I review the canonical form for gravitational waves in Linearized Gravity, using conventions established in e.g. [158, 165].

The real valued solutions to Eq.(2.112) have the form

$$h_{\mu\nu}(t, x) = \sum_k \epsilon_{\mu\nu}(k) e^{ik^\alpha x_\alpha} + c.c., \quad (2.114)$$

where $\epsilon_{\mu\nu}$ is the polarization tensor. To be a valid solution of the wave equation

$$\square h_{\mu\nu} = 0 , \quad (2.115)$$

it must hold that $k^2 = 0$, and therefore the available modes are linearly dispersing

$$k_0 = \pm |\mathbf{k}| . \quad (2.116)$$

To find the physical degrees of freedom, conventionally one chooses harmonic gauge, ie

$$k^\nu \tilde{h}^\alpha{}_\nu = k^\nu \tilde{h}_{\mu\nu} = 0 . \quad (2.117)$$

Explicitly,

$$k^\nu \epsilon_{\mu\nu} - \frac{1}{2} k^\nu \eta_{\mu\nu} \epsilon^\alpha{}_\alpha = k^\nu \epsilon_{\mu\nu} - \frac{1}{2} k_\mu \epsilon^\alpha{}_\alpha = 0 . \quad (2.118)$$

Since we also apply the condition

$$\square \xi_\nu = 0 , \quad (2.119)$$

the degrees of freedom ξ will also be solutions of the wave equation, such that

$$\xi_\nu = \sum_k c_\nu(k) e^{ikx} . \quad (2.120)$$

Then the polarization tensor will transform in harmonic gauge as

$$\epsilon'_{\mu\nu} = \epsilon_{\mu\nu} - \xi_{\mu,\nu} - \xi_{\nu,\mu} = \epsilon_{\mu\nu} - k_\mu c_\nu - k_\nu c_\mu . \quad (2.121)$$

The explicit form of the polarization tensor—and importantly its surviving components—can now be determined. Making the choice of z as the propagation axis, we can write in units $c = 1$

$$k^\nu = (k, 0, 0, k) , \quad (2.122a)$$

$$k_\mu = (-k, 0, 0, k) . \quad (2.122b)$$

From the components of Eq.(2.118), we find

$$\mu = 0 : k(\epsilon_{00} + \epsilon_{30}) = -\frac{1}{2}k(-\epsilon_{00} + \epsilon_{11} + \epsilon_{22} + \epsilon_{33}) , \quad (2.123a)$$

$$\mu = 1 : k(\epsilon_{01} + \epsilon_{31}) = 0 , \quad (2.123b)$$

$$\mu = 2 : k(\epsilon_{02} + \epsilon_{32}) = 0 , \quad (2.123c)$$

$$\mu = 3 : k(\epsilon_{03} + \epsilon_{33}) = \frac{1}{2}k(-\epsilon_{00} + \epsilon_{11} + \epsilon_{22} + \epsilon_{33}) , \quad (2.123d)$$

which sets 4 conditions on the ϵ_{0i} and ϵ_{22} components of the polarization tensor

$$\epsilon_{01} = -\epsilon_{31} , \quad (2.124a)$$

$$\epsilon_{02} = -\epsilon_{32} , \quad (2.124b)$$

$$\epsilon_{03} = \epsilon_{30} = -\frac{1}{2}(\epsilon_{00} + \epsilon_{33}) , \quad (2.124c)$$

$$\epsilon_{22} = -\epsilon_{11} . \quad (2.124d)$$

In addition, the transformation property of the polarization tensor Eq.(2.118) leads to

$$\boxed{\epsilon'_{00} = \epsilon_{00} - 2kc_0} \quad (2.125a)$$

$$\epsilon'_{0i} = \epsilon_{0i} - kc_i , \quad (2.125b)$$

$$\epsilon'_{11} = \epsilon_{11} + 0 + 0 , \quad (2.125c)$$

$$\epsilon'_{12} = \epsilon_{12} + 0 + 0 , \quad (2.125d)$$

$$\boxed{\epsilon'_{13} = \epsilon_{13} - kc_1} \quad (2.125e)$$

$$\epsilon'_{22} = \epsilon_{22} + 0 + 0 , \quad (2.125f)$$

$$\boxed{\epsilon'_{23} = \epsilon_{23} + kc_2} \quad (2.125g)$$

$$\boxed{\epsilon'_{33} = \epsilon_{33} + kc_3} \quad (2.125h)$$

Choosing the c 's such that the boxed components defined in Eqs. (2.125a, 2.125e, 2.125g, 2.125h), vanish in the original, unprimed frame gives four more independent constraints. Note that Eq. (2.125b) describes the transformation of components which are already gauged away at this point. However, if one works first from the transformation property of the polarization tensor prior to applying any other gauge condition, then this set of equations is important to consider, and implies that elements that mixing in temporal components can always be gauged away. Collecting the non-vanishing results

$$\epsilon_{\mu\nu} = \begin{pmatrix} 0 & 0 & 0 & 0 \\ 0 & \epsilon_{11} & \epsilon_{12} & 0 \\ 0 & \epsilon_{21} & \epsilon_{22} & 0 \\ 0 & 0 & 0 & 0 \end{pmatrix} , \quad (2.126)$$

where explicitly the gauge conditions Eq. (2.105) lead to

$$\text{Tr}(\epsilon) = \epsilon_{22} + \epsilon_{11} = 0 , \quad (2.127a)$$

$$\epsilon_{12} = \epsilon_{21} . \quad (2.127b)$$

We can define the two independent polarization modes by

$$\epsilon_+ = \epsilon_{11} = -\epsilon_{22} , \quad (2.128a)$$

$$\epsilon_x = \epsilon_{12} = \epsilon_{21} . \quad (2.128b)$$

Specifically, without loss of generality, we can consider the case of a gravitational wave propagating along z , for which the classical field $h_{\mu\nu}$ can take a linear superposition of

the two dynamically independent forms

$$\mathbf{h}^+ = e^{ik^\mu x_\mu} \epsilon_+ \begin{pmatrix} 0 & 0 & 0 & 0 \\ 0 & 1 & 0 & 0 \\ 0 & 0 & -1 & 0 \\ 0 & 0 & 0 & 0 \end{pmatrix}, \quad (2.129a)$$

$$\mathbf{h}^\times = e^{ik^\mu x_\mu} \epsilon_x \begin{pmatrix} 0 & 0 & 0 & 0 \\ 0 & 0 & 1 & 0 \\ 0 & 1 & 0 & 0 \\ 0 & 0 & 0 & 0 \end{pmatrix}. \quad (2.129b)$$

We here anticipate for the reader that the mode counting argument presented here will be echoed by a similar set of physical restrictions on the modes of the ferroquadrupolar ordered magnet (see Chapter 3), which in turn leads to the same number of relativistically dispersing excitations in the low-energy limit.

In conclusion, we see explicitly that the symmetric polarization tensor is traceless and has two surviving transverse degrees of freedom.

Finally, let's generalize the degree of freedom counting argument to arbitrary dimension: as a symmetric tensor $g_{\mu\nu}$ and also $\epsilon_{\mu\nu}$ have

$$\left(d + \frac{d^2 - d}{2}\right) = \frac{d(d+1)}{2} \quad (2.130)$$

independent components, and d components will be determined by the choice of gauge, followed by a further d to fix the residual gauge freedom. Then we find

$$\frac{d(d+1)}{2} - d - d = \frac{d(d-3)}{2}, \quad (2.131)$$

such that there are no degrees of freedom left for freely propagating modes in a (2+1)D theory of gravitation. Therefore generically, lower dimensional theories of GR have no physical excitations, while the (3+1)D Universe has two degrees of freedom available for gravitational waves. This is also a critical point that we will allude to in discussion of the connection with excitations in spin nematics in Chapter 4.

2.3.5 Quantized spin-2 excitations

The treatments above describe gravitational waves as excitations of a classical field (the metric) in the canonical approach, [139, 158, 165, 166]. A next natural step is to quantize the excitations of the gravitational wave, which leads to a consistent theory in the linearized limit of gravity at least [43]. We assume from the harmonic form of the equations of motion that we can express the field with the Fourier decomposition

$$h_{\mu\nu}(x, t) = \sum_{\sigma=+, \times} \int d^3k \frac{1}{\sqrt{\omega(\mathbf{k})}} \left[\epsilon_{\mu\nu}^\sigma a_\sigma^\dagger(\mathbf{k}) e^{ik_\rho x^\rho} + (\epsilon_{\mu\nu}^\sigma)^* a_\sigma(\mathbf{k}) e^{-ik_\rho x^\rho} \right], \quad (2.132)$$

where $\epsilon_{\mu\nu}^\sigma$ is a tensor encoding information about polarization, and $a_\sigma(\mathbf{k})$ satisfies

$$[a_\sigma(\mathbf{k}), a_{\sigma'}^\dagger(\mathbf{k}')] = \delta_{\sigma\sigma'} \delta(\mathbf{k} - \mathbf{k}') . \quad (2.133)$$

For a wave with linear polarization, propagating along the z -direction, $\epsilon_{\mu\nu}^\sigma$ take the specific form

$$\epsilon^+ = \frac{1}{\sqrt{2}} \begin{pmatrix} 0 & 0 & 0 & 0 \\ 0 & 1 & 0 & 0 \\ 0 & 0 & -1 & 0 \\ 0 & 0 & 0 & 0 \end{pmatrix}, \quad \epsilon^\times = \frac{1}{\sqrt{2}} \begin{pmatrix} 0 & 0 & 0 & 0 \\ 0 & 0 & 1 & 0 \\ 0 & 1 & 0 & 0 \\ 0 & 0 & 0 & 0 \end{pmatrix}. \quad (2.134)$$

Next we will see that the graviton consistent with linearized gravity corresponds to a spin-2 particle. Recall that spin is the property which defines how the state of a particle transforms under action of the rotation subgroup $SO(1, 3)$ of the Lorentz group, with generators J_i defined in Eq. (2.35). For an arbitrary state ϕ , under rotation through θ

$$R_i[\theta]\phi = e^{i\theta J_i} \phi . \quad (2.135)$$

For a spin- γ particle with internal state described by ϵ , the internal state picks up a phase

$$R_z[\theta]\epsilon = e^{i2\theta} \epsilon . \quad (2.136)$$

If $\gamma = 1$, the state returns to itself for every rotation through 2π . However, if $\gamma = 2$, the state returns to itself for every rotation through π .

To verify this transformation property of the graviton and determine its helicity, consider

$$\epsilon'_{\mu\nu} = R_z^T[\theta]\epsilon^+ R_z[\theta] + R_z^T[\theta]\epsilon^\times R_z[\theta], \quad (2.137)$$

where explicitly

$$R_z[\theta] = \begin{pmatrix} 1 & 0 & 0 & 0 \\ 0 & \cos \theta & -\sin \theta & 0 \\ 0 & \sin \theta & \cos \theta & 0 \\ 0 & 0 & 0 & 1 \end{pmatrix}. \quad (2.138)$$

We can then define two polarizations

$$\epsilon_R = \epsilon_+ - i\epsilon_x, \quad (2.139a)$$

$$\epsilon_L = \epsilon_+ + i\epsilon_x. \quad (2.139b)$$

such that

$$\epsilon_+ = \frac{1}{2}(\epsilon_R + \epsilon_L), \quad (2.140a)$$

$$\epsilon_x = \frac{i}{2}(\epsilon_R - \epsilon_L), \quad (2.140b)$$

the result of the transformation reveals that

$$\epsilon'_R = e^{2i\theta} \epsilon_R , \quad (2.141a)$$

$$\epsilon'_L = e^{-2i\theta} \epsilon_L . \quad (2.141b)$$

Rotations through π therefore return the particle to the same state, and therefore the graviton must be a spin-2 particle.

2.4 Chapter summary

In concluding this Chapter, we have discussed Goldstone modes, with examples from the context of symmetry breaking magnetic phases. We are now equipped to identify analogues of photons as massless spin-1 Bosons and of gravitons as massless spin-2 Bosons. This now sets the stage for Chapter 3, where I will review and present magnetic analogues of light, and Chapter 4, where I will present a novel one-to-one magnetic analogue of gravitational waves.

Chapter 3

Analogues of electromagnetism in magnetic phases

“As simple as possible, as complex as necessary.” -paraphrased, attribution to Albert Einstein

Quantum field theories are the most effective tool yet developed for the description of the vacuum of the Universe, and we learned in the last Chapter how they can be used to describe the excitations of electromagnetism and gravity.

In this Chapter we will be concerned with analogues of electromagnetism arising in magnetism, and we will see how effective low-energy field theories of magnetic insulators play a key role in making such identifications. I will first review the known toy example of the XY ferromagnet, which reproduces a (2+1)D theory of electromagnetism.

A discussion of magnetic analogues of electromagnetism would not be complete without mention of the emergent electromagnetism in spin ice. For completeness this will also be briefly reviewed in this Chapter.

I will finally turn attention to the Heisenberg antiferromagnet, and make explicit a connection between its spin wave excitations and photons, a fact that has been often alluded to in the folklore of magnetism, but to the best of my knowledge, never made explicit. In this Chapter, I make this correspondence concrete and present a dictionary for explicitly connecting the degrees of freedom.

The Heisenberg model describes the exchange interaction between spins in a magnetic solid. As we learned in the last Chapter, there are at least two ordered phases of the Heisenberg model which are distinguished one from the other on the basis of whether the order breaks time-reversal symmetry or not. The effective field theories corresponding to these two cases are respectively not Lorentz invariant or they are.

In this Chapter, I will motivate a Lorentz covariant form of the effective Lagrangian, first from semiclassical arguments. Then, I introduce the reader to $SU(2)$ spin coherent states, and how to use this basis to derive the quantum mechanical low-energy field theory for the Heisenberg antiferromagnet, whose action is that of a non-linear sigma model. From the form of this field theory and its excitations, it will become explicit that the Goldstone modes are in one-to-one correspondence with photons in electromagnetism.

I conclude the Chapter with brief comments on where these photon analogues could be observed in experiment.

3.1 The XY model as a toy model for electromagnetism on a lattice

Analogies to electromagnetism have a long history in magnetism. In this Section, I will review the reduced dimensional electromagnetism analogue that arises in the (2+1)D XY ferromagnet [45, 48], which possesses minimally a U(1) symmetry, and is known possess analogue charges corresponding to the topological point defects, namely, XY vortices. I will also briefly provide a visual intuition for why vector field theories are necessarily repulsive for like charges and attractive for charges of opposite sign.

Recall the definition established in Eq. (1.36) for classical $O(2)$ spins, or rotors, repeated below

$$\mathbf{S} = S \begin{pmatrix} \cos \theta \\ \sin \theta \end{pmatrix}, \quad (3.1)$$

using which the XY model can be expressed

$$\mathcal{H} = J \sum_{\langle ij \rangle} \mathbf{S}_i \cdot \mathbf{S}_j = Js^2 \sum_{\langle ij \rangle} \cos(\theta_i - \theta_j). \quad (3.2)$$

This model has a ferromagnetic ground state when $J > 0$. Due to the spin length constraint, the state space is spanned by the U(1) generator and each spin has only one dynamical degree of freedom θ . I next briefly describe why this dynamical degree of freedom corresponds to a scalar Goldstone Boson.

3.1.1 Goldstone modes of the $O(2)$ XY ferromagnet

Here I describe the number of Goldstone modes present in the XY ferromagnet. For the ferromagnetically ordered states of the $O(2)$ XY model, there is only one broken rotational symmetry. This is broken by the orientation of the spins in the ground state, for which a general order parameter is a vector of the form

$$\mathbf{S}_0 = \begin{pmatrix} S_x \\ S_y \end{pmatrix}. \quad (3.3)$$

Notice that the spin degrees of freedom in this case are planar rotors that do not share the gyroscopic nature of $O(3)$ spins. They are not axial vectors, and as such, do not break time reversal symmetry. In this case, Goldstone's theorem is minimally satisfied by the existence of a single linearly dispersing Goldstone mode, which must have scalar character since there is only one leftover degree of freedom in the ground state for each spin. In Chapter 5, I reproduce this result in simulation, cf. Fig 5.5a.

3.1.2 Hydrodynamic model of planar rotors: a sigma model for the XY ferromagnet

I now review the hydrodynamic limit of the XY ferromagnet, and show how the lattice description of the XY ferromagnet is described in the low-energy limit by a continuum field theory which takes the form of a Gaussian action known as a sigma model.

For the purpose of this discussion, we can without loss of generality set $s^2 = 1$. We again consider the long wavelength limit, for which the single degree of freedom θ_i per rotor is assumed to vary smoothly over small scales and can be cast into a continuous field $\theta(\vec{r})$. In this limit, the potential energy associated with a field configuration becomes

$$U = \int \frac{d^2r}{a^2} J \cos(a \nabla \theta(\vec{r})) , \quad (3.4a)$$

$$\approx \int d^2r \frac{J}{a} \left(1 - \frac{1}{2} \nabla \theta^2\right) . \quad (3.4b)$$

We can phenomenologically introduce a term capturing the energy stored in the motion of the field degrees of freedom. Defining a notion of effective mass to be proportional to the spin susceptibility χ , the effective classical kinetic energy contribution from the entire field will take the form

$$K = \int \frac{d^2r}{a^2} \frac{\chi \dot{\theta}^2}{2} , \quad (3.5)$$

The Lagrangian describing the system up to constants and terms of $\mathcal{O}(3)$ is then

$$\mathcal{L} = K - U = \int \frac{d^2r}{2} \left[\chi \dot{\theta}^2 - \rho \nabla \theta^2 \right] , \quad (3.6)$$

which has linearly dispersing dynamics described by the wave equation

$$\chi \partial_t^2 \theta = \rho \partial_i^2 \theta. \quad (3.7)$$

We next remind the reader explicitly that the low-energy action of the XY model is equivalent to that of (2+1)D electromagnetism.

3.1.3 A mapping to (2+1)D electromagnetism, its photon and charges

I now explain how the XY ferromagnet is connected to (2+1)D electromagnetism. To make the connection, there are two key ingredients we need from (2+1)D electromagnetism beforehand. First, we must describe the field theory and the freely propagating field modes (i.e. the photon), and second, the allowed charges. Both of these characteristics will be shown to have analogues in the XY ferromagnet.

First, consider that (2+1)D electromagnetism has a structural peculiarity, namely, in two dimensions three simultaneously perpendicular vectors in the ordinary sense cannot exist. As a consequence, the structure of electric and magnetic fields cannot

be on the same footing while also allowing a propagating mode. This necessitates a breaking of the symmetry between E and B fields observed in (3+1)D electromagnetism. Before deciding on a convention that breaks this symmetry, let us introduce the conventional gauge potential \vec{A} and a dual potential \vec{h}^1 , such that the electric and magnetic fields could be expressed in one of the following ways

$$\vec{E} = -\partial_t \vec{A}, \quad \text{or} \quad E = \nabla_{\perp} \cdot \vec{h}, \quad (3.8)$$

$$B = \nabla_{\perp} \cdot \vec{A}, \quad \text{or} \quad \vec{B} = -\partial_t \vec{h}, \quad (3.9)$$

where

$$\nabla_{\perp} = (\partial_y, -\partial_x), \quad (3.10)$$

is a 2D equivalent of curl², and

$$\nabla = (\partial_x, \partial_y). \quad (3.12)$$

The underlying symmetry between these two formulations is apparent, but each represents an exclusive choice. The option on the left is the conventional choice, for which the dual potential field h is chosen to have a scalar nature such that

$$\vec{E} = -\partial_t \vec{A} = \nabla_{\perp} h, \quad (3.13)$$

$$B = \nabla_{\perp} \cdot \vec{A} = -\partial_t h. \quad (3.14)$$

In this conventional choice, the EM physics in the XY ferromagnet can be mapped onto the dual gauge field

$$\theta(\vec{r}) \iff h(\vec{r}), \quad (3.15)$$

such that

$$\partial_t \theta \equiv B = \partial_x A_y - \partial_y A_x, \quad (3.16)$$

$$-\partial_x \theta \equiv E_y = -\partial_t A_x, \quad (3.17)$$

$$\partial_y \theta \equiv E_x = -\partial_t A_y, \quad (3.18)$$

¹Both of these gauge fields have only one independent degree of freedom, but can be cast in vector form for conventional convenience. Depending on which formulation we work in, it is conventional to gauge fix the primary gauge field and treat the second gauge field as a scalar.

²I am using here the notation $\vec{a}_{\perp} = (a_y, -a_x)$ for a 2D vector defined by the property

$$\vec{a} \cdot \vec{a}_{\perp} = 0, \quad (3.11)$$

such that

1. $(\vec{a}_{\perp})_{\perp} = -\vec{a}$,
2. $\vec{a}_{\perp} \cdot \vec{a}_{\perp} = \vec{a} \cdot \vec{a}$,
3. $(\vec{a} \cdot \vec{b})_{\perp} = \vec{a}_{\perp} \cdot \vec{b}_{\perp}$.

(2+1)D EM formulation	v1	v2
Vector and scalar fields	\vec{E}, B	\vec{B}, E
E and B fields	$-\partial_t \vec{A} = \vec{E}, -\partial_t h_x = B$ $\nabla_{\perp} \cdot \vec{A} = B, \nabla_{\perp} h_x = \vec{E}$	$\partial_t \vec{h} = \vec{B}, \partial_t A_x = E$ $\nabla_{\perp} A_x = \vec{B}, \nabla_{\perp} \cdot \vec{h} = E,$
Gauss' Law	$\oint \vec{d}r \cdot \vec{E} = 2\pi Q_e$	$\oint \vec{d}r \cdot \vec{B} = 2\pi Q_m$
Gauge potential	\vec{A}	Gauge fixed to scalar e.g. A_x
Dual gauge potential	Gauge fixed to scalar e.g. h_x	\vec{h}
Maxwell's equation	$\partial_t B - \partial_x E_y + \partial_y E_x = 0$	$\partial_t E - \partial_x B_y + \partial_y B_x = 0$

Table 3.1: Summary of the two dual formulations of electromagnetism in (2+1)D.

for which the fields obey the 2D expression of Maxwell's equations

$$\partial_t B - \partial_x E_y + \partial_y E_x = 0. \quad (3.19)$$

In this formulation, the electric field has vector character, and the electric field alone will possess field monopoles, measured by the Gauss law

$$\oint \vec{d}r \cdot \vec{E} = 2\pi Q_e. \quad (3.20)$$

A more natural way to extract the EM physics of the XY ferromagnet is to map the rotor degree of freedom θ directly onto the physical degree of freedom of the gauge field \vec{A} . For this purpose, we work with the remaining degree of freedom A of a gauge fixed \vec{A} , leading to

$$\vec{E} = \nabla_{\perp} A = -\partial_t \vec{h}, \quad (3.21)$$

$$B = -\partial_t A = \nabla_{\perp} \cdot \vec{A}. \quad (3.22)$$

Here note that it is the magnetic field that acquires vector character, and therefore the charges of the gauge theory are magnetic monopoles, described by the Gauss law

$$\oint \vec{d}r \cdot \vec{B} = 2\pi Q_m. \quad (3.23)$$

The reason that either of these approaches is ultimately well-defined is due to the fact that there is no equivalent of precessional dynamics in (2+1)D, and therefore there is no restriction on the existence of either kind of monopole, cf. Appendix C.

In summary, there is only one independent physical degree of freedom present in either gauge field and its dual, which maps onto the relevant degree of freedom of the XY model. The two approaches to this mapping are summarized in Table 3.1.

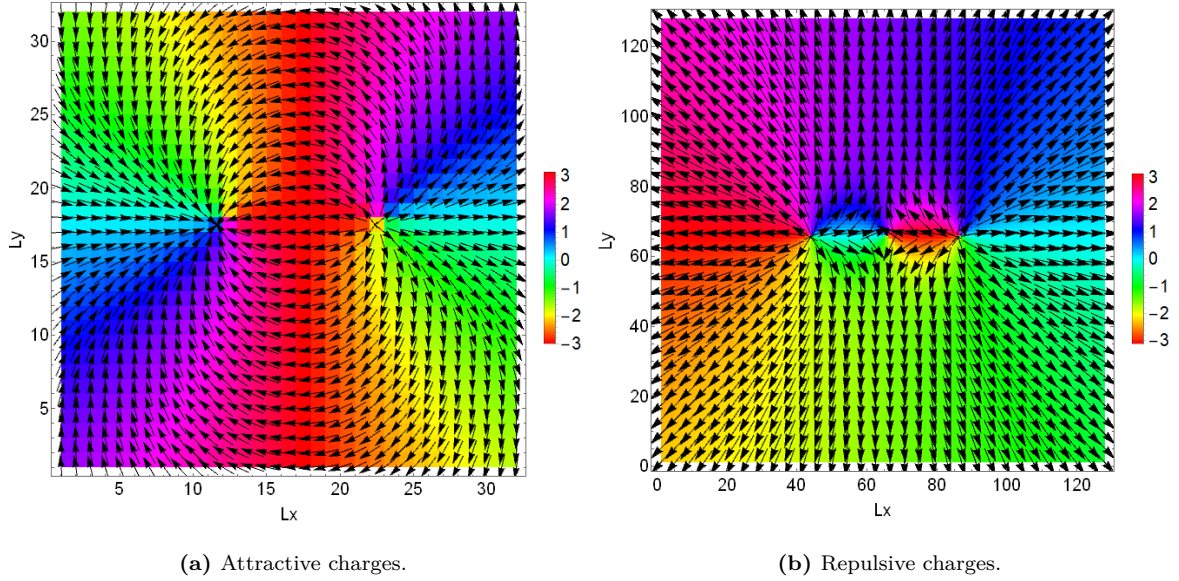


Figure 3.1: Spin configurations in an XY magnet, showing the connection with electric charges. Colour bars represent the angle $\theta \in [-\pi, \pi]$ associated to the spins. **(a)** Charges with opposite winding number generate a field configuration whose energy can be minimized by bringing the charges closer together. **(b)** Charges with both positive winding number generate a field configuration whose energy can be minimized by moving charges further apart.

Homotopy of the XY magnet: charges and Gauss' law

The XY ferromagnet possesses topologically stable point defects, corresponding to the homotopy group π_1 of the order parameter space $O(2)$. There are two distinct windings that can be made around this space, leading to two infinitely degenerate families of point charge with independent signatures of winding. In the context of electromagnetism, the charge and the field are related via the Gauss' law, Eq. (3.23). The analogous relation in the XY model relates each source to a distinct pattern of effective electric field.

The interactions between such point charges follow naturally from the Hamiltonian we started with, such that the system at low energies will endeavour to maximize the area of domains with parallel or nearly parallel spins.

This leads to effective attractive or repulsive interactions in the dynamics of the point defects of a vector field, which is consistent with the fact that a vector field theory must mediate repulsive interactions between similarly charged particles and attractive interactions between oppositely charged particles.

In summary, in this Section we have discussed the reduced dimensional analogue of electromagnetism which emerges in the XY model. Due to the reduced dimensional nature of the theory, it has an unusual formulation in terms of gauge fields, as summarized in Table. 3.1, with one scalar degree of freedom corresponding to the photon mode, equivalent to the magnon mode in the XY ferromagnet. The homotopy group of the XY order parameter space permits the existence of point defects which correspond to sources of the vector electric field.

In the next Section, I review the next analogue to have been developed in the magnetism context, namely that of spin ice to (3+1)D electromagnetism.

3.2 Emergent electromagnetism in spin ice

No discussion of electromagnetism analogues in magnets would be complete without reference to spin ice. I include here a short discussion for historical completeness and refer the interested reader to other excellent reviews on the subject, such as [52, 167].

Spin ice phases can be effectively modeled as a classical Ising antiferromagnet. Unlike Heisenberg magnets, whose collective behaviour is determined primarily by spin exchange interactions, spin ice arises from long-range dipolar interactions which induce an Ising anisotropy on spins.

On the pyrochlore lattice, spin ice exhibits a parallel with water ice through the ground state rules which apply to the degrees of freedom on each tetrahedron. In water ice, the pyrochlore lattice is built from oxygen atoms, which live at the centres of the tetrahedra of the lattice, and hydrogen atoms which form bonds bridging neighbouring oxygen atoms. There are four such bonds per oxygen, but they are not equivalent. The position of each hydrogen atom is either close to or farther from a given oxygen atom, such that the ground state manifold of water ice is comprised of all the states for which there are two hydrogen atoms close and two further away. This two-in two-out structure was first discussed by Bernal and Fowler [49] and receives the name Ice rules. For classical pyrochlore spin ice, the Ising spins live on the vertices of the lattice, and each tetrahedron exhibits an equivalent to the Ice rules in water ice, namely a two-in two-out configuration of Ising spins. This behaviour is captured by the divergence free condition on the effective field \mathbf{E} generated by the Ising spins

$$\nabla \cdot \mathbf{E} = 0 . \quad (3.24)$$

This is the classical spin ice equivalent of Gauss' law. The experimental signature of this in the equal-time structure factor is the appearance of pinch points, see Fig. 1.3b.

On the pyrochlore lattice, configurations satisfying the Ice rules form a highly-degenerate ground state manifold. The inclusion of the possibility of quantum tunneling between the states within this manifold, by allowing spin flips on entire hexagonal plaquettes, allows for description of quantum spin ice. Including these quantum fluctuations, the sharp pinch points become diffuse e.g. [56, 59].

The effective Hamiltonian

$$H_{\text{eff}} = (\nabla \cdot \mathbf{E})^2 , \quad (3.25)$$

combined with the dynamical term arising from quantum tunneling between different states obeying the ice rules, one arrives at an effective action equivalent to Maxwell's electromagnetism [55, 56]

$$\mathcal{S} = \int dt dx^3 \left((\mathbf{E})^2 - \frac{1}{c^2} (\mathbf{B})^2 \right) , \quad (3.26)$$

where the wave speed here implicitly encapsulates parameters arising from microscopic details of the model [56]

$$c = \sqrt{UK} a_0 \hbar^{-1} , \quad (3.27)$$

with U and K corresponding to the constants in the potential and kinetic terms of the model.

The quantum spin ice analogue is the most complete electromagnetism analogue which arises in the context of magnetism, and has been the focus of many works of fundamental interest [55, 56, 168], with particular attention drawn to the presence of magnetic monopoles [53, 54], and an effective fine structure constant [57]. The photons of quantum spin ice, have been inferred in $\text{Pr}_2\text{Hf}_2\text{O}_7$ [59] through the broadening of the pinch-point line shape indicative of quantum fluctuations, allowing estimation of the photon speed in this material, which is on the order of $3.6 \frac{m}{s}$.

Other features of emergent electrodynamics have been identified in candidate materials such as magnetic monopoles in $\text{Yb}_2\text{Ti}_2\text{O}_7$ [58], and several other dipole-octupolar quantum spin-ice candidate materials have also been verified, including $\text{Ce}_2\text{Zr}_2\text{O}_7$ [60, 61], $\text{Ce}_2\text{Hf}_2\text{O}_7$ [62] and $\text{Ce}_2\text{Sn}_2\text{O}_7$ [63].

This makes quantum spin ice a promising platform for electrodynamics analogues realizable in experiment. However, a strategy for generalization to higher-rank gauge theories distinct from Maxwell's $U(1)$ electromagnetism and which instead parallels gravity is yet unknown. For this reason, I next develop an explicit connection between the excitations of the Heisenberg antiferromagnet and photons which will serve as the template for an explicit connection between the Goldstone modes in spin nematics and gravitational waves, see Chapter 4.

3.3 Low energy excitations of the Heisenberg model and the collinear Néel Antiferromagnet

The purpose of this Section is to show that in the low-energy limit, excitations of the collinear Néel antiferromagnetic ground state are in one-to-one correspondence with the distinct photon polarizations of electromagnetism, where in both cases the excitations are massless spin-1 Bosons. I conclude this Section having developed the pieces needed for such a correspondence, and make explicit the connection between photons and collinear antiferromagnons, starting from a microscopic description of ordered magnetic phases.

3.3.1 Lorentz covariance from semiclassical treatment of the equations of motion

In the previous Chapter, we saw briefly in the case of the Heisenberg antiferromagnet that—contrary to the Heisenberg ferromagnet—there is no explicit time-reversal symmetry breaking across the unit cell, and therefore the Goldstone modes arising from the two broken rotational symmetries remain independent. Therefore, its Lagrangian description is expected to be Lorentz covariant.

A more explicit way to see why indeed the Lorentz covariance is preserved for the antiferromagnet, and not for the ferromagnet, is to examine how the presence or absence of a bipartite lattice affects the respective equations of motion.

The equations of motion for spins described by the Heisenberg Hamiltonian follow

from the corresponding Heisenberg equations of motion [86], as first conceived of and named by Dirac [78], namely

$$\partial_t S_i^\gamma = \frac{1}{i\hbar} [S_i^\gamma, \mathcal{H}] , \quad (3.28)$$

which for the Heisenberg Hamiltonian [cf.Eq. (1.16)]

$$\mathcal{H} = J \sum_{\langle ij \rangle} \mathbf{S}_i \cdot \mathbf{S}_j \quad (3.29)$$

takes the form

$$\partial_t S_i^\gamma = \frac{J}{\hbar} \sum_{\delta} S_i^\alpha S_{i+\delta}^\beta \epsilon_{\alpha\beta}^\gamma . \quad (3.30)$$

Let's consider first a semiclassical description of the ferromagnetic case, specifically assuming large s . Despite our interest here in the spin- $\frac{1}{2}$ Heisenberg model, this approximation nevertheless produces a valid result, which can be motivated by observing that the Hilbert space of the spin- $\frac{1}{2}$ degrees of freedom is spanned by the generators of SU(2). Since SU(2) is isomorphic to O(3), then we can semiclassically think of each spin degree of freedom as an O(3) vector with components S^γ . Choosing a basis where the ground state is ordered along the z -direction

$$\mathbf{S}_0 = S^\gamma , \quad (3.31)$$

the fluctuations about the ordered S^z moment are captured by

$$\phi_i^\gamma = S_i^\gamma - \delta_z^\gamma S_i^z , \quad (3.32)$$

where δ_z^γ is the Kronecker delta function. In the small fluctuation limit we assume

$$S^z \approx s . \quad (3.33)$$

Without loss of generality, we can consider the equation of motion on a chain where

$$\partial_t S_i^\gamma = \frac{J}{\hbar} (S_i^\alpha S_{i+1}^\beta - S_i^\beta S_{i+1}^\alpha + S_i^\alpha S_{i-1}^\beta - S_i^\beta S_{i-1}^\alpha) , \quad (3.34a)$$

$$\partial_t S_i^x \approx \frac{Js}{\hbar} (2S_i^y - S_{i+1}^y - S_{i-1}^y) , \quad (3.34b)$$

$$\partial_t S_i^y \approx -\frac{Js}{\hbar} (2S_i^x - S_{i+1}^x - S_{i-1}^x) , \quad (3.34c)$$

$$\partial_t S_i^z \approx 0 . \quad (3.34d)$$

At low energies, the wavelengths of fluctuations are much longer than the lattice constant, and we can treat the insulator in the continuum limit, also referred to as the hydrodynamic limit. Under this condition, the equations of motion become

$$\partial_t S_i^x \approx \frac{Js}{a^2 \hbar} \nabla^2 S^y , \quad (3.35a)$$

$$\partial_t S_i^y \approx -\frac{Js}{a^2 \hbar} \nabla^2 S^x, \quad (3.35b)$$

$$\partial_t S_i^z \approx 0, \quad (3.35c)$$

or in terms of the non-trivial components of the fluctuations ϕ^γ

$$\partial_t \phi_i^x \approx \frac{Js}{\hbar} \nabla^2 \phi^y, \quad (3.36a)$$

$$\partial_t \phi_i^y \approx -\frac{Js}{\hbar} \nabla^2 \phi^x, \quad (3.36b)$$

which are clearly coupled, and admit plane wave solutions with quadratic dispersion. The equations of motion are therefore not Lorentz covariant.

Next, let us consider the Heisenberg antiferromagnet, which will have Lorentz covariant equations of motion. Taking the Néel state to be the ground state, we can define two sublattices A and B for which

$$S_i^z \approx s \quad \text{for } i \in A, \quad (3.37a)$$

$$S_j^z \approx -s \quad \text{for } j \in B. \quad (3.37b)$$

Then for sublattice A

$$\partial_t S_i^x \approx \frac{Js}{\hbar} \left(-2S_i^y - S_{i+1}^y - S_{i-1}^y \right), \quad (3.38a)$$

$$\partial_t S_i^y \approx \frac{Js}{\hbar} \left(2S_i^x + S_{i+1}^x + S_{i-1}^x \right), \quad (3.38b)$$

$$\partial_t S_i^z \approx 0, \quad (3.38c)$$

while for sublattice B

$$\partial_t S_j^x \approx \frac{Js}{\hbar} \left(2S_j^y + S_{j+1}^y + S_{j-1}^y \right), \quad (3.39a)$$

$$\partial_t S_j^y \approx -\frac{Js}{\hbar} \left(-2S_j^x - S_{j+1}^x - S_{j-1}^x \right), \quad (3.39b)$$

$$\partial_t S_j^z \approx 0. \quad (3.39c)$$

Making use of the ladder operators Eq. (1.8) to condense the dynamical expressions, we find

$$\partial_t S_i^+ \approx \frac{iJs}{\hbar} \left(2S_i^+ + S_{i+1}^+ + S_{i-1}^+ \right), \quad (3.40a)$$

$$\partial_t S_j^+ \approx \frac{-iJs}{\hbar} \left(2S_j^+ + S_{j+1}^+ + S_{j-1}^+ \right), \quad (3.40b)$$

which can be recast for each sublattice by taking one more time derivative

$$\partial_t^2 S_i^+ \approx \left(\frac{Js}{\hbar} \right)^2 \left(-2S_i^+ + S_{i+2}^+ + S_{i-2}^+ \right), \quad (3.41a)$$

$$\partial_t^2 S_j^+ \approx \left(\frac{Js}{\hbar} \right)^2 \left(-2S_j^+ + S_{j+2}^+ + S_{j-2}^+ \right). \quad (3.41b)$$

In the hydrodynamic limit in terms of the staggered field S^α or its fluctuations ϕ^α , the equations of motion become respectively

$$\partial_t^2 S^\alpha = \nabla^2 S^\alpha , \quad (3.42a)$$

$$\partial_t^2 \phi^\alpha = \nabla^2 \phi^\alpha , \quad (3.42b)$$

which is exactly the Lorentz covariant wave equation.

Let us next consider an explicit wave ansatz for antiferromagnetic excitations on a one-dimensional chain

$$S_i^+ = u e^{i(2nka - \omega t)} , \quad (3.43a)$$

$$S_j^+ = v e^{i((2n+1)ka - \omega t)} , \quad (3.43b)$$

where a is the lattice spacing. Substituting into the equations of motion Eq. (3.40) and defining

$$\omega_0 = \frac{4JS}{\hbar} , \quad (3.44)$$

leads to the following system of equations

$$u(\omega + \omega_0) + v \omega_0 \cos(ka) = 0 , \quad (3.45a)$$

$$v(\omega - \omega_0) + u \omega_0 \cos(ka) = 0 , \quad (3.45b)$$

from which we obtain the one-dimensional dispersion relation

$$\omega = \omega_0 |\sin ka| . \quad (3.46)$$

Notice that indeed this is linear at low energies, i.e. small k , and consistent with the Lorentz covariance of the equations of motion, where

$$\omega \approx v|k| . \quad (3.47)$$

Explicitly we now identify the components of the fluctuation ϕ^γ , for a ground state oriented along e.g. z . Remembering the definition

$$S^+ = S^x + iS^y , \quad (3.48)$$

it is therefore clear that the y -component of the fluctuation will be $\pi/2$ out of phase with the ansatz specified for the x -component. We can then write the two possible circularly polarized excitations as

$$\vec{\phi}_\circlearrowright = \begin{pmatrix} \cos(kx - \omega t) \\ \sin(kx - \omega t) \\ 0 \end{pmatrix} , \quad (3.49a)$$

$$\vec{\phi}_\circlearrowleft = \begin{pmatrix} \cos(kx - \omega t) \\ -\sin(kx - \omega t) \\ 0 \end{pmatrix} , \quad (3.49b)$$

which resemble the non-trivial part of the electromagnetic gauge potential, cf. Eq. (2.52), and hints at the correspondence we develop in this section. The vector transformation properties of the fluctuations ϕ correspond to a spin $s = 1$ Boson, consistent with the difference in angular momentum induced by creation of the S^+ Boson, defined as

$$S^+ |m\rangle = \sqrt{s(s+1) - m(m+1)} |m+1\rangle . \quad (3.50)$$

An alternative approach arriving at the equations of motion for both the ferromagnetic and antiferromagnetic cases above is to utilize a Holstein-Primakoff transformation of the quantum mechanical operators S^+ and S^- to diagonalize the Hamiltonian [72, 169], and leads to the same results as this section. This alternative quantum mechanical treatment holds in the limit of small magnon numbers $a^\dagger a$ relative to the spin length s . This approach is fundamental to spin-wave theory, but will not be necessary in this Thesis.

In conclusion, in the absence of any sublattice, the dipolar spin order characteristic of the ferromagnet must break time-reversal symmetry and does not lead to Lorentz covariant equations of motion. However, the presence of a bipartite lattice as in the collinear antiferromagnet restores time-reversal symmetry. As we shall see in Chapter 4, with the addition of a biquadratic term, there are non-magnetic forms of order which do not break time-reversal symmetry, and for which a bipartite structure is therefore not necessary to obtain Lorentz covariance in the equations of motion.

3.3.2 $SU(2)$ $S = \frac{1}{2}$ spin coherent states for spin path integrals

The classical intuitions for how spins behave are fundamental for developing a path integral language applicable to spins, and is therefore an essential part of building a quantum mechanical field theory. For the unfamiliar reader, these are further developed in Appendix C. In order to proceed to describe quantum mechanically the low energy behaviour of the Heisenberg antiferromagnet, it is necessary to introduce the spin coherent state basis. Further details on this basis can be found in e.g. [169–171]. Coherent states were summarized by Glauber in 1963 [172] to mean three equivalent things: first, that they are states of minimum Heisenberg uncertainty, and therefore of minimum distance to an equivalent classical state; second, that coherent states are eigenstates of the annihilation operator; and third, that they are generated from the vacuum state of a harmonic oscillator by action of displacement operators specifically of the Heisenberg-Weyl group. This latter fact was later extended to arbitrary Lie groups [173, 174]. Coherent states for spin consistent with these definitions were first formulated by Radcliffe in 1972 [175], perhaps unknown to Feynman who, despite formulating the path integral, did not succeed in generalizing its application to the quantum mechanics of spin [169].

Recall that we can think of spin as the internal property leftover by action of the Wigner group. For massive particles, what is leftover is $O(3)$ or the quantized angular momentum representations of $SU(2)$, where as for massless particles, this is the Euclidean group $E(2)$, the algebra of transformations on the flat plane which, after fixing redundant degrees of freedom, correspond to transverse modes.

For a massive spin- $\frac{1}{2}$ particle such as an electron, the irreducible representation of

the generators of SU(2) is the set of Pauli matrices

$$S_x = \frac{1}{2} \begin{pmatrix} 0 & 1 \\ 1 & 0 \end{pmatrix}, \quad S_y = \frac{1}{2} \begin{pmatrix} 0 & -i \\ i & 0 \end{pmatrix}, \quad S_z = \frac{1}{2} \begin{pmatrix} 0 & 1 \\ 1 & 0 \end{pmatrix}. \quad (3.51)$$

Using these, the spin coherent state can be expressed in the following way

$$|\Omega\rangle = e^{iS_\alpha\lambda^\alpha} |\uparrow\rangle = e^{\frac{i\lambda_3}{2}} |\uparrow\rangle + e^{\frac{i}{2}(\lambda_1+i\lambda_2)} |\downarrow\rangle. \quad (3.52)$$

In this expression, one degree of freedom is used to fix the global phase of the state, another degree of freedom specifies the relative phase between the two basis states, and the last degree of freedom fixes the normalization, such that any arbitrary state in the Hilbert space can be described in this way. This is the quantum mechanical representation of the semiclassical O(3) vector we worked with previously. In this case however, the angular momentum commutation relations must be satisfied, so a single O(3) vector does not uniquely describe a quantum state. However, Heisenberg spins can still be appropriately represented by the unit vectors of the spin coherent state basis

$$|n(\phi, \theta, \psi)\rangle = e^{-i\phi\hat{S}_x} e^{-i\theta\hat{S}_y} e^{-i\psi\hat{S}_z} |\uparrow\rangle, \quad (3.53)$$

where recall that

$$[S_\alpha, S_\beta] = i\epsilon_{\alpha\beta\gamma} S_\gamma, \quad (3.54)$$

and $|\uparrow\rangle$ is the highest weight state of the representation that points along a direction \vec{n}_0 which I have taken to by convention to be the z-axis. This tells us that any arbitrary state can be thought of as a rotation away from the highest weight state. The implication of this representation is that

$$(\vec{n} \cdot \mathbf{S}) |\vec{n}\rangle = s |\vec{n}\rangle. \quad (3.55)$$

Since the phase factor ψ around the z -axis does not provide new measurable information, we can therefore restrict attention to a polar coordinate representation

$$\vec{n} = |n(\phi, \theta)\rangle = (\sin \theta \cos \phi, \sin \theta \sin \phi, \cos \phi). \quad (3.56)$$

At face value, this would allow a description of spins on a continuous manifold, the two-sphere S^2 , as was the case for classical O(3) spins. However, Heisenberg spins live in a discrete state space, one conventionally represented by the S_z eigenstates, which satisfy

$$S_z |s, m\rangle = m |s, m\rangle, \quad (3.57a)$$

$$\mathbf{S}^2 |s, m\rangle = s(s+1) |s, m\rangle, \quad (3.57b)$$

where

$$-s \leq (m = \frac{p}{2}) \leq s \quad \text{with} \quad p \in \mathcal{Z}. \quad (3.58)$$

To reconcile this fact, we observe that the spin coherent state basis must form an overcomplete basis, with a one-to-many mapping of the form

$$|\vec{n}\rangle = \sum_{m=-s}^s D^{(s)}(\vec{n}, m) |s, m\rangle , \quad (3.59)$$

where the $3 \times s$ -dimensional matrices $D^{(s)}$ satisfy the algebra[171]

$$D^{(s)}(\vec{n}_1, m) D^{(s)}(\vec{n}_2, m) = D^{(s)}(\vec{n}_0, m) e^{i\Phi(\vec{n}_1, \vec{n}_2, \vec{n}_0) S_z} . \quad (3.60)$$

The phase Φ of the exponential term is defined as the area of a spherical triangle formed by the unit vectors $\hat{n}_1, \hat{n}_2, \hat{n}_0$. Since the spin coherent state vectors live on the the closed manifold S^2 , this is not uniquely defined. In particular, each set of three vectors defines two spherical triangles over the sphere (one interior, one exterior), such that one can only specify the area Φ modulo the total area of the sphere 4π . Therefore it must hold that

$$e^{i4\pi m} = 1 , \quad (3.61)$$

which provides a geometric intuition for why spins must have integer or half-integer quantization for m .

Next, to set the stage for building an action, we will need a few properties of spin coherent states. The first is that since these are not classical vectors, they are not orthogonal. In particular, since there are multiple ways to map onto a spin coherent state as seen above, they form an overcomplete basis, with the overlap between two states given by

$$\langle \vec{n}_i | \vec{n}_j \rangle = e^{i\Phi(\vec{n}_i, \vec{n}_j, \vec{n}_0)} \left(\frac{1 + \vec{n}_i \cdot \vec{n}_j}{2} \right)^s . \quad (3.62)$$

In addition, by considering the appropriate integration measure that normalizes the overcomplete mapping, the resolution of identity for the spin coherent states defined on the surface of the sphere is given by

$$\mathbb{1} = \int_{S^2} d\mu[\vec{n}] |\vec{n}\rangle \langle \vec{n}| \quad (3.63a)$$

$$= \frac{2S+1}{4\pi} \int d\vec{n}^3 \delta(\vec{n}^2 - 1) |\vec{n}\rangle \langle \vec{n}| . \quad (3.63b)$$

With this, we are now equipped with the prerequisite definitions and properties to derive the low-energy field theory for the Heisenberg antiferromagnet.

3.3.3 Quantum non-linear sigma model for a Heisenberg antiferromagnet

In this section I review the mapping of the quantum Heisenberg antiferromagnet onto the $O(3)$ non-linear sigma model, following a combination of treatments found in [5, 169, 171].

Historically this mapping was first developed by Haldane [176] in order to understand the behaviour of excitations beyond the elementary magnons captured by linear

spin wave theory, ie. topological magnons, leading ultimately to the discovery of the Haldane gap for which he was awarded the 2016 Nobel Prize. For further historical details, see [177–182].

For the purposes of this Chapter, this mapping provides a more direct parallel to the relativistically covariant theory of electromagnetism. The construction starts from the path integral formulation of the partition function. To explicitly calculate the path integral, we need a convenient way to sum over all possible paths, for which an appropriate representation for the quantum mechanical spins is the spin coherent basis.

The (Euclidean) action for quantum spins

At finite temperatures, the partition function for a quantum system can be evaluated in terms of the Hamiltonian operator

$$Z = \text{Tr}\left(e^{-\beta H}\right), \quad (3.64)$$

which takes account of the states in principle accessible to the system via thermal fluctuations. We will not use the specific form of the Heisenberg Hamiltonian yet in this subsection.

At zero temperature, there are no longer thermal fluctuations, and the relevant quantity of interest is the time evolution operator and its propagator

$$U(t_0, t) = \text{Tr}\left(e^{i\frac{(t-t_0)}{\hbar}H}\right), \quad (3.65a)$$

$$K(n_{t_0}, n_t) = \langle n_{t_0} | e^{i(t-t_0)H} | n_t \rangle. \quad (3.65b)$$

For real β , if we identify

$$\beta = \tau = -it, \quad (3.66)$$

then the Boltzmann weight at finite temperature can be thought of as being equivalent to the time evolution operator in imaginary ³ time τ . Working with $\hbar = 1$

$$U(\tau) = \text{Tr}\left(e^{itH}\right) = \text{Tr}\left(e^{-\tau H}\right). \quad (3.67)$$

This allows us to evaluate the partition function as a path integral. First, the finite imaginary time is subdivided into small steps $\delta\tau$ such that

$$\beta = \tau = N\delta\tau. \quad (3.68)$$

Substituting this into the expression for the partition function we find

$$Z = \text{Tr}\left(e^{-\beta H}\right) = \lim_{\substack{N \rightarrow \infty \\ \delta\tau \rightarrow 0}} \text{Tr}\left[\hat{T}(e^{-\delta\tau H})^N\right], \quad (3.69)$$

where \hat{T} is the time ordering operator. Taking the trace over \vec{n}_α and inserting the

³Also known as Euclidean time, imaginary time can be thought of as an abstract dimension that shares the transformation properties of spatial dimensions.

resolution of identity

$$Z = \lim_{\substack{N \rightarrow \infty \\ \delta\tau \rightarrow 0}} \left(\frac{2S+1}{4\pi} \right)^N \sum_{\vec{n}_\alpha} \langle \vec{n}_\alpha | \hat{T} \left(\int d\vec{n}^3 \delta(\vec{n}^2 - 1) |\vec{n}\rangle \langle \vec{n}| e^{-\delta\tau H} \right)^N | \vec{n}_\alpha \rangle, \quad (3.70a)$$

$$= \lim_{\substack{N \rightarrow \infty \\ \delta\tau \rightarrow 0}} \int d\mu[\vec{n}_{t_1}] \dots d\mu[\vec{n}_{t_N}] \sum_{\vec{n}_\alpha} \langle \vec{n}_\alpha | \vec{n}_{t_1} \rangle \langle \vec{n}_{t_1} | e^{-\delta\tau H} | \vec{n}_{t_2} \rangle \dots \langle \vec{n}_{t_{N-1}} | e^{-\delta\tau H} | \vec{n}_{t_N} \rangle \langle \vec{n}_{t_N} | e^{-\delta\tau H} | \vec{n}_\alpha \rangle, \quad (3.70b)$$

$$= \lim_{\substack{N \rightarrow \infty \\ \delta\tau \rightarrow 0}} \left(\prod_{j=1}^N \int d\mu[\vec{n}_{\tau_j}] \langle \vec{n}_{\tau_j} | e^{-\delta\tau H} | \vec{n}_{\tau_{j+1}} \rangle \right), \quad (3.70c)$$

where periodic boundary conditions apply on τ . Expanding the matrix elements of the Hamiltonian in the limit $\delta\tau \rightarrow 0$

$$\langle \vec{n}_{\tau_j} | e^{-\delta\tau H} | \vec{n}_{\tau_j + \delta\tau} \rangle \approx \langle \vec{n}_{\tau_j} | \vec{n}_{\tau_{j+1}} \rangle - \delta\tau \langle \vec{n}_{\tau_j} | H | \vec{n}_{\tau_{j+1}} \rangle, \quad (3.71a)$$

$$\approx e^{i\Phi(\vec{n}_{\tau_j}, \vec{n}_{\tau_{j+1}}, \vec{n}_0)} \left(\frac{1 + \vec{n}_{\tau_j} \vec{n}_{\tau_{j+1}}}{2} \right)^S - \delta\tau \langle \vec{n}_{\tau_j} | H | \vec{n}_{\tau_j} \rangle. \quad (3.71b)$$

When evaluating the product over j , we keep only the terms up to first order in $\delta\tau$, such that

$$\prod_{j=1}^N \left(e^{i\Phi(\vec{n}_{\tau_j}, \vec{n}_{\tau_{j+1}}, \vec{n}_0)} \left(\frac{1 + \vec{n}_{\tau_j} \vec{n}_{\tau_{j+1}}}{2} \right)^S - \delta\tau \langle \vec{n}_{\tau_j} | H | \vec{n}_{\tau_j} \rangle \right), \quad (3.72a)$$

$$\approx \left(\prod_{j=1}^N e^{i\Phi(\vec{n}_{\tau_j}, \vec{n}_{\tau_{j+1}}, \vec{n}_0)} \left(\frac{1 + \vec{n}_{\tau_j} \vec{n}_{\tau_{j+1}}}{2} \right)^S \right) - \delta\tau \sum_{j=1}^N \left(\prod_{i \neq j} e^{i\Phi(\vec{n}_{\tau_i}, \vec{n}_{\tau_{i+1}}, \vec{n}_0)} \left(\frac{1 + \vec{n}_{\tau_i} \vec{n}_{\tau_{i+1}}}{2} \right)^S \langle \vec{n}_{\tau_j} | H | \vec{n}_{\tau_j} \rangle \right), \quad (3.72b)$$

$$= \left(\prod_{j=1}^N e^{i\Phi(\vec{n}_{\tau_j}, \vec{n}_{\tau_{j+1}}, \vec{n}_0)} \left(\frac{1 + \vec{n}_{\tau_j} \vec{n}_{\tau_{j+1}}}{2} \right)^S \right) \left(1 - \delta\tau \sum_{j=1}^N \frac{\langle \vec{n}_{\tau_j} | H | \vec{n}_{\tau_j} \rangle}{e^{i\Phi(\vec{n}_{\tau_j}, \vec{n}_{\tau_{j+1}}, \vec{n}_0)} \left(\frac{1 + \vec{n}_{\tau_j} \vec{n}_{\tau_{j+1}}}{2} \right)^S} \right), \quad (3.72c)$$

$$= \left(\prod_{j=1}^N e^{i\Phi(\vec{n}_{\tau_j}, \vec{n}_{\tau_{j+1}}, \vec{n}_0)} \left(\frac{1 + \vec{n}_{\tau_j} \vec{n}_{\tau_{j+1}}}{2} \right)^S \right) \left(1 - \delta\tau \sum_{j=1}^N \frac{\langle \vec{n}_{\tau_j} | H | \vec{n}_{\tau_j} \rangle}{1 + \mathcal{O}(\delta\tau)} \right), \quad (3.72d)$$

$$\approx \prod_{j=1}^N e^{i\Phi(\vec{n}_{\tau_j}, \vec{n}_{\tau_{j+1}}, \vec{n}_0)} e^{\ln \left(\frac{1 + \vec{n}_{\tau_j} \vec{n}_{\tau_{j+1}}}{2} \right)^S} e^{-\delta\tau \langle \vec{n}_{\tau_j} | H | \vec{n}_{\tau_j} \rangle}. \quad (3.72e)$$

Then the partition function can be expressed

$$Z = \lim_{\substack{N \rightarrow \infty \\ \delta\tau \rightarrow 0}} \int \mathcal{D}\vec{n} e^{-S_E[\vec{n}]}, \quad (3.73)$$

using

$$\mathcal{D}\vec{n} = \prod_{j=1}^N \int d\vec{n}_{\tau_j}^3 \delta(\vec{n}_{\tau_j}^2 - 1) \left(\frac{2S+1}{4\pi} \right), \quad (3.74)$$

and with the Euclidean action

$$S_E[\vec{n}] = -iS \sum_{j=1}^N \Phi(\vec{n}_{\tau_j}, \vec{n}_{\tau_{j+1}}, \vec{n}_0) - S \sum_{j=1}^N \ln \left(\frac{1 + \vec{n}_{\tau_j} \cdot \vec{n}_{\tau_{j+1}}}{2} \right) + \sum_{j=1}^N \delta\tau \langle \vec{n}_{\tau_j} | H | \vec{n}_{\tau_j} \rangle, \quad (3.75a)$$

$$= S_{kin} + S_H, \quad (3.75b)$$

which is the object we are interested in. Note that the contribution of the logarithmic term is effectively a constant, and will be ignored⁴. Let's consider the first term, which is of the form

$$S_{kin} = iSA[\vec{n}], \quad (3.76)$$

where the solid angle spanned by the spherical triangle formed by $\vec{n}_{\tau_j}, \vec{n}_{\tau_{j+1}}$ and \vec{n}_0 given by

$$A[\vec{n}] = \Phi(\vec{n}_{\tau_j}, \vec{n}_{\tau_{j+1}}, \vec{n}_0), \quad (3.77)$$

is the Berry phase accumulated by a single spin at each step along its trajectory. In the semiclassical approximation, it is sufficient to assume that the spin trajectories are closed orbits on the $O(3)$ sphere that do not exhibit any jumps. That is, the evolution of the spin precession is smooth. This may not always be justifiable for quantum mechanical objects, and so the path integral method should ideally be checked against alternative procedures.

The full solid angle swept out cannot be uniquely defined. In particular for every closed contour there are two areas that can be defined on the sphere such that

$$A[\Sigma^+] + A[\Sigma_-] = 4\pi. \quad (3.78)$$

Therefore, modulo 4π and in the continuum limit $\delta\tau \rightarrow 0$

$$A[\Sigma^+] = \int_0^\beta d\tau \int_0^1 d\lambda \vec{n}_\tau \cdot (\partial_\tau \vec{n}_\tau \times \partial_\lambda \vec{n}_\tau), \quad (3.79)$$

$$(3.80)$$

where λ smoothly parametrizes the path from $\vec{n}(\tau, \lambda) = \vec{n}(\tau, 0) = \vec{n}_\tau$ to the top of the solid angle cap $\vec{n}(\tau, \lambda) = \vec{n}(\tau, 1) = \vec{n}_0$. Per spin, the contribution to the action then becomes

$$S_{kin} = iS \int d\tau \int_0^1 d\lambda \vec{n}_\tau \cdot (\partial_\tau \vec{n}_\tau \times \partial_\lambda \vec{n}_\tau). \quad (3.81)$$

Depending on the body of literature, this type of term is called a Chern-Simons term, or also Wess-Zumino term.

On a lattice of spins, we must sum over the contributions from each spin. In the

⁴Notice that $\vec{n}_{\tau_j} \cdot \vec{n}_{\tau_{j+1}} = \vec{n}_{\tau_j} \cdot (\vec{n}_{\tau_j} + d\vec{n}_{\tau_j})$, where $\vec{n}_{\tau_j} \perp d\vec{n}_{\tau_j}$

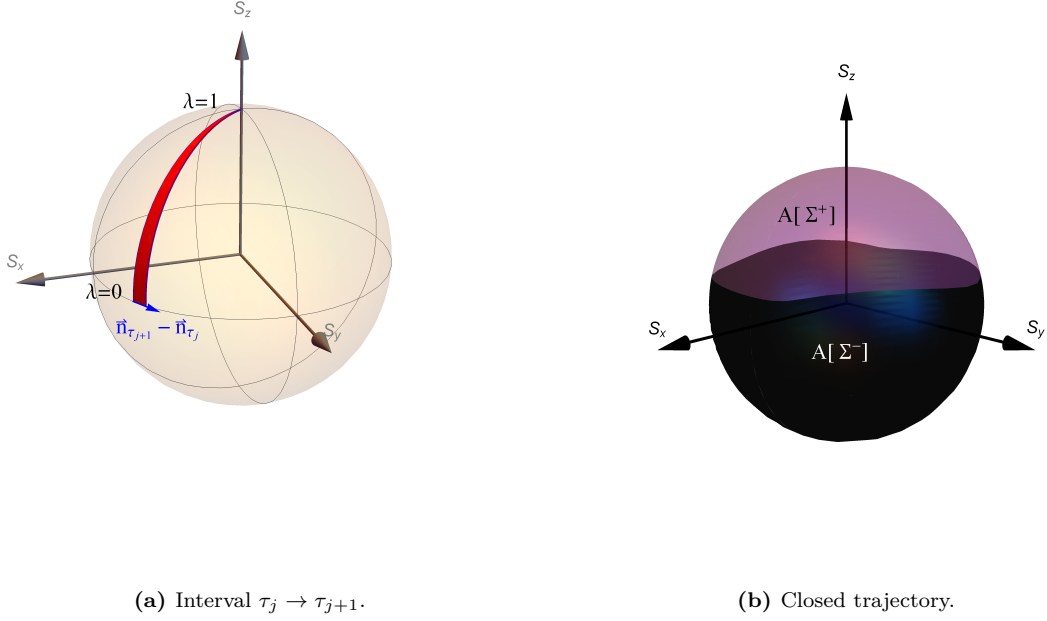


Figure 3.2: Illustration of the origin of the Berry phase arising in quantum magnets. **(a)** Sketch of the Berry phase swept out between times τ_j and τ_{j+1} . **(b)** An arbitrary closed trajectory in the space of spin coherent states delineates two patches of the sphere, showing the ambiguity in defining areas of closed loops on the sphere.

continuum limit we can write

$$S_{kin} = iS \int d\tau dr^d \vec{n}(\vec{r}, \tau) \cdot (\delta \vec{n}(\vec{r}, \tau) \times \partial_\tau \vec{n}(\vec{r}, \tau)). \quad (3.82)$$

Next, to evaluate the Hamiltonian term of the action, we restrict focus to the antiferromagnetic Heisenberg model.

From the Heisenberg Antiferromagnet to an O(3) NLSM

The ordered phase of a non frustrated Heisenberg antiferromagnetic model is characterized by a non-zero staggered magnetization of the form (up to three dimensions x, y, z)

$$\vec{m}_s = \frac{1}{N} \sum_{\vec{r}} (-1)^{x+y+z} \vec{n}(\vec{r}), \quad (3.83)$$

and described by the Heisenberg Hamiltonian Eq. (C.9) for $J < 0$. The classical ground state for this model consists of spins of alternating orientation (the Néel state). While this picture is not strictly true for the quantum antiferromagnet, it is acceptable to assume that the true ground state is close to the Néel state and therefore that at least over short-range we observe the characteristic staggered Néel ordering, consistent with the range of approximations made so far. This justifies the decomposition of the spin field $\vec{n}(\vec{r})$ into a staggered order component $\vec{m}_s(\vec{r})$ and its orthogonal component \vec{l} describing the fluctuations, which have a tendency to ferromagnetically align spins.

Specifically this decomposition looks like

$$\vec{n} = \frac{\vec{m}_s + \vec{l}}{\sqrt{\vec{m}^2 + \vec{l}^2}}, \quad (3.84)$$

In the limit of small fluctuations, the normalization in the denominator is just unity. Further, due to the spin length constraint, as in the semiclassical case, the fluctuations must be orthogonal to the order parameter, i.e.

$$\vec{m}_s \cdot \vec{l} = 0. \quad (3.85)$$

For simplicity of notation, in the hydrodynamic limit I denote \vec{m}_s by simply \vec{m} . For arbitrary lattice dimension d , the Hamiltonian term then becomes

$$\mathcal{S}_H = \int d\tau dx^d \langle \vec{n}(\vec{r}, \tau) | H | \vec{n}(\vec{r}, \tau) \rangle, \quad (3.86a)$$

$$= -J \int d\tau dx^d \sum_{\vec{\delta}} \langle \vec{n}(\vec{r}, \tau) | \vec{S}_{\vec{r}} \cdot \vec{S}_{\vec{r}+\vec{\delta}} | \vec{n}(\vec{r}, \tau) \rangle, \quad (3.86b)$$

$$= -JS^2 \int d\tau dx^d \sum_{\vec{\delta}} \vec{n}(\vec{r}, \tau) \cdot \vec{n}(\vec{r} + \vec{\delta}, \tau), \quad (3.86c)$$

$$= -\frac{JS^2}{2} \int d\tau dx^d \sum_{\vec{\delta}} (\vec{n}(\vec{r}, \tau) + \vec{n}(\vec{r} + \vec{\delta}, \tau))^2 + \text{const}, \quad (3.86d)$$

$$= -\frac{JS^2}{2} \int d\tau dx^d \sum_{\vec{\delta}} ((-1)^{x+y} \vec{m}(\vec{r}, \tau) + \vec{l}(\vec{r}, \tau) + (-1)^{x+y} \vec{m}(\vec{r} + \vec{\delta}, \tau) + \vec{l}(\vec{r} + \vec{\delta}, \tau))^2, \quad (3.86e)$$

$$\approx -\frac{JS^2}{2} \int d\tau dx^d (\partial_x \vec{m}(\vec{r}, \tau) + 2\vec{l}(\vec{r}, \tau))^2 + (\partial_y \vec{m}(\vec{r}, \tau) + 2\vec{l}(\vec{r}, \tau))^2 \quad (3.86f)$$

$$\approx -\frac{JS^2}{2} \int d\tau dx^d (\partial_x \vec{m}(\vec{r}, \tau))^2 + (\partial_y \vec{m}(\vec{r}, \tau))^2 + 8\vec{l}(\vec{r}, \tau) + \mathcal{O}(|\vec{l}|^2). \quad (3.86g)$$

Following a similar expansion in the fluctuations to first order in \vec{l} for the kinetic term, we arrive at

$$\mathcal{S}_{kin} = iS \int d\tau dx^d \vec{l}(\vec{r}, \tau) \cdot (\vec{m}(\vec{r}, \tau) \times \partial_\tau \vec{m}(\vec{r}, \tau)). \quad (3.87)$$

By saddle-point approximation of the action, the fluctuating field \vec{l} can be shown again to be dependent on the staggered magnetization field \vec{m} .

$$\vec{l} = \frac{i}{8JS} \vec{m}(\vec{r}, \tau) \times \partial_\tau \vec{m}(\vec{r}, \tau), \quad (3.88)$$

The action then becomes

$$S_E = \int d\tau dx^d \left[\frac{1}{8J} (\partial_\tau \vec{m})^2 + \frac{JS^2}{2} ((\partial_x \vec{m})^2 + (\partial_y \vec{m})^2) \right]. \quad (3.89)$$

After Wick rotation back to Minkowski time, we recover the same result as Eq. (C.33a)

$$\mathcal{S}_{AFM} = \int dt dx^d \left[\frac{\chi S^2}{2} (\partial_t \vec{m}_i)^2 - \frac{\rho}{2} (\partial_j \vec{m}_i)^2 \right]. \quad (3.90)$$

The magnetization can be expressed component-wise in terms of the fields ϕ_x and ϕ_y that act as generators for the two rotations breaking the continuous $O(3)$ symmetry of the action. That is,

$$\vec{m} = (\phi_x, \phi_y, \sqrt{1 - \phi_x^2 - \phi_y^2}), \quad (3.91)$$

with dynamics described by

$$\mathcal{S}_{AFM} = \frac{\rho}{2} \int d\tau dx^d \left[\frac{1}{c^2} (\partial_\tau \vec{\phi})^2 - \sum_{i \in x_d} (\partial_i \vec{\phi})^2 \right], \quad (3.92)$$

where again I define the wave speed

$$c = \sqrt{\frac{\rho}{\chi S^2}}, \quad (3.93)$$

We will now compare the excitations as predicted by this low-energy theory with electromagnetism.

3.4 Light, magnons, action! A dictionary for spin-1 excitations

In Chapter 2, we saw how the masslessness of photons in electromagnetism is connected to the existence of transverse modes. Here, I explicitly identify a one-to-one correspondence between photons and the antiferromagnons of electromagnetism. This correspondence is at times alluded to within the magnetism community, but has not been explicitly documented to the best of my knowledge, and I here provide the missing details.

From Eq. (3.43) we can identify semiclassical solutions which correspond to effective electric and magnetic fields that allow us to visualize the antiferromagnons in parallel with photons, see Fig. 3.3, cf. Fig 1.5. Without loss of generality, consider an antiferromagnet with order oriented along the z -direction, propagating along the z -axis.

$$\vec{\phi}_\circ = \frac{B_0}{k} \begin{pmatrix} \cos(kz - \omega t) \\ \sin(kz - \omega t) \\ 0 \end{pmatrix} = \vec{A}_\circ, \quad (3.94)$$

with fields

$$-\partial_t \vec{\phi}_\circ = E_0 \begin{pmatrix} -\sin(kz - \omega t) \\ \cos(kz - \omega t) \\ 0 \end{pmatrix} = \vec{E}_\circ, \quad (3.95)$$

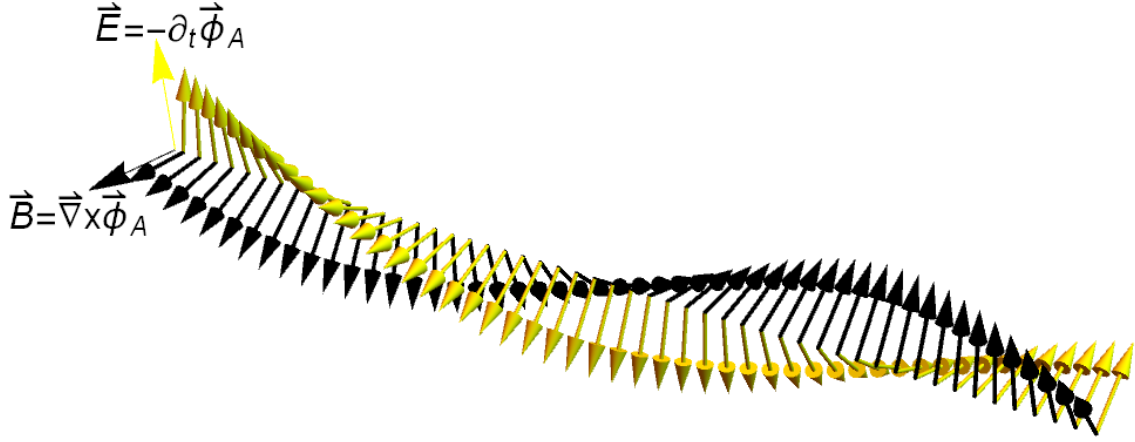


Figure 3.3: Analogue E and B fields arising in the continuum field description of the antiferromagnetic Goldstone modes of the Heisenberg antiferromagnet. The field $\vec{\phi}_A$ represents the non-trivial transverse components of the staggered magnon field ϕ^μ and equivalently of the gauge field A^μ .

and

$$\vec{\nabla} \times \vec{\phi}_\circlearrowleft = B_0 \begin{pmatrix} \cos(kz - \omega t) \\ \sin(kz - \omega t) \\ 0 \end{pmatrix} = \vec{B}_\circlearrowleft, \quad (3.96)$$

using $\frac{B_0}{c^2} = E_0$ and $c^2 = \frac{\omega}{k}$. This provides a concrete mapping between the magnetic canting field $\vec{\phi}$ and an effective vector gauge potential \vec{A} with respective electric and magnetic fields.

Meanwhile, the other polarization takes the form

$$\vec{\phi}_\circlearrowright = \frac{B_0}{k} \begin{pmatrix} \cos(kz - \omega t) \\ -\sin(kz - \omega t) \\ 0 \end{pmatrix} = \vec{A}_\circlearrowright, \quad (3.97)$$

with fields

$$-\partial_t \vec{\phi}_\circlearrowright = E_0 \begin{pmatrix} \sin(kz - \omega t) \\ \cos(kz - \omega t) \\ 0 \end{pmatrix} = \vec{E}_\circlearrowright, \quad (3.98)$$

and

$$\vec{\nabla} \times \vec{\phi}_\circlearrowright = B_0 \begin{pmatrix} -\cos(kz - \omega t) \\ \sin(kz - \omega t) \\ 0 \end{pmatrix} = \vec{B}_\circlearrowright, \quad (3.99)$$

again using $\frac{B_0}{c^2} = E_0$ and $c^2 = \frac{\omega}{k}$. This completes the explicit mapping onto electric and magnetic fields for the Heisenberg antiferromagnet, summarized in Table 3.2.

	Collinear Néel AFM	(3+1)D EM
Lagrangian	$\mathcal{L} = \frac{1}{2} \left[\chi(\partial_t \vec{\phi})^2 - \rho(\partial_i \vec{\phi})^2 \right]$	$\mathcal{L} = \frac{1}{2} \left[\frac{1}{c^2}(\partial_t \vec{A})^2 - (\partial_i \vec{A})^2 \right]$
DOFs	$\vec{\phi}_\circ, \vec{\phi}_\circ$ $-\partial_t \vec{\phi}_\circ, \nabla \times \vec{\phi}_\circ$ $-\partial_t \vec{\phi}_\circ, \nabla \times \vec{\phi}_\circ$	$\vec{A}_\circ, \vec{A}_\circ$ $\vec{E}_\circ, \vec{B}_\circ$ $\vec{E}_\circ, \vec{B}_\circ$

Table 3.2: Dictionary connecting AFM and EM excitations

Consider now defining a relativistic tensor for the Heisenberg antiferromagnet

$$F_{\mu\nu} = (\partial_\mu \phi_\nu - \partial_\nu \phi_\mu), \quad (3.100)$$

by promoting the magnon degrees of freedom ϕ to a four-vector, with the necessary physical restrictions that

$$\phi^0 = 0, \quad (3.101a)$$

$$k_\mu \phi^\mu = 0, \quad (3.101b)$$

for

$$\vec{k} \parallel \vec{m}_0 \implies \partial_i \phi^i = 0. \quad (3.102)$$

such that the antiferromagnons ϕ can be consistently defined in four-vector notation, and will transform under the elements of the Lorentz group as four-vectors.

We can then redefine the action Eq. (3.92)

$$\mathcal{S}_{AFM} = - \int d\tau dx^3 g_{\mu\nu} \tilde{g}_{\rho\sigma} \partial^\mu \phi^\rho \partial^\nu \phi^\sigma, \quad (3.103)$$

where

$$\partial_\mu = \left(\frac{1}{c} \partial_0, \partial_1, \partial_2, \partial_3 \right), \quad (3.104)$$

and $g_{\mu\nu}$ is a 4-dimensional metric defined as

$$g_{\mu\nu} = \begin{pmatrix} -1 & 0 & 0 & 0 \\ 0 & 1 & 0 & 0 \\ 0 & 0 & 1 & 0 \\ 0 & 0 & 0 & 1 \end{pmatrix}, \quad (3.105)$$

clearly equivalent to the Minkowski metric in flat spacetime, and $\tilde{g}_{\rho\sigma}$ is also a 4-

dimensional metric which can be defined as

$$\tilde{g}_{\rho\sigma} = \begin{pmatrix} \pm 1 & 0 & 0 & 0 \\ 0 & 1 & 0 & 0 \\ 0 & 0 & 1 & 0 \\ 0 & 0 & 0 & 1 \end{pmatrix}, \quad (3.106)$$

where the signature of the component \tilde{g}_{00} does not influence any physical quantity and can be chosen arbitrarily, since the components ϕ^0 are trivial. Therefore, for convenience, this metric also can take to be to the Minkowski metric in flat spacetime. Fundamentally, this metric defines the inner product in the Hilbert space between the promoted spin degrees of freedom. It is clear from this decomposition that a notion of a curved spacetime for field degrees of freedom requires modification of the inner product in Hilbert space. Such modifications will not be discussed in this Thesis, and the gravitational wave analogue I establish next in Chapter 4 will be discussed only in flat spacetime. The distinction the Hilbert space and the real space that the atoms are embedded in is important, since the Hilbert space remains 3-dimensional even in the lower dimensional systems. This means that we can still nevertheless establish a parallel to (3+1)D electromagnetism in reduced dimensional magnetic systems. This point will also hold for the gravitational wave analogy, even more importantly in that case, since, unlike (2+1)D electromagnetism, there are no self-supporting excitations allowed in (2+1)D gravity.

In conclusion, we can establish an analogue between the magnons—traveling parallel to \vec{m}_0 —in the Heisenberg antiferromagnet with the physical degrees of freedom of the relativistic vector gauge potential in a gauge (e.g. Lorenz gauge) which minimizes redundant components of A_μ , leaving only the transverse degrees of freedom.

3.5 Analogue photons in experiment

3.5.1 Analogue photons in magnetic insulators

In the context of magnetic insulators, several candidate materials exhibit Néel antiferromagnetism with linearly dispersing excitations at low-energy, including e.g. Rb_2MnF_4 [183], La_2CuO_4 [8], La_2NiO_4 [183]. The square lattice spin- $\frac{1}{2}$ insulators, in particular the cuprates and niquelates, have independently attracted significant attention due to the appearance of superconductivity at large doping [184].

The linear dispersion, see Fig. 1.4a, is the neutron scattering hallmark of the analogue photon excitations described in this Chapter. Direct observation of these analogue photons is readily available with measurements of the dynamical spin-spin correlations $S(\mathbf{q}, \omega)$ defined in Eq. 1.41. Such dynamical structure factors are very revealing of properties of quantum magnets, and for example within the context of quantum spin-ice, the analogue photons described in Section 3.2 have also been indirectly inferred from inelastic neutron scattering measurements of candidate materials, e.g. [59, 60]. Another powerful tool is Resonant Inelastic X-ray Scattering, from which the dynamical structure factors have also been measured for a variety of antiferromagnetic cuprates such as La_2CuO_4 [185, 186], and e.g. CaCuO_2 [187, 188].

In discussing candidates for Néel antiferromagnetism, in practice, there is often more than just the Heisenberg interaction at play. Other effects arising from Dzyaloshinskii-Moriya interactions, ring exchange and/or longer range exchange interactions, can complicate the direct analogue to electromagnetic photons [189–191]. Furthermore, relativistic effects such as spin-orbit coupling can gap out the low-energy excitations as in Ca_2Ru_4 , where compression of the crystal induces distortion gapping out the low-energy modes [192], in an analogue of the Anderson-Higgs mechanism. Additionally in regimes where quantum fluctuations are large, or other exotic excitations become important, spin-wave theory is insufficient to make full detailed predictions in several compounds, such as at high energies for La_2CuO_4 [193].

3.5.2 Analogue photons in cold atoms

Néel antiferromagnets are also accessible in cold atomic gases in optical lattices, see e.g. [194–197]. In these systems of neutral atoms, relativistic effects originating from spin-orbit coupling do not play a role, and there is no impact on the associated analogue photon spectrum .

An optical lattice consists of a periodic array made from interfering optical laser beams, e.g. [125], that binds atoms in-situ at the locations of extremized intensity of the light. This works as follows: the time-varying electric field induces a changing dipole moment on the rarified atoms, primarily affecting the electrons, in the cold atomic gas. Choosing laser frequencies that are far from any transition energies in the atomic species under study, the energy of the electrons in the atoms changes in response to the field in proportion to the field intensity

$$\Delta E = \sum_{m,n \in x,y,z} \alpha_{mn}(\omega) \langle E_m(\mathbf{r}, t) E_n(\mathbf{r}, t) \rangle, \quad (3.107)$$

where n and m are spatial indices, $\alpha_{nm}(\omega)$ is the electric polarizability tensor corresponding to the frequency ω of the laser's electric field E_m . As a result, the atoms experience an effective potential

$$V = \Delta E. \quad (3.108)$$

The use of optical frequencies allows for relatively large sizes of the emerging lattice, which facilitates significant control at the resolution of individual lattice sites [122, 125].

In addition to the use of optical lattices, it is important to consider the species of atom being trapped. Alkali atoms used in cold atomic gases can possess different internal spin states, allowing for simulation of spin systems and preparations of mixtures of spin components, as required for a Néel antiferromagnet. The spin of a particle determines if it will behave as a Boson or a Fermion. This also applies to atoms in their interactions with one another. For neutral atoms, the number of neutrons is the variable that determines if the atom will have an integer or half-integer total spin. An even number of neutrons leads to integer total spin, corresponding to bosonic exchange statistics. An odd number of neutrons leads to half-integer total spin, corresponding in turn to fermionic exchange statistics.

For the cleanest cold atom realization of the Heisenberg Hamiltonian, we can con-

sider a Fermi gas, such as $^{40}\text{K}^5$, with two distinct species realized by two hyperfine states denoted

$$\sigma \in \{\uparrow, \downarrow\}, \quad (3.109)$$

in an optical lattice. Such interacting Fermions in an optical lattice can be described by the Hubbard Hamiltonian

$$\mathcal{H} = -t \sum_{\langle ij \rangle} \sum_{\sigma} [c_{i\sigma}^{\dagger} c_{j\sigma} + c_{j\sigma}^{\dagger} c_{i\sigma}] + U \sum_i c_{i\uparrow}^{\dagger} c_{i\uparrow} c_{i\downarrow}^{\dagger} c_{i\downarrow}, \quad (3.110)$$

where t is the hopping parameter, U captures the strength of the potential, and $c_{i\sigma}^{\dagger}$ and $c_{i\sigma}$ are fermionic creation and annihilation operators with anticommutation relations

$$\{c_{i\sigma}, c_{j\sigma'}^{\dagger}\} = \delta_{ij} \delta_{\sigma\sigma'}. \quad (3.111)$$

In the tight-binding limit where

$$U \gg t, \quad (3.112)$$

the Hubbard model reduces to [67]

$$\mathcal{H} = \frac{4t^2}{U} \sum_{\langle ij \rangle} \mathbf{S}_i \cdot \mathbf{S}_j \quad (3.113)$$

equivalent to the Heisenberg Hamiltonian Eq. (1.16).

Cold atom simulations of the Néel antiferromagnet are also motivated by the search for d-wave superconductivity in the Hubbard model [196, 197], but as the work in this Chapter suggests, such experimental realizations also possess interest for their analogue photonic excitations.

Integer-spin alkali atoms, such as ^{23}Na and ^{87}Rb , are in fact more common than their fermionic counterparts, since it is energetically less favourable for an atom to have both an unpaired neutron in addition to the unpaired proton in the nucleus [125, 198]. We will see in Chapter 4 that such species can realize the ferroquadrupolar nematic phase whose excitations are in Chapter 4 shown to be in correspondence to gravitational waves.

3.6 Chapter summary

In concluding this Chapter, we have learned that magnetic phases can exhibit Goldstone modes which are in one-to-one correspondence with vector field theories of electromagnetism in (2+1)D and (3+1)D. In addition, we have learned that in models

⁵ ^{40}K is an atom with total spin $\frac{9}{2}$, which in principle possesses a spin manifold with 9 distinct states. However, for the present discussion, we are interested in mixtures of two distinct hyperfine species at most. In practice, for ^{40}K it is known that the pair of states $m_F = \frac{9}{2}$ and $m_F = \frac{7}{2}$ have populations robust against scattering into other m_F states at low temperature, such that their respective populations are conserved [194].

where stable point defects are supported, there is an analogue of the charges of the vector field theory of electromagnetism. We have also seen examples of how such analogues have been realized in experiment.

In the next Chapter, we will see how the Goldstone modes of a spin nematic are in one-to-one correspondence with gravitational waves. We will also see that (2+1)D spin nematics can support stable point defects that behave like charges, i.e. mass, which gravitate.

Chapter 4

Analogue of linearized gravity in spin nematics and spinor condensates

“More is different.” - Philip Warren Anderson

As we have seen in Chapter 2, in their non-interacting limit, gravitational waves are harmonic excitations of a free spin-2 field, and are therefore described by a rank-2 tensor field theory. The massless, spin-2 excitations of linearized gravity in (3+1)D can be characterized by two independent dynamical components of a rank-2 polarization tensor. Such massless, spin-2 excitations are not exclusive to the context of linearized gravity, also arising as Goldstone modes in systems with nematic order.

In this Chapter we will dive into the description of quantum spin nematics and their Goldstone modes, focusing on the realization of ferroquadrupolar order as found in the Bilinear-Biquadratic model. This system presents tensorial Goldstone modes that I identify to be in one-to-one correspondence with gravitational waves. To understand this connection, I will first review spin nematics as realized in spin-1 systems in a model independent way before introducing the Bilinear-Biquadratic model. I then introduce the spin coherent states for spin-1 and use this to rederive the corresponding low-energy limit, which leads to a non-linear sigma model in direct correspondence with the action of linearized gravity.

I then present the reader with a key result of this Thesis, namely, the dictionary which explicitly connects the excitations of a ferroquadrupolar spin nematic to gravitational waves in flat spacetime. I present further intuitions that gravitational waves and the nematic excitations are both quadrupolar excitations with the same fundamental character. To set the stage for results I will discuss in Chapter 5, I then briefly review the homotopy class of spin nematics based on their respective order parameter, and discuss the attractive nature of the point defects, consistent with a spin-2 field theory.

Finally, I review the state of the art in both solid state and cold atom experiments involving spin nematics, and discuss in particular techniques applicable to spinor condensates for observing quadrupolar order.

4.1 Quadrupolar order and spin nematics

In this Section I will introduce the reader to nematic phases of matter, historically discovered in the context of classical liquid crystals, and will motivate their relevance as a candidate platform for analogue gravitational waves.

Ultimately, the goal is to identify an ordered phase which preserves time-reversal symmetry, and has two independent Goldstone Bosons which are spin-2 excitations. We saw previously in the case of the Heisenberg antiferromagnet that dipolar order on the bipartite lattice restores time-reversal symmetry as far as the long wavelength physics is concerned. The corresponding vector order parameter gives us two dynamically independent spin-1 excitations. We will now see how nematic liquid crystals and spin nematics are ordered phases whose order parameters are symmetric, traceless, rank-2 tensors, which in addition preserve time-reversal symmetry. This already signals possible comparison with the structure of gravitational waves Eq. (1.56).

The first liquid crystals, discovered by Reinitzer in 1888 [199], arose in cholesterol benzoates extracted from carrot root, a molecule with inversion symmetry along the long axis. Reinitzer discovered that this substance exhibited two distinct phase transitions from the low temperature crystalline phase to the liquid phase. The intermediate phase, dubbed a liquid crystal, was characterized by anisotropy of the molecular degrees of freedom and led to unique optical properties. Following their initial discovery, it took a long time for the existence of such liquid crystal phases to be widely accepted [200].

Much of the early theory of liquid crystals was developed by Oseen by 1933 [201]. In order to revive interest in the topic, this was much later expanded upon by Charles Frank in his seminal 1958 paper [202]. These works laid out the classification for liquid crystal phases, one of which is the nematic phase characterized by loss of orientational symmetry without loss of translational symmetry. In the nematic phase, it is energetically favourable for the long axis of the molecules to align, thus breaking rotational symmetry through the selection of a direction characterized by the vector \mathbf{u} , called a director. Due to the inversion symmetry of the molecules, there is no way to distinguish any sense of their orientation between \mathbf{u} and $-\mathbf{u}$, therefore the order parameter must be a symmetric product of the vector \mathbf{u} [203]. As discussed in [110], the minimal and conventional choice describing a uniaxial nematic phase is the symmetric, traceless tensor of the form

$$\mathcal{Q}^{\alpha\beta} = \left(u^\alpha u^\beta \right) - \frac{1}{3} \delta^{\alpha\beta} u^\gamma u^\gamma . \quad (4.1)$$

As alluded to in Chapter 1, ordered phases of magnetic materials can exhibit phases characterized by an order parameter analogous to that of nematic liquid crystals, as shown in Eq. (1.31), defined again here explicitly on the lattice in terms of the SU(2) spin operators S_i^α

$$\langle Q_{ij}^{\alpha\beta} \rangle = \frac{1}{N} \left\langle \left[\frac{1}{2} \left(S_i^\alpha S_j^\beta + S_i^\beta S_j^\alpha \right) - \frac{1}{3} \delta^{\alpha\beta} S_i^\gamma S_j^\gamma \right] \right\rangle . \quad (4.2)$$

In analogy with the nematic liquid crystal, such phases receive the name spin nematics.

The most general definition of the order parameter here encompasses the possibility of bond ordered nematics formed by triplet pairs of spin- $\frac{1}{2}$ atoms [89–91], in addition to the case of on-site spin-1 (or higher) atoms. The latter case will occupy the attention of this Thesis, since spin-1 nematics are expected both in candidate magnetic insulators e.g. [99, 100] and spinor condensates e.g. [107].

Analogous to the $O(3)$ symmetry breaking of the high-temperature liquid phase in the transition to the nematic liquid crystal phase, spin nematics break $SU(2)$ symmetry while preserving time-reversal symmetry, leading to two independent Goldstone Bosons. In addition, and also in analogy with liquid crystals, spin nematics are characterized by a well-understood homotopy class and corresponding topological defects which will be discussed later in this Chapter.

The on-site operator $Q^{\alpha\beta}$ arises as the symmetric and traceless component of a general tensor operator [11, 78, 79, 82]

$$A^{\alpha\beta} = S^{\dagger\alpha} S^{\beta} . \quad (4.3)$$

The A operator decomposes into three spherical tensors which transform under rotation like objects of angular momentum $l = 0$, $l = 1$ and $l = 2$ respectively. The first is the scalar

$$\rho = S^{\dagger\alpha} S^{\alpha} , \quad (4.4)$$

which measures the length of the spin degree of freedom. Next, the antisymmetric components define the dipole moment

$$S^{\gamma} = \epsilon^{\alpha\beta\gamma} S^{\dagger\alpha} S^{\beta} , \quad (4.5)$$

Finally there is the symmetric and traceless rank-2 tensor operator

$$Q^{\alpha\beta} = \frac{1}{2} (S^{\alpha} S^{\beta} + S^{\beta} S^{\alpha}) - \frac{1}{3} \delta^{\alpha\beta} S^{\gamma} S^{\gamma} . \quad (4.6)$$

corresponding to the quadrupole moment. The symmetric and traceless conditions

$$Q^{\alpha\beta} = Q^{\beta\alpha} , \quad (4.7a)$$

$$\text{Tr}(Q) = 0 , \quad (4.7b)$$

mean that there are five independent quadrupole moments. These are conventionally defined by [10]

$$\mathbf{Q} = \begin{pmatrix} \frac{1}{2}(Q^{xx} - Q^{yy}) \\ \frac{1}{\sqrt{3}}(2Q^{zz} - Q^{xx} - Q^{yy}) \\ Q^{xy} \\ Q^{yz} \\ Q^{zx} \end{pmatrix} , \quad (4.8)$$

whose components satisfy the relation

$$\sum_{\alpha,\beta} Q^{\alpha\beta} Q^{\alpha\beta} = 2\mathbf{Q} \cdot \mathbf{Q} . \quad (4.9)$$

The operators $Q^{\alpha\beta}$ are non-trivial for all irreducible representations of $SU(2)$ with

$$s \geq 1 , \quad (4.10)$$

and on-site spin-nematic phases can be thus supported in spin systems with, at least, spin-1.

In summary, for spin-nematic phases characterized by a non-trivial expectation value of the single-site quadrupole operators, Eq. (4.2), the following generically holds

$$\langle \rho \rangle = s(s+1) , \quad (4.11a)$$

$$\langle S^\alpha \rangle = 0 , \quad (4.11b)$$

$$\langle Q^{\alpha\beta} \rangle \neq 0 , \quad (4.11c)$$

such that $SU(2)$ symmetry is spontaneously broken while simultaneously preserving time-reversal symmetry. The operator ρ is non-dynamical in the spin nematic phase, such that there are no longitudinal oscillations of the spin degree of freedom.

In the next Section, we will see how to describe the dynamical modes of such phases, and how in the low-energy limit, these modes are purely quadrupolar, corresponding to spin-2 Goldstone Bosons. I will review the spin coherent state formalism required to describe a Hilbert space in which quadrupolar degrees of freedom are non-trivial. This will be necessary to build a low-energy field theory for a quantum spin nematic.

4.2 Representation of nematic order and nematic Goldstone modes in spin-1 magnets

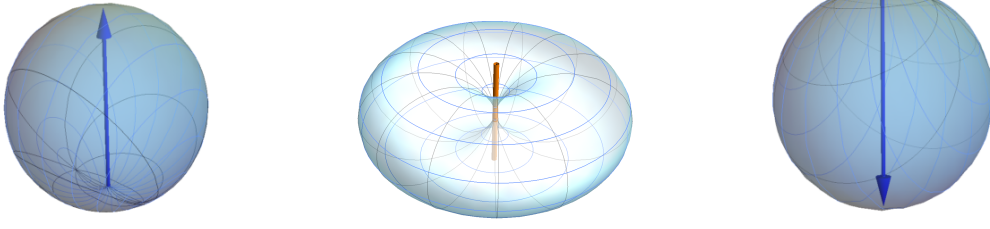
After having introduced the order parameter for spin nematics, I aim in this Section to extract the corresponding description of tensor Goldstone Bosons, as they appear in magnetic insulators and spinor condensates. To this end, I first describe conventional representations for spin-1 magnets [10] and their excitations. Later in this Chapter, I will show how the nature of these excitations are in one-to-one correspondence with the tensor modes of linearized gravity, a key result in this Thesis.

The on-site rank-2 tensor operator describing spin nematic order is only non-trivially defined for systems with spin-1 or greater. For the purpose of this Thesis, I will focus on the case of spin-1 magnets and spinor condensates. In this case, the Hilbert space is spanned by the magnetic basis states

$$|s = 1, m = 1\rangle \equiv |1\rangle , \quad (4.12)$$

$$|s = 1, m = 0\rangle \equiv |0\rangle , \quad (4.13)$$

$$|s = 1, m = -1\rangle \equiv |\bar{1}\rangle , \quad (4.14)$$


 (a) Magnetic state $|1\rangle$.

 (b) Nematic state $|0\rangle$.

 (c) Magnetic state $|\bar{1}\rangle$.

Figure 4.1: (a) The magnetic state with quantum number $m = 1$ can be represented by an $O(3)$ vector pointing along the positive z direction. (b) The spin probability surface of the $|0\rangle$ state is characterized by absence of favoured dipolar orientation, and showcases inversion symmetry reflective of the preserved time-reversal symmetry. This state is clearly quadrupolar. (c) The magnetic state with quantum number $m = -1$ can be represented by an $O(3)$ vector pointing along the negative z direction. See e.g. [10] or Appendix E for descriptions of how to define these surfaces.

whose probability density surfaces are shown in Fig. 4.1.

For each of the three magnetic basis states, visualized in Fig. 4.1, we find the following operator expectation values

$$\langle 1|S^\alpha|1\rangle = \delta^{\alpha z}, \quad \langle 0|S^\alpha|0\rangle = 0, \quad \langle \bar{1}|S^\alpha|\bar{1}\rangle = \delta^{\alpha z} \quad (4.15a)$$

$$\langle 1|(S^\alpha)^2|1\rangle = \langle \bar{1}|(S^\alpha)^2|\bar{1}\rangle = 0, \quad (4.15b)$$

$$\langle 0|(S^x)^2|0\rangle = \langle 0|(S^y)^2|0\rangle = 0, \quad (4.15c)$$

$$\langle 0|(S^z)^2|0\rangle \neq 0. \quad (4.15d)$$

This indicates that the magnetic states $|1\rangle$ and $|\bar{1}\rangle$ have dipolar character, and the nematic state $|0\rangle$ has a quadrupolar character. For the description of spin nematics in which the ground state has quadrupolar character, I will adopt a more suitable basis, following e.g. [10]. This basis is the time reversal invariant basis, see Fig. 4.2, defined as follows in terms of the magnetic basis ¹

$$|x\rangle = i\frac{|1\rangle - |\bar{1}\rangle}{\sqrt{2}}, \quad |y\rangle = \frac{|1\rangle + |\bar{1}\rangle}{\sqrt{2}}, \quad |z\rangle = -i|0\rangle, \quad (4.17)$$

In time-reversal invariant basis, the representation of any state in the spin-1 Hilbert space is described by a vector \mathbf{d} , which takes the form

$$|\mathbf{d}\rangle = \sum_{\alpha} d^{\alpha} |\alpha\rangle, \quad (4.18)$$

¹The inverse basis mapping takes the form

$$|1\rangle = |x\rangle + i|y\rangle, \quad |0\rangle = i|z\rangle, \quad |\bar{1}\rangle = -|x\rangle + i|y\rangle. \quad (4.16)$$

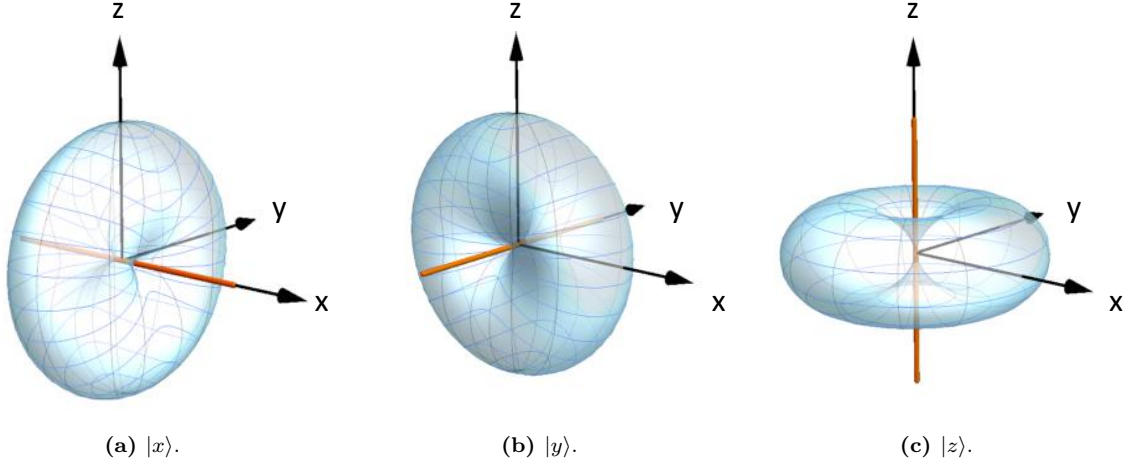


Figure 4.2: The three time-reversal invariant states defined in Eq. 4.17, with orientations along the respective coordinate axes. States in this basis are described by the complex vector \mathbf{d} defined in Eq. 4.18.

where the coefficients d^α of the director \mathbf{d} are generically complex-valued, and with

$$|\mathbf{d}| = 1, \quad (4.19)$$

In the time-reversal invariant basis it is explicitly clear that quadrupolar states are purely real (or purely imaginary), while the dipolar states necessarily mix linear superpositions of real and imaginary components. It is therefore convenient to decompose the director in terms of its real and imaginary components

$$\mathbf{d} = \mathbf{u} + i\mathbf{v}, \quad (4.20)$$

where the normalization of \mathbf{d} remains fixed, and the norms of \mathbf{u} and \mathbf{v} are not independent.

Since the dipolar components are finite when \mathbf{u} and \mathbf{v} are simultaneously finite, the dipolar expectation value can also be expressed by the antisymmetric composition of the director components

$$\langle \mathbf{S} \rangle = \mathbf{u} \times \mathbf{v}, \quad (4.21)$$

while the quadrupolar components take the form

$$\begin{aligned} \langle Q^{\alpha\beta} \rangle &= \frac{1}{2} (\mathbf{d}^{\dagger\alpha} \mathbf{d}^\beta + \mathbf{d}^{\dagger\beta} \mathbf{d}^\alpha) - \frac{1}{3} \delta^{\alpha\beta} \mathbf{d}^{\dagger\gamma} \mathbf{d}^\gamma \\ &= (u^\alpha u^\beta + v^\alpha v^\beta) - \frac{1}{3} \delta^{\alpha\beta} (u^\gamma u^\gamma + v^\gamma v^\gamma). \end{aligned} \quad (4.22)$$

Equipped with this description, we can return to assessing the expectation value of the quadrupole operator within a spin nematic, in order to explicitly determine the channels available to dynamical fluctuations. Explicitly in terms of the spin-1 director components, the expectation value of the quadrupole operator in matrix representation

is

$$\langle Q^{\alpha\beta} \rangle = \frac{1}{2} \begin{pmatrix} 2(u^x)^2 + 2(v^x)^2 - \frac{2}{3} & u^x u^y + v^x v^y & u^x u^z + v^x v^z \\ u^x u^y + v^x v^y & 2(u^y)^2 + 2(v^y)^2 - \frac{2}{3} & u^y u^z + v^y v^z \\ u^x u^z + v^x v^z & u^y u^z + v^y v^z & 2(u^z)^2 + 2(v^z)^2 - \frac{2}{3} \end{pmatrix}. \quad (4.23)$$

Assuming a quadrupolar ordered ground state, with purely real director \mathbf{d} aligned with one of the coordinate axes, e.g. the z -axis,

$$\mathbf{d} = (0, 0, u^z) = (0, 0, 1), \quad (4.24)$$

then the expectation value of the order parameter in the spin nematic ground state takes a simpler form

$$Q = \begin{pmatrix} -\frac{1}{3} & 0 & 0 \\ 0 & -\frac{1}{3} & 0 \\ 0 & 0 & \frac{2}{3} \end{pmatrix}. \quad (4.25)$$

To leading order, we can semi-classically express the fluctuations away from the ground state, cf.[11]

$$\tilde{\mathbf{d}} = (\phi^x + i\psi^x, \phi^y + i\psi^y, 1 - \mathcal{O}(\phi^2) - \mathcal{O}(\psi^2)), \quad (4.26)$$

for real fields ϕ^α and ψ^α . The oscillations of the ϕ field correspond to real rotations, and cost no energy at long wavelength. These are the two symmetry restoring Goldstone modes for the spin nematic. On the other hand, the oscillations of the ψ field correspond to imaginary transformations which deform a quadrupolar distribution into a dipolar one, and only play a role at finite energies. Therefore in the low-energy limit, the semi-classical fluctuations of the ground state take the form

$$\tilde{Q}^{xz} = \begin{pmatrix} 0 & 0 & \phi^x \\ 0 & 0 & 0 \\ \phi^x & 0 & 0 \end{pmatrix}, \quad \tilde{Q}^{yz} = \begin{pmatrix} 0 & 0 & 0 \\ 0 & 0 & \phi^y \\ 0 & \phi^y & 0 \end{pmatrix}, \quad (4.27)$$

and as symmetric tensors, correspond to quadrupolar part of the general tensor Eq. (4.3). Using the transformation described in Eq. (2.135), these tensors transform as

$$R_z[\theta] \tilde{Q}^{xz} = e^{i2\theta} \tilde{Q}^{xz}, \quad (4.28)$$

$$R_z[\theta] \tilde{Q}^{yz} = e^{i2\theta} \tilde{Q}^{yz}, \quad (4.29)$$

where $R_z[\theta]$ is the matrix encoding a rotation about the z -axis, defined previously in Eq. 2.138. These excitations thus respectively correspond to two independent spin-2 Goldstone Bosons. Fluctuations of the diagonal elements would correspond to longitudinal spin oscillations, which on physical grounds are disallowed. The remaining off-diagonal elements contribute to the oscillations only to quadratic order in the fluctuation amplitude ϕ^α .

We can thus conclude that spin nematics harbour spin-2 Goldstone Bosons. It remains to be shown how these oscillations are harmonic in nature, akin to the spin-2

field excitations of linearized gravity, and that they are in clear one-to-one correspondence with gravitational waves. In the next Section, I will introduce the reader to spin-coherent states for spin-1, as will be later used for the development of an effective low-energy field theory for the spin nematic.

4.3 The $s = 1$ spin coherent states

Recall that in Section 3.3.2 we saw how to construct coherent states for spin- $\frac{1}{2}$. Following treatments in e.g. [5, 10] we will now learn why this representation is insufficient for spin greater than $\frac{1}{2}$, and equip ourselves with the equivalent notion of spin coherent states for the spin-1 case. This will be used later in this Chapter in order to later construct a low-energy field theory for a spin nematic phase.

It is reasonable to assume that the magnetic basis states are at least partly connected by the generators of $SU(2)$. The internal spin state of a massive particle arises from the part of the Lorentz group that does not affect the four-momentum. That corresponds to $O(3)$, or its isomorphism $SU(2)$. In the case of spin-1, the $SU(2)$ generators are given by

$$S^x = \frac{1}{\sqrt{2}} \begin{pmatrix} 0 & 1 & 0 \\ 1 & 0 & 1 \\ 0 & 1 & 0 \end{pmatrix}, \quad S^y = \begin{pmatrix} 0 & -i & 0 \\ i & 0 & -i \\ 0 & i & 0 \end{pmatrix}, \quad S^z = \begin{pmatrix} 1 & 0 & 0 \\ 0 & 0 & 0 \\ 0 & 0 & -1 \end{pmatrix}. \quad (4.30)$$

This is also a representation of Wigner's Little group for massive particles, and these generators internally transform spin states within their respective Hilbert space [204]. However, it turns out that these generators are insufficient to span the landscape of all possible internal states. To see why this is so, consider the arbitrary superposition expressed in terms of the magnetic basis of states

$$|\Omega\rangle = \alpha |1\rangle + \beta |0\rangle + \gamma |\bar{1}\rangle, \quad (4.31)$$

where α, β, γ are arbitrary complex coefficients. There are in total six real degrees of freedom associated to these coefficients, though two are not independent. This is due, firstly, to the normalization constraint, and secondly, to the gauge freedom associated to the global phase of the wavefunction. Therefore, to describe an arbitrary spin-1 state we must be able to transform the following number of degrees of freedom

$$6 - 2 = 4. \quad (4.32)$$

If we next examine the states spanned by the generators of $SU(2)$ acting on the magnetic basis states

$$e^{iS_\alpha \lambda^\alpha} |1\rangle = e^{\frac{i\lambda_3}{2}} |1\rangle + e^{\frac{i}{2}(\lambda_1 + i\lambda_2)} |0\rangle + |\bar{1}\rangle, \quad (4.33a)$$

$$e^{iS_\alpha \lambda^\alpha} |0\rangle = e^{\frac{i}{2}(\lambda_1 - i\lambda_2)} |1\rangle + |0\rangle + e^{\frac{i}{2}(\lambda_1 + i\lambda_2)} |\bar{1}\rangle, \quad (4.33b)$$

$$e^{iS_\alpha \lambda^\alpha} |\bar{1}\rangle = |1\rangle + e^{\frac{i}{2}(\lambda_1 - i\lambda_2)} |0\rangle + e^{\frac{-i\lambda_3}{2}} |\bar{1}\rangle, \quad (4.33c)$$

it is clear that $SU(2)$ transformations cannot map each basis state onto any other arbitrary basis state. Therefore, we cannot obtain a general expression for $|\Omega\rangle$ by $SU(2)$ transformation. The best we could do is to reach a subsection of the Hilbert space spanned by

$$|\Omega\rangle = \frac{(1 + \cos \theta)}{2} e^{-i\phi} |1\rangle + \frac{\sin \theta}{\sqrt{2}} |0\rangle + \frac{(1 - \cos \theta)}{2} e^{-i\phi} |\bar{1}\rangle . \quad (4.34)$$

Pragmatically we can see why this is the case: there are only three degrees of freedom λ associated to the $SU(2)$ transformations, and as we have seen before in Section 3.3.2, one of these corresponds to a trivial redefinition of phase. However, to describe an arbitrary normalized spin-1 coherent state, we need four degrees of freedom at minimum. This means that there are generators missing from our attempt to describe the spin-coherent states.

Recall that for the spin- $\frac{1}{2}$ case, the Hilbert space has only two independent degrees of freedom. In that case the Hilbert space is coincidentally spanned by the Little group. However, for spins greater than $\frac{1}{2}$, there are more internal degrees of freedom than can be described by the $SU(2)$ generators alone.

We can reconcile this in the spin-1 case by observing that there is a quadrupole sector in the Hilbert space. We can see from Eq. (4.33b) that for a state with angular momentum quantum number

$$m = 0 , \quad (4.35)$$

there is no net dipole. The corresponding eigenstate of S_z cannot be rotated into a purely dipolar state. Conversely, by considering e.g. Eq. (4.33a) we see that neither of the dipolar states can be rotated exclusively onto the $|0\rangle$ state. As observed in the previous Section, it is clear that real rotations remain within the respective spaces of dipole and quadrupole, while imaginary rotations mix the states between these two sectors of the Hilbert space. It is further worth noting that the symmetries of the Hilbert space are not necessarily in correspondence with the symmetries of the action. In the spin nematic, the Goldstone modes arise from the broken $SU(2)$ symmetry present in the action, corresponding to the real rotations that map quadrupoles to quadrupoles. For a time-reversal preserving state, there will be a purely real or purely imaginary director. Thus there are two broken generators, and these correspond to the two Goldstone modes. However, at higher energies the imaginary rotations allowed by the symmetry generators of the Hilbert space become available.

With these properties in mind, the off-diagonal generators of $SU(3)$ form a natural representation for transformations between states in the Hilbert space [5, 6]. This can be generalized to $U(3)$ generators where required, and will be discussed briefly in Chapter 5 [11, 82].

A complete representation of $SU(3)$ is given by the Gell-Mann matrices

$$\lambda_1 = \begin{pmatrix} 0 & -i & 0 \\ i & 0 & 0 \\ 0 & 0 & 0 \end{pmatrix} \quad \lambda_2 = \begin{pmatrix} 0 & 0 & -i \\ 0 & 0 & 0 \\ i & 0 & 0 \end{pmatrix} \quad \lambda_3 = \begin{pmatrix} 0 & 0 & 0 \\ 0 & 0 & -i \\ 0 & i & 0 \end{pmatrix} \quad (4.36a)$$

$$\lambda_4 = \begin{pmatrix} 0 & -1 & 0 \\ 1 & 0 & 0 \\ 0 & 0 & 0 \end{pmatrix} \quad \lambda_5 = \begin{pmatrix} 0 & 0 & -1 \\ 0 & 0 & 0 \\ 1 & 0 & 0 \end{pmatrix} \quad \lambda_6 = \begin{pmatrix} 0 & 0 & 0 \\ 0 & 0 & -1 \\ 0 & 1 & 0 \end{pmatrix} \quad (4.36b)$$

$$\lambda_7 = \begin{pmatrix} 1 & 0 & 0 \\ 0 & -1 & 0 \\ 0 & 0 & 0 \end{pmatrix} \quad \lambda_8 = \frac{1}{\sqrt{3}} \begin{pmatrix} 1 & 0 & 0 \\ 0 & 1 & 0 \\ 0 & 0 & -2 \end{pmatrix} \quad (4.36c)$$

where $\lambda_1, \lambda_2, \lambda_3$ are spatial rotation generators and $\lambda_4, \lambda_5, \lambda_6$ are the generators of complex rotations and the diagonal generators λ_7, λ_8 do not physically alter the states. Let us now use the SU(3) rotation generators to specify the coherent state representation for an arbitrary spin-1 state. Recall we can decompose the director into real and imaginary parts as follows

$$|\mathbf{d}\rangle = |\mathbf{u}\rangle + i|\mathbf{v}\rangle \equiv |\mathbf{u}, \mathbf{v}\rangle . \quad (4.37)$$

The general spin coherent state for spin-1 can then be expressed as

$$|\mathbf{u}, \mathbf{v}\rangle = \sum_{j \in x, y, z} U |j\rangle , \quad (4.38)$$

with unitary operator U defined as

$$U = e^{i \sum_{m=1}^6 \lambda_m \phi_m} , \quad (4.39)$$

where ϕ_m are the respective angles through which the state $|j\rangle$ is rotated by the corresponding generators of SU(3).

For these spin coherent states, the resolution of identity takes the form

$$\mathbb{1} = \int_{\Omega} d\mu[\mathbf{d}] |\mathbf{d}\rangle \langle \mathbf{d}| \quad (4.40a)$$

$$= \frac{2S+1}{2\pi} \int d\mathbf{u}^3 d\mathbf{v}^3 \delta(\mathbf{u}^2 + \mathbf{v}^2 - 1) |\mathbf{u}, \mathbf{v}\rangle \langle \mathbf{u}, \mathbf{v}| . \quad (4.40b)$$

where the area of the spheres spanned by the fields \mathbf{u} and \mathbf{v} is

$$\Omega_{\text{RP}^2} = \frac{1}{2} 4\pi . \quad (4.41)$$

In conclusion, we have now seen why more general SU(N) representations are needed to capture the Hilbert space of N-level spin systems, and have seen explicitly the spin coherent state basis for the spin-1 case. Next we will examine a microscopic spin-1 model and use the spin coherent state basis to rederive the non-linear sigma model for a ferroquadrupolar spin nematic.

4.4 Quantum non-linear sigma model for a spin-1 nematic

In this Section, I showcase how the low-energy physics of a ferroquadrupolar spin-nematic exhibits a Gaussian action, which I here establish to be in correspondence with that of linearized gravity. Until this point, all the framework developed has been model independent. In order to provide a more concrete derivation of the analogue to linearized gravity, and to place it on microscopic grounds, in this Section I first review the Bilinear-Biquadratic model, and its ferroquadrupolar phase—which is a spin nematic phase as thus far presented. I then rederive that its low-energy field theory is a non-linear sigma model, as first shown by Ivanov and Kolezhuk [93], inspired by treatments in [5, 170, 171, 205].

4.4.1 The minimal spin-1 model: the Bilinear Biquadratic model

The Bilinear-Biquadratic model is the simplest exchange model which describes both dipolar and quadrupolar degrees of freedom, as present in magnetic systems whose atoms possess a spin-1 moment. In terms of dipolar spin operators, its Hamiltonian takes the following form

$$H_{BBQ} = \sum_{\langle ij \rangle} J_1 \mathbf{S}_i \cdot \mathbf{S}_j + \sum_{\langle ij \rangle} J_2 (\mathbf{S}_i \cdot \mathbf{S}_j)^2 . \quad (4.42)$$

This model is generally SU(2) symmetric [11], except at the high symmetry point defined at

$$J_1 = J_2 , \quad (4.43)$$

where the model becomes SU(3) symmetric [206, 207]. In terms of the quadrupole operators

$$Q_i^{\alpha\beta} Q_j^{\alpha\beta} = 4(\mathbf{S}_i \mathbf{S}_j)^2 + 2\mathbf{S}_i \mathbf{S}_j - \frac{4}{3}s^2(s+1)^2 , \quad (4.44)$$

the quadrupole contribution in the Hamiltonian can be explicitly expressed

$$H_{BBQ} = \sum_{\langle ij \rangle} \left(J_1 - \frac{J_2}{2} \right) \mathbf{S}_i \cdot \mathbf{S}_j + \sum_{\langle ij \rangle} \frac{J_2}{4} Q_i^{\alpha\beta} \cdot Q_j^{\alpha\beta} - J_2 \frac{2}{3} s^2 (s+1)^2 . \quad (4.45)$$

Examination of Eq. (4.45) reveals that where the bilinear exchange term in Q is dominant, it is energetically favourable for the quadrupolar degrees of freedom to order. Therefore, a spin nematic phase characterized by ferroquadrupolar order is dominant in this model where negative J_2 interactions are much larger than the J_1 interactions

e.g.[10]. Specifically on the triangular lattice, the ferroquadrupolar phase spans [4, 95]

$$J_2 < 0 \quad J_1 \ll J_2 \quad -\frac{\sqrt{2}}{2} < J_1 < \frac{5\pi}{4}. \quad (4.46)$$

This expectation has been confirmed through both mean field calculations and numerical studies on different lattices [4, 6, 95, 208], see e.g. Fig. 1.2a. Ferroquadrupolar alignment is expected in the region of the phase diagram where negative J_2 interactions dominate extending until the enhanced symmetry boundary.

We next use this model to construct a field theory valid for the ferroquadrupolar phase.

4.4.2 Effective low-energy field theory of the ferroquadrupolar spin nematic

In this Section, using the spin-coherent states and the bilinear-biquadratic model, as outlined in [93, 171, 205], we will arrive at a spin-2 field theory for the nematic ground state.

As we have seen in Chapter 3, the Hamiltonian of a finite temperature quantum system is related to the partition function through the path integral representation

$$Z = \text{Tr}(e^{-\beta H}) = \lim_{\substack{N \rightarrow \infty \\ \delta\tau \rightarrow 0}} \text{Tr}[\hat{T}(e^{-\delta\tau H})^N], \quad (4.47)$$

where \hat{T} is the time ordering operator. The partition function is also in turn connected to the Euclidean action

$$Z = \lim_{\substack{N \rightarrow \infty \\ \delta\tau \rightarrow 0}} \int \mathcal{D}[\mathbf{d}] e^{-S_E[\mathbf{d}]}, \quad (4.48)$$

From Eq. (4.47), the partition function can be expressed using the spin-coherent states

$$Z = \lim_{\substack{N \rightarrow \infty \\ \delta\tau \rightarrow 0}} \left(\frac{2S+1}{4\pi} \right)^N \sum_{\mathbf{d}_\alpha} \langle \mathbf{u}_\alpha, \mathbf{u}_\alpha | \hat{T} \left(\int d\mu[\mathbf{d}] |\mathbf{u}, \mathbf{v}\rangle \langle \mathbf{u}, \mathbf{v}| e^{-\delta\tau H} \right)^N | \mathbf{u}_\alpha, \mathbf{u}_\alpha \rangle, \quad (4.49)$$

$$= \lim_{\substack{N \rightarrow \infty \\ \delta\tau \rightarrow 0}} \prod_{t=1}^N \left[\int d\mu[\mathbf{d}_t] e^{-\delta\tau (\langle A \rangle + \langle H \rangle)} \right], \quad (4.50)$$

$$= \lim_{\substack{N \rightarrow \infty \\ \delta\tau \rightarrow 0}} \int d\mu[\mathbf{d}_t] e^{-\sum_{t=1}^N \delta\tau (\langle A \rangle + \langle H \rangle)}, \quad (4.51)$$

where the geometrical Berry-phase term takes the form

$$\langle A \rangle = \frac{1}{\delta\tau} (\langle \mathbf{u}_t, \mathbf{v}_t | \mathbf{u}_t, \mathbf{v}_t \rangle - \langle \mathbf{u}_t, \mathbf{v}_t | \mathbf{u}_{t+1}, \mathbf{v}_{t+1} \rangle), \quad (4.52a)$$

$$= \frac{1}{\delta\tau} ((\mathbf{u}_t - i\mathbf{v}_t)(\mathbf{u}_t + i\mathbf{v}_t) - (\mathbf{u}_t - i\mathbf{v}_t)(\mathbf{u}_{t+1} + i\mathbf{v}_{t+1})), \quad (4.52b)$$

$$= -\frac{1}{\delta\tau} (\mathbf{u}_t(\mathbf{u}_{t+1} - \mathbf{u}_t) + \mathbf{v}_t(\mathbf{v}_{t+1} - \mathbf{v}_t) - i\mathbf{v}_t(\mathbf{u}_{t+1} - \mathbf{u}_t) + i\mathbf{u}_t(\mathbf{v}_{t+1} - \mathbf{v}_t)) , \quad (4.52c)$$

which after evaluating the limit $\delta\tau \rightarrow 0$ becomes

$$A \approx -(\mathbf{u}\partial_\tau\mathbf{u} + \mathbf{v}\partial_\tau\mathbf{v} + i\mathbf{u}\partial_\tau\mathbf{v} - i\mathbf{v}\partial_\tau\mathbf{u}) . \quad (4.53)$$

The Hamiltonian term can be most clearly derived by expressing the Bilinear-Biquadratic model in terms of the expectation value of the director [5]

$$\langle H_{BBQ} \rangle = \sum_{\langle ij \rangle} J_1 |\mathbf{d}_i \cdot \bar{\mathbf{d}}_j|^2 + \sum_{\langle ij \rangle} (J_2 - J_1) |\mathbf{d}_i \cdot \mathbf{d}_j|^2 + J_2 . \quad (4.54)$$

In the low-energy limit, we can approximate the on-site degrees of freedom by continuous fields

$$\mathbf{d}_i \approx \mathbf{d}(\mathbf{r}, \tau) . \quad (4.55)$$

The fields at each of the nearest-neighbour sites can be described to first order in terms of the Taylor series expansion

$$\begin{aligned} d_j &\approx \mathbf{d}(\mathbf{r} + \boldsymbol{\alpha}_j, \tau) \\ &\approx \mathbf{d}(\mathbf{r}, \tau) + \alpha_j^m \partial_m \mathbf{d}(\mathbf{r}, \tau) + \mathcal{O}(\partial_m^2 \mathbf{d}) , \end{aligned} \quad (4.56)$$

where $\boldsymbol{\alpha}_j$ is the vector connecting each site to the j^{th} -neighbour, with Cartesian components denoted by m . Note that we can always decompose the contributions in the Taylor expansion for any lattice geometry into the derivatives along the Cartesian directions m with α_j^m representing the appropriate numerical prefactors².

²On the triangular lattice, there are six nearest neighbour positions defined by

$$\mathbf{r} + \boldsymbol{\alpha}_j = \mathbf{r} + \left(\cos\left(\frac{2\pi}{6}j\right), \sin\left(\frac{2\pi}{6}j\right), 0 \right) , \quad (4.57)$$

for j taking integer values from 1 to 6, where

$$\mathbf{r} + \boldsymbol{\alpha}_1 = \mathbf{r} - \boldsymbol{\alpha}_4 , \quad (4.58a)$$

$$\mathbf{r} + \boldsymbol{\alpha}_2 = \mathbf{r} - \boldsymbol{\alpha}_5 , \quad (4.58b)$$

$$\mathbf{r} + \boldsymbol{\alpha}_3 = \mathbf{r} - \boldsymbol{\alpha}_6 . \quad (4.58c)$$

and where

$$|\boldsymbol{\alpha}_j| = a , \quad (4.59)$$

with lattice spacing a . Then, for the triangular lattice

$$\mathbf{d}(\mathbf{r} + \boldsymbol{\alpha}_1, \tau) \approx \mathbf{d}(\mathbf{r}, \tau) + a\partial_x\mathbf{d}(\mathbf{r}, \tau) + \mathcal{O}(\partial_m^2 \mathbf{d}) , \quad (4.60a)$$

$$\mathbf{d}(\mathbf{r} + \boldsymbol{\alpha}_2, \tau) \approx \mathbf{d}(\mathbf{r}, \tau) + \frac{a}{2}\partial_x\mathbf{d}(\mathbf{r}, \tau) + \frac{\sqrt{3}a}{2}\partial_y\mathbf{d}(\mathbf{r}, \tau) + \mathcal{O}(\partial_m^2 \mathbf{d}) , \quad (4.60b)$$

$$\mathbf{d}(\mathbf{r} + \boldsymbol{\alpha}_3, \tau) \approx \mathbf{d}(\mathbf{r}, \tau) - \frac{a}{2}\partial_x\mathbf{d}(\mathbf{r}, \tau) + \frac{\sqrt{3}a}{2}\partial_y\mathbf{d}(\mathbf{r}, \tau) + \mathcal{O}(\partial_m^2 \mathbf{d}) . \quad (4.60c)$$

We can then express the interaction terms

$$\begin{aligned} \mathbf{d}_i \bar{\mathbf{d}}_j &\equiv \mathbf{d}(\mathbf{r}, \tau) \bar{\mathbf{d}}(\mathbf{r} + \boldsymbol{\alpha}_j, \tau) \\ &\approx \mathbf{d}(\mathbf{r}, \tau) \left(\bar{\mathbf{d}}(\mathbf{r}, \tau) + \alpha_j^m \partial_m \bar{\mathbf{d}}(\mathbf{r}, \tau) + \mathcal{O}(\partial_m^2 \bar{\mathbf{d}}) \right) , \end{aligned} \quad (4.61a)$$

$$\begin{aligned} \mathbf{d}_i \mathbf{d}_j &\equiv \mathbf{d}(\mathbf{r}, \tau) \mathbf{d}(\mathbf{r} + \boldsymbol{\alpha}_j, \tau) \\ &\approx \mathbf{d}(\mathbf{r}, \tau) \left(\mathbf{d}(\mathbf{r}, \tau) + \alpha_j^m \partial_m \mathbf{d}(\mathbf{r}, \tau) + \mathcal{O}(\partial_m^2 \mathbf{d}) \right) . \end{aligned} \quad (4.61b)$$

Simplifying the notation by representing the fields $\mathbf{d}(\mathbf{r}, \tau)$ instead as \mathbf{d} , leads to the following formulation of the continuum expectation value of the Hamiltonian

$$\langle H_{BBQ} \rangle \approx \int \frac{d^d r}{a^d} \sum_{j=1}^{\frac{z}{2}} J_1 \left| \mathbf{d} \bar{\mathbf{d}} + \alpha_j^m \mathbf{d} \partial_m \bar{\mathbf{d}} \right|^2 + (J_2 - J_1) \left| \mathbf{d} \mathbf{d} + \alpha_j^m \mathbf{d} \partial_m \mathbf{d} \right|^2 , \quad (4.62)$$

where z is the coordination number of the lattice, specifying the number of nearest neighbours.

Working explicitly in terms of the component fields \mathbf{u} and \mathbf{v} , we can explicitly choose coordinates such that the ferroquadrupolar ground state is described by the purely real field \mathbf{u} , as is convention [93]. This allows the following simplifying assumptions to apply

$$\mathbf{u}^2 \gg \mathbf{v}^2 , \quad (4.63)$$

such that the terms

$$\mathbf{v} \partial_m \mathbf{v} , (\partial_m \mathbf{v})^2 \approx 0 . \quad (4.64)$$

One can also make the conventional choice [5, 6]

$$\mathbf{u} \cdot \mathbf{v} = 0 , \quad (4.65a)$$

$$\implies \partial_\tau (\mathbf{u} \cdot \mathbf{v}) = 0 , \quad (4.65b)$$

$$\implies \mathbf{u} \partial_\tau \mathbf{v} = -\mathbf{v} \partial_\tau \mathbf{u} . \quad (4.65c)$$

which fixes the global phase degree of freedom of the state \mathbf{d} , and allows further simplification using Eq. (4.65c). Neglecting terms $\mathcal{O}(v^3)$, the interaction terms become respectively

$$H_j^{J_1} \equiv J_1 \left| (\mathbf{u} + i\mathbf{v})(\mathbf{u} - i\mathbf{v}) + \alpha_j^m (\mathbf{u} + i\mathbf{v}) \partial_m (\mathbf{u} - i\mathbf{v}) \right|^2 \quad (4.66a)$$

$$= J_1 \left(1 + \alpha_j^m (\mathbf{u} \partial_m \mathbf{u} + 2i\mathbf{v} \partial_m \mathbf{u}) + (\alpha_j^m \mathbf{u} \partial_m \mathbf{u})^2 + 2i\alpha_j^m \mathbf{u} \partial_m \mathbf{u} \alpha_j^n \mathbf{v} \partial_n \mathbf{u} \right) , \quad (4.66b)$$

and

$$H_j^{J_2 - J_1} \equiv (J_2 - J_1) \left| (\mathbf{u} + i\mathbf{v})(\mathbf{u} + i\mathbf{v}) + \alpha_j^m (\mathbf{u} + i\mathbf{v}) \partial_m (\mathbf{u} + i\mathbf{v}) \right|^2 \quad (4.67a)$$

$$= (J_2 - J_1) \left(1 - 4\mathbf{u}^2 \mathbf{v}^2 + \alpha_j^m (\mathbf{u} \partial_m \mathbf{u} + 2i\mathbf{v} \partial_m \mathbf{u}) (\mathbf{u}^2 + 2i\mathbf{u} \mathbf{v} - \mathbf{v}^2) \right)$$

$$+ (\alpha_j^m \mathbf{u} \partial_m \mathbf{u})^2 + 2i\alpha_j^m \mathbf{u} \partial_m \mathbf{u} \alpha_j^n \mathbf{v} \partial_n \mathbf{u} \Big). \quad (4.67b)$$

Substituting back into the Hamiltonian term of the action, the terms linear in α_j^m cancel when summed over j , leaving the sufficiently general result

$$\mathcal{S}_{\mathcal{H}} = \int d\tau dx^d \left[2z(J_1 - J_2) \mathbf{u}^2 \mathbf{v}^2 + J_2 \sum_{j=1}^{\frac{z}{2}} (\alpha_j^m \partial_m \mathbf{u})^2 \right]. \quad (4.68)$$

We now return to the Berry phase term, noticing that

$$\mathbf{u}^2 + \mathbf{v}^2 = 1 \implies \mathbf{u} \partial_\tau \mathbf{u} + \mathbf{v} \partial_\tau \mathbf{v} = 0, \partial_\tau (\mathbf{u} \cdot \mathbf{v}) = 0 \implies \mathbf{u} \partial_\tau \mathbf{v} = -\mathbf{v} \partial_\tau \mathbf{u}, \quad (4.69a)$$

$$(4.69b)$$

such that,

$$\langle A \rangle = -2i\mathbf{u} \partial_\tau \mathbf{v} = 2i\mathbf{v} \partial_\tau \mathbf{u}. \quad (4.70)$$

Then, the full Euclidean action then takes the form

$$\mathcal{S}_E = \int d\tau dx^d \left[2z(J_1 - J_2) \mathbf{u}^2 \mathbf{v}^2 - 2i\mathbf{u} \partial_\tau \mathbf{v} + J_2 \sum_{j=1}^{\frac{z}{2}} (\alpha_j^m \partial_m \mathbf{u})^2 \right], \quad (4.71)$$

The Euler-Lagrange equations allow us to identify that one field is constrained in terms of the other. In this case

$$\mathbf{v} = \frac{-i\partial_\tau \mathbf{u}}{2z(J_1 - J_2)\mathbf{u}^2} \equiv i\chi_\perp \partial_\tau \mathbf{u}, \quad (4.72)$$

where I have defined the susceptibility

$$\chi_\perp = \frac{1}{2z(J_1 - J_2)}. \quad (4.73)$$

This means we can interpret \mathbf{v} as the fluctuating field, and ultimately the dynamics of the dominant field will depend exclusively on the configuration of the purely real \mathbf{u} field. This implies that in the small fluctuation limit the surviving components of the fluctuations will be almost exclusively quadrupolar. At higher energies, where fluctuations deviate more greatly from the ground state, the mutual dependence of the real and imaginary fields \mathbf{u} and \mathbf{v} leads to the mixing of the modes into the dipole channel. We will see this exemplified in dynamical simulation in the next Chapter.

In addition, we can identify a stiffness associated to the order

$$\rho = -J_2 \sum_{j=1}^{\frac{z}{2}} (\alpha_j^m)^2, \quad (4.74)$$

with the minus sign introduced on physical grounds that the stiffness be a positive quantity.

Transforming back to real time, finally, the ferroquadrupolar action in the low-energy limit has the form

$$\mathcal{S}_{FQ} = \int dt dx^d \left[\chi (\partial_t \mathbf{u})^2 - \rho (\partial_m \mathbf{u})^2 \right], \quad (4.75)$$

which is again a non-linear sigma model defined in terms of the real part of a director, \mathbf{u} , whose excitations are the quadrupolar spin-2 field excitations given in Eq. (4.27). To make explicit the quadrupolar nature of the action and its excitations, consider the field

$$Q^{\alpha\beta} = Q_{GS}^{\alpha\beta} + \tilde{Q}^{\alpha\beta}. \quad (4.76)$$

Choosing coordinates such that ground state is oriented along the z -axis, and the excitations are as described in Eq. (4.27), we find that the scalar contraction

$$\partial_\mu Q^{\dagger\alpha\beta} \partial^\mu Q^{\alpha\beta} = \partial_\mu \tilde{Q}^{\dagger\alpha\beta} \partial^\mu \tilde{Q}^{\alpha\beta}, \quad (4.77a)$$

$$= 2\partial_\mu (\phi^x - i\psi^x) \partial^\mu (\phi^x + i\psi^x) + 2\partial_\mu (\phi^y - i\psi^y) \partial^\mu (\phi^y + i\psi^y), \quad (4.77b)$$

$$= 2 \left(\partial_\mu (\phi)^2 + \partial_\mu (\psi)^2 \right), \quad (4.77c)$$

reduces to the Lagrangian for the dynamical part of the director. From this, it is clear that the action can be expressed as

$$\mathcal{S}_{FQ} = -\frac{1}{2} \int dt dr^d \left[-\chi_\perp (\partial^t Q^{\alpha\beta} \partial_t Q_{\alpha\beta}) + \rho_s (\partial^m Q^{\alpha\beta} \partial_m Q_{\alpha\beta}) \right], \quad (4.78)$$

by defining

$$Q_{\alpha\beta} = Q^{\dagger\alpha\beta}. \quad (4.79)$$

This form of the action parallels the linearized gravity action 2.111, and gives rise to a wave equation

$$\frac{1}{v^2} \partial_t \partial^t \tilde{Q}^{\alpha\beta} - \partial_n \partial^n \tilde{Q}^{\alpha\beta} = 0, \quad (4.80)$$

with wave speed ³

$$v = \sqrt{\rho_s / \chi_\perp}, \quad (4.82)$$

³For the triangular lattice, we can evaluate explicitly

$$\begin{aligned} v &= \sqrt{2z(J_1 - J_2)(-J_2) \sum_{j=1}^{\frac{z}{2}} (\alpha_j^m)^2} \\ &= 2\sqrt{3}\sqrt{3} J_2 a = 6 J_2 a. \end{aligned} \quad (4.81)$$

and relativistic dispersion

$$\omega(\mathbf{k}) = v|\mathbf{k}|. \quad (4.83)$$

The solutions to the equations of motion are harmonic spin-2 waves

$$Q^{\alpha\beta}(x, t) = \sum_{\sigma=1,2} \int d^3k \frac{1}{\sqrt{\omega(\mathbf{k})}} \left[\epsilon_{\alpha\beta}^{\sigma} a_{\sigma}^{\dagger}(\mathbf{k}) e^{ik_{\rho}x^{\rho}} + \left(\epsilon_{\alpha\beta}^{\sigma} \right)^* a_{\sigma}(\mathbf{k}) e^{-ik_{\rho}x^{\rho}} \right]. \quad (4.84)$$

that in the next Section I will prove to be in one-to-one correspondence with gravitational waves.

In conclusion, the ferroquadrupolar phase exhibits two tensorial Goldstone modes which in the low-energy limit remain purely quadrupolar, and are described by a non-linear sigma model reminiscent of the linearized gravity action.

4.5 What starts with action ends with action: a dictionary for spin-2 excitations

We have shown explicitly that the microscopic Bilinear-Biquadratic model is equivalent in the low-energy limit to a spin-2 field theory, whose fluctuations share the same Gaussian form as captured by the field theory for linearized gravity. Next I will expand concretely on how to map these respective fluctuations onto one another, and will present a deeper interpretation of the nature of the fluctuations.

4.5.1 Mapping linearized gravity gauge constraints onto the physical constraints of ferroquadrupolar order

We have seen that the low-energy field theory for the ferroquadrupolar phase takes a form reminiscent of the action for linearized gravity Eq. (2.111) after applying the gauge conditions

$$h_{\mu}^{\mu} = 0, \text{ [traceless]} \quad (4.85a)$$

$$h_{0\mu} = 0, \text{ [no scalar or vector components]} \quad (4.85b)$$

$$\partial^n h_{nm} = 0, \text{ [no longitudinal dynamics]}. \quad (4.85c)$$

Promoting the tensor description of \tilde{Q} to a 4×4 representation for closer comparison to the structure of gravitational waves, we can re-express the ground state and the fluctuating modes respectively as

$$Q^{\mu\nu} = Q_{GS}^{\mu\nu} + \tilde{Q}^{\mu\nu}, \quad (4.86)$$

such that the action can be expressed

$$\mathcal{S}_{\text{FQ}} = -\frac{1}{2} \int dt d^d x \left[-\chi_{\perp} (\partial^t \tilde{Q}^{\mu\nu} \partial_t \tilde{Q}_{\mu\nu}) + \rho_s (\partial^n \tilde{Q}^{\mu\nu} \partial_n \tilde{Q}_{\mu\nu}) \right]. \quad (4.87)$$

Note that the background metric in linearized gravity (nor full general relativity) is not traceless, no matter whether we consider Minkowski or Euclidean backgrounds. As in the case of the antiferromagnet analogue, it is best not to confuse the symmetry breaking ground state with the spacetime background that controls the coupling between terms in the action.

In this representation, the dynamical modes of the spin nematic are subject at minimum to the following physical constraints which in part mimic the conditions of Eq. (2.105).

$$\tilde{Q}_{\mu}^{\mu} = 0, \text{ [traceless]}, \quad (4.88a)$$

$$\tilde{Q}_{0\mu} = 0, \text{ [no scalar or vector components]}, \quad (4.88b)$$

The freedom to choose the orientation of the ground state means there is not automatically a parallel constraint to Eq. (2.105c).

For a system with order captured by a director pointing along the z -axis, the polarization tensors for the corresponding excitations [5, 11] can be described to leading order by the promoted objects

$$\tilde{\epsilon}_{\mu\nu}^1 = \frac{1}{2} \begin{pmatrix} 0 & 0 & 0 & 0 \\ 0 & 0 & 0 & 1 \\ 0 & 0 & 0 & 0 \\ 0 & 1 & 0 & 0 \end{pmatrix}, \quad \tilde{\epsilon}_{\mu\nu}^2 = \frac{1}{2} \begin{pmatrix} 0 & 0 & 0 & 0 \\ 0 & 0 & 0 & 0 \\ 0 & 0 & 0 & 1 \\ 0 & 0 & 1 & 0 \end{pmatrix}. \quad (4.89)$$

The general condition that describes this structure of the degrees of freedom for the ferroquadrupolar phase is

$$d_{\alpha} d_{\beta} Q^{\alpha\beta} = 0, \quad (4.90)$$

which is explicitly analogous to Eq. (2.105c)⁴, assuming that the director \mathbf{d} and the wavevector \mathbf{k} are parallel.

This therefore motivates the need to develop a unitary basis transformation such that we can identify a full dictionary between the excitations of the ferroquadrupolar phase in spin space and deformations of real space effected by a gravitational wave.

To connect these representations, we can define a transformation from real-space

⁴Note however that this condition does contain matrices $\tilde{Q}^{\alpha\beta}$ that satisfy the condition analogous to

$$d_{\alpha} \tilde{Q}^{\alpha} = 0. \quad (4.91)$$

to spin-space and back using a subset of the generators of $SU(4)$, namely, those which correspond to the real-valued generators of $SU(3)$ up to a zero padded row and column

$$\lambda_1 = \begin{pmatrix} 0 & 0 & 0 & 0 \\ 0 & 0 & 1 & 0 \\ 0 & 1 & 0 & 0 \\ 0 & 0 & 0 & 0 \end{pmatrix}, \quad \lambda_3^{xy} = \begin{pmatrix} 0 & 0 & 0 & 0 \\ 0 & 1 & 0 & 0 \\ 0 & 0 & -1 & 0 \\ 0 & 0 & 0 & 0 \end{pmatrix}, \quad (4.92a)$$

$$\lambda_6 = \begin{pmatrix} 0 & 0 & 0 & 0 \\ 0 & 0 & 0 & 0 \\ 0 & 0 & 0 & 1 \\ 0 & 0 & 1 & 0 \end{pmatrix}, \quad \lambda_3^{yz} = \begin{pmatrix} 0 & 0 & 0 & 0 \\ 0 & 0 & 0 & 0 \\ 0 & 0 & 1 & 0 \\ 0 & 0 & 0 & -1 \end{pmatrix}, \quad (4.92b)$$

$$\lambda_4 = \begin{pmatrix} 0 & 0 & 0 & 0 \\ 0 & 0 & 0 & 1 \\ 0 & 0 & 0 & 0 \\ 0 & 1 & 0 & 0 \end{pmatrix}, \quad \lambda_3^{xz} = \begin{pmatrix} 0 & 0 & 0 & 0 \\ 0 & 1 & 0 & 0 \\ 0 & 0 & 0 & 0 \\ 0 & 0 & 0 & -1 \end{pmatrix}, \quad (4.92c)$$

whose action on any ϵ or $\tilde{\epsilon}$ modifies only the spatial components of the polarization tensor, and corresponds to rotation of quadrupole moments without mixing in any spin dipole moments.

I here define a protocol to identify the excitation tensor for arbitrarily oriented ferroquadrupolar order with the structure of the tensor for a gravitational wave propagating along an arbitrary direction. This protocol can be divided into three steps.

1. The director \mathbf{d} is mapped onto the z -axis by rotating the polarization tensor through an angle $-\arccos(\mathbf{d} \cdot \hat{\mathbf{z}})$ around the orthogonal vector \mathbf{v}_d

$$\mathbf{v}_d = \frac{\mathbf{d} \times \hat{\mathbf{z}}}{|\mathbf{d} \times \hat{\mathbf{z}}|}, \quad \cos \theta = \hat{\mathbf{d}} \cdot \hat{\mathbf{z}}. \quad (4.93)$$

2. Then apply an $SU(4)$ transformation that maps the spin-space excitations to the form of real-space excitations.
3. The $\hat{\mathbf{z}}$ aligned excitation now represents a gravitational wave propagating along the z -axis. To describe an arbitrary direction of propagation, the excitation tensor is rotated through an angle $\arccos(\mathbf{k} \cdot \hat{\mathbf{z}})$ around the orthogonal vector \mathbf{v}_k

$$\mathbf{v}_k = \frac{\mathbf{k} \times \hat{\mathbf{z}}}{|\mathbf{k} \times \hat{\mathbf{z}}|}, \quad \cos \phi = \hat{\mathbf{k}} \cdot \hat{\mathbf{z}}, \quad (4.94)$$

This transformation can also be carried out in reverse to find the appropriate description for arbitrarily oriented ferroquadrupolar order from the structure of the tensor for a gravitational wave. I then combine these three steps into the general transformations

of the form [7]

$$Q_{\mu\nu} = R[\mathbf{v}_d, \theta]^\alpha{}_\mu R[\mathbf{v}_d, \theta]^\beta{}_\nu \left[R[\mathbf{v}_k, \phi]^\gamma{}_\rho R[\mathbf{v}_k, \phi]^\kappa{}_\sigma \right. \\ \left. h_{\gamma\kappa} [\lambda_1 \otimes \lambda_4 + \lambda_{3xy} \otimes \lambda_6]^\rho{}_\sigma \right], \quad (4.95)$$

$$h_{\mu\nu} = R[\mathbf{v}_k, \phi]^\alpha{}_\mu R[\mathbf{v}_k, \phi]^\beta{}_\nu \left[R[\mathbf{v}_d, \theta]^\gamma{}_\rho R[\mathbf{v}_d, \theta]^\kappa{}_\sigma \right. \\ \left. Q_{\gamma\kappa} [\lambda_4 \otimes \lambda_1 + \lambda_6 \otimes \lambda_{3xy}]^\rho{}_\sigma \right], \quad (4.96)$$

where $R[\mathbf{m}, \theta]$ is a padded SO(3) rotation matrix

$$\mathbf{R}[\mathbf{m}, \theta] = \begin{pmatrix} 0 & 0 & 0 & 0 \\ 0 & \text{Cos}[\theta] + (1 - \text{Cos}[\theta])m_1^2 & (1 - \text{Cos}[\theta])m_1m_2 - \text{Sin}[\theta]m_3 & \text{Sin}[\theta]m_2 + (1 - \text{Cos}[\theta])m_1m_3 \\ 0 & (1 - \text{Cos}[\theta])m_1m_2 + \text{Sin}[\theta]m_3 & \text{Cos}[\theta] + (1 - \text{Cos}[\theta])m_2^2 & -\text{Sin}[\theta]m_1 + (1 - \text{Cos}[\theta])m_2m_3 \\ 0 & -\text{Sin}[\theta]m_2 + (1 - \text{Cos}[\theta])m_1m_3 & \text{Sin}[\theta]m_1 + (1 - \text{Cos}[\theta])m_2m_3 & \text{Cos}[\theta] + (1 - \text{Cos}[\theta])m_3^2 \end{pmatrix}. \quad (4.97)$$

The action of this operator is to rotate a state oriented along the direction of a vector \mathbf{m} to a final state oriented along direction \hat{z} as described in the former protocol.

There is one additional point worth significant remark, namely, that the spin nematic excitations exist in a three-dimensional Hilbert space (trivially promoted here to three dimensions plus one null dimension for ease of representation) independent of the physical dimension of the system. This means that such analogue waves also exist in low-dimensional spin nematic phases. Recall however that for gravitational waves, three dimensions of space and one of time are minimally required to support their existence. However, the analogue in spin nematics allows us to explore analogue gravitational waves in systems of arbitrary dimension, a point which I will use to motivate attractive charges for this analogue in Section 4.5.3, and an approach to experimental observation in Chapter 5.

In conclusion, the action describing excitations about a ferroquadrupolar ground state is in direct correspondence with that of linearized gravity. The quadrupolar Goldstone modes are in one-to-one correspondence with gravitational waves in flat spacetime: we can always identify a mapping that transcribes the excitations of a ferroquadrupolar spin nematic onto those of a gravitational wave in flat spacetime and viceversa.

4.5.2 Quadrupolar nature of excitations in linearized gravity and spin nematics

Having so far seen the connection between the Goldstone modes of spin nematics and gravitational waves, I now turn to a deeper investigation of the nature of the excitations themselves, and showcase the relationship between the nature of fluctuations in the Hilbert space to those of spacetime.

In order to visualize the effect of a gravitational wave, and show that it has an

analogous notion in the spin nematic wave, I will first derive the form for a surface of constant induced strain and then show the analogous quantity in a spin nematic.

Consider the following measure of distance between spacetime events

$$ds^2 \stackrel{def}{=} (x - x')^2 \quad (4.98a)$$

$$= g_{\mu\nu}(x - x')^\mu(x - x')^\nu, \quad (4.98b)$$

which is invariant under transformations of the Poincaré group

$$x^\mu \rightarrow \bar{x}^\mu = \Lambda^\mu_\nu x^\nu + a^\mu, \quad (4.99)$$

and general coordinate transformations Eq. (2.88a-2.88b). Now if the metric is perturbed by $h_{\mu\nu}$ separable from the background due to shorter time and length scales involved, then this becomes

$$ds^2 = (g_{\mu\nu} + h_{\mu\nu})(x - x')^\mu(x - x')^\nu \quad (4.100a)$$

$$= g_{\mu\nu}(x - x')^\mu(x - x')^\nu + h_{\mu\nu}(x - x')^\mu(x - x')^\nu \quad (4.100b)$$

$$= ds_0^2 + \tilde{d}s^2, \quad (4.100c)$$

where

$$\tilde{d}s^2 \stackrel{def}{=} (x - x')^2, \quad (4.101a)$$

$$= h_{\mu\nu}(x - x')^\mu(x - x')^\nu, \quad (4.101b)$$

defines an appropriate contraction over indices to give a scalar measure of distance. Consider then the quantity

$$\frac{\tilde{d}s^2}{(x - x')^\mu(x - x')_\mu} = \frac{h_{\mu\nu}(x - x')^\mu(x - x')^\nu}{(x - x')^\mu(x - x')_\mu}. \quad (4.102)$$

If we now define the strain induced by a gravitational wave on the distance separating two spacetime events.

$$\epsilon = \frac{\tilde{d}s}{|x - x'|}, \quad (4.103)$$

we see that we can identify surfaces of constant induced strain, which can be represented by

$$\epsilon = \pm \left(\frac{h_{\mu\nu}(x - x')^\mu(x - x')^\nu}{|(x - x')|^2} \right)^{\frac{1}{2}}, \quad (4.104)$$

with corresponding surfaces of constant strain squared

$$V(t, \mathbf{x}) = \frac{h_{mn}(t, \mathbf{x})x^m x^n}{|\mathbf{x}|^2}, \quad (4.105)$$

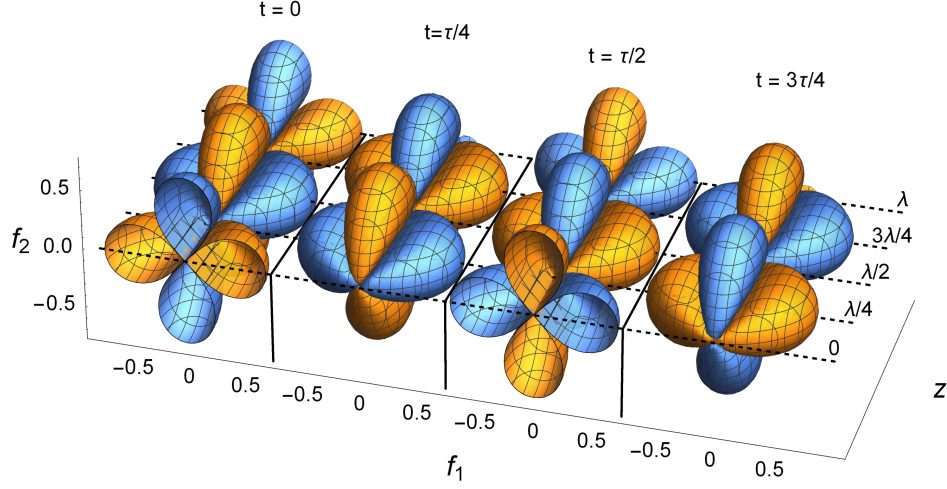


Figure 4.3: Equipotential surfaces demonstrating the equivalent quadrupolar breathing behaviour of the modes of both gravity [cf. Eq. 4.105] and the spin nematic [cf. Eq. (4.107)]. Figure reproduced from [7] with permission.

where for comparison with the spin nematic, the time and space components of four-vectors have been explicitly separated. This quantity is visualized in Fig. 4.3 which we can call a surface of equal field strength, and provides a scalar representation of the quadrupolar nature of the gravitational wave.

Next I show how we can identify a parallel quantity in the spin nematic. Consider the expectation value

$$\langle \tilde{Q}_{\alpha\beta} \rangle = \frac{\langle d^\alpha | \tilde{Q}_{\alpha\beta} | d^\beta \rangle}{|d^\alpha|^2}. \quad (4.106)$$

This defines surfaces of equal probability to measure a given superposition of the quadrupole components.

We can also examine the wavefunction amplitude, defined as an analogous equipotential surface to Eq. (4.105)

$$V(\mathbf{S}, (t, \mathbf{x})) = \frac{S^m \tilde{Q}_{mn}(t, \mathbf{x}) S^n}{|\mathbf{S}|^2}, \quad (4.107)$$

which is functionally identical to the equal strain surface for the gravitational wave visualized in Fig. 4.3, and insensitive to which basis we are in. Both of these quantities showcase the characteristic oscillation of quadrupolar degrees of freedom, and we can conclude that independent of any basis choice, the underlying nature of such modes is the same.

4.5.3 Homotopy and defects of the spin nematic phase

Here I will briefly review the order parameter space of the spin nematic, and corresponding topological windings present in two dimensions, with an eye to identification

of charges which behave like mass.

The Lagrangians of the nematic phases discussed in this Chapter share $SU(2)$ as their full symmetry group. The nature of symmetry breaking order preserved inversion symmetry is characterized by the infinite dihedral group, and this in turn defines the order parameter manifold as [209, 210]

$$SU(2)/D_\infty = \mathbb{RP}^2 \quad (4.108)$$

The order parameter space of the nematic liquid crystal and ferroquadrupolar spin nematic therefore correspond to the topological space \mathbb{RP}^2 , see Fig. 4.4a.

The order parameter manifold provides us clear predictions about the defects that can arise. The π_1 defects in two dimensions—corresponding to point defects—for \mathbb{RP}^2 are \mathbb{Z}^2 defects, namely, they are their own antidefect, and so their topological charge does not carry any signature. In fact, all such defects are topologically equivalent, since any non-trivial loop on \mathbb{RP}^2 can be continuously deformed into any other.

Recall another key property of spin-2 field theories, namely, that they mediate attractive interactions. As in the case of the XY analogue, the spin nematic state provides us here with visual confirmation of this fact. Observe in Fig. 4.4c how nearby domains of directors can reach maximal alignment if the defects are free to approach one another and annihilate. This provides a visual confirmation of the fact that a spin-2 field theory mediates attractive interactions between sources of the field, as in the case of gravity.

4.6 Spin nematics in experiment

Quantum spin nematic candidates have been long investigated, in both the context of magnetic insulators and spinor condensates. Here I briefly review progress in both areas, with a view to identify analogue gravitational waves proposed here in experiment.

4.6.1 Spin nematics in magnetic insulators

In the context of magnetic insulators, the possible existence of quadrupolar order in spin-1 magnets was suggested in 1969 [87]. For spin-1, well known candidate spin-nematic materials are FeGa_2S_4 and NiGa_2S_4 , which have an effective triangular lattice structure of Fe or Ni atoms with effective spin-1. These materials have motivated extensive investigation to explore the possibility of their spin nematic character [95, 99–101, 211, 212]. However, quadrupolar order is directly hidden from most solid state probes, a challenge that has motivated the ongoing search for detectable signatures that could serve as a smoking gun signatures of nematic order, not exclusive to the triangular lattice materials [5, 213–216].

In addition to work on spin-1 candidate materials, focus has also been shared by spin- $\frac{1}{2}$ candidate materials. In spin- $\frac{1}{2}$ materials, the possibility of nematic order was first discussed to arise from the collective interactions between pairs of spin- $\frac{1}{2}$ degrees of freedom in the triplet state on bonds [89–91]. Indirect evidence suggests that such bond spin-nematic phases can appear in materials such as the frustrated spin-chain

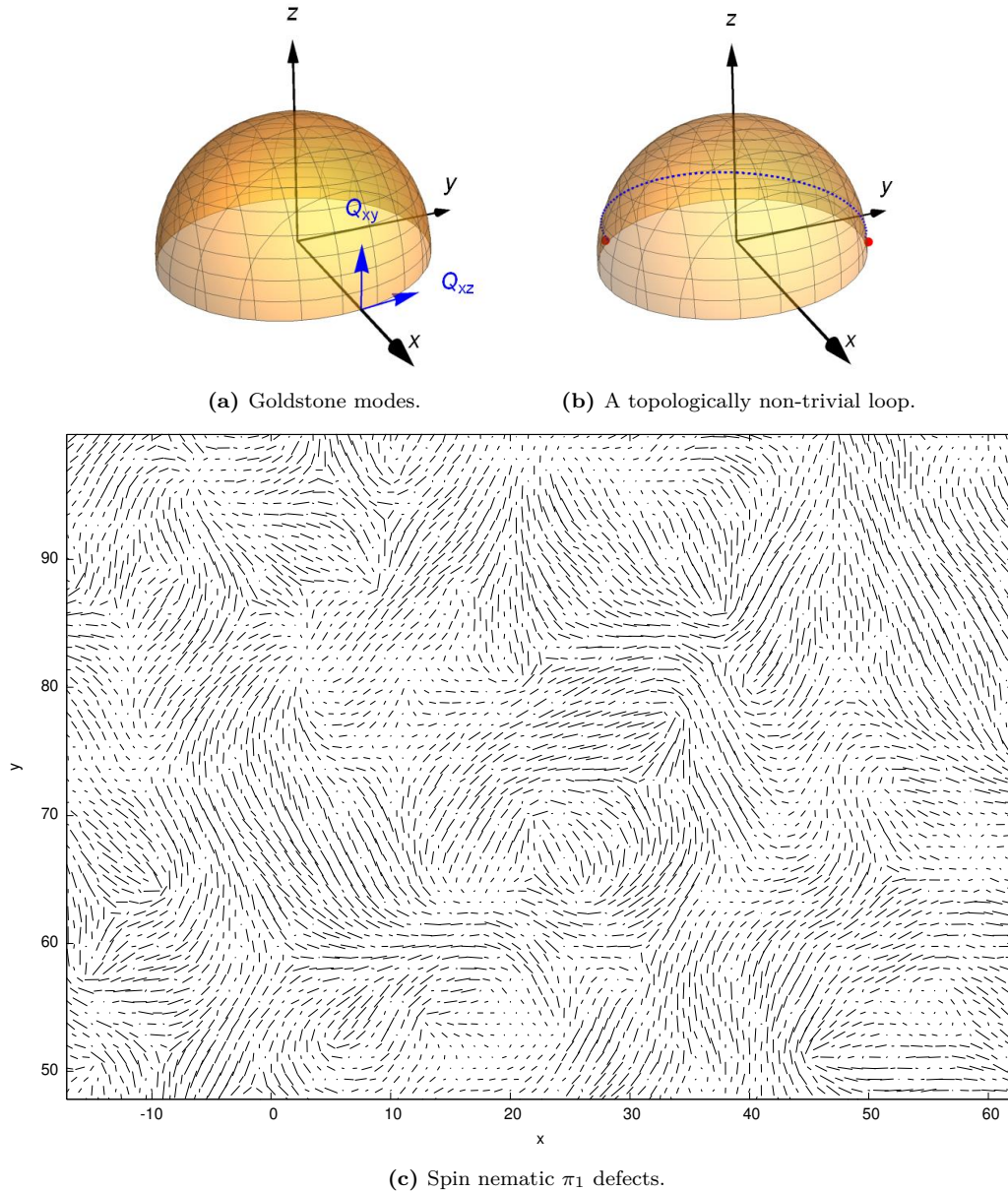


Figure 4.4: The manifold \mathbb{RP}^2 , the order parameter space of both the nematic liquid crystal and the ferroquadrupolar liquid crystal, its symmetry restoring excitations, and topological defects in order parameter space and real-space. All antipodal points on the boundary of the hemisphere are identified. (a) For a ground state ordered along the x -direction, the two transverse Goldstone modes are indicated by the blue arrows, denotes Q_{xy} and Q_{yz} respectively. (b) The π_1 point defects on this manifold correspond to topologically non-trivial loops such as shown in the blue dashed line, where the red antipodal points are identified. Such loops are not oriented, as loops of two distinct orientations can always be smoothly deformed into one another on this manifold, leading to the \mathbb{Z}^2 nature of the defects. (c) Topological point defects of a spin nematic on a two dimensional lattice as observed in the two-dimensional projection of the director field, obtained by Monte Carlo simulation.

compound LiCuVO_4 [217], Volborthite [215], and other candidate materials such as solid ^3He films [218] are also suspected to realize bond spin-nematics. It is worth note that experimental work on these materials has been carried out in-field, and the applied magnetic field reduces the available Goldstone modes from two to one, not ideal for work with the analogue gravitational waves here proposed. Bond-nematic antiferroquadrupolar order has also been discussed in theoretical works [219, 220], and is also described at low-energies by a non-linear sigma model with linearly dispersing Goldstone Bosons.

In conclusion, as for the spin-1 materials, definitive experimental evidence has yet to be provided. For this reason, even though the candidate materials described here present the correct number of low-temperature Goldstone modes at zero-field, and could in principle realize analogue gravitational waves, the lack of methods to conclusively detect these in solid state experiments currently prevent use of magnetic insulators for their realization.

4.6.2 Spin nematics in spinor condensates

In contrast to the ongoing investigation within the solid state community, the experimental existence of spin nematic phases have been clearly established in spinor condensates. Within cold atoms, the investigation of quantum spin nematics spans several decades [102, 221, 222], with the last decade uncovering the successful detection of spin nematic phases described by the order parameter Eq. (4.23) in condensates of ^{23}Na [107, 223, 224]. Additionally, spin-1 alkali condensates are known to be described in the tight binding limit by the Bilinear-Biquadratic model Eq. (1.19) [104], with ^{23}Na atoms presenting the appropriate scattering parameters to exhibit a ferroquadrupolar nematic ground state.

The characterization of spin nematic order is also, at present, more directly accessible in cold atoms than in magnetic insulators due to the existence of a variety of probes that are free of the technical difficulties associated with magnetic insulators.

Firstly, in spinor condensates the characterization of the relative populations of the condensate in each of the states $|1\rangle$, $|0\rangle$ and $|\bar{1}\rangle$ can be directly measured, and nematic phases populating the $|0\rangle$ state alone can be distinguished, using for example Stern-Gerlach measurement after releasing the gas from the trap [103, 121, 223].

Additionally, for phases in which the spin populations are mixtures of the three levels, it has been shown that the relevant population composition can be deciphered from statistical treatment of the phase information following spin rotation operations applied to multiple realizations of the system [107].

In addition, it has also been shown that information from the quadrupolar channel can be extracted from the interaction between light and the atomic gas [225]. The optical properties of the atomic gas can be characterized in terms of the internal spin structure of the atom

$$\alpha_{mn} = c_0 \langle \rho \rangle \delta_{mn} - i c_1 \epsilon_{mnl} \langle S^l \rangle + c_2 \langle Q_{mn} \rangle, \quad (4.109)$$

where α_{mn} is the electric polarizability tensor, with monopole, dipole and quadrupole distributions ρ , \mathbf{S} and Q_{mn} , and corresponding coefficients c_i . The vector and tensor

properties contribute to the optical birefringence. In terms of passing electromagnetic wave, which is transverse in nature, the transverse polarizability can be measured from the phase imprinted on the electric field by passage through a slice of thickness dz [121]

$$\mathbf{E}_{out}(x, y, z + dz) = e^{ik[1 + \frac{1}{2}\alpha_{\perp}]dz} \mathbf{E}_{in}(x, y, z) . \quad (4.110)$$

where k is the frequency of the light used, and α_{\perp} are the components of the polarizability tensor defined by equation Eq. (4.109) which are orthogonal to the the direction of the light (in this case the z -direction). Assuming a thin gas cloud, such as for a quasi-two-dimensional system, the phase imprinted on the transverse wave takes the form [121]

$$\mathbf{E}_{out}^{\perp}(x, y) \approx e^{[i\frac{k}{2}(c_0\rho(x,y) + \frac{c_2}{2}(Q_{xx}(x,y) + Q_{yy}(x,y)))]} \left[1 + \frac{ik}{2} \begin{pmatrix} \frac{c_2}{2}(Q_{xx}(x,y) - Q_{yy}(x,y)) & ic_1S_z(x,y) + c_2Q_{xy}(x,y) \\ -ic_1S_z(x,y) + c_2Q_{xy}(x,y) & -\frac{c_2}{2}(Q_{xx}(x,y) - Q_{yy}(x,y)) \end{pmatrix} \right] \mathbf{E}_{in}^{\perp} \quad (4.111)$$

such that quadrupolar information in the transverse plane is in principle extractable from direct imaging of the sample with light.

Independently, the direct measurement of the expectation values of dipole and quadrupole operators has also been carried out [109]. This technique consists in using microwave pulses to selectively couple states from distinct hyperfine manifolds, specifically from the $F = 1$ manifold to the $F = 2$ manifold. Since there are more states in the larger hyperfine manifold, non-commuting observables can be encoded in a recoverable way, such that dipole and quadrupole components can be obtained from the populations of each state in the two respective manifolds e.g.

$$S^x = n_{2,+2} - n_{2,-2} , \quad (4.112)$$

$$Q^{yz} = n_{1,+1} - n_{1,-1} , \quad (4.113)$$

where $n_{F,m}$ represents the population of each species in the F manifold with magnetic quantum number m .

All of these independent strategies for measuring nematic order and its quadrupolar components suggests that the cold atom toolbox is well-suited for the simulation of analogue gravitational waves discussed here. We will return to the prospect of simulating analogue gravitational waves in cold atoms in Chapter 5.

4.7 Chapter summary

This Chapter has treated spin nematics and their particular realization in spin-1 magnets. We have seen that spin nematics are described in the low-energy limit by a non-linear sigma model, whose action is in direct correspondence with the action for linearized gravity. Building on this, I have presented a novel analogue between the Goldstone modes of ferroquadrupolar spin nematics and gravitational waves—both of which are massless, quadrupolar waves described by symmetric, traceless tensors—

which holds independent of the spatial dimension of the realization of the spin nematic. This is the case since the Hilbert space of the nematic waves is automatically three dimensional in our Universe, independent of the dimension of the system. With this in mind, I have then hinted at the existence of attractive defects that mimic the behaviour of gravitating bodies in two-dimensional spin nematics. I have also reviewed current state of spin nematics in experiment, with a view to realizing the analogue presented here in spinor condensates. I will discuss these last two points in more depth in the next Chapter.

Chapter 5

Numerical investigation of gravitational wave analogues

“The more one fails, the greater the chance that it works.” - Les Shadoks

The analytic results developed in Chapter 4 identify a connection between the Goldstone modes of spin nematics and gravitational waves in linearized gravity.

In this Chapter, I expand on this connection by carrying out numerical simulation leading to the identification of gravitating vortices in a two-dimensional ferroquadrupolar spin nematic which shed analogue gravitational waves during their attractive in-spiral towards annihilation [7].

I first provide a brief overview of the semiclassical simulation methods I have used to produce the results in this Thesis. I first review Markov-chain Monte Carlo methods for the generation of thermodynamic properties and other data at thermal equilibrium, such as spin-spin correlations. I then review the Molecular dynamics scheme applied to spin systems. These simulations in combination are then used to produce the keystone results of this Thesis, corroborating the existence of gravitational wave analogues in spin nematics. Building on this, I finally outline an experimental protocol for this analogue in cold atoms.

5.1 Classical Monte Carlo methods

Monte Carlo methods refer to a huge class of numerical methods of continued relevance within physics and beyond [226]. Named for the famed casino in Monaco, within the context of statistical physics, these methods refer to simulation techniques from which specific properties of a physical system can be estimated in polynomial time. In this Section, I provide an overview of classical Markov-chain Monte Carlo simulation, discussed further in e.g. [227, 228] and its specific application to spin models discussed in this Thesis.

The key idea behind Monte Carlo methods is to numerically estimate observables by averaging over a series of statistically-independent samples drawn from an appropriate ensemble. For very large state spaces, it is not realistic to wait until the simulation has sampled the whole space before being able to make an average measurement. Therefore, one typically employs an appropriate sampling distribution, chosen such

that the estimator corresponding to the observable converges for a large number of samples N_s . This strategy is referred to as Importance Sampling [227].

A Markov-chain Monte Carlo algorithm is one way to achieve just this. The strategy is to generate a sequence of states drawn from a physically appropriate probability distribution, where each element of the sequence is obtained from the previous by updates satisfying a condition called “detailed balance”.

This condition arises from choice of the sampling distribution which describes the equilibrium distribution of the system. This equilibrium condition is equivalent to conservation of the probability n_a to occupy state a

$$\frac{dn_a(t)}{dt} = 0, \quad (5.1)$$

where

$$\sum_a n_a = 1. \quad (5.2)$$

Given that the rate of change for the probability to be occupying configuration a is determined by all the ways to enter or leave the configuration a , we can define

$$\frac{dn_a(t)}{dt} = \sum_b n_b(t)P(b \rightarrow a) - n_a(t)P(a \rightarrow b). \quad (5.3)$$

It is necessary that the Markov chain be able to sample in principle every state in the configuration space. Therefore, we expect the transition probabilities $P(a \rightarrow b)$ of moving from one configuration a to the next b to be always non-zero, even if very small. An appropriately chosen distribution function, such as the Gibb’s distribution we will see momentarily, will ensure this condition holds. This corresponds to the property that in the large time limit the Markov chain explores the whole configuration space, and receives the name ergodicity.

Combining Eq. (5.1) and Eq. (5.3) leads to the condition

$$\sum_b n_b(t)P(b \rightarrow a) = \sum_b n_a(t)P(a \rightarrow b), \quad (5.4)$$

which is the Detailed Balance condition. A Markov-chain Monte Carlo algorithm thus provides an artificial kind of dynamics that evolves the configuration of the system towards the equilibrium manifold of configurations.

The simplest Markov-chain Monte Carlo algorithm is the Metropolis algorithm [229], in which we define the Gibb’s distribution for an ensemble by the set of probabilities

$$n_a = \frac{e^{-\frac{E_a}{k_B T}}}{Z}, \quad (5.5)$$

$$Z = \sum_i e^{-\frac{E_i}{k_B T}}, \quad (5.6)$$

with Z representing the partition function. Direct sampling of such distributions is

hard in general since it requires calculating E_i for all possible configurations. Instead, by working with the Detailed Balance condition

$$\frac{P(a \rightarrow b)}{P(b \rightarrow a)} = \frac{n_b}{n_a} = e^{-\frac{(E_b - E_a)}{k_B T}}, \quad (5.7)$$

we can define the ratio of transition probabilities without reference to the partition function, and depending solely on the gradient of relative energy between two configurations. Therefore, the probability with which we should accept a proposed move from a to b is

$$P_{accept} = \min\left(1, \frac{n_b}{n_a}\right), \quad (5.8)$$

where in the case

$$\frac{n_b}{n_a} \geq 1, \quad (5.9)$$

the energy is reduced by accepting the move. Otherwise, the move is energetically unfavourable, but can still occur with finite probability, as required by ergodicity. For a system of size N , we define a set of N such moves as a Monte Carlo sweep.

In conclusion, with clever choice of update rule, we can sample from the probability distribution without us ever having to directly evaluate the full distribution and this is the most fundamental tool for simulating spin models. There are many additional tricks one can apply, some specific to certain categories of models, and I will here review the techniques I have employed in my simulations of $O(N)$ and $U(3)$ models. I will first describe how we make thermodynamic measurements using Markov chain Monte Carlo.

5.1.1 Equilibrium measurements, estimators and block averaging

When simulating spin models using Markov-chain Monte Carlo, the goal is to make reliable estimates of the thermodynamic behaviour of the system at a given temperature T or other model specific parameters, such as applied field h or internal coupling strength J . Extracting the dependence of observable equilibrium properties on these variables teaches us something about the phase of the system. For simple ordered phases, such as the ferromagnet, while we may a priori know what the low-energy configurations look like, for many systems we do not always know in advance what the equilibrium subspace may look like. Indeed, exploring the unknown is the strength of simulation methods, once appropriately calibrated.

Models with simple interactions, such as the Ising model or the Heisenberg model, exhibit well-known exactly soluble limits in which we have knowledge in advance of the observable macroscopic properties of the system. These known limits serve as benchmarks to help iron out systematic errors.

One key observable we can measure in this way is the system energy. Other quantities include macroscopic order parameters, such as the staggered magnetization. We

can then extract the thermodynamic behaviour of such quantities by constructing quantities such as the heat capacity C or the magnetic susceptibility χ

$$C = \frac{\partial_T \langle E \rangle}{T} \Big|_h = \frac{\langle E^2 \rangle - \langle E \rangle^2}{T^2} \quad (5.10a)$$

$$\chi = \frac{\partial_T \langle M \rangle}{T} \Big|_h = \frac{\langle M^2 \rangle - \langle M \rangle^2}{T} \quad (5.10b)$$

where the energy E and macroscopic magnetization M are averaged over the states sampled at a given temperature and at fixed values of other variables. The heat capacity sensitively encodes information about how the energy stored per degree of freedom changes as a function of temperature, and can exhibit critical scaling near phase transitions.

With a functional algorithm free of systematic error for the simulation of a given problem, the primary source of errors arising in Monte Carlo data is statistical in origin. Good approximations to the actual values of the observables rely on large numbers of measurements N_s , over which we define the estimator for the variable of interest x as the average

$$\bar{x} = \frac{1}{N_s} \sum_i x_i, \quad (5.11)$$

with standard deviation defined [227]

$$\sigma_N = \sqrt{\frac{\langle \bar{x}^2 \rangle - \bar{x}^2}{N - 1}}, \quad (5.12)$$

that provides a measure of the statistical distribution of individual instances x_i , assuming these are statistically uncorrelated. However, by virtue of the Markov chain method, subsequent samples are not uncorrelated. It is therefore important to only measure again after enough time has passed that the individual instances no longer are correlated. To quantify this, the degree of autocorrelation for a given observable after some time t can be estimated

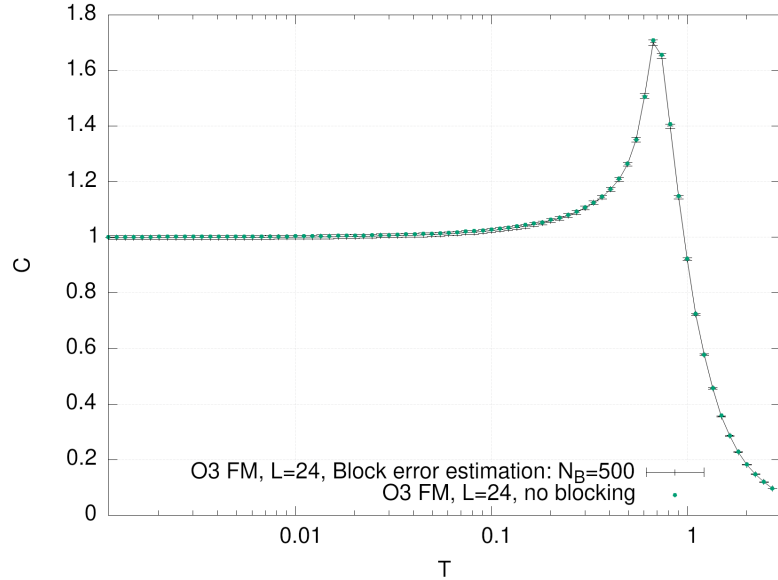
$$\lambda(t) = \sum_{t'}^t x(t')x(t'+t) - \bar{x}^2 \quad (5.13)$$

where this quantity typically decays exponentially,

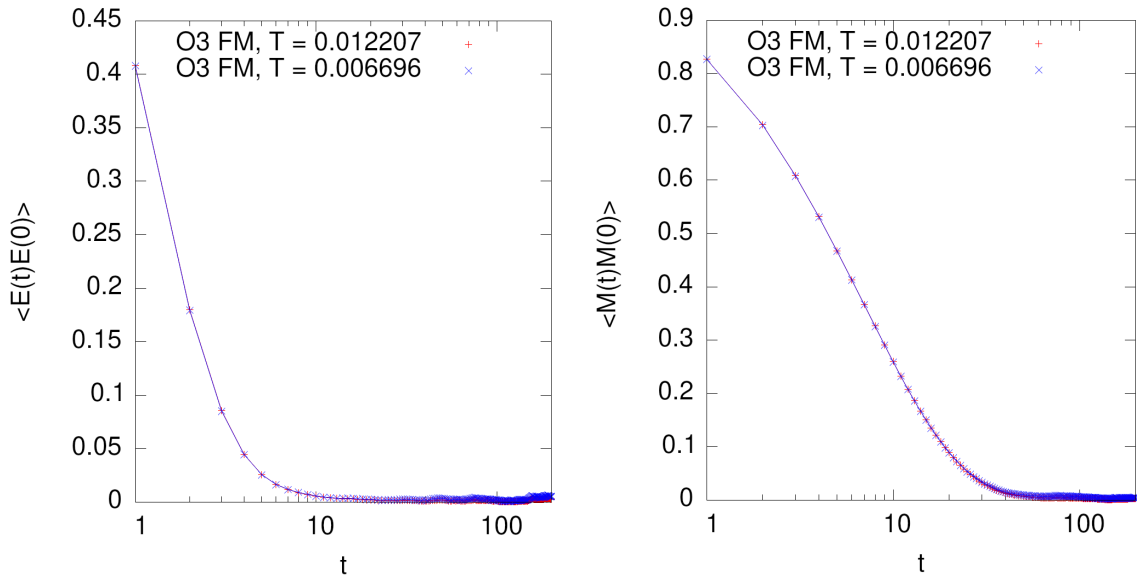
$$\lambda(t) \sim e^{-\frac{t}{\tau}} \quad (5.14)$$

in which case the autocorrelation time τ can be estimated from examination of the exponential behaviour, and measurements should be spaced accordingly. It was also shown by Muller-Krumbhaar and Binder [230] that the standard deviation can be corrected to account for autocorrelations with knowledge of the autocorrelation time τ .

If we are interested in estimating the error in derived quantities, we can propagate the error measured by the standard deviation in the originally measured observable.



(a) Heat capacity benchmark for blocking method.



(b) Energy and magnetization autocorrelation at low temperatures.

Figure 5.1: Benchmarks for the blocking procedure for error estimation of derived quantities. **(a)** Heat capacity as a function of temperature in the $O(3)$ square lattice Heisenberg model at $J = 1$, calculated with and without the blocking strategy, both results overlaid. The results are in agreement within statistical uncertainty. **(b)** Energy E and order parameter M autocorrelations as a function of simulation time allow determination of an appropriate choice of N_B , valid to the lowest temperatures of interest in the system. The autocorrelation decays rapidly, such that N_B on the order of 100 is more than sufficient.

This is straightforward to do in the case of simple dependence on the observable, such as a linear combination. However, in e.g. the case of specific heat, error propagation to the derivative can be cumbersome, though technically plausible via Taylor expansion.

For this reason, I employ an alternative strategy, called the Blocking method [227, 231]. This involves grouping measurements into blocks of uncorrelated measurements which are used to make estimates of the derived observable and its uncertainty. To see how this approach can lead to an appropriate estimate, let us consider specifically the case of the heat capacity. The relevant estimator without blocking measurements is given by

$$\langle C \rangle = \frac{1}{T^2} \left(\frac{1}{N_s} \sum_{i=1}^{N_s} E_i^2 - \frac{1}{N_s^2} \left(\sum_{i=1}^{N_s} E_i \right)^2 \right). \quad (5.15)$$

Next I define the equivalent estimator using the blocking procedure. Breaking down the total measurements into a number of bins N_{bins} of respective bin-size N_B

$$N_s = N_B \cdot N_{bins}, \quad (5.16)$$

the heat capacity estimator then takes the form

$$\langle C \rangle_B = \frac{1}{T^2} \sum_{j=1}^{N_{bins}} \left(\frac{1}{N_B} \sum_{i=1}^{N_B} E_i^2 - \frac{1}{N_B^2} \left(\sum_{i=1}^{N_B} E_i \right)^2 \right). \quad (5.17)$$

The first term in this estimator is equivalent to that of Eq. (5.15). However, the second terms are distinct

$$\frac{1}{N_s^2} \left(\sum_{i=1}^{N_s} E_i \right)^2 \neq \sum_{j=1}^{N_{bins}} \frac{1}{N_B^2} \left(\sum_{i=1}^{N_B} E_i \right)^2 \quad (5.18)$$

though are known to converge in the case that the measurements E_i are uncorrelated [231], see Fig. 5.1.

In general any derived observable can be evaluated using this procedure, in combination with careful assessment of the maximum autocorrelation time down to the lowest simulated temperature, thus providing a statistical distribution of values over which to average and evaluate the statistical deviation of the derived quantity. Having reviewed the process of measurement in a classical Markov chain Monte Carlo simulation, I will next provide some background on best practices to equilibrate the system prior to beginning any measurements.

5.1.2 Simulated Annealing

The process of reaching equilibrium takes time, particularly if the starting configuration of the system is far from the subspace describing equilibrium. For this reason, one cannot simply start to measure desired observables right from the beginning of the simulation, particularly if the starting point is somehow out of the ordinary in the

ensemble. Instead, some time will need to be allowed for the system to thermalize¹.

The high temperature state of any system is always entropy dominated. Once we pick an initial temperature for the system which is roughly an order of magnitude above the interaction scale of the problem, then any completely random initial configuration is an equally valid description of the thermally equilibrated state at that temperature. From this starting point, we can gradually turn the simulation temperature down to the target temperature of interest. This process of simulating a hot sample which is gradually cooled receives the name simulated annealing.

The annealing to the target temperature must always be followed by an appropriate thermalization time. Depending on the details of the system being simulated, annealing timescales and thermalization timescales on the order of $\mathcal{O}(10^5 - 10^6)$ can be sufficient. For the systems I consider in this Thesis, these timescales are sufficient.

For some systems, particularly frustrated or glassy systems, the free energy landscape across the configuration space may have many local minima. In such cases there could be a danger that local updates such as the Metropolis update in combination with the annealing as a strategy to reach equilibrium may fail. In such circumstances, this approach should be used with care in combination with strategies such as parallel tempering, introduced by Marinari and Parisi [232] or non-local updates e.g. [233, 234]. For the results I show in this Thesis, I will not employ parallel tempering.

5.1.3 Overrelaxation

Another strategy to improve the efficiency of the Monte Carlo sampling consists in locally decorrelating configurations of the system through a process known as overrelaxation [235, 236]. In this section, I briefly review how this works for the O(3) Heisenberg model.

Consider the local environment of an O(3) spin \mathbf{S}_i , defined by

$$\mathbf{H}_i = \sum_{j=i+\delta} \mathbf{S}_j, \quad (5.19)$$

where site j represents any lattice site in the immediate neighbourhood of site i .

Now suppose we take the spin at site i and bump it randomly to another configuration within the space of states with equal energies. For O(3) spins, the states with equal energy are all those whose inner product with \mathbf{H}_i is constant, and so describes the boundary of a cone on the sphere. The process of updating the spin i is equivalent to performing the rotation

$$\mathbf{S}'_i = R(\mathbf{H}_i, \phi) \mathbf{S}_i, \quad (5.20)$$

defined around the axis \mathbf{H}_i and by an angle ϕ . We could then choose random numbers

¹To motivate this, it is helpful to think of the simulation like a real experiment. If we want to make measurements on a physical sample that we took from the shelf at room temperature and the target temperature is much lower, then putting the sample too quickly into the low temperature environment will quench the system far from its equilibrium state and it will take time for the induced dynamics to quiesce. A better strategy if we are interested in the equilibrium properties is to slowly cool the sample, allowing it to remain in quasi-equilibrium throughout the process.

ϕ on the interval $[0, 2\pi]$ and perform these rotations in combination with every sweep of the Monte Carlo update. However the generation of random numbers is computationally expensive in the context of Monte Carlo simulation, where we are repeating large numbers of such operations to obtain statistically valid data. It is therefore enough instead to simply rotate every time by a constant $\phi = \pi$.

In this case, the corresponding update takes the simple form

$$\mathbf{S}'_i = -\mathbf{S}_i + 2\mathbf{H}_i \cdot \mathbf{S}_i . \quad (5.21)$$

Until this point, I have not presented the reader with any reason to suspect that the local Metropolis update rule may not sample correctly from certain continuous manifolds of states, such as that of $O(3)$ spins. However, the same non-linearity present implicitly in the length constraint on $|\mathbf{S}_i|^2$ leads to incorrect sampling if the spin components are directly sampled with this constraint in effect. An efficient method to overcome this is discussed in the next Section.

5.1.4 Marsaglia method

An efficient method for sampling points randomly on a 2-sphere was presented by Marsaglia in 1972 [237]. Starting with the generation of two random and uniformly distributed variables x_1 and x_2 , subject to the constraint

$$x_1^2 + x_2^2 < 1 , \quad (5.22)$$

one can define a random point on the surface of the sphere with coordinates

$$\mathbf{S} = \left(2x_1\sqrt{1-x_1^2-x_2^2}, 2x_2\sqrt{1-x_1^2-x_2^2}, 1-2\sqrt{x_1^2+x_2^2} \right) . \quad (5.23)$$

This scheme and its generalizations are of use for random sampling of constrained variables in the context of Metropolis update algorithms, such as for general $O(N)$ systems and, as I will review in the next Section, for the $U(3)$ representation of spin-1 systems.

5.1.5 $U(3)$ representation for spin-1 in simulation

I here briefly describe how to carry out simulations using the $U(3)$ formalism developed in [11]. In Chapter 4, we saw that the Gell-Mann basis for $SU(3)$ is sufficient to describe transformations between states in the Hilbert space. However, the expression of the commutation relations between \mathbf{S} and \mathbf{Q} operators in $SU(3)$ is more cumbersome than it needs to be. An alternative method is to use the $U(3)$ algebra, as originally observed by Papanicolau [82]. This formalism, explicitly developed in [11], exploits the simplicity of the commutators in the $U(3)$ representation to provide a linear form for the equations of motion. While this is not necessary for the thermodynamic simulation discussed in this Section, it becomes extremely relevant for dynamical simulation. For this reason, I apply this formalism in both Monte Carlo and later Molecular Dynamics simulations of the spin-1 Bilinear-Biquadratic model introduced in Chapter 1 and Chapter 4.

The key idea is to observe that a tensor operator defined in terms of a complex director \mathbf{d}

$$\mathcal{A}_{\alpha\beta} = d_i^\dagger d_j, \quad (5.24)$$

spans U(3), c.f. Eq. (4.3). This operator has scalar, vector and tensor components

$$\rho = \langle d_\alpha^\dagger d_\alpha \rangle, \quad (5.25)$$

which equivalently measures the length of the spin,

$$S_\gamma = \langle \epsilon_{\alpha\beta\gamma} d_\alpha^\dagger d_\beta \rangle, \quad (5.26)$$

which corresponds to the dipole component, and

$$Q_{\alpha\beta} = \langle \frac{1}{2}(d_\alpha^\dagger d_\beta + d_\beta^\dagger d_\alpha) - \frac{1}{3}\delta_{\alpha\beta} d_\gamma^\dagger d_\gamma \rangle, \quad (5.27)$$

which has no orientation and measures quadrupole components. This set contains one scalar operator that is not required for the description of the SU(3) Hilbert space, and in order to ensure that it does not mix with the other operators, its magnitude is fixed by setting the trace of the operator \mathcal{A} to 1.

In terms of these operators, the Bilinear-Biquadratic Hamiltonian Eq. (1.19) introduced in Chapter 4 then becomes

$$\mathcal{H}_{BBQ} = \sum_{\langle ij \rangle} \left(J_1 \mathcal{A}_i^{\alpha\beta} \mathcal{A}_j^{\beta\alpha} + (J_2 - J_1) \mathcal{A}_i^{\alpha\beta} \mathcal{A}_j^{\alpha\beta} + J_2 \right) \quad (5.28)$$

where the new operators encode the antisymmetric dipole component and traceless symmetric quadrupole components in the following way

$$S^\alpha = -i\epsilon^{\alpha\beta\gamma} \mathcal{A}^{\beta\gamma} \quad (5.29a)$$

$$Q^{\alpha\beta} = -\mathcal{A}^{\alpha\beta} - \mathcal{A}^{\beta\alpha} + \frac{2}{3}\delta^{\alpha\beta} \text{Tr}(\mathcal{A}). \quad (5.29b)$$

Due to implicit constraint on the length of the director defining the U(3) spins, a naive Metropolis update in which components of \mathcal{A} are directly sampled will not uniformly sample the 5-sphere² corresponding to the state space. I employ a generalization of the Marsaglia method that was established in [11]. In this generalization, we consider five random variables

$$\theta_1, \theta_2 \in [0, 1], \quad (5.30)$$

$$\phi_1, \phi_2, \phi_3 \in [0, 2\pi], \quad (5.31)$$

²Recall that the director has a total of six real degrees of freedom, and the length constraint fixes one of these. Therefore in the scheme described here, the global phase degree of freedom is also be sampled over, though in principle could be removed, restrictin instead to sampling over the 4-sphere.

from which the corresponding random director takes the form

$$\mathbf{d} = (x_1 + ix_2, x_3 + ix_4, x_5 + ix_6), \quad (5.32)$$

with

$$x_1 = \theta_2^{\frac{1}{4}} \theta_1^{\frac{1}{2}} \sin(\phi_1), \quad (5.33a)$$

$$x_2 = \theta_2^{\frac{1}{4}} \theta_1^{\frac{1}{2}} \cos(\phi_1), \quad (5.33b)$$

$$x_3 = \theta_2^{\frac{1}{4}} \sqrt{1 - \theta_1} \sin(\phi_2), \quad (5.33c)$$

$$x_4 = \theta_2^{\frac{1}{4}} \sqrt{1 - \theta_1} \cos(\phi_2), \quad (5.33d)$$

$$x_5 = \sqrt{1 - \theta_2^{\frac{1}{2}}} \sin(\phi_3), \quad (5.33e)$$

$$x_6 = \sqrt{1 - \theta_2^{\frac{1}{2}}} \cos(\phi_3). \quad (5.33f)$$

The statistical independence of the six resulting components x_i is valid in the limit of large numbers of samples, as showcased by the convergence of the second moments of the components, see Fig. 5.2.

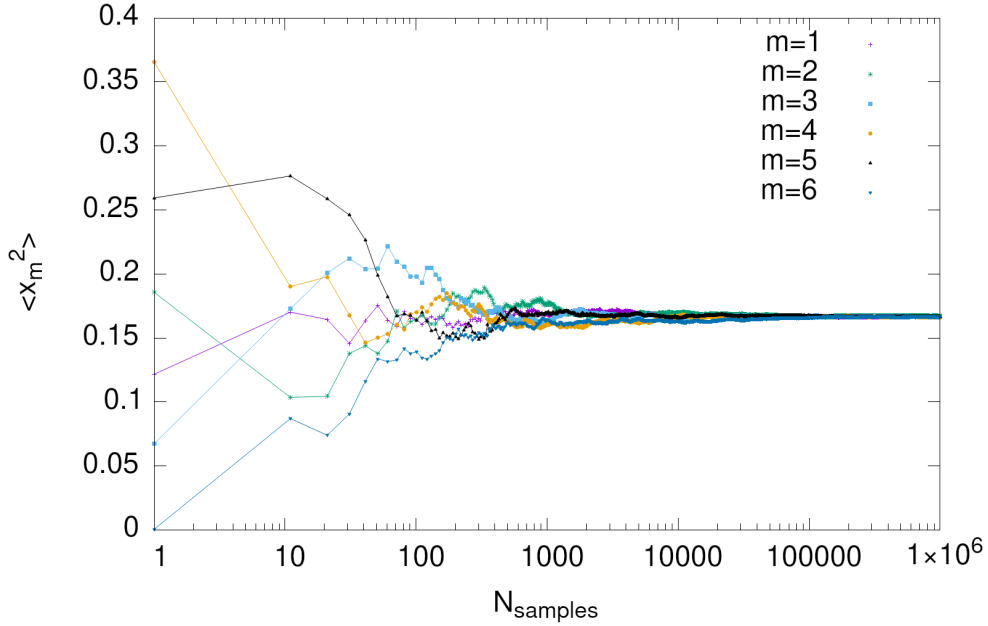


Figure 5.2: Convergence of the second moments of the derived components x_m at large sampling number, revealing firstly that the statistical errors in all components respect the central-limit theorem and secondly that the expressions Eq. (5.33) components are not biased or correlated.

Within the U(3) formalism, in addition to the equal-time structure factor corresponding to dipole-dipole correlations (c.f. Eq. (1.40)), we define the equal-time structure factors corresponding to the two-point correlations of the \mathcal{A} and \mathcal{Q} tensor

operators

$$S_{\mathcal{Q}}(\mathbf{q}) = \frac{1}{N} \sum_{\alpha\beta} \sum_{i,j}^N \langle \mathcal{Q}^{\alpha\beta}(\mathbf{r}_i) \mathcal{Q}^{\alpha\beta}(\mathbf{r}_j) \rangle e^{-\mathbf{q} \cdot (\mathbf{r}_i - \mathbf{r}_j)} , \quad (5.34a)$$

$$S_{\mathcal{A}}(\mathbf{q}) = \frac{1}{N} \sum_{\alpha\beta} \sum_{i,j}^N \langle \mathcal{A}^{\alpha\beta}(\mathbf{r}_i) \mathcal{A}^{\alpha\beta}(\mathbf{r}_j) \rangle e^{-\mathbf{q} \cdot (\mathbf{r}_i - \mathbf{r}_j)} , \quad (5.34b)$$

As a necessary precursor for studying the dynamical structure factors, I use these quantities as benchmarks for my U(3) triangular lattice simulation and obtain results in agreement with [11], as shown in Fig. 5.3. All Fourier transformations are carried out using the FFTW3 library [238].

In the next Section, I will describe the procedure I follow for carrying out dynamical simulations, which can be applied to any model system whose equations of motion can be decoupled into a system of linear differential equations.

5.2 Molecular Dynamics

The dynamics of the spin systems of interest are governed by sets of linear differential equations. In this Section, I will review the Runge-Kutta method for integration of coupled sets of linear differential equations, and showcase its application on XY, Heisenberg and spin-1 systems, reproducing their excitation spectrum.

5.2.1 Runge-Kutta methods

Following the treatment in [239], I will briefly review how Runge-Kutta methods can be used to simulate the dynamics of a system whose initial state is known, provided the equations of motion can be decomposed into a set of linear differential equations. The application of such techniques to the study of spin systems has been long established, e.g. [240, 241], and the name Molecular Dynamics has been used in analogy to its use in the simulation of the positional degrees of freedom of atoms and molecules.

Assume the dynamical quantity of interest is a multivariable function y , with equation of motion

$$\frac{dy}{dt} = f(y, t) . \quad (5.35)$$

If we know the initial condition y_0 , then we can to high degree of accuracy approximate the value of y at the next timestep

$$y_1 = y_0 + h \sum_{i=1}^N b_i k_i \quad (5.36)$$

where h denotes the size of the timestep and we can specify the number of stages n that we wish to include

$$k_1 = f(y_0, t_0) , \quad (5.37a)$$

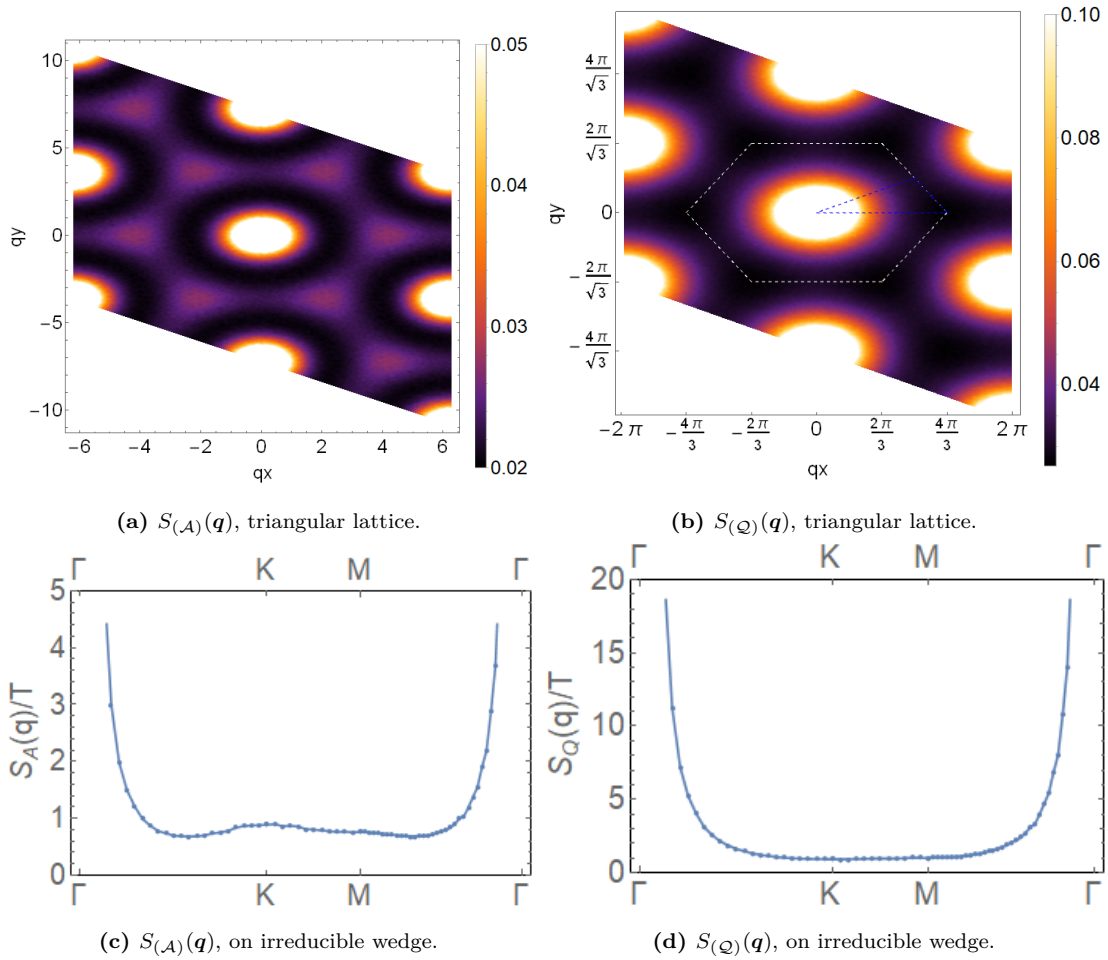


Figure 5.3: Sample benchmark plots for classical Monte Carlo simulation of the spin-1 Bilinear-Biquadratic model Eq. 5.28 on the triangular lattice, showing agreement with results Fig. 15 in [11]. (a) Equal-time structure factor measuring correlations of the \mathcal{A} degrees of freedom, evaluated at $T = 0.030J$ for the triangular lattice Bilinear-Biquadratic model, for $J_1 = 0$ and $J_2 = -1$. (b) Equal-time structure factor for \mathcal{Q} degrees of freedom, evaluated for the same parameters. The Brillouin zone boundary is depicted in white dashed line, and the blue dashed line delineates the irreducible wedge. (c) Corresponding slice of $S_{\mathcal{A}}(\mathbf{q})$ along the irreducible wedge, evaluated at $T = 0.030J$ for the triangular lattice Bilinear-Biquadratic model, for $J_1 = 0$ and $J_2 = -1$. (d) Corresponding slice of $S_{\mathcal{Q}}(\mathbf{q})$ along the irreducible wedge, evaluated at $T = 0.030J$ for the triangular lattice Bilinear-Biquadratic model, for $J_1 = 0$ and $J_2 = -1$.

$$k_2 = f(y_0 + ha_{21}k_1, t_0 + c_2h) , \quad (5.37b)$$

$$k_3 = f(y_0 + h(a_{31}k_1 + a_{32}k_2), t_0 + c_3h) \quad (5.37c)$$

$$\vdots \quad (5.37d)$$

$$k_n = f(y_0 + h \sum_{i=1}^{n-1} a_{ni}k_i, t_0 + c_nh) , \quad (5.37e)$$

where choice of coefficients that obey

$$c_i = \sum_{j=1}^{n-1} a_{ij} \quad (5.38a)$$

$$\sum_i b_i = 1 , \quad (5.38b)$$

will produce best results. Note that for equations of motion in which time does not explicitly feature, the c coefficients do not play a role.

Higher order Runge-Kutta schemes provide more accurate results at times far removed from the initial condition. The fourth order Runge-Kutta method is empirically known to exhibit an ideal balance between algorithmic complexity and accuracy of results [239], and I employ the fourth-order method in all dynamical simulation results I present here.

5.2.2 Dynamical structure factors from simulation

One reason to carry out dynamical simulations of magnetic systems can be to study their real-space dynamics. Another is to reveal statistical properties about the excitation structure of a model. In this Section, I will describe how I use Runge-Kutta integration to reproduce the dynamical structure factors for the XY, Heisenberg and U3 spin models to further benchmark my simulations, before moving on to study the real-space dynamics of analogue gravitational waves.

The dynamics of two-point spin correlations are an important observable which can be probed in magnetic materials using inelastic neutron scattering experiments. The relevant observable quantity for spin dipoles is

$$S(\mathbf{q}, \omega) = \sum_{\alpha} \frac{1}{2\pi N} \int_{-\infty}^{\infty} dt e^{i\omega t} \sum_{i,j} e^{i\mathbf{q}(\mathbf{r}_i - \mathbf{r}_j)} \langle S^{\alpha}(\mathbf{r}_i, 0) S^{\alpha}(\mathbf{r}_j, t) \rangle , \quad (5.39)$$

and can be defined in terms of a discrete equivalent measured from numerical simulation

$$S^{\alpha}(\mathbf{q}, \omega) = \sum_{\alpha} \frac{1}{NN_t} \sum_{t=1}^{N_t} e^{i\omega t} \sum_{i,j=1}^N e^{i\mathbf{q}(\mathbf{r}_i - \mathbf{r}_j)} \langle S^{\alpha}(\mathbf{r}_i, 0) S^{\alpha}(\mathbf{r}_j, t) \rangle , \quad (5.40)$$

with the average defined as the thermal ensemble average over a statistically significant number of independent spin configurations³, which can be generated by classical Monte Carlo simulation.

³For the results in this Thesis, I average over $\mathcal{O}(10^5)$ configurations.

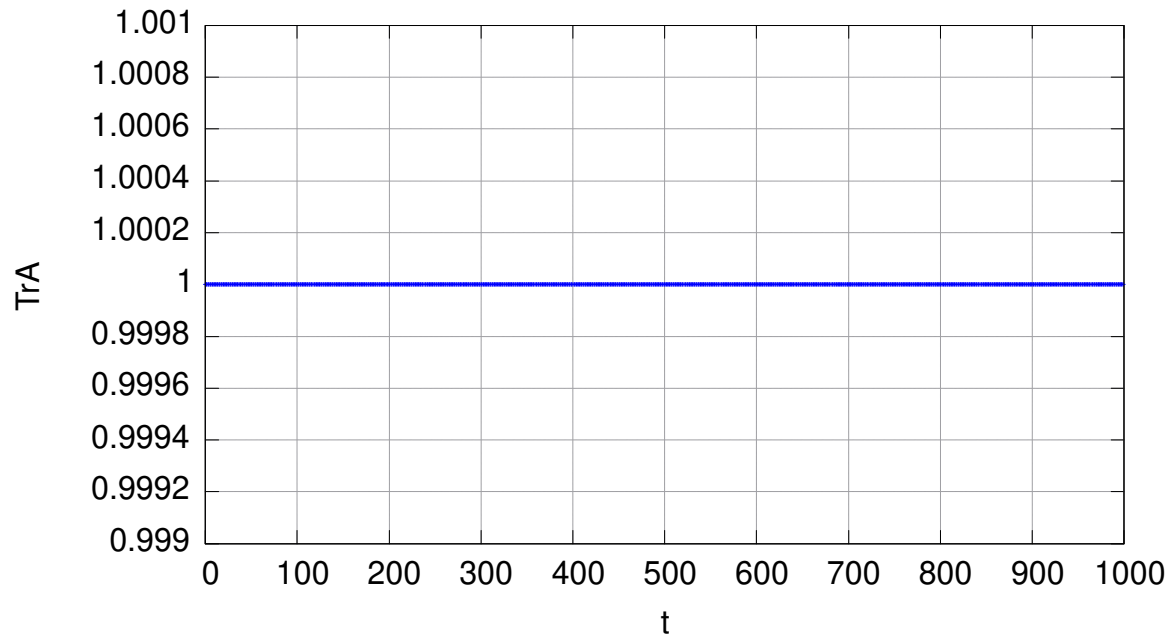
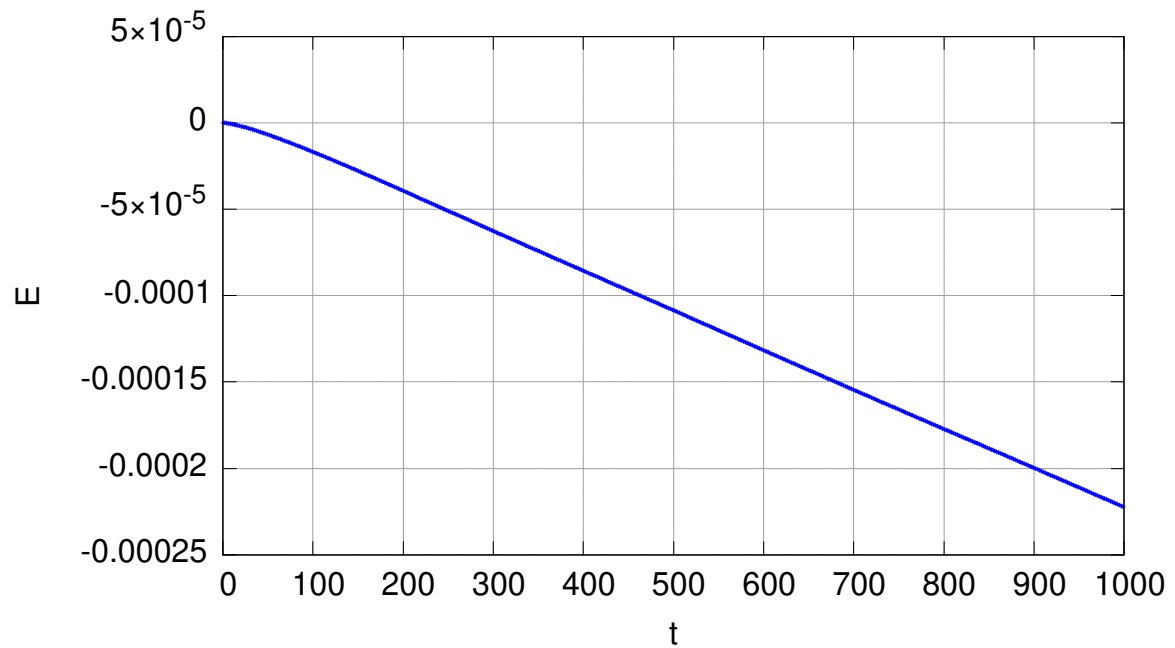
(a) $\text{Tr}(\mathcal{A})(t)$.(b) $E(t)$.

Figure 5.4: Benchmark plots for fourth-order Runge-Kutta simulation of the $U(3)$ equations of motion Eq. 5.46. **(a)** Conserved quantities related to the spin length, such as $\text{Tr}(\mathcal{A})$ shown here, are useful diagnostics for correct implementation of the simulation. For all states simulated $\text{Tr}(\mathcal{A}) = 1$, and it remains so to machine precision for the duration of simulation. **(b)** Deviation of the energy from the initial configuration for a $U(3)$ ferroquadrupolar state as the system is time evolved with a fourth-order Runge-Kutta method. Small errors are accrued and can be further reduced in magnitude by decreasing the simulation stepsize h .

For the case of spin-1 within the U(3) representation, we can additionally define the dynamical structure factors for the quadrupole degree of freedom

$$\begin{aligned} S_{\mathcal{Q}}(\mathbf{q}, \omega) &= \sum_{\alpha, \beta} \int \frac{dt}{2\pi} e^{i\omega t} \langle \mathcal{Q}^{\alpha\beta}(\mathbf{q}, t) \mathcal{Q}^{\alpha\beta}(-\mathbf{q}, 0) \rangle, \\ &= \frac{1}{NN_t} \sum_{t=1}^{N_t} e^{i\omega t} \sum_{i,j=1}^N e^{i\mathbf{q}(\mathbf{r}_i - \mathbf{r}_j)} \langle \mathcal{Q}^{\alpha\beta}(\mathbf{r}_i, 0) \mathcal{Q}^{\alpha\beta}(\mathbf{r}_j, t) \rangle. \end{aligned} \quad (5.41)$$

and the tensor operator \mathcal{A}

$$S_{\mathcal{A}}(\mathbf{q}, \omega) = \frac{1}{NN_t} \sum_{t=1}^{N_t} e^{i\omega t} \sum_{i,j=1}^N e^{i\mathbf{q}(\mathbf{r}_i - \mathbf{r}_j)} \langle \mathcal{A}^{\alpha\beta}(\mathbf{r}_i, 0) \mathcal{A}^{\alpha\beta}(\mathbf{r}_j, t) \rangle. \quad (5.42)$$

In previous chapters of this Thesis we have discussed several connections between the Goldstone modes of certain ordered phases of spin systems, such as known for the ferromagnetic XY magnet, implicitly known for the Heisenberg antiferromagnet and now established here for spin nematics. The common thread amongst these systems is the linearly-dispersive character of the low-energy excitations which can be obtained by Molecular Dynamics simulation.

I next briefly list the equations of motion for XY, O(3) and U(3) spins, which all can be cast into linear differential equations.

For the classical XY model, the Hamiltonian dynamics give us

$$\dot{p}_i = -\frac{\partial H}{\partial \theta_i} = JS^2 \sum_{\langle ij \rangle} \sin(\theta_i - \theta_j), \quad (5.43a)$$

$$\dot{\theta}_i = p_i, \quad (5.43b)$$

for which I use a fourth-order Runge-Kutta method to simulate dynamics. In Fig. 5.5a, we observe the linearly dispersing Goldstone mode at low energies, which is analogous to an electromagnetic wave in flatland.

For Heisenberg spins, we have already seen in Chapter 3 the form of the equations of motion

$$\partial_t \vec{S}_i = \sum_{\delta} \vec{S}_i \times \vec{S}_{i+\delta} \quad (5.44)$$

for which I again use a fourth-order Runge-Kutta method to simulate dynamics. In Fig. 5.5b, we observe the linearly dispersing Goldstone mode corresponding to transverse photons at low energies.

For U(3) spins, it was established in [11] that the equations of motion reduce to a linear differential equation

$$\partial_t A_i^{\alpha\beta} = -i[A_i^{\alpha\beta}, H] \quad (5.45)$$

$$= -i \sum_{\delta} \left(J_1 (A_i^{\alpha\sigma} A_{i+\delta}^{\sigma\beta} - A_i^{\sigma\beta} A_{i+\delta}^{\alpha\sigma}) + (J_2 - J_1) (A_i^{\alpha\sigma} A_{i+\delta}^{\beta\sigma} - A_i^{\sigma\beta} A_{i+\delta}^{\sigma\alpha}) \right), \quad (5.46)$$

for which I also employ a fourth-order Runge-Kutta method to simulate dynamics,

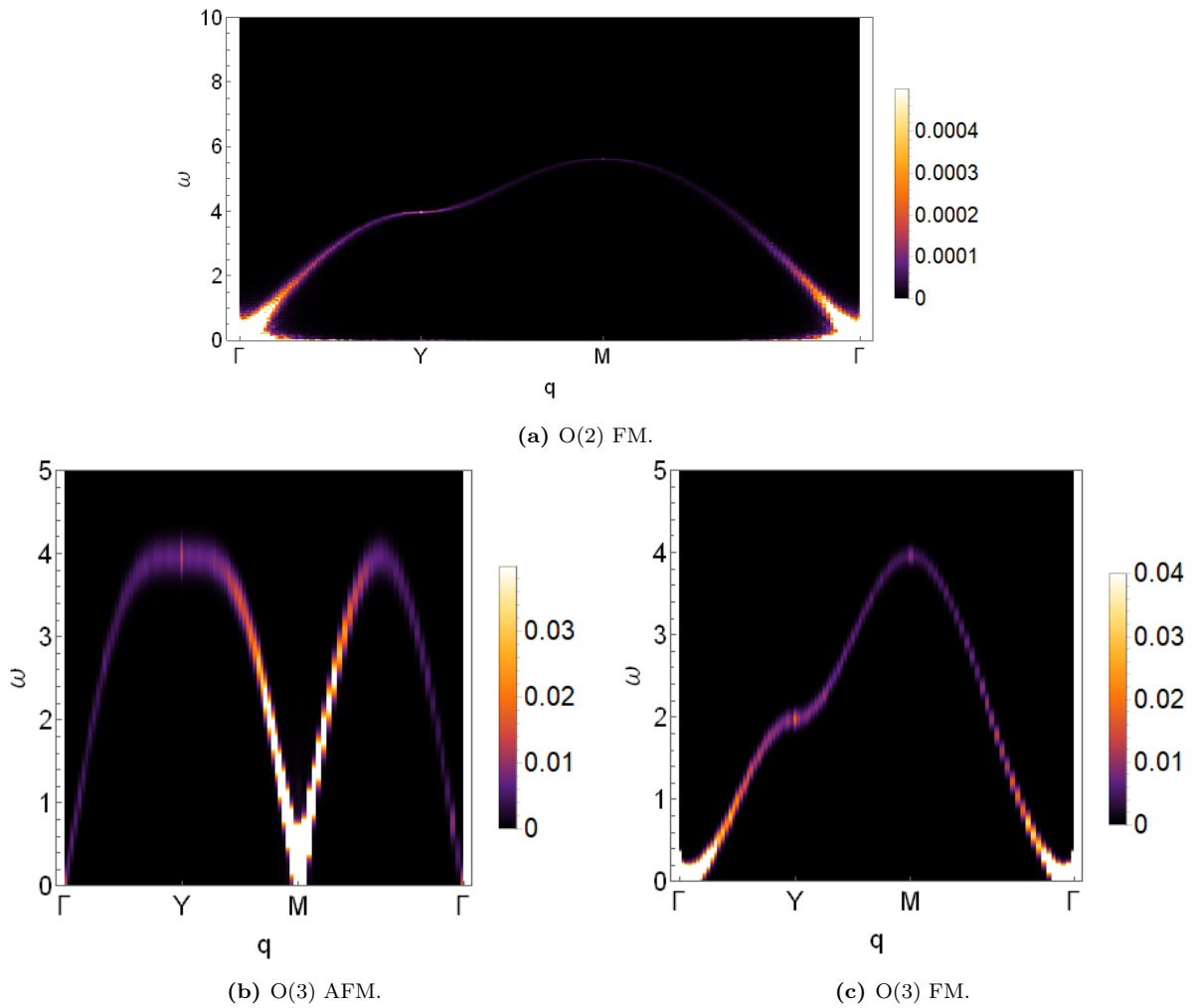


Figure 5.5: $S(\mathbf{q}, \omega)$ evaluated from Molecular Dynamics simulations for different models on the square lattice, showcasing the different character of the low-energy excitations. (a) $S(\mathbf{q}, \omega)$ on the irreducible wedge for the square lattice XY ferromagnet at $T = 0.010J$, showing the linearly dispersing Goldstone mode. (b) $S(\mathbf{q}, \omega)$ on the irreducible wedge for the square lattice O(3) antiferromagnet at $T = 0.010$, showing the linearly dispersing Goldstone modes. (c) $S(\mathbf{q}, \omega)$ on the irreducible wedge for the square lattice O(3) ferromagnet at $T = 0.010J$, showing the quadratically dispersing Goldstone mode.

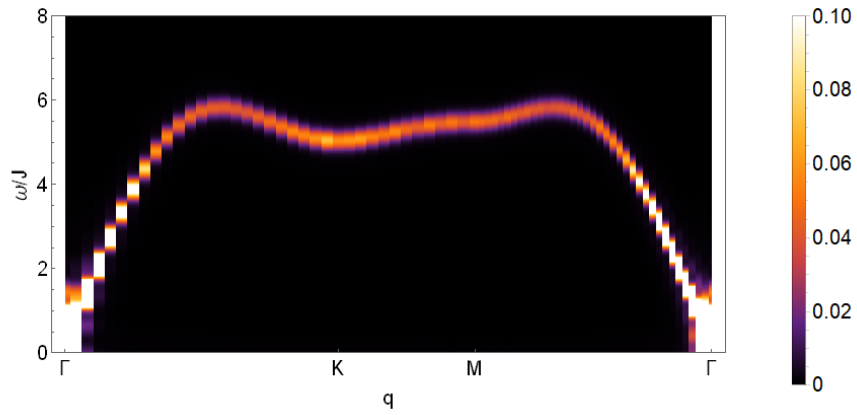
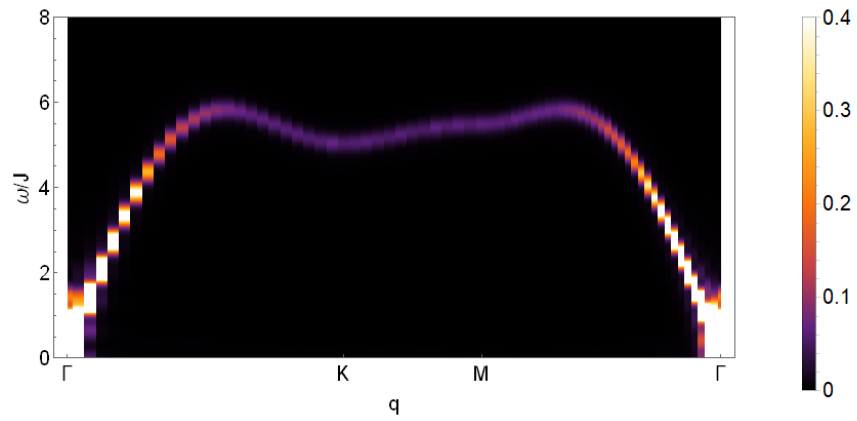
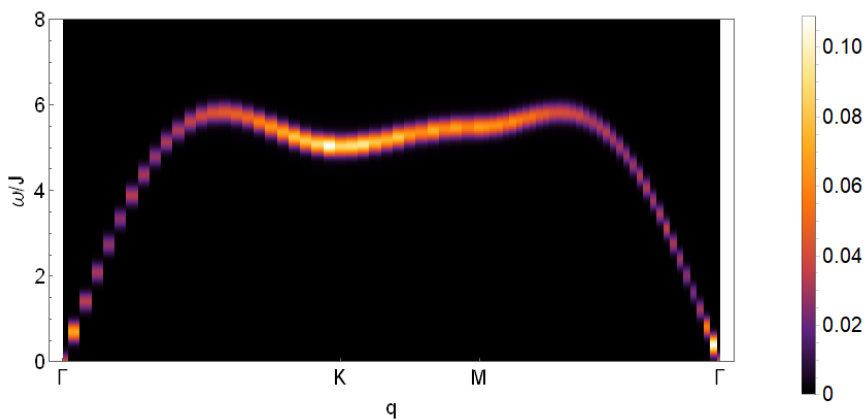
(a) $S_{\mathcal{A}}(\mathbf{q}, \omega)$.(b) $S_{\mathcal{Q}}(\mathbf{q}, \omega)$.(c) $S(\mathbf{q}, \omega)$.

Figure 5.6: Molecular dynamics simulations showing the excitation spectra of a ferroquadrupolar spin nematic, on the triangular lattice Bilinear-Biquadratic model at $J_1 = 0$ and $J_2 = -1$, at $T = 0.050$. These results are in agreement with Fig. 16 in [11]. (a) $S_{\mathcal{A}}(\mathbf{q}, \omega)$, (b) $S_{\mathcal{Q}}(\mathbf{q}, \omega)$ and (c) $S(\mathbf{q}, \omega)$ on the irreducible wedge for the specified parameters.

with stepsize

$$h = \frac{2\pi}{10 \omega_{\max}}, \quad (5.47)$$

where ω_{\max} is the largest frequency present in the spectrum, which is model dependent. This resolution of time steps yields an acceptable accuracy for the simulation timescales of interest, see Fig. 5.4b. Note crucially that in Fig. 5.6b we observe maximal weight corresponding to the linearly dispersing Goldstone mode corresponding to transverse gravitational waves at low energies. At higher energies, the weight mixes into the dipole channel, as alluded to in Chapter 4.

Having discussed my simulation methods and respective benchmarks for both thermodynamic measurements and dynamics, I turn to their application to the context of spin nematic gravitational waves and how these can be generated.

5.3 Connecting it all: nematic gravitational waves in simulation

We have seen in this Thesis arguments for the ferroquadrupolar spin-nematic phase to exhibit two quadrupolar Goldstone modes, which are strikingly like gravitational waves in vacuum. In this final Section, I show numerical results confirming that such waves exist at low-energies in the quadrupolar channel, by examining the specific case of a two-dimensional spin nematic⁴ in which they can be generated by the annihilation of two \mathbb{Z}^2 vortices. Furthermore, the dynamics of the \mathbb{Z}^2 vortices is attractive, suggestive of further parallels with mass.

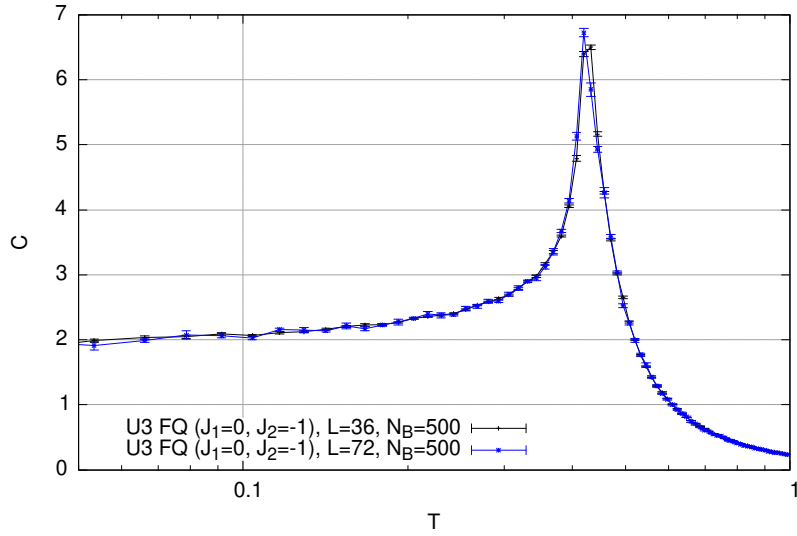
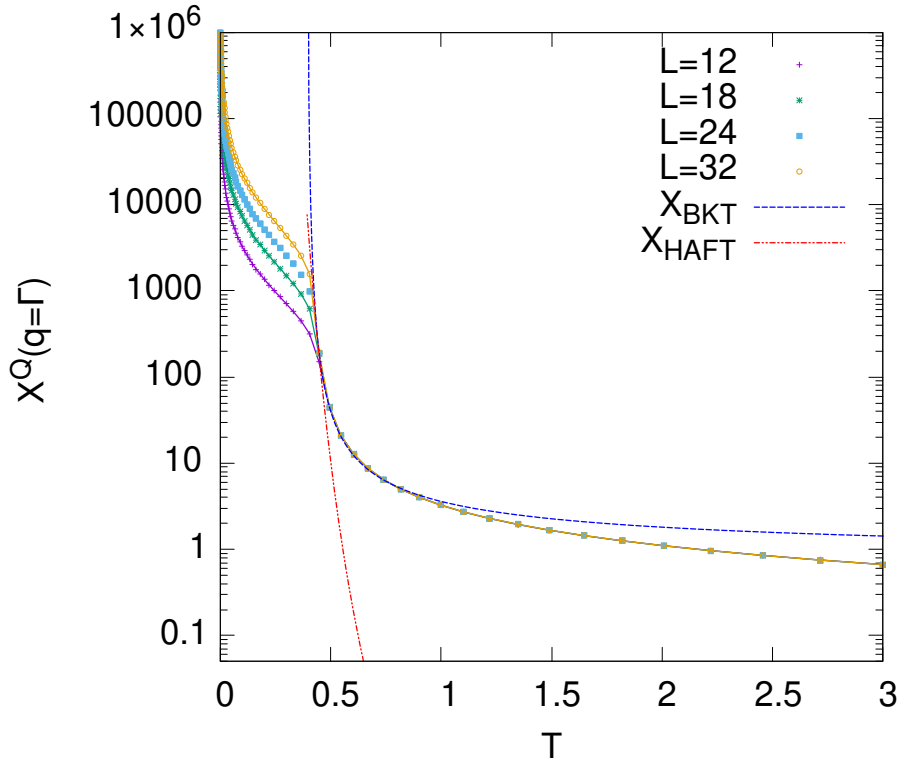
5.3.1 Possible topologically mediated transition in 2D spin nematics

As was discussed in Chapter 2, true long-range order cannot exist in reduced dimensional quantum systems at finite temperature unless mediated by another mechanism such as topological excitations, as exemplified by the XY ferromagnet. Previous work on the triangular lattice $O(3)$ Bilinear-Biquadratic model in Monte Carlo simulation shows evidence for a topological phase transition [242]. However, recent results from tensor network calculations do not find evidence for such a topological phase transition in 2D [243]. The question can also be raised whether in the triangular lattice $U(3)$ Bilinear-Biquadratic model there is a topologically mediated phase transition.

Here I provide a phenomenological argument to suggest that the ferroquadrupolar phase in the triangular lattice Bilinear-Biquadratic model could exhibit a topologically mediated phase transition. This analysis builds on earlier unpublished work by my collaborator Rico Pohle [244].

The ferroquadrupolar phase of the Bilinear-Biquadratic model exhibits a peak in the heat capacity at finite temperature, see Fig. 5.7a. As discussed in Chapter 2,

⁴Recall as discussed at the end of Section 4.5.1 that the dimensionality of the system is unimportant for the validity of the analogue, which relies on the internal dimensions of the Hilbert space.

(a) Heat capacity for the Bilinear-Biquadratic model with $J_1 = 0.0$, $J_2 = 1.0$.

(b) Order parameter susceptibility

Figure 5.7: Exploration of topological phase transition into the ferroquadrupolar phase. **(a)** Heat capacity as a function of temperature in the U(3) triangular lattice Bilinear-Biquadratic model at $J_1 = 0$ and $J_2 = -1$, exhibiting a peak in the heat capacity. **(b)** Order parameter susceptibility as a function of temperature in the U(3) triangular lattice Bilinear-Biquadratic model at $J_1 = 0$ and $J_2 = -1$, exhibiting as scaling behaviour in good agreement with the scaling analytically predicted for the BKT transition. This is consistent with the onset of a topologically mediated phase transition into the ferroquadrupolar phase.

the Mermin-Wagner theorem prevents the system from undergoing a transition to a true long-range ordered phase at finite temperature. One could hypothesize that the heat capacity peak arises for one of two reasons: either the peak is a finite-size effect driven by the Goldstone modes, and should migrate towards zero-temperature in the thermodynamic limit; or the finite-size feature is indicative of vortices, signaling that there is a temperature below which there is an underlying change in the structure of correlations, akin to the BKT transition in the XY model, characterized by algebraic correlations at temperatures below the critical temperature.

Specifically, the correlation length in the paramagnetic regime for the BKT transition in the 2D XY model scales as [45, 47, 245]

$$\xi_{\text{BKT}} \sim e^{\frac{b}{\sqrt{T-T_c}}} , \quad (5.48)$$

where b is a critical exponent, in this case specific to the BKT universality class, and T_c is the critical temperature. The structure factor is expected to scale as [45, 246]

$$S(\mathbf{q}) \sim \xi_{\text{BKT}}^{2-\eta} , \quad (5.49)$$

where for the BKT transition

$$\eta = \frac{1}{4} . \quad (5.50)$$

The equivalent scaling behaviours for the ferroquadrupolar nematic phase has not been derived to the best of our knowledge, and was beyond the scope of this project to derive independently. In the absence of an established RG calculation, we construct a phenomenological description of the paramagnetic regime, borrowing scaling relations applicable to other models which share some similarities and compare their scaling to results from simulation. We consider comparison to the XY ferromagnet and the O(3) antiferromagnet, each presented in turn below.

We first examine if a parallel to the vortex physics exhibited by the XY model and its BKT transition can be established. For comparison with simulation we define a quantity derived from the two-point correlations, called the order parameter susceptibility, which for the ferroquadrupolar phase takes the form

$$\chi^{(Q)}(\mathbf{q}) = \frac{S_Q(\mathbf{q})}{T} , \quad (5.51)$$

which contains information about the correlations in the paramagnetic regime.

For the BKT transition, the scaling behaviour for this quantity follows from Eq. (5.49)

$$\chi_{\text{BKT}}^{(Q)} = C_{\text{BKT}} e^{\frac{7b}{4\sqrt{T-T_c}}} . \quad (5.52)$$

Fitting the order parameter susceptibility Eq. (5.51) from simulation in the paramagnetic regime at the Γ -point to the form of the scaling relation Eq. (5.52) leads to the following values for the exponent b and parameters

$$b \approx 0.8 , \quad (5.53a)$$

$$T_c = 0.39 , \quad (5.53b)$$

$$C_{KT} \approx 6.0 , \quad (5.53c)$$

and the result of the fit is shown in Fig. 5.7b.

Next we analyze the relevance of Goldstone modes on the scaling behaviour, borrowing existing treatments for an O(3) antiferromagnet. The low-energy physics corresponding to the ferroquadrupolar phase is described by a non-linear sigma model Eq. (4.87), with degrees of freedom inhabiting a Hilbert space larger than just SU(2) alone. That said, we have also seen how the low-energy physics of the Heisenberg antiferromagnet maps onto an O(3) non-linear sigma model. Therefore, we can phenomenologically motivate a comparison between scaling relations for the classical O(3) triangular-lattice antiferromagnet (HAFT) and the triangular lattice ferroquadrupole. The scaling behaviour of the correlation length for the former has been established [246–248]

$$\xi_{\text{HAFT}} \sim \left(\frac{T}{B}\right)^{\frac{1}{2}} e^{2\frac{B}{T}} , \quad (5.54)$$

where B is a parameter specific to the model, and with the corresponding scaling for the order parameter susceptibility [246]

$$\chi_{\text{HAFT}}^{(Q)} = C_{\text{HAFT}} \left(\frac{T}{B}\right)^4 e^{2\frac{B}{T}} , \quad (5.55)$$

where C_{HAFT} is a constant. Unlike the 2D XY model, the triangular lattice antiferromagnet is not believed to exhibit any order at finite temperature. There is no associated proliferation of vortices mediating a topological phase transition, and the correlation length diverges at zero temperature.

Fitting the order parameter susceptibility Eq. (5.51) from simulation again in the paramagnetic regime at the Γ -point to this case Eq. (5.55) leads to the following values for the parameters

$$B \approx 6.994 , \quad (5.56a)$$

$$C_{\text{HAFT}} \approx 3 \cdot 10^{-7} , \quad (5.56b)$$

and the result of the fit is also shown in Fig. 5.7b.

The thermodynamic results for the order parameter susceptibility at the ferroquadrupolar ordering vector $\mathbf{q} = \Gamma$ shown in Fig. 5.7b reveal that it exhibits a scaling behaviour in the paramagnetic regime remarkably close to that predicted for the BKT transition. This is consistent with the possibility that the two-dimensional ferroquadrupolar phase exhibits a topologically mediated crossover. However, given the approximations made in the current analysis, we cannot provide a definitive answer regarding the nature of the phase transition in the U(3) Bilinear-Biquadratic model. That said, the presence of vortices is self-evident in 2D, both in experiment [249] and in the simulations which are presented next in this Chapter. It is these vortices in the low temperature phase that will next occupy our attention for the purposes of this Thesis.

5.3.2 Attractive interactions between vortex pairs

As discussed in Chapter 4, the order parameter space supports vortex point defects. These show up in abundance in Monte Carlo simulations when the high temperature paramagnet is quenched quickly to the low temperature phase, freezing in the higher-energy vortex states that would otherwise be highly improbable to find using local updates alone. The configurations obtained from Monte Carlo can then be time-evolved using the Molecular Dynamics scheme described Section 5.2. As briefly alluded to at the end of Chapter 4, the dynamical simulations reveal patterns of attractive interaction between vortices, much like gravitational interactions, see Fig. 5.8 and Fig. 5.9, described in more detail below. However, it should be noted that—in contrast to massive objects in gravity—the \mathbb{Z}^2 nature of the vortices ultimately leads to the annihilation of the attracted defect pair, rather than their coalescence. Nevertheless, as for the case of massive gravitating objects—such as neutron stars and black-holes—on their in-spiral leading up to a merger event, there are analogue gravitational waves emitted by pairs of interacting vortices in close proximity. The amplitude of these waves can be seen even at finite temperature above the thermal fluctuations of the background.

In Fig. 5.8, we see a series of images from simulation showing the total quadrupole operator, defined as

$$\sum_{\alpha\beta} Q^{\alpha\beta}. \quad (5.57)$$

The first image, labeled $t = 0$, shows a sample configuration extracted from Monte-Carlo simulation of the Bilinear-Biquadratic model, in which periodic boundary conditions were used, at a finite-temperature below the threshold temperature $T_c \approx 0.39$. In this image, there are many \mathbb{Z}^2 vortices present. The sample configuration is then time evolved using the Molecular Dynamics simulation previously described, with periodic boundary conditions. The next image is taken from the simulation at timestep $t = 11$, by which time several pairs of vortices that were in close proximity within the original configuration have annihilated. By timestep $t = 25$, several other defect pairs have attracted and undergone annihilation events. Each annihilation event is both preceded and followed by emission of ripples in the quadrupolar channel, which I will show in closer detail in Fig. 5.9.

In order to study the waves emitted by such events in more detail, I initialize a vortex pair in terms of director configurations as defined in the context of classical 2D nematic liquid crystals [250]

$$\mathbf{d}(\mathbf{r}) = \begin{cases} (-\sin \theta(\mathbf{r}), \cos \theta(\mathbf{r}), 0) & \text{for } x_1 \leq x \leq x_2, \\ (\cos \theta(\mathbf{r}), \sin \theta(\mathbf{r}), 0) & \text{otherwise} \end{cases}, \quad (5.58a)$$

where

$$\theta(\mathbf{r}) = \frac{1}{2} \tan^{-1} \left(\frac{y - y_1}{x - x_1} \right) - \frac{1}{2} \tan^{-1} \left(\frac{y - y_2}{x - x_2} \right). \quad (5.59)$$

with vortices located at

$$\mathbf{r}_i = (x_i, y_i) \text{ s.} \quad (5.60)$$

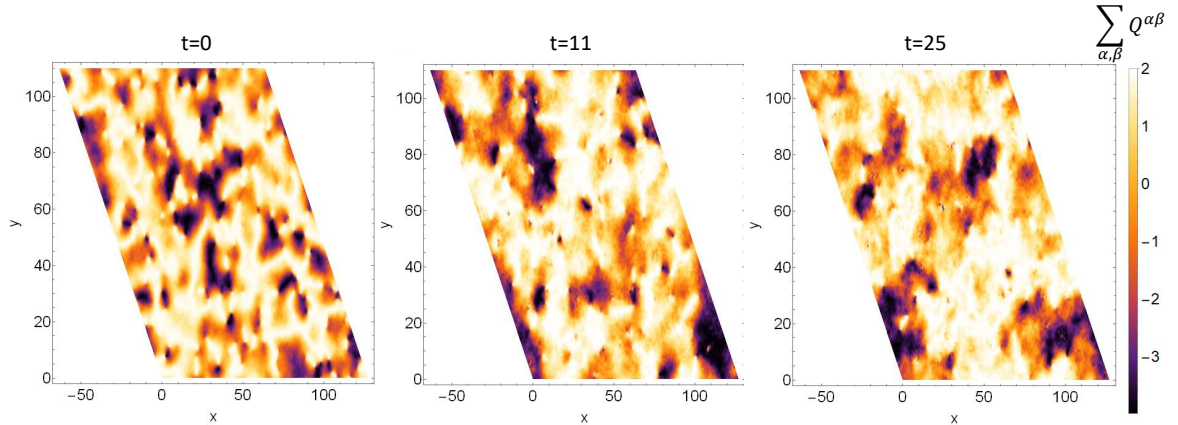


Figure 5.8: Sequence of images showing the total quadrupolar operator $\sum_{\alpha\beta} Q^{\alpha\beta}$ in real-space, obtained by time-evolution acting on a single configuration extracted from Monte Carlo simulation. The image is riddled with Z^2 vortices, which experience attractive interactions and generate analogue gravitational waves during the in-spiral leading up to, during and after annihilation events, see also Fig 5.9.

This indeed describes the point defects that arise in the Monte Carlo study: vortices whose core has zero radius. In the context of the ferroquadrupolar phase, the sign associated to either of the above defined defects is in fact not important, since the nature of the order parameter space connects all such defects, see Fig. 4.4. In this way, a simulation effectively at zero temperature—therefore free of thermal noise—can be carried out. Using this scheme, I study the evolution of wave emission from an interacting defect pair, shown in Fig. 5.9. At the start of the simulation, two vortices sit at a distance of 15 lattice sites on a lattice of $L_x = L_y = 180$ sites. They experience an attractive interaction, which starts slowly and gradually accelerates, and is associated with an outpouring of quadrupolar wave trains. There is significant motion occurring beyond timestep $t = 500$. Until timestep $t = 630$, there are still two distinguishable vortices. After that time, they are annihilated, with a fresh wave train released associated to the annihilation event. This large amplitude front can be seen in the subsequent images as it propagates outwards. Waves continue to be emitted immediately following the annihilation, as is the case for gravitational merger events.

Note that there is a different source of systematic error in this simulation, arises from the top and bottom boundaries of the system where periodic boundary conditions provide an interface between regions of distinct director alignment. This noise reaches the field-of-view shown in these images by timestep $t \approx 350$, and can be seen faintly in the results of Fig. 5.9 and Fig. 5.10.

5.3.3 The “chirp” of nematic gravitational waves

The results of dynamical simulation shown in Fig. 5.9 reveal that for each vortex-pair annihilation there are emitted wavefronts in the quadrupolar channel that correspond to analogue gravitational waves. To make further comparison of this phenomena with that of real gravitational wave observations, I next study the frequency decomposition of the wavefronts as a function of time. We will see that the frequency distribution changes

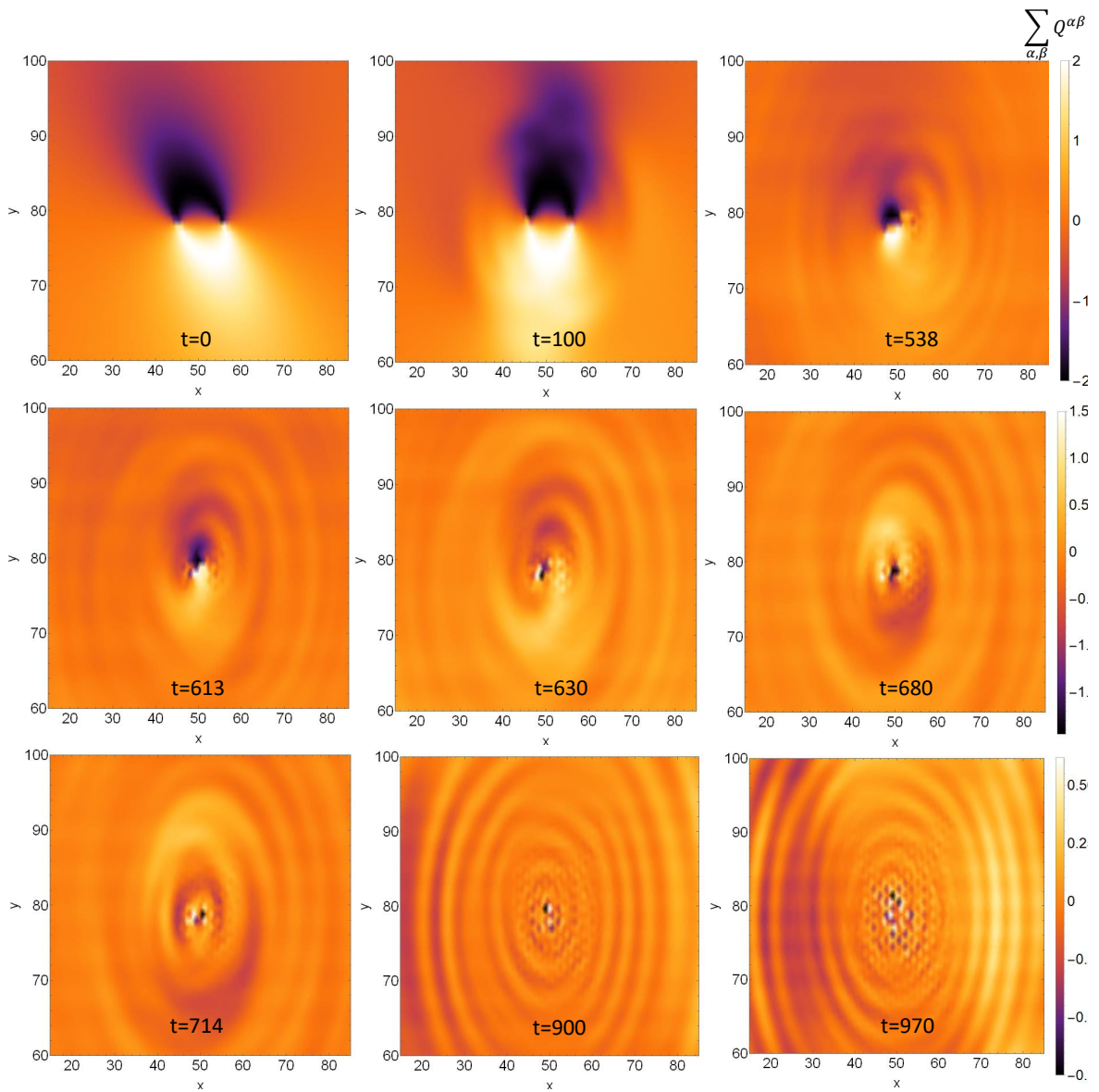


Figure 5.9: Sequence of close-up images showing the total quadrupolar operator $\sum_{\alpha,\beta} Q^{\alpha\beta}$ in real-space, obtained by time-evolution of an initialized pair of defects. The emission of analogue gravitational waves leading to and after the annihilation event is shown.

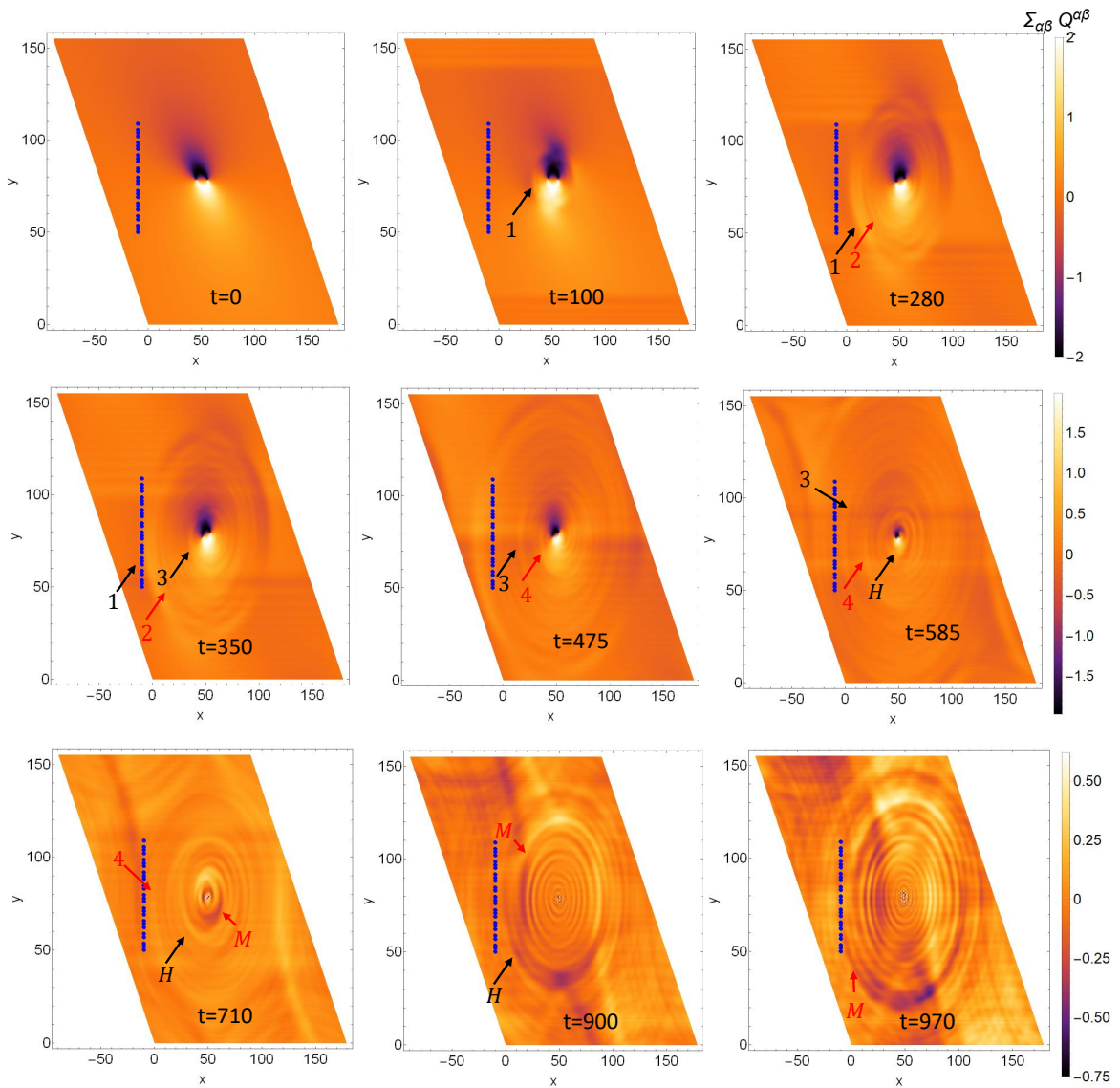
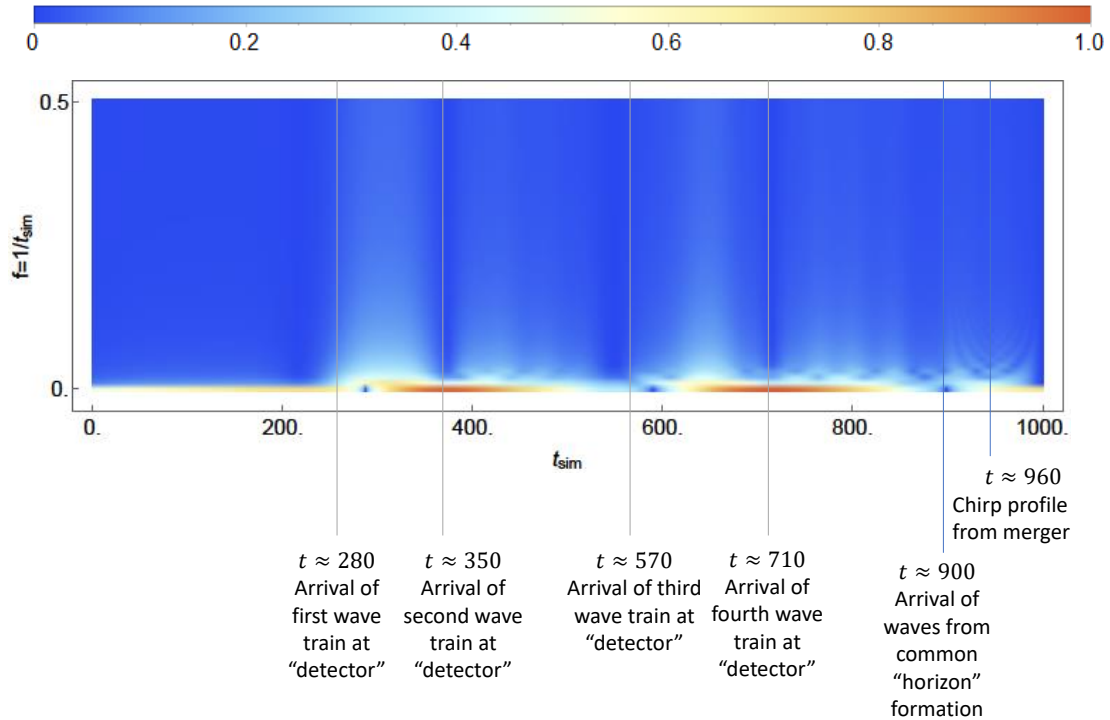
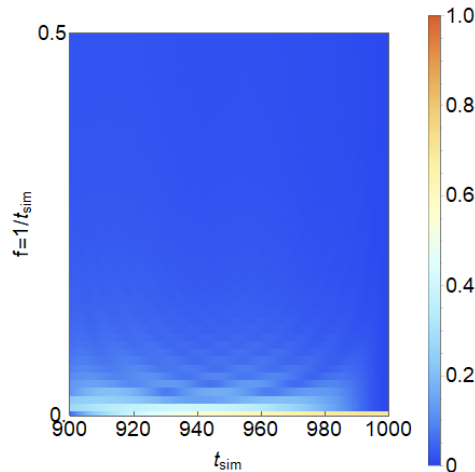


Figure 5.10: Sequence of images showing the total quadrupolar operator $\sum_{\alpha\beta} Q^{\alpha\beta}$ in real-space, obtained by time-evolution of an initialized pair of defects. The distinct wave trains corresponding to events identified in Fig. 5.11 are marked by arrows.



(a) Spectrogram from simulated gravitational wave emission.



(b) Chirp signal corresponding to vortex annihilation.

Figure 5.11: (a) Spectrogram of the time-resolved signal corresponding to the total quadrupolar operator $\sum_{\alpha\beta} Q^{\alpha\beta}$, as "measured" by a line of "detectors" placed on the triangular lattice orthogonal to the passing wavefront. The line of "detectors" is placed at a positions marked in blue in Fig. 5.10. (b) A zoom-in on the chirp emitted by the vortex annihilation, characterized by the upturn in the frequency composition of the wavefronts towards late times. Windowing artifacts are present in the signal, due to the large size of the time window relative to the duration of the merger event.

approaching the annihilation event, and that the annihilation event is associated with a sudden increase in higher frequencies called a “chirp”, in analogy to the result from the LIGO collaboration reproduced in Fig. 1.7.

Focusing on the real-space data corresponding to the total quadrupolar operator $\sum_{\alpha\beta} Q^{\alpha\beta}$, I extract a time-dependent signal corresponding to the amplitude of a wavefront at a distance from the source, a pair of in-spiraling vortices. To better sample the wavefronts and to improve the signal-to-noise ration, I do not extract this signal at a single point. Rather, I choose a line of points orthogonal to the wavefront and orthogonal to the boundary noise—therefore along the y -direction in this case—to serve as “detectors” of the quadrupolar deformation. The chosen points correspond to those shown in blue in Fig. 5.10, with some discontinuities present along this line of points due to the geometry of the triangular lattice. In real-space, we can observe by eye that there are several wave trains which are emitted prior to the annihilation event. The leading front associated to each of these is tracked in Fig. 5.10, and the selected timesteps correspond roughly to those at which each leading front arrives at the “detector” line.

To construct a spectrogram which displays time-frequency information for the signal extracted from the “detector”, I choose a time window of $\mathcal{O}(100)$ units of simulation time. This is sufficient to resolve features in the time-frequency domain without distorting their position in the time domain, as compared to the real-space data shown in Fig. 5.10. Smaller windows do not provide sufficient resolution in the frequency domain. Larger windows risk the overlap of features in the time-domain. The resulting spectrogram is shown in Fig 5.11. The events visible at marked times in the spectrogram are in turn also marked in real-space in Fig. 5.10, corresponding to the aforementioned leading wavefronts. The annihilation is associated with a special burst of wave emissions, as can be seen by eye in real-space, and which is characterized by a rapid upsweep in frequency content known as a “chirp”. The emissions during the approach and annihilation process are qualitatively similar to those of gravitational merger events, and the merger itself in the spin nematic case is also characterized by a chirp in the spectrogram, see Fig. 5.11.

In summary, the two-dimensional ferroquadrupolar spin nematic harbours vortices that experience attractive interactions, and emit analogue gravitational waves, shown in Chapter 4 to be in one-to-one correspondence with gravitational waves. The gravitational wave profile originating from a vortex-annihilation event qualitatively resembles a black-hole or neutron star merger event through the generation of a characteristic chirp.

5.4 A proposal to realize nematic gravitational waves in spinor condensates

In this Chapter, I have simulated analogue gravitational waves in spin nematics and showcased some characteristic signatures. I now develop estimates suggesting these waves can be seen with present day experiments.

5.4.1 Experimental protocol

As discussed in Chapter 4, ferroquadrupolar spin nematics have been realized in spinor condensates of ^{23}Na , e.g. [103, 107, 223], with several techniques available for measuring quadrupolar observables in real-space [109, 223, 225].

I now describe an experimental protocol that would lead to the production of analogue gravitational waves in a spinor condensate. The key to this, as illustrated in this Chapter, is to rely on the annihilation of \mathbb{Z}^2 vortex pairs to excite the quadrupolar modes. Starting with a spinor condensate of ^{23}Na atoms, a transverse optical lattice should be applied in order to isolate quasi-2D slices of the system, as done in e.g. [115]. Another optical lattice may be applied to reproduce the triangular lattice, however this is unnecessary as this spin-1 condensate is known to reproduce a nematic state without a microscopic lattice [103, 107, 223].

In order to induce the formation of vortices, the system should go through a rapid quench from a non-nematic state to the nematic state. In simulation here, I have quenched temperature from the paramagnetic to ferroquadrupolar phase. However, an easier strategy within a cold atomic gas is to perform a quench in the parameter space from a neighbouring low-temperature phase. This has already been carried out [249] by quenching from the antiferromagnetic phase to the ferroquadrupolar phase, resulting in \mathbb{Z}^2 defect formation.

Then, as illustrated in simulation here, the vortices will attract and annihilate pairwise, behaviour which can be measured in real-time using imaging with light [225], and coupling to higher hyperfine manifolds to make readouts of the quadrupolar and dipolar channels [109], as previously discussed in Chapter 4.

5.4.2 Timescales for gravitational wave analogues

There are two relevant dynamical scales that further determine the experimental accessibility of the analogue I propose. The first is the wave speed in the condensed matter medium, and the second is the vortex lifetime. On the triangular lattice, the microscopic speed of propagation I predict from the field theory is

$$v = \sqrt{2z(-J_2)(J_1 - J_2)(\alpha_1^2 + \alpha_2^2 + \alpha_3^2)}. \quad (5.61)$$

For spinor condensates, the coupling parameters J_1 and J_2 can be related to the scattering lengths [104]. I use this to make a back-of-the-envelope estimate for the wave speeds to be on the order $\mathcal{O}(1 - 10^3) \frac{\mu\text{m}}{s}$. In the solid state context, the coupling J_2 could be on the order of meV, leading to a wave speed on the order $\mathcal{O}(10^2) \frac{\text{m}}{s}$.

From simulation, the timescale associated with the annihilation of \mathbb{Z}^2 vortices is of order $10^2 J_2^{-1}$, and this can be taken as an order of magnitude estimate for the vortex lifetime. Converting this figure in terms of the value of the coupling J_2 , the back-of-the-envelope estimates I obtain for the relevant timescale are $\mathcal{O}(1)ns$ in the solid state context and $\mathcal{O}(0.1 - 10)s$.

Observation of topological defects in nematics has been carried out [249], with dynamical timescale on the order 1s, consistent with estimates I provide. In combination with the rest of the experimental achievements in the observation of spin nematics in

spinor condensates, it is highly likely that the dynamics I have studied in this Thesis can be observed without new experimental breakthroughs.

In conclusion, cold atom experiments can today reproduce all of the elements necessary to recreate and observe the gravitational wave analogues that I have investigated, and work in magnetic insulator candidates may not be far behind.

5.5 Chapter summary

In concluding this Chapter, we have provided evidence for a topologically mediated phase transition into the ferroquadrupolar phase of the triangular lattice Bilinear-Biquadratic model. The corresponding defects experience attractive interactions in analogy with gravity, and generate a wave profile analogous to that of massive inspiraling objects. These simulation results corroborate the analogue presented from the field theory, and provide a clearer connection with gravitational waves and the processes that generate them. Finally, I have outlined an experimental protocol for the realization of these analogue gravitational waves in cold atoms.

Chapter 6

Conclusions and outlook

“There is a theory which states that if anyone ever discovers exactly what the Universe is for and why it is here, it will instantly disappear and be replaced by something even more bizarre and inexplicable.” - Douglas Adams

In the beginning, it was once said, there was light. But there were also gravitational waves, we just couldn't detect them. Observational astronomy of gravitational waves promises to provide fresh and clean information to test the limits of General Relativity in the strong gravity context. However, from such observations alone, we cannot expect to derive insight into the regime of overlap between quantum mechanics and general relativity.

In this Thesis, I have combined analytical insights from low-energy field theories and numerical simulation to make the case for analogues of light and gravity in ordered phases of quantum magnets. Following a review of relevant background material in Chapters 1-2, in Chapter 3, I have explicitly shown how the non-linear sigma model that describes the low-energy physics of the collinear Néel antiferromagnet is equivalent to a gauge fixed action for electromagnetism in vacuum, and have constructed a dictionary mapping the excitations of the Heisenberg antiferromagnet onto the photons of electromagnetism.

In Chapter 4, I have used a similar strategy to identify analogue gravitational waves in a ferroquadrupolar spin nematic. The dynamics of the quadrupolar order parameter are enshrined in the action, which shares the same form as that of linearized gravity, allowing a precise connection to be established between the Goldstone modes of a ferroquadrupolar spin nematic and gravitational waves. There a one-to-one correspondence between the two modes of each theory, and I have made explicit the dictionary for mapping to and from real-space and spin-space, illustrating both the appropriate transformation and that the underlying excitations share the same quadrupolar nature in their respective spaces: gravitational waves induce surfaces of constant strain that are equivalent to the surface of equal wavefunction amplitude of a quadrupolar wave in Hilbert space.

In Chapter 5, I have illustrated in simulation that the spin-2 massless excitations of the spin nematic mediate attractive interactions between \mathbb{Z}^2 vortices, which have only one signature of charge. This resembles the nature of gravity and gravitational mass. However, while gravitationally in-spiraling objects merge with total cumulative

total mass, this is not the case for the ferroquadrupolar \mathbb{Z}^2 vortices, which annihilate. Nevertheless, the in-spiraling ferroquadrupolar vortices emit analogue gravitational waves, whose frequency profile undergoes a sudden chirp during the part of the process associated with vortex annihilation. How much of this process can be described in analogy with the strong gravity limit remains an open question, and one worth future attention in the search for a curved spacetime analogue. I finally outline a experimental strategy for realizing these gravitational waves and the vortex annihilation process in spinor condensates.

As discussed in Chapter 1, cold atom simulators of scalar gravitational waves and curved spacetimes have been already developed [39, 41]. The tensor wave analogue I have developed here provides a new and more complete analogue for the structure of gravitational waves. Having distilled both sides of the correspondence to the simplest ingredients needed, this analogue offers a clean, and experimentally accessible avenue to access the physics of linearized gravity in a laboratory context, once one can realize a quantum spin nematic. As reviewed in Chapters 4-5, there is a long history of studying spin nematic candidates in both magnetic insulators and spinor condensates, and spin nematic states along with quadrupolar observables are detectable in real-space with techniques applicable to systems of cold atoms.

Linearized gravity, like electromagnetism, is a relativistic gauge theory. These manifest unitarity, locality and Lorentz invariance. That said, with a given gauge choice, some of these properties are brought to the foreground while others are suppressed, and this is what allows for the explicit connections explored in this Thesis. However, the recipe for condensed matter analogues presented in this Thesis does not lead to gauge theories. Each analogue exhibits unitarity and locality, though is not Lorentz invariant in the sense that different choice of inertial reference frame change the expression of the fields in Hilbert space.

To go beyond this, the case of emergent QED in the context of spin ice [55, 56] may provide inspiration. The emergent gauge theories that can emerge in the context of magnetism are suggestive that a higher-rank gauge theory analogous—at least in part—gravity could be found. While investigation of higher rank gauge theories has been the subject of ongoing research [168], and some features such as attraction between exotic particles [38] have been identified, no complete gravity analogue has yet been identified. This interesting line of inquiry merits further development.

A second ingredient missing in the work presented here is curvature. In magnetic models, aspects of geometry have long been identified [251, 252], and recently similar notions of geometry are also identified in graphene [253, 254]. A parallel notion of geometry is needed to bring to bear an analogue with general relativity.

Within the context of more traditional condensed matter questions, this Thesis work also raises interesting avenues to be further explored.

The thermodynamic properties seen in simulation are here predictive of a topologically mediated phase transition or crossover. A full characterization this behaviour using a model specific analysis remains open. One open end here is the field theoretical derivation of the nematic stiffness and its scaling in association with the vortex mediated transition.

In fact, future work focusing on such characterization need not be confined to the ferroquadrupolar nematic phase studied here. The antiferroquadrupolar nematic

phase, for example, is characterized by an $SU(2)$ symmetry breaking order, similar to the ferroquadrupole. However, the introduction of the sublattice structure changes in turn which symmetry group is broken, and the corresponding homotopy class predicts quaternion point defects, which do not annihilate, but instead merge [209, 255].

In both the ferroquadrupolar and antiferroquadrupolar cases, the nature of the vortex merger processes merits closer study with analogy to gravitational behaviour beyond the linearized limit. It is unclear to what order the analogy holds as one introduces stronger gravitational fields.

If nothing else, in now coming to the end, then let us conclude from this Thesis that you don't have to look to the extremes of the Universe to find something extraordinary.

Bibliography

- [1] P. J. Wasilewski, “Lodestone: Nature’s own permanent magnet,” NASA-TM-X-71145, 1976.
- [2] P. Wasilewski and G. Kletetschka, “Lodestone: Natures only permanent magnet-what it is and how it gets charged,” *Geophysical Research Letters*, vol. 26, no. 15, pp. 2275–2278, 1999.
- [3] F. Annett, *Electrical Machinery: A Practical Study Course on Installation, Operation and Maintenance*. McGraw-Hill book Company, Incorporated, 1921.
- [4] A. Läuchli, F. Mila, and K. Penc, “Quadrupolar Phases of the $S = 1$ Bilinear-Biquadratic Heisenberg Model on the Triangular Lattice,” *Physical Review Letters*, vol. 97, p. 087205, Aug. 2006.
- [5] A. Smerald, *Theory of the Nuclear Magnetic $1/T_1$ Relaxation Rate in Conventional and Unconventional Magnets*. Springer Theses, Cham: Springer International Publishing, 2013.
- [6] A. Smerald and N. Shannon, “Theory of spin excitations in a quantum spin-nematic state,” *Physical Review B*, vol. 88, p. 184430, Nov. 2013.
- [7] L. Chojnacki, R. Pohle, H. Yan, Y. Akagi, and N. Shannon, “Gravitational wave analogs in spin nematics and cold atoms,” *Phys. Rev. B*, vol. 109, p. L220407, Jun 2024.
- [8] R. Coldea, S. M. Hayden, G. Aeppli, T. G. Perring, C. D. Frost, T. E. Mason, S.-W. Cheong, and Z. Fisk, “Spin waves and electronic interactions in La_2CuO_4 ,” *Phys. Rev. Lett.*, vol. 86, pp. 5377–5380, Jun 2001.
- [9] B. P. Abbott *et al.*, “Observation of gravitational waves from a binary black hole merger,” *Phys. Rev. Lett.*, vol. 116, p. 061102, Feb 2016.
- [10] C. Lacroix, P. Mendels, and F. Mila, eds., *Introduction to Frustrated Magnetism*, vol. 164 of *Springer Series in Solid-State Sciences*. Berlin, Heidelberg: Springer Berlin Heidelberg, 2011.
- [11] K. Remund, R. Pohle, Y. Akagi, J. Romhányi, and N. Shannon, “Semi-classical simulation of spin-1 magnets,” *Phys. Rev. Research*, vol. 4, p. 033106, Aug. 2022. Publisher: American Physical Society.

-
- [12] J. E. Enderby, “Sir Frederick Charles Frank (1911-98),” *Nature*, vol. 393, pp. 314–314, May 1998.
- [13] P. W. Anderson, “Plasmons, Gauge Invariance, and Mass,” *Phys. Rev.*, vol. 130, pp. 439–442, Apr. 1963. Publisher: American Physical Society.
- [14] F. Englert and R. Brout, “Broken symmetry and the mass of gauge vector mesons,” *Phys. Rev. Lett.*, vol. 13, pp. 321–323, Aug 1964.
- [15] P. W. Higgs, “Broken symmetries and the masses of gauge bosons,” *Phys. Rev. Lett.*, vol. 13, pp. 508–509, Oct 1964.
- [16] G. S. Guralnik, C. R. Hagen, and T. W. B. Kibble, “Global conservation laws and massless particles,” *Phys. Rev. Lett.*, vol. 13, pp. 585–587, Nov 1964.
- [17] G. E. Volovik, *The universe in a helium droplet*. No. 117 in International series of monographs on physics, Oxford: Oxford University Press, repr ed., 2009.
- [18] M. J. Jacquet, S. Weinfurtner, and F. König, “The next generation of analogue gravity experiments,” *Philosophical Transactions of the Royal Society A: Mathematical, Physical and Engineering Sciences*, vol. 378, p. 20190239, Aug. 2020.
- [19] G. Volovik, “Superfluid ^3He -b and gravity,” *Physica B: Condensed Matter*, vol. 162, no. 3, pp. 222–230, 1990.
- [20] G. E. Volovik, “Simulation of quantum field theory and gravity in superfluid ^3He ,” *Low Temperature Physics*, vol. 24, pp. 127–129, 02 1998.
- [21] W. G. Unruh, “Experimental black-hole evaporation?,” *Phys. Rev. Lett.*, vol. 46, pp. 1351–1353, May 1981.
- [22] W. G. Unruh, “Sonic analogue of black holes and the effects of high frequencies on black hole evaporation,” *Physical Review D*, vol. 51, pp. 2827–2838, Mar. 1995.
- [23] G. Rousseaux, C. Mathis, P. Maïssa, T. G. Philbin, and U. Leonhardt, “Observation of negative-frequency waves in a water tank: a classical analogue to the hawking effect?,” *New Journal of Physics*, vol. 10, p. 053015, May 2008.
- [24] S. Weinfurtner, E. W. Tedford, M. C. J. Penrice, W. G. Unruh, and G. A. Lawrence, “Measurement of stimulated hawking emission in an analogue system,” *Phys. Rev. Lett.*, vol. 106, p. 021302, Jan 2011.
- [25] O. Lahav, A. Itah, A. Blumkin, C. Gordon, S. Rinott, A. Zayats, and J. Steinhauer, “Realization of a sonic black hole analog in a Bose-Einstein condensate,” *Phys. Rev. Lett.*, vol. 105, p. 240401, Dec 2010.
- [26] M. Hotta, Y. Nambu, Y. Sugiyama, K. Yamamoto, and G. Yusa, “Expanding edges of quantum hall systems in a cosmology language: Hawking radiation from de Sitter horizon in edge modes,” *Phys. Rev. D*, vol. 105, p. 105009, May 2022.

-
- [27] Y. Rosenberg, “Optical analogues of black-hole horizons,” *Philosophical Transactions of the Royal Society A: Mathematical, Physical and Engineering Sciences*, vol. 378, p. 20190232, Aug. 2020.
- [28] J. Petty and F. König, “Optical analogue gravity physics: resonant radiation,” *Philosophical Transactions of the Royal Society A: Mathematical, Physical and Engineering Sciences*, vol. 378, p. 20190231, Aug. 2020.
- [29] G. E. Volovik, “Black hole and Hawking radiation by type-II Weyl fermions,” *JETP Letters*, vol. 104, pp. 645–648, Nov. 2016.
- [30] H. Liu, J.-T. Sun, C. Song, H. Huang, F. Liu, and S. Meng, “Fermionic Analogue of High Temperature Hawking Radiation in Black Phosphorus,” *Chinese Physics Letters*, vol. 37, p. 067101, June 2020.
- [31] H. Kleinert, “Gravity as a Theory of Defects in a Crystal with Only Second Gradient Elasticity,” *Annalen der Physik*, vol. 499, no. 2, pp. 117–119, 1987.
- [32] H. Kleinert and J. Zaanen, “Nematic world crystal model of gravity explaining absence of torsion in spacetime,” *Physics Letters A*, vol. 324, pp. 361–365, Apr. 2004.
- [33] Y. Zhu and Y. Jiang, “World crystal: extending to four dimensional,” *General Relativity and Gravitation*, vol. 43, pp. 2935–2941, Nov. 2011.
- [34] J. Zaanen and A. Beekman, “The emergence of gauge invariance: The stay-at-home gauge versus local–global duality,” *Annals of Physics*, vol. 327, pp. 1146–1161, Apr. 2012.
- [35] A. J. Beekman, J. Nissinen, K. Wu, K. Liu, R.-J. Slager, Z. Nussinov, V. Cvetkovic, and J. Zaanen, “Dual gauge field theory of quantum liquid crystals in two dimensions,” *Physics Reports*, vol. 683, pp. 1–110, Apr. 2017.
- [36] A. J. Beekman, J. Nissinen, K. Wu, and J. Zaanen, “Dual gauge field theory of quantum liquid crystals in three dimensions,” *Physical Review B*, vol. 96, p. 165115, Oct. 2017.
- [37] M. Pretko and L. Radzihovsky, “Fracton-Elasticity Duality,” *Physical Review Letters*, vol. 120, p. 195301, May 2018. arXiv: 1711.11044.
- [38] M. Pretko, “Emergent gravity of fractons: Mach’s principle revisited,” *Physical Review D*, vol. 96, p. 024051, July 2017.
- [39] C. Viermann, M. Sparn, N. Liebster, M. Hans, E. Kath, Á. Parra-López, M. Tolosa-Simeón, N. Sánchez-Kuntz, T. Haas, H. Strobel, S. Floerchinger, and M. K. Oberthaler, “Quantum field simulator for dynamics in curved spacetime,” *Nature*, vol. 611, pp. 260–264, Nov. 2022.

-
- [40] M. Tolosa-Simeón, Á. Parra-López, N. Sánchez-Kuntz, T. Haas, C. Viermann, M. Sparn, N. Liebster, M. Hans, E. Kath, H. Strobel, M. K. Oberthaler, and S. Floerchinger, “Curved and expanding spacetime geometries in Bose-Einstein condensates,” *Physical Review A*, vol. 106, p. 033313, Sept. 2022.
- [41] T. Bravo, C. Sabín, and I. Fuentes, “Analog quantum simulation of gravitational waves in a Bose-Einstein condensate,” *EPJ Quantum Technology*, vol. 2, p. 3, Dec. 2015.
- [42] C. Sabín, J. Kohlrus, D. E. Bruschi, and I. Fuentes, “Thermal noise in BEC-phononic gravitational wave detectors,” *EPJ Quantum Technology*, vol. 3, p. 8, Dec. 2016.
- [43] B. S. DeWitt, “Quantum theory of gravity. II. the manifestly covariant theory,” *Phys. Rev.*, vol. 162, pp. 1195–1239, Oct 1967.
- [44] S. Weinberg, *The Quantum Theory of Fields*, vol. 1. Cambridge University Press, 1995.
- [45] J. M. Kosterlitz, “The critical properties of the two-dimensional XY model,” *Journal of Physics C: Solid State Physics*, vol. 7, pp. 1046–1060, Mar. 1974. Publisher: IOP Publishing.
- [46] V. L. Berezinskii, “Destruction of Long-range Order in One-dimensional and Two-dimensional Systems Possessing a Continuous Symmetry Group. II. Quantum Systems,” *Soviet Journal of Experimental and Theoretical Physics*, vol. 34, p. 610, Jan. 1972.
- [47] J. M. Kosterlitz and D. J. Thouless, “Ordering, metastability and phase transitions in two-dimensional systems,” *Journal of Physics C: Solid State Physics*, vol. 6, p. 1181, apr 1973.
- [48] S. Dasgupta, S. Zhang, I. Bah, and O. Tchernyshyov, “Quantum Statistics of Vortices from a Dual Theory of the XY Ferromagnet,” *Phys. Rev. Lett.*, vol. 124, p. 157203, Apr. 2020. Publisher: American Physical Society.
- [49] J. D. Bernal and R. H. Fowler, “A Theory of Water and Ionic Solution, with Particular Reference to Hydrogen and Hydroxyl Ions,” *The Journal of Chemical Physics*, vol. 1, pp. 515–548, Aug. 1933.
- [50] L. Pauling, “The structure and entropy of ice and of other crystals with some randomness of atomic arrangement,” *Journal of the American Chemical Society*, vol. 57, no. 12, pp. 2680–2684, 1935.
- [51] M. J. Harris, S. T. Bramwell, D. F. McMorrow, T. Zeiske, and K. W. Godfrey, “Geometrical frustration in the ferromagnetic pyrochlore $\text{Ho}_2\text{Ti}_2\text{O}_7$,” *Phys. Rev. Lett.*, vol. 79, pp. 2554–2557, Sep 1997.
- [52] M. Udagawa and L. Jaubert, *Spin Ice*. Springer Series in Solid-State Sciences, Springer International Publishing, 2021.

-
- [53] I. A. Ryzhkin, “Magnetic relaxation in rare-earth oxide pyrochlores,” *Journal of Experimental and Theoretical Physics*, vol. 101, pp. 481–486, Sept. 2005.
- [54] C. Castelnovo, R. Moessner, and S. L. Sondhi, “Magnetic monopoles in spin ice,” *Nature*, vol. 451, pp. 42–45, Jan. 2008.
- [55] M. Hermele, M. P. A. Fisher, and L. Balents, “Pyrochlore photons: The U(1) spin liquid in a $S = \frac{1}{2}$ three-dimensional frustrated magnet,” *Physical Review B*, vol. 69, p. 064404, Feb. 2004.
- [56] O. Benton, O. Sikora, and N. Shannon, “Seeing the light: Experimental signatures of emergent electromagnetism in a quantum spin ice,” *Physical Review B*, vol. 86, Aug. 2012.
- [57] S. D. Pace, S. C. Morampudi, R. Moessner, and C. R. Laumann, “Emergent Fine Structure Constant of Quantum Spin Ice Is Large,” *Physical Review Letters*, vol. 127, p. 117205, Sept. 2021.
- [58] Y. Tokiwa, T. Yamashita, M. Udagawa, S. Kittaka, T. Sakakibara, D. Terazawa, Y. Shimoyama, T. Terashima, Y. Yasui, T. Shibauchi, and Y. Matsuda, “Possible observation of highly itinerant quantum magnetic monopoles in the frustrated pyrochlore $\text{Yb}_2\text{Ti}_2\text{O}_7$,” *Nature Communications*, vol. 7, p. 10807, Feb. 2016.
- [59] R. Sibille, N. Gauthier, H. Yan, M. Ciomaga Hatnean, J. Ollivier, B. Winn, U. Filges, G. Balakrishnan, M. Kenzelmann, N. Shannon, and T. Fennell, “Experimental signatures of emergent quantum electrodynamics in $\text{Pr}_2\text{Hf}_2\text{O}_7$,” *Nature Physics*, vol. 14, pp. 711–715, July 2018.
- [60] J. Gaudet, E. M. Smith, J. Dudemaine, J. Beare, C. R. C. Buhariwalla, N. P. Butch, M. B. Stone, A. I. Kolesnikov, G. Xu, D. R. Yahne, K. A. Ross, C. A. Marjerrison, J. D. Garrett, G. M. Luke, A. D. Bianchi, and B. D. Gaulin, “Quantum spin ice dynamics in the dipole-octupole pyrochlore magnet $\text{Ce}_2\text{Zr}_2\text{O}_7$,” *Phys. Rev. Lett.*, vol. 122, p. 187201, May 2019.
- [61] B. Gao, T. Chen, D. W. Tam, C.-L. Huang, K. Sasmal, D. T. Adroja, F. Ye, H. Cao, G. Sala, M. B. Stone, C. Baines, J. A. T. Verezhak, H. Hu, J.-H. Chung, X. Xu, S.-W. Cheong, M. Nallaiyan, S. Spagna, M. B. Maple, A. H. Nevidomskyy, E. Morosan, G. Chen, and P. Dai, “Experimental signatures of a three-dimensional quantum spin liquid in effective spin-1/2 $\text{Ce}_2\text{Zr}_2\text{O}_7$ pyrochlore,” *Nature Physics*, vol. 15, pp. 1052–1057, Oct. 2019.
- [62] V. Porée, E. Lhotel, S. Petit, A. Krajewska, P. Puphal, A. H. Clark, V. Pomjakushin, H. C. Walker, N. Gauthier, D. J. Gawryluk, and R. Sibille, “Crystal-field states and defect levels in candidate quantum spin ice $\text{Ce}_2\text{Hf}_2\text{O}_7$,” *Phys. Rev. Mater.*, vol. 6, p. 044406, Apr 2022.
- [63] R. Sibille, N. Gauthier, E. Lhotel, V. Porée, V. Pomjakushin, R. A. Ewings, T. G. Perring, J. Ollivier, A. Wildes, C. Ritter, T. C. Hansen, D. A. Keen, G. J. Nilsen, L. Keller, S. Petit, and T. Fennell, “A quantum liquid of magnetic octupoles on the pyrochlore lattice,” *Nature Physics*, vol. 16, pp. 546–552, May 2020.

-
- [64] K. Shimizu, S. Okumura, Y. Kato, and Y. Motome, “Spin moiré engineering of topological magnetism and emergent electromagnetic fields,” *Phys. Rev. B*, vol. 103, p. 184421, May 2021.
- [65] A. A. Mills, “The lodestone: History, physics, and formation,” *Annals of Science*, vol. 61, no. 3, pp. 273–319, 2004.
- [66] S. Blundell, *Magnetism in Condensed Matter*. Oxford Master Series in Condensed Matter Physics, OUP Oxford, 2001.
- [67] A. Auerbach, *Interacting Electrons and Quantum Magnetism*. Springer Science, 2012.
- [68] P. Anderson, *Basic Notions Of Condensed Matter Physics*. Advanced Book Classics, Taylor & Francis Limited (Sales), 2019.
- [69] D. P. Kozlenko, L. S. Dubrovinsky, S. E. Kichanov, E. V. Lukin, V. Cerantola, A. I. Chumakov, and B. N. Savenko, “Magnetic and electronic properties of magnetite across the high pressure anomaly,” *Scientific Reports*, vol. 9, p. 4464, Mar. 2019.
- [70] E. Pachoud, J. Cumby, G. Perversi, J. P. Wright, and J. P. Attfield, “Site-selective doping of ordered charge states in magnetite,” *Nature Communications*, vol. 11, p. 1671, Apr. 2020.
- [71] S.-W. Cheong and F.-T. Huang, “Altermagnetism with non-collinear spins,” *npj Quantum Materials*, vol. 9, p. 13, Jan. 2024.
- [72] P. Fazekas, *Lecture Notes on Electron Correlation and Magnetism*. World Scientific, 1999.
- [73] P. A. M. Dirac, “Quantum mechanics of many-electron systems,” *Proceedings of the Royal Society of London. Series A, Containing Papers of a Mathematical and Physical Character*, vol. 123, no. 792, pp. 714–733, 1929.
- [74] W. Heisenberg, “Zur Theorie des Ferromagnetismus,” *Zeitschrift für Physik*, vol. 49, pp. 619–636, Sept. 1928.
- [75] A. Yoshimori and S. Inagaki, “Fourth order interaction effects on the antiferromagnetic structures. ii. a phenomenological model for NiS₂,” *Journal of the Physical Society of Japan*, vol. 50, no. 3, pp. 769–773, 1981.
- [76] M. Hoffmann and S. Blügel, “Systematic derivation of realistic spin-models for beyond-Heisenberg solids,” *Physical Review B*, vol. 101, p. 024418, Jan. 2020. arXiv:1803.01315 [cond-mat].
- [77] P. Mellado, “Spin model for the honeycomb NiPS₃,” *Applied Physics Letters*, vol. 123, p. 242403, 12 2023.
- [78] J. J. Sakurai and J. Napolitano, *Modern quantum mechanics*. Boston: Addison-Wesley, 2nd ed ed., 2011.

-
- [79] A. Messiah, *Quantum Mechanics*. Dover Books on Physics, Dover Publications, 2014.
- [80] H. Zhang and C. D. Batista, “Classical spin dynamics based on SU(N) coherent states,” *Physical Review B*, vol. 104, p. 104409, Sept. 2021. arXiv: 2106.14125.
- [81] D. Dahlbom, C. Miles, H. Zhang, C. D. Batista, and K. Barros, “Langevin dynamics of generalized spins as SU(N) coherent states,” *Physical Review B*, vol. 106, p. 235154, Dec. 2022. arXiv:2209.01265 [cond-mat].
- [82] N. Papanicolaou, “Unusual phases in quantum spin-1 systems,” *Nuclear Physics B*, vol. 305, no. 3, pp. 367 – 395, 1988.
- [83] J. C. Maxwell, “On the Dynamical Evidence of the Molecular Constitution of Bodies,” *Nature*, vol. 11, pp. 357–359, Mar. 1875.
- [84] L. Landau, “On the theory of phase transitions,” *Phys.Z.Sowjetunion*, vol. 11, 1965.
- [85] M. Plischke and B. Bergersen, *Equilibrium statistical physics*. Hackensack, NJ: World Scientific, 3rd ed ed., 2006.
- [86] C. Kittel, *Introduction to Solid State Physics*. Wiley, 8th edition ed., 2005.
- [87] M. Blume and Y. Y. Hsieh, “Biquadratic Exchange and Quadrupolar Ordering,” *Journal of Applied Physics*, vol. 40, pp. 1249–1249, Mar. 1969.
- [88] H. H. Chen and P. M. Levy, “Quadrupole phase transitions in magnetic solids,” *Phys. Rev. Lett.*, vol. 27, pp. 1383–1385, Nov 1971.
- [89] A. Andreev and I. Grishchuk, “Spin Nematics,” *JETP*, vol. 87, pp. 467–475, 1984.
- [90] A. V. Chubukov, “Chiral, nematic, and dimer states in quantum spin chains,” *Phys. Rev. B*, vol. 44, pp. 4693–4696, Sep 1991.
- [91] N. Shannon, T. Momoi, and P. Sindzingre, “Nematic order in square lattice frustrated ferromagnets,” *Phys. Rev. Lett.*, vol. 96, p. 027213, Jan 2006.
- [92] K. Harada and N. Kawashima, “Quadrupolar order in isotropic Heisenberg models with biquadratic interaction,” *Phys. Rev. B*, vol. 65, p. 052403, Jan 2002.
- [93] B. A. Ivanov and A. K. Kolezhuk, “Effective field theory for the $S = 1$ quantum nematic,” *Physical Review B*, vol. 68, Aug. 2003.
- [94] D. Podolsky and E. Demler, “Properties and detection of spin nematic order in strongly correlated electron systems,” *New Journal of Physics*, vol. 7, p. 59, feb 2005.
- [95] H. Tsunetsugu and M. Arikawa, “Spin nematic phase in $s=1$ triangular antiferromagnets,” *Journal of the Physical Society of Japan*, vol. 75, no. 8, p. 083701, 2006.

-
- [96] E. M. Stoudenmire, S. Trebst, and L. Balents, “Quadrupolar correlations and spin freezing in $s = 1$ triangular lattice antiferromagnets,” *Phys. Rev. B*, vol. 79, p. 214436, Jun 2009.
- [97] R. K. Kaul, “Spin nematic ground state of the triangular lattice $S = 1$ biquadratic model,” *Phys. Rev. B*, vol. 86, p. 104411, Sep 2012.
- [98] A. Völl and S. Wessel, “Spin dynamics of the bilinear-biquadratic $s = 1$ Heisenberg model on the triangular lattice: A quantum monte carlo study,” *Phys. Rev. B*, vol. 91, p. 165128, Apr 2015.
- [99] S. Nakatsuji, Y. Nambu, H. Tonomura, O. Sakai, S. Jonas, C. Broholm, H. Tsunetsugu, Y. Qiu, and Y. Maeno, “Spin Disorder on a Triangular Lattice,” *Science*, vol. 309, pp. 1697–1700, Sept. 2005.
- [100] M. E. Valentine, T. Higo, Y. Nambu, D. Chaudhuri, J. Wen, C. Broholm, S. Nakatsuji, and N. Drichko, “Impact of the Lattice on Magnetic Properties and Possible Spin Nematicity in the $S = 1$ Triangular Antiferromagnet NiGa_2S_4 ,” *Physical Review Letters*, vol. 125, p. 197201, Nov. 2020.
- [101] K. Guratinder, M. Schmidt, H. C. Walker, R. Bewley, M. Wörle, D. Cabra, S. A. Osorio, M. Villalba, A. K. Madsen, L. Keller, A. Wildes, P. Puphal, A. Cervellino, C. Rüegg, and O. Zaharko, “Magnetic correlations in the triangular antiferromagnet FeGa_2S_4 ,” *Phys. Rev. B*, vol. 104, p. 064412, Aug 2021.
- [102] T. Ohmi and K. Machida, “Bose-Einstein condensation with internal degrees of freedom in alkali atom gases,” *Journal of the Physical Society of Japan*, vol. 67, no. 6, pp. 1822–1825, 1998.
- [103] J. Stenger, S. Inouye, D. M. Stamper-Kurn, H.-J. Miesner, A. P. Chikkatur, and W. Ketterle, “Spin domains in ground-state Bose–Einstein condensates,” *Nature*, vol. 396, pp. 345–348, Nov. 1998.
- [104] A. Imambekov, M. Lukin, and E. Demler, “Spin-exchange interactions of spin-one bosons in optical lattices: Singlet, nematic, and dimerized phases,” *Physical Review A*, vol. 68, p. 063602, Dec. 2003.
- [105] F. Zhou, M. Snoek, J. Wiemer, and I. Affleck, “Magnetically stabilized nematic order: Three-dimensional bipartite optical lattices,” *Phys. Rev. B*, vol. 70, p. 184434, Nov 2004.
- [106] D. Jacob, L. Shao, V. Corre, T. Zibold, L. De Sarlo, E. Mimoun, J. Dalibard, and F. Gerbier, “Phase diagram of spin-1 antiferromagnetic Bose-Einstein condensates,” *Physical Review A*, vol. 86, p. 061601, Dec. 2012.
- [107] T. Zibold, V. Corre, C. Frapolli, A. Invernizzi, J. Dalibard, and F. Gerbier, “Spin-nematic order in antiferromagnetic spinor condensates,” *Phys. Rev. A*, vol. 93, p. 023614, Feb 2016.

-
- [108] L. M. Symes and P. B. Blakie, “Nematic ordering dynamics of an antiferromagnetic spin-1 condensate,” *Physical Review A*, vol. 96, p. 013602, July 2017.
- [109] P. Kunkel, M. Prüfer, S. Lannig, R. Rosa-Medina, A. Bonnin, M. Gärttner, H. Strobel, and M. K. Oberthaler, “Simultaneous Readout of Noncommuting Collective Spin Observables beyond the Standard Quantum Limit,” *Physical Review Letters*, vol. 123, p. 063603, Aug. 2019.
- [110] P. Chaikin and T. Lubensky, *Principles of Condensed Matter Physics*. Cambridge University Press, 2000.
- [111] P. Olmsted, “Lectures on Landau theory of phase transitions,” 2015.
- [112] E. Roddick and D. Stroud, “Effect of phase fluctuations on the low-temperature penetration depth of high- T_c superconductors,” *Phys. Rev. Lett.*, vol. 74, pp. 1430–1433, Feb 1995.
- [113] V. J. Emery and S. A. Kivelson, “Superconductivity in bad metals,” *Phys. Rev. Lett.*, vol. 74, pp. 3253–3256, Apr 1995.
- [114] E. W. Carlson, S. A. Kivelson, V. J. Emery, and E. Manousakis, “Classical phase fluctuations in high temperature superconductors,” *Phys. Rev. Lett.*, vol. 83, pp. 612–615, Jul 1999.
- [115] Z. Hadzibabic, P. Krüger, M. Cheneau, B. Battelier, and J. Dalibard, “Berezinskii–Kosterlitz–Thouless crossover in a trapped atomic gas,” *Nature*, vol. 441, pp. 1118–1121, June 2006.
- [116] J. Coey, *Magnetism and Magnetic Materials*. Cambridge University Press, 2010.
- [117] D. Yudilevich, R. Stöhr, A. Denisenko, and A. Finkler, “Mapping single electron spins with magnetic tomography,” *Phys. Rev. Appl.*, vol. 18, p. 054016, Nov 2022.
- [118] A. Furrer, J. Mesot, and T. Straessle, *Neutron Scattering In Condensed Matter Physics*. Series On Neutron Techniques And Applications, World Scientific Publishing Company, 2009.
- [119] J. C. Wheatley, “Experimental properties of superfluid ^3He ,” *Rev. Mod. Phys.*, vol. 47, pp. 415–470, Apr 1975.
- [120] A. J. Leggett, “A theoretical description of the new phases of liquid ^3He ,” *Rev. Mod. Phys.*, vol. 47, pp. 331–414, Apr 1975.
- [121] D. M. Stamper-Kurn and M. Ueda, “Spinor Bose gases: Symmetries, magnetism, and quantum dynamics,” *Reviews of Modern Physics*, vol. 85, pp. 1191–1244, July 2013.
- [122] I. Bloch, J. Dalibard, and W. Zwerger, “Many-body physics with ultracold gases,” *Rev. Mod. Phys.*, vol. 80, pp. 885–964, July 2008.

-
- [123] S. Inouye, M. R. Andrews, J. Stenger, H.-J. Miesner, D. M. Stamper-Kurn, and W. Ketterle, “Observation of Feshbach resonances in a Bose–Einstein condensate,” *Nature*, vol. 392, pp. 151–154, Mar. 1998.
- [124] T. Köhler, K. Góral, and P. S. Julienne, “Production of cold molecules via magnetically tunable Feshbach resonances,” *Rev. Mod. Phys.*, vol. 78, pp. 1311–1361, Dec. 2006.
- [125] M. Lewenstein, A. Sanpera, and V. Ahufinger, *Ultracold atoms in Optical Lattices*. Oxford University Press, 2012.
- [126] K. D. Nelson, X. Li, and D. S. Weiss, “Imaging single atoms in a three-dimensional array,” *Nature Physics*, vol. 3, p. 556, June 2007.
- [127] W. S. Bakr, J. I. Gillen, A. Peng, S. Fölling, and M. Greiner, “A quantum gas microscope for detecting single atoms in a Hubbard-regime optical lattice,” *Nature*, vol. 462, p. 74, Nov. 2009.
- [128] F. M. Surace, P. Fromholz, N. D. Oppong, M. Dalmonte, and M. Aidelsburger, “*Ab Initio* Derivation of Lattice-Gauge-Theory Dynamics for Cold Gases in Optical Lattices,” *PRX Quantum*, vol. 4, p. 020330, May 2023.
- [129] K. Nemoto, “Generalized coherent states for SU(N) systems,” *Journal of Physics A: Mathematical and General*, vol. 33, p. 3493, may 2000.
- [130] E. K. Laird, Z.-Y. Shi, M. M. Parish, and J. Levinsen, “SU(N) fermions in a one-dimensional harmonic trap,” *Phys. Rev. A*, vol. 96, p. 032701, Sep 2017.
- [131] C. Sabín, D. E. Bruschi, M. Ahmadi, and I. Fuentes, “Phonon creation by gravitational waves,” *New Journal of Physics*, vol. 16, p. 085003, Aug. 2014. Publisher: IOP Publishing.
- [132] J. C. Maxwell, *A dynamical theory of the electromagnetic field*, vol. 8. 1865.
- [133] J. C. Maxwell, *A treatise on electricity and magnetism*, vol. 1. Clarendon press, 1873.
- [134] O. Heaviside, *Electromagnetic theory*, vol. 1. The Electrician Publishing, 1893.
- [135] H. Hertz and D. Jones, *Electric Waves: Being Researches on the Propagation of Electric Action with Finite Velocity Through Space*. Macmillan, 1893.
- [136] J. Jackson, *Classical Electrodynamics*. Wiley, 2021.
- [137] A. A. Michelson and E. W. Morley, “On the relative motion of the earth and the luminiferous ether,” *American Journal of Science*, vol. s3-34, pp. 333–345, 11 1887.
- [138] A. Einstein, “Zur elektrodynamik bewegter körper,” *Annalen der Physik*, vol. 322, no. 10, pp. 891–921, 1905.

-
- [139] C. W. Misner, K. S. Thorne, and J. A. Wheeler, *Gravitation*. San Francisco: W. H. Freeman, 1973.
- [140] E. Noether, “Invariante variationsprobleme,” *Nachrichten von der Gesellschaft der Wissenschaften zu Göttingen, Mathematisch-Physikalische Klasse*, vol. 1918, pp. 235–257, 1918.
- [141] Y. Nambu, “Quasi-particles and gauge invariance in the theory of superconductivity,” *Phys. Rev.*, vol. 117, pp. 648–663, Feb 1960.
- [142] J. Goldstone, “Field theories with Superconductor solutions,” *Il Nuovo Cimento (1955-1965)*, vol. 19, pp. 154–164, Jan. 1961.
- [143] Y. Nambu and G. Jona-Lasinio, “Dynamical model of elementary particles based on an analogy with superconductivity. I,” *Phys. Rev.*, vol. 122, pp. 345–358, Apr 1961.
- [144] J. Goldstone, A. Salam, and S. Weinberg, “Broken Symmetries,” *Physical Review*, vol. 127, pp. 965–970, Aug. 1962.
- [145] H. Watanabe and H. Murayama, “Unified Description of Nambu-Goldstone Bosons without Lorentz Invariance,” *Physical Review Letters*, vol. 108, p. 251602, June 2012.
- [146] R. Ferrari and L. Picasso, “Spontaneous breakdown in quantum electrodynamics,” *Nuclear Physics B*, vol. 31, pp. 316–330, Sept. 1971.
- [147] A. J. Beekman, L. Rademaker, and J. van Wezel, “An introduction to spontaneous symmetry breaking,” *SciPost Phys. Lect. Notes*, p. 11, 2019.
- [148] H. B. Nielsen and S. Chadha, “On how to count Goldstone bosons,” *Nuclear Physics B*, vol. 105, no. 3, pp. 445 – 453, 1976.
- [149] Y. Hidaka, “Counting rule for Nambu-Goldstone modes in nonrelativistic systems,” *Phys. Rev. Lett.*, vol. 110, p. 091601, Feb 2013.
- [150] Y. Hidaka, “Generalization of the Nambu-Goldstone theorem.” Seed Seminar of Mathematics and Physics, 2021.
- [151] F. Bloch, “Zur Theorie des Ferromagnetismus,” *Zeitschrift für Physik*, vol. 61, pp. 206–219, Mar. 1930.
- [152] R. Peierls, “Quelques propriétés typiques des corps solides,” *Annales de l’institut Henri Poincaré*, vol. 5, no. 3, pp. 177–222, 1935.
- [153] P. C. Hohenberg, “Existence of long-range order in one and two dimensions,” *Phys. Rev.*, vol. 158, pp. 383–386, Jun 1967.
- [154] N. D. Mermin and H. Wagner, “Absence of ferromagnetism or antiferromagnetism in one- or two-dimensional isotropic Heisenberg models,” *Phys. Rev. Lett.*, vol. 17, pp. 1133–1136, Nov 1966.

-
- [155] S. Coleman, “There are no Goldstone bosons in two dimensions,” *Communications in Mathematical Physics*, vol. 31, pp. 259–264, Dec. 1973.
- [156] B. I. Halperin, “On the Hohenberg-Mermin-Wagner theorem and its limitations,” *Journal of Statistical Physics*, vol. 175, pp. 521–529, May 2019. arXiv: 1812.00220.
- [157] M. Srednicki, *Quantum Field Theory*. Cambridge University Press, 2007.
- [158] N. Turok, “PSI general relativity core lectures,” 2015.
- [159] Y. S. Kim and E. P. Wigner, “Cylindrical group and massless particles,” *Journal of Mathematical Physics*, vol. 28, pp. 1175–1179, 05 1987.
- [160] Y. S. Kim and E. P. Wigner, “Space-time geometry of relativistic particles,” *Journal of Mathematical Physics*, vol. 31, pp. 55–60, 01 1990.
- [161] Y. Kim, “Internal space-time symmetries of massive and massless particles and their unification,” *Nuclear Physics B - Proceedings Supplements*, vol. 102-103, pp. 369–376, 2001. Proceedings of the International Conference on Supersymmetry and Quantum Field Theory dedicated to the 75th birthday anniversary of Dmitrij V. Volkov.
- [162] M. E. Peskin and D. V. Schroeder, *An Introduction to quantum field theory*. Reading, USA: Addison-Wesley, 1995.
- [163] D. Gaiotto, A. Kapustin, N. Seiberg, and B. Willett, “Generalized global symmetries,” *Journal of High Energy Physics*, vol. 2015, p. 172, Feb. 2015.
- [164] Y. Hidaka, Y. Hirono, and R. Yokokura, “Counting Nambu-Goldstone modes of higher-form global symmetries,” *Phys. Rev. Lett.*, vol. 126, p. 071601, Feb 2021.
- [165] M. Maggiore, *Gravitational Waves: Volume 1: Theory and Experiments*. Oxford: Oxford University Press, 2007.
- [166] S. M. Carroll, *Spacetime and Geometry: An Introduction to General Relativity*. Cambridge University Press, 2019.
- [167] C. Castelnovo, R. Moessner, and S. Sondhi, “Spin ice, fractionalization, and topological order,” *Annual Review of Condensed Matter Physics*, vol. 3, no. 1, pp. 35–55, 2012.
- [168] H. Yan, O. Benton, L. D. C. Jaubert, and N. Shannon, “Rank-2 U(1) spin liquid on the breathing pyrochlore lattice,” *Phys. Rev. Lett.*, vol. 124, p. 127203, Mar 2020.
- [169] A. Altland and B. D. Simons, *Condensed Matter Field Theory, Second Edition*. Cambridge University Press, 2010.
- [170] N. Nagaosa, *Quantum Field Theory in Condensed Matter Physics*. Berlin, Heidelberg: Springer Berlin Heidelberg, 1999.

-
- [171] E. Fradkin, *Field Theories of Condensed Matter Physics*. Cambridge: Cambridge University Press, 2 ed., 2013.
- [172] R. J. Glauber, “Coherent and incoherent states of the radiation field,” *Phys. Rev.*, vol. 131, pp. 2766–2788, Sep 1963.
- [173] A. M. Perelomov, “Coherent states for arbitrary Lie group,” *Communications in Mathematical Physics*, vol. 26, pp. 222–236, Sept. 1972.
- [174] R. Gilmore, “Geometry of symmetrized states,” *Annals of Physics*, vol. 74, pp. 391–463, 1972.
- [175] J. M. Radcliffe, “Some properties of coherent spin states,” *Journal of Physics A: General Physics*, vol. 4, pp. 313–323, May 1971.
- [176] F. D. M. Haldane, “Nonlinear Field Theory of Large-Spin Heisenberg Antiferromagnets: Semiclassically Quantized Solitons of the One-Dimensional Easy-Axis Néel State,” *Physical Review Letters*, vol. 50, pp. 1153–1156, Apr. 1983.
- [177] J. Villain, “Quantum theory of one- and two-dimensional ferro- and antiferromagnets with an easy magnetization plane . I. ideal 1-d or 2-d lattices without in-plane anisotropy,” *Journal de Physique*, vol. 35, no. 1, pp. 27–47, 1974.
- [178] F. D. M. Haldane, “Ground state properties of antiferromagnetic chains with unrestricted spin: Integer spin chains as realisations of the $O(3)$ non-linear sigma model,” *ILL preprint*, vol. SP-81/95, 1981.
- [179] F. D. M. Haldane, “Continuum dynamics of the 1-D Heisenberg antiferromagnet: Identification with the $O(3)$ nonlinear sigma model,” *Physics Letters A*, vol. 93, no. 9, pp. 464 – 468, 1983.
- [180] I. Affleck, “Quantum spin chains and the haldane gap,” *Journal of Physics: Condensed Matter*, vol. 1, pp. 3047–3072, May 1989.
- [181] M. Stone, “Supersymmetry and the quantum mechanics of spin,” *Nuclear Physics B*, vol. 314, no. 3, pp. 557 – 586, 1989.
- [182] M. Oshikawa, “Lecture notes on the Haldane gap,” April 2018.
- [183] A. N. Petsch, N. S. Headings, D. Prabhakaran, A. I. Kolesnikov, C. D. Frost, A. T. Boothroyd, R. Coldea, and S. M. Hayden, “High-energy spin waves in the spin-1 square-lattice antiferromagnet La_2NiO_4 ,” *Phys. Rev. Res.*, vol. 5, p. 033113, Aug 2023.
- [184] J. G. Bednorz and K. A. Müller, “Possible high T_c superconductivity in the BaLaCuO system,” *Zeitschrift für Physik B Condensed Matter*, vol. 64, pp. 189–193, June 1986.

-
- [185] H. C. Robarts, M. García-Fernández, J. Li, A. Nag, A. C. Walters, N. E. Headings, S. M. Hayden, and K.-J. Zhou, “Dynamical spin susceptibility in La_2CuO_4 studied by resonant inelastic x-ray scattering,” *Phys. Rev. B*, vol. 103, p. 224427, Jun 2021.
- [186] D. Betto, R. Fumagalli, L. Martinelli, M. Rossi, R. Piombo, K. Yoshimi, D. Di Castro, E. Di Gennaro, A. Sambri, D. Bonn, G. A. Sawatzky, L. Braicovich, N. B. Brookes, J. Lorenzana, and G. Ghiringhelli, “Multiple-magnon excitations shape the spin spectrum of cuprate parent compounds,” *Phys. Rev. B*, vol. 103, p. L140409, Apr 2021.
- [187] Y. Y. Peng, G. Dellea, M. Minola, M. Conni, A. Amorese, D. Di Castro, G. M. De Luca, K. Kummer, M. Salluzzo, X. Sun, X. J. Zhou, G. Balestrino, M. Le Tacon, B. Keimer, L. Braicovich, N. B. Brookes, and G. Ghiringhelli, “Influence of apical oxygen on the extent of in-plane exchange interaction in cuprate superconductors,” *Nature Physics*, vol. 13, pp. 1201–1206, Dec. 2017.
- [188] L. Martinelli, D. Betto, K. Kummer, R. Arpaia, L. Braicovich, D. Di Castro, N. B. Brookes, M. Moretti Sala, and G. Ghiringhelli, “Fractional spin excitations in the infinite-layer cuprate CaCuO_2 ,” *Phys. Rev. X*, vol. 12, p. 021041, May 2022.
- [189] A. A. Katanin and A. P. Kampf, “Spin excitations in La_2CuO_4 : consistent description by inclusion of ring exchange,” *Phys. Rev. B*, vol. 66, p. 100403, Sep 2002.
- [190] A. A. Katanin and A. P. Kampf, “Theoretical analysis of magnetic raman scattering in La_2CuO_4 : two-magnon intensity with the inclusion of ring exchange,” *Phys. Rev. B*, vol. 67, p. 100404, Mar 2003.
- [191] S. Yamamoto and Y. Noriki, “Spin-wave thermodynamics of square-lattice antiferromagnets revisited,” *Phys. Rev. B*, vol. 99, p. 094412, Mar 2019.
- [192] A. Jain, M. Krautloher, J. Porras, G. Ryu, D. Chen, D. Abernathy, J. Park, A. Ivanov, J. Chaloupka, G. Khaliullin, B. Keimer, and B. Kim, “Higgs mode and its decay in a two-dimensional antiferromagnet,” *Nature Physics*, vol. 13, pp. 633–637, July 2017.
- [193] N. S. Headings, S. M. Hayden, R. Coldea, and T. G. Perring, “Anomalous high-energy spin excitations in the high- T_c superconductor-parent antiferromagnet La_2CuO_4 ,” *Phys. Rev. Lett.*, vol. 105, p. 247001, Dec 2010.
- [194] B. DeMarco and D. S. Jin, “Onset of Fermi degeneracy in a trapped atomic gas,” *Science*, vol. 285, no. 5434, pp. 1703–1706, 1999.
- [195] R. Jördens, N. Strohmaier, K. Günter, H. Moritz, and T. Esslinger, “A Mott insulator of fermionic atoms in an optical lattice,” *Nature*, vol. 455, pp. 204–207, Sept. 2008.

-
- [196] A. Koetsier, R. A. Duine, I. Bloch, and H. T. C. Stoof, “Achieving the Néel state in an optical lattice,” *Phys. Rev. A*, vol. 77, p. 023623, Feb 2008.
- [197] C. J. M. Mathy, D. A. Huse, and R. G. Hulet, “Enlarging and cooling the Néel state in an optical lattice,” *Phys. Rev. A*, vol. 86, p. 023606, Aug 2012.
- [198] C. Pethick and H. Smith, *Bose-Einstein condensation in dilute gases*. Cambridge, New York: Cambridge University Press, 2002.
- [199] F. Reinitzer, “Contributions to the knowledge of cholesterol,” *Liquid Crystals*, vol. 5, no. 1, pp. 7–18, 1989.
- [200] M. Mitov, “Liquid-crystal science from 1888 to 1922: Building a revolution,” *ChemPhysChem*, vol. 15, no. 7, pp. 1245–1250, 2014.
- [201] C. W. Oseen, “The theory of liquid crystals,” *Trans. Faraday Soc.*, vol. 29, pp. 883–899, 1933.
- [202] F. C. Frank, “I. Liquid crystals. On the theory of liquid crystals,” *Discussions of the Faraday Society*, vol. 25, p. 19, 1958.
- [203] P. de Gennes and J. Prost, *The Physics of Liquid Crystals*. International Series of Monographs on Physics, Clarendon Press, 1993.
- [204] Y. Kim and M. Noz, *New Perspectives On Einstein’s $E = Mc^2$* . World Scientific Publishing Company, 2018.
- [205] A. Smerald, “Relaxation rates in the presence of nematic order,” 2012.
- [206] B. Sutherland, “Model for a multicomponent quantum system,” *Phys. Rev. B*, vol. 12, pp. 3795–3805, Nov 1975.
- [207] A. Schmitt, K.-H. Mütter, and M. Karbach, “The spin-1 Lai-Sutherland model with external and internal fields: I. the phase diagram,” *Journal of Physics A: Mathematical and General*, vol. 29, p. 3951, jul 1996.
- [208] I. Niesen and P. Corboz, “Ground-state study of the spin-1 bilinear-biquadratic Heisenberg model on the triangular lattice using tensor networks,” *Phys. Rev. B*, vol. 97, p. 245146, Jun 2018.
- [209] N. D. Mermin, “The topological theory of defects in ordered media,” *Reviews of Modern Physics*, vol. 51, pp. 591–648, July 1979.
- [210] G. P. Alexander, B. G.-g. Chen, E. A. Matsumoto, and R. D. Kamien, “Colloquium : Disclination loops, point defects, and all that in nematic liquid crystals,” *Reviews of Modern Physics*, vol. 84, pp. 497–514, Apr. 2012.
- [211] S. Bhattacharjee, V. B. Shenoy, and T. Senthil, “Possible ferro-spin nematic order in NiGa_2S_4 ,” *Phys. Rev. B*, vol. 74, p. 092406, Sep 2006.

-
- [212] N. Caci, P. Mühlbacher, D. Ueltschi, and S. Wessel, “Poisson-dirichlet distributions and weakly first-order spin-nematic phase transitions,” *Phys. Rev. B*, vol. 107, p. L020409, Jan 2023.
- [213] F. Michaud, F. Vernay, and F. Mila, “Theory of inelastic light scattering in spin-1 systems: Resonant regimes and detection of quadrupolar order,” *Phys. Rev. B*, vol. 84, p. 184424, Nov 2011.
- [214] S. C. Furuya and T. Momoi, “Electron spin resonance for the detection of long-range spin nematic order,” *Phys. Rev. B*, vol. 97, p. 104411, Mar 2018.
- [215] Y. Kohama, H. Ishikawa, A. Matsuo, K. Kindo, N. Shannon, and Z. Hiroi, “Possible observation of quantum spin-nematic phase in a frustrated magnet,” *PNAS*, vol. 116, 2019.
- [216] X. Bai, S.-S. Zhang, Z. Dun, H. Zhang, Q. Huang, H. Zhou, M. B. Stone, A. I. Kolesnikov, F. Ye, C. D. Batista, and M. Mourigal, “Hybridized quadrupolar excitations in the spin-anisotropic frustrated magnet FeI_2 ,” *Nature Physics*, vol. 17, pp. 467–472, Apr. 2021.
- [217] A. Orlova, E. L. Green, J. M. Law, D. I. Gorbunov, G. Chanda, S. Krämer, M. Horvatić, R. K. Kremer, J. Wosnitza, and G. L. J. A. Rikken, “Nuclear magnetic resonance signature of the spin-nematic phase in LiCuVO_4 at high magnetic fields,” *Phys. Rev. Lett.*, vol. 118, p. 247201, Jun 2017.
- [218] T. Momoi, P. Sindzingre, and K. Kubo, “Spin nematic order in multiple-spin exchange models on the triangular lattice,” *Phys. Rev. Lett.*, vol. 108, p. 057206, Feb 2012.
- [219] R. Shindou, S. Yunoki, and T. Momoi, “Dynamical spin structure factors of quantum spin nematic states,” *Phys. Rev. B*, vol. 87, p. 054429, Feb 2013.
- [220] A. Smerald, H. T. Ueda, and N. Shannon, “Theory of inelastic neutron scattering in a field-induced spin-nematic state,” *Phys. Rev. B*, vol. 91, p. 174402, May 2015.
- [221] E. Demler and F. Zhou, “Spinor bosonic atoms in optical lattices: Symmetry breaking and fractionalization,” *Phys. Rev. Lett.*, vol. 88, p. 163001, Apr 2002.
- [222] A. Imambekov, M. Lukin, and E. Demler, “Spin-exchange interactions of spin-one bosons in optical lattices: Singlet, nematic, and dimerized phases,” *Physical Review A*, vol. 68, p. 063602, Dec. 2003.
- [223] D. Jacob, L. Shao, V. Corre, T. Zibold, L. De Sarlo, E. Mimoun, J. Dalibard, and F. Gerbier, “Phase diagram of spin-1 antiferromagnetic Bose-Einstein condensates,” *Physical Review A*, vol. 86, p. 061601, Dec. 2012.
- [224] L. de Forges de Parny, H. Yang, and F. Mila, “Anderson tower of states and nematic order of spin-1 bosonic atoms on a 2D lattice,” *Phys. Rev. Lett.*, vol. 113, p. 200402, Nov 2014.

-
- [225] I. Carusotto and E. J. Mueller, “Imaging of spinor gases,” *Journal of Physics B: Atomic, Molecular and Optical Physics*, vol. 37, pp. S115–S125, Apr. 2004.
- [226] D. P. Kroese, T. Brereton, T. Taimre, and Z. I. Botev, “Why the Monte Carlo method is so important today,” *WIREs Computational Statistics*, vol. 6, no. 6, pp. 386–392, 2014.
- [227] M. E. J. Newman and G. T. Barkema, *Monte Carlo methods in statistical physics*. Oxford : New York: Clarendon Press ; Oxford University Press, 1999.
- [228] W. Krauth, *Statistical mechanics: algorithms and computations*. No. 13 in Oxford master series in physics, Oxford: Oxford University Press, 2006.
- [229] N. Metropolis, A. W. Rosenbluth, M. N. Rosenbluth, A. H. Teller, and E. Teller, “Equation of state calculations by fast computing machines,” *The Journal of Chemical Physics*, vol. 21, no. 6, pp. 1087–1092, 1953.
- [230] H. Müller-Krumbhaar and K. Binder, “Dynamic properties of the Monte Carlo method in statistical mechanics,” *Journal of Statistical Physics*, vol. 8, pp. 1–24, May 1973.
- [231] H. Flyvbjerg and H. G. Petersen, “Error estimates on averages of correlated data,” vol. 91, p. 7, 1989.
- [232] E. Marinari and G. Parisi, “Simulated tempering: A new Monte Carlo scheme,” *Europhysics Letters*, vol. 19, p. 451, jul 1992.
- [233] U. Wolff, “Collective Monte Carlo updating for spin systems,” *Phys. Rev. Lett.*, vol. 62, pp. 361–364, Jan 1989.
- [234] H. G. Evertz, “The loop algorithm,” *Advances in Physics*, vol. 52, no. 1, pp. 1–66, 2003.
- [235] F. R. Brown and T. J. Woch, “Overrelaxed heat-bath and metropolis algorithms for accelerating pure gauge Monte Carlo calculations,” *Phys. Rev. Lett.*, vol. 58, pp. 2394–2396, Jun 1987.
- [236] M. Creutz, “Overrelaxation and Monte Carlo simulation,” *Phys. Rev. D*, vol. 36, pp. 515–519, Jul 1987.
- [237] G. Marsaglia, “Choosing a Point from the Surface of a Sphere,” *Annals of Mathematical Statistics*, vol. 43, no. 2, pp. 645–646, 1972. Publisher: The Institute of Mathematical Statistics.
- [238] H. for the FFTW library. <https://www.fftw.org/index.html>.
- [239] E. Hairer, S. Norsett, and G. Wanner, *Solving Ordinary Differential Equations I*, vol. 8 of *Springer Series in Computational Mathematics*. Berlin, Heidelberg: Springer Berlin Heidelberg, 1993.

-
- [240] J. M. Loveluck and E. Balcar, “Propagating energy modes in the classical Heisenberg chain: “magnons” and “second magnons”,” *Phys. Rev. Lett.*, vol. 42, pp. 1563–1566, Jun 1979.
- [241] T. Schneider and H. R. Jauslin, “Spin dynamics of the ferromagnetic Heisenberg chain in a magnetic field: Evidence for “second magnons”,” *Phys. Rev. B*, vol. 27, pp. 1919–1921, Feb 1983.
- [242] H. Kawamura and A. Yamamoto, “Vortex-Induced Topological Transition of the Bilinear–Biquadratic Heisenberg Antiferromagnet on the Triangular Lattice,” *Journal of the Physical Society of Japan*, vol. 76, p. 073704, July 2007.
- [243] A. Ueda and M. Oshikawa, “Tensor network renormalization study on the crossover in classical heisenberg and sp^2 models in two dimensions,” *Phys. Rev. E*, vol. 106, p. 014104, Jul 2022.
- [244] R. Pohle [*Unpublished*].
- [245] M. Wintel, H. U. Everts, and W. Apel, “The heisenberg antiferromagnet on a triangular lattice: Topological excitations,” *Europhysics Letters (EPL)*, vol. 25, pp. 711–716, Mar. 1994.
- [246] B. W. Southern and A. P. Young, “Spin stiffness in frustrated antiferromagnets,” *Phys. Rev. B*, vol. 48, pp. 13170–13173, Nov 1993.
- [247] S. Chakravarty, B. I. Halperin, and D. R. Nelson, “Two-dimensional quantum Heisenberg antiferromagnet at low temperatures,” *Phys. Rev. B*, vol. 39, pp. 2344–2371, Feb. 1989. Publisher: American Physical Society.
- [248] P. Azaria, B. Delamotte, and D. Mouhanna, “Low-temperature properties of two-dimensional frustrated quantum antiferromagnets,” *Phys. Rev. Lett.*, vol. 68, pp. 1762–1765, Mar 1992.
- [249] S. Kang, S. W. Seo, H. Takeuchi, and Y. Shin, “Observation of wall-vortex composite defects in a spinor Bose-Einstein condensate,” *Phys. Rev. Lett.*, vol. 122, p. 095301, Mar 2019.
- [250] X. Tang and J. V. Selinger, “Orientation of topological defects in 2D nematic liquid crystals,” *Soft Matter*, vol. 13, no. 32, pp. 5481–5490, 2017.
- [251] I. Dzyaloshinskii and G. Volovik, “On the concept of local invariance in the theory of spin glasses,” *Journal de Physique*, vol. 39, no. 6, pp. 693–700, 1978.
- [252] D. Hill, V. Slastikov, and O. Tchernyshyov, “Chiral magnetism: a geometric perspective,” *SciPost Phys.*, vol. 10, p. 078, 2021.
- [253] M. M. Roberts and T. Wiseman, “Analog gravity and the continuum effective theory of the graphene tight binding lattice model,” 2023.

- [254] A. Motavassal and S. A. Jafari, “Circuit realization of a tilted Dirac cone: Platform for fabrication of curved spacetime geometry on a chip,” *Phys. Rev. B*, vol. 104, p. L241108, Dec 2021.
- [255] J. Takano and H. Tsunetsugu, “Theory of impurity effects on the spin nematic state,” *Journal of the Physical Society of Japan*, vol. 80, no. 9, p. 094707, 2011.
- [256] A. Eichhorn, A. Held, and C. Wetterich, “Quantum-gravity predictions for the fine-structure constant,” *Physics Letters B*, vol. 782, pp. 198–201, 2018.
- [257] O. Tchernyshyov, “PSI condensed matter core lectures,” 2015.
- [258] S. K. Kim, Y. Tserkovnyak, and O. Tchernyshyov, “Propulsion of a domain wall in an antiferromagnet by magnons,” *Physical Review B*, vol. 90, p. 104406, Sept. 2014.
- [259] S. Dasgupta and O. Tchernyshyov, “Theory of spin waves in a hexagonal antiferromagnet,” *Physical Review B*, vol. 102, p. 144417, Oct. 2020. arXiv: 2004.02790.

Appendix A

Comparing the strength of electromagnetism to gravity

If you stop to think about it, it's quite an extraordinary fact that a small chunk of lodestone can hold up a steel nail off the floor against gravity that the entire Earth is otherwise conspiring to draw back down to the ground. That there is such a large difference of scales between the strengths of electromagnetic and gravitational interactions is an empirical fact with no known fundamental justification.

That said, to develop a more concrete sense of the discrepancy than the example above can convey, it is more precise to compare the order of magnitude difference between the electromagnetic interactions—as described by Coulomb's law—and gravitational interactions—as described classically by Newton's law—between two equivalent charge and mass distributions at the same distance.

Consider two electrons, of mass $m_e = 9.11 \cdot 10^{-31} kg$ and charge $q = 1.60 \cdot 10^{-19} C$ respectively, separated by a distance of $r = 1m$. The Coulomb force experienced between the electrons will repel them with a force

$$F_e = \frac{q_1 q_2}{4\pi\epsilon_0 r^2} \approx \frac{10^{-19} \cdot 10^{-19}}{10^9} N \approx 10^{-29} N \quad (\text{A.1})$$

while they experience a gravitational attraction on the order

$$F_G = \frac{Gm_1 m_2}{r^2} \approx 10^{-11} \cdot 10^{-31} \cdot 10^{-31} \approx 10^{-73} N \quad (\text{A.2})$$

from which we see that for electrons the electrostatic interaction is on the order of 10^{46} times greater than the gravitational attraction.

There are attempts to derive the fundamental constants on consistency grounds from theories of quantum gravity, which represent an open area of inquiry. The interested reader is directed to e.g. [256], since a deeper discussion is well beyond the scope of this Thesis.

Appendix B

Gravitational-wave-induced deformation on an object of known shape

To visualize the deformation induced by the gravitational wave on the spacetime (and subsequently on objects of known shape and size), we must retain directional information in addition to the strain amplitude. Consider a parametric surface given by $r(x^\mu)$, which describes an object of given shape. From the definition of the scalar invariant

$$x^2 \stackrel{def}{=} g_{\mu\nu} x_0^\mu x_0^\nu \quad (\text{B.1})$$

$$x^\mu x_\mu = \eta_{\mu\nu} x_0^\mu x_0^\nu + h_{\mu\nu} x_0^\mu x_0^\nu \quad (\text{B.2})$$

we can obtain an expression for x_μ , considering that for $h_{\mu\nu} \ll 1$, $x^\mu \approx x_0^\mu$

$$x_\mu = x_{0\mu} + h_{\mu\nu} x_0^\nu \quad (\text{B.3})$$

From this, we can identify the resulting strain to each of the components

$$\frac{\Delta x^\mu}{|x|} = \frac{h_\nu^\mu x_0^\nu}{|x|}. \quad (\text{B.4})$$

Substituting into the given function $r(x^\mu)$ provides a parametric description of the object's deformation. For example, Fig. 1.6 shows the induced deformation on a circle resulting from the passage of a gravitational wave.

Appendix C

Semiclassical intuitions: from classical spins to Dirac strings

I here define a classical spin field, and see how this leads to the concept of a Dirac string. Throughout this section, I review arguments laid out in [66, 257] and the appendix of [258].

On the basis of their mechanical properties, classical spins are like gyroscopes, with angular momentum $\vec{S}(\vec{r}) = S\vec{m}(\vec{r})$. To understand their motion, we can examine the equations of motion for a classical gyroscopic object

$$\frac{d\vec{S}}{dt} = \vec{\tau} = \vec{r} \times \vec{F}, \quad (\text{C.1a})$$

$$= -\vec{r} \times \frac{\partial U}{\partial \vec{r}}, \quad (\text{C.1b})$$

where \vec{r} must be carefully defined. There is no physical length associated with the spin. However, we can identify $\vec{r} = S\vec{m}$, where $|\vec{m}|^2 = 1$. Then the equations of motion become

$$\frac{Sd\vec{m}}{dt} + \vec{m} \times \frac{\partial U}{\partial \vec{m}} = 0, \quad (\text{C.2a})$$

$$\vec{m} \times \left(\frac{Sd\vec{m}}{dt} + \vec{m} \times \frac{\partial U}{\partial \vec{m}} \right) = 0, \quad (\text{C.2b})$$

$$\left(\vec{m} \cdot \frac{\partial U}{\partial \vec{m}} \right) \vec{m} - |\vec{m}|^2 \frac{\partial U}{\partial \vec{m}} - S\partial_t \vec{m} \times \vec{m} = 0, \quad (\text{C.2c})$$

$$\frac{\partial U}{\partial \vec{m}} = -S\partial_t \vec{m} \times \vec{m} = 0. \quad (\text{C.2d})$$

This tells us that the restoring force generates a precessional movement of the spin vector. The form of this force is also analogous to a Lorentz-like force law $q\vec{v} \times \vec{B}$, if we identify $\vec{v} = \partial_t \vec{m}$ and $q\vec{B} = S\vec{m}$. We can then define a fictitious vector gauge field \vec{A} , which satisfies

$$q\vec{\nabla}_m \times \vec{A} = S\vec{m}, \quad (\text{C.3a})$$

$$\vec{A} \rightarrow \vec{A} + \vec{\nabla}_m f(\vec{m}(\vec{r}, t)), \quad (\text{C.3b})$$

The term in the Lagrangian corresponding to a Lorentz-like force takes the form $q\vec{v}\cdot\vec{A}$. Terms of this form have geometric properties, and can also contain a kinetic term of the form $(\partial_t\vec{m})^2$ as we shall see for the antiferromagnet. So for d -dimensional systems in which the spin degrees of freedom can be described by a single spatially varying field $\vec{m}(\vec{r}, t)$ related to the order parameter (no sublattice order, ex. ferromagnet) the action is of the form

$$\mathcal{S} = \int dt dr^d \vec{A} \cdot \partial_t \vec{m} - U(\vec{m}), \quad (\text{C.4})$$

where $U(\vec{m}) = \frac{\rho}{2} \partial_i \vec{m} \partial_i \vec{m}$.

Let us examine more closely the physical implications of this analogy. The space of allowed \vec{m} is the 2-sphere with radially outpointing vectors. Therefore, we can describe the physical degrees of freedom \vec{m} by

$$\vec{m} = \frac{1}{r} \vec{e}_r, \quad (\text{C.5})$$

once we restrict attention to the sector where $|\vec{m}|^2 = 1$, and now I use polar coordinates (r, θ, ϕ) to denote the coordinates of the space of \vec{m} . In this abstract space, this is the field of a monopole. Let's examine more closely what happens to the vector field \vec{A} itself. It will have a general form

$$\vec{A} = A_r \vec{e}_r + A_\theta \vec{e}_\theta + A_\phi \vec{e}_\phi, \quad (\text{C.6})$$

For simplicity in identifying a valid form for \vec{A} , we can set $A_r = A_\theta = 0$. Then A_ϕ can be found by

$$S\vec{m} = q\vec{\nabla}_m \times \vec{A} = \frac{q}{r^2 \sin \theta} \begin{vmatrix} \vec{e}_r & \vec{e}_\theta & \vec{e}_\phi \\ \partial_r & \partial_\theta & \partial_\phi \\ A_r & rA_\theta & r \sin \theta A_\phi \end{vmatrix}, \quad (\text{C.7a})$$

$$S\vec{m} = \frac{q}{r^2 \sin \theta} \partial_\theta (r \sin \theta A_\phi) \vec{e}_r \quad (\text{C.7b})$$

$$Sr \sin \theta = q \partial_\theta (r \sin \theta A_\phi) \quad (\text{C.7c})$$

$$Sr \int d\theta \sin \theta = qr \sin \theta A_\phi \quad (\text{C.7d})$$

$$qA_\phi = S \left(\frac{\cos \theta + C}{\sin \theta} \right) \quad (\text{C.7e})$$

On physical grounds that will become clear, $C \pm 1$, and $q = 1$. Additionally, the field becomes unphysical at $\theta = \pi$. To shed light on both of these properties, consider the flux of the gauge field through a solid angle defined on the 2-sphere by the angle θ away from z . Choosing $C = -1$

$$\Phi = \oint d\vec{m} \vec{A} = \oint r \sin \theta d\phi A_\phi, \quad (\text{C.8a})$$

$$= 2\pi S (\cos \theta - 1) \quad (\text{C.8b})$$

The sign convention I use for the flux is such that a negative flux points downwards through the solid angle of the 2-sphere. Therefore, near the North pole $\Phi = -\pi S \theta^2$ is

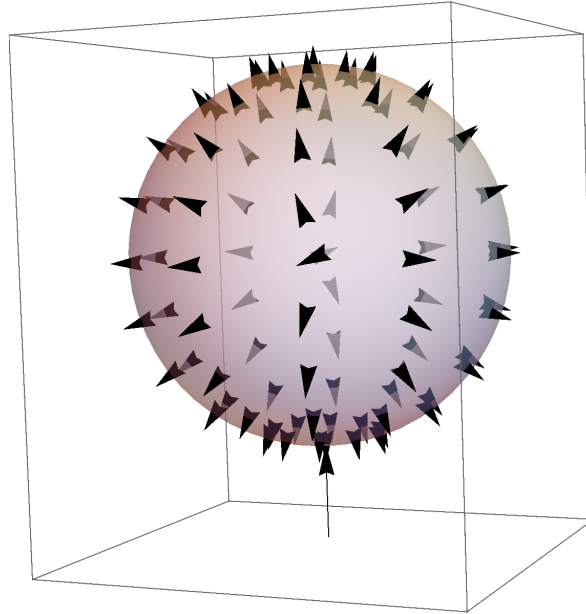


Figure C.1: Sketch of the gauge field A , with Dirac string at South pole

the flux entering the sphere. See Fig. C.1

Consider the flux at the South pole of the 2-sphere ($\theta = \pi$). There is a finite flux $4\pi S$ exiting the sphere through this point, exactly canceling the total flux entering through the remaining surface of the sphere. This artifact is called the Dirac string, see Fig. C.1.

For the description of spin waves, where the spin degrees of freedom remain within a finite solid angle about the ordering vector, placing the Dirac string in the opposite hemisphere allows for a problem free description. A choice of $C = 1$ places the Dirac string at the North pole ($\theta = 0$) instead.

The physical implication of the Dirac string is that nature does not allow monopoles to arise from such gyroscopic/magnetic forces. Additionally, notice that if the Berry phase Φ is a multiple of 2π , then the presence of the Dirac string is effectively invisible since no relative phase shift is accumulated that could lead to a measurable phase difference. This is satisfied for $S = \frac{b}{2}$ for $b \in \mathcal{N}$, which is consistent with physical spins coming in integer and half-integer values.

C.1 Building a semiclassical low-energy field theory: the hydrodynamic limit of the Heisenberg model

In this section, we continue to make use of insight derived from treatment of spin degrees of freedom semiclassically, and review an effective low-energy field theory for the Heisenberg antiferromagnet, as has been shown previously in e.g. [259]. In the following Sections, I will review the fully quantum mechanical treatment, first derived by [179].

The Heisenberg Hamiltonian [Eq. (1.16)] penalizes spin configurations that deviate from the ordered state, with energetic contributions arising from the scalar product between neighbouring spins, which we will continue to think of as $O(3)$ vectors. Deviations from order that have high spatial frequency are energetically heavily penalized, and therefore unexpected in the low-energy limit. It is therefore reasonable to assume that all equilibrium dynamical processes taking place in the lattice are long wavelength in nature, far exceeding the scale of the lattice spacing a , and we can approximate the lattice by a continuum. This long wavelength limit is also referred to as the hydrodynamic limit, in analogy with the continuum approximations made in the context of fluid mechanics.

To facilitate the transition to the continuum notation, I denote position on the lattice by the set of d -dimensional vectors \vec{r} , with neighbouring sites separated by $\vec{\delta}$, such that the Hamiltonian looks like

$$H = \sum_{\vec{r}, \vec{\delta}} J \mathbf{S}(\vec{r}) \cdot \mathbf{S}(\vec{r} + \vec{\delta}) , \quad (\text{C.9})$$

In the long wavelength limit, we can effectively describe the behaviour of spins on the lattice by use of a continuous order parameter field

$$\mathbf{S}(\vec{r}) = s \vec{m}(\vec{r}) , \quad (\text{C.10})$$

where \vec{m} is a unit vector field valued on the $O(3)$ sphere. Using this hydrodynamic description, the lattice points \vec{r} are spaced infinitesimally closely such that

$$\partial_i \vec{m} \partial_i \vec{m} \approx (\vec{m}(\vec{r}) - \vec{m}(\vec{r} + \vec{\delta}))^2 , \quad (\text{C.11a})$$

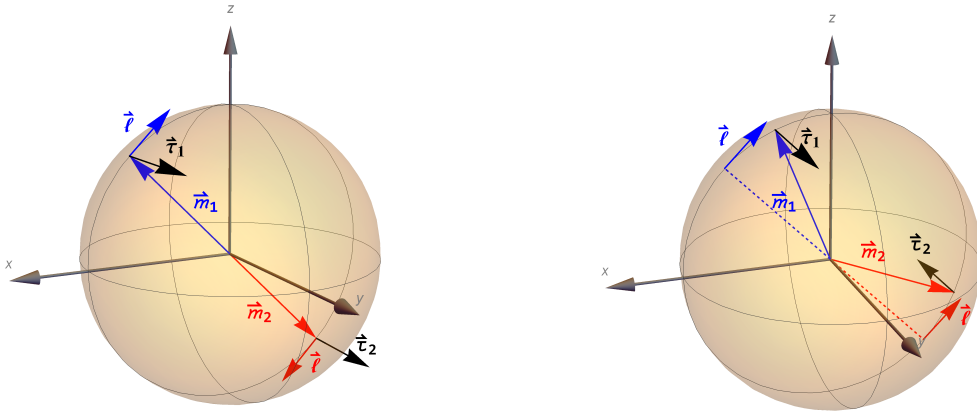
$$= 2\vec{m}(\vec{r}) \cdot \vec{m}(\vec{r} + \vec{\delta}) + \vec{m}(\vec{r})^2 + \vec{m}(\vec{r} + \vec{\delta})^2 , \quad (\text{C.11b})$$

where defining

$$\rho a \sim J s^2 . \quad (\text{C.12})$$

leads to an effective low-energy description of the Heisenberg model

$$H = \frac{\rho a^2}{2} \int dr \sum_{i=1}^d \partial_i \vec{m} \partial_i \vec{m} + \text{const.} , \quad (\text{C.13})$$



(a) Torque model for spins that do not cant, as defined by the condition $m_1 = -m_2$. (b) Model allowing for canting between sublattices.

Figure C.2: (a) If the mode of excitation is assumed to locally move spins from both lattices away from the ground state rigidly as shown here, then the resulting restoring force that counteracts the fluctuation \vec{l} leads to torques τ_1 and τ_2 whose actions oppose each other and the spins cannot move. This means such fluctuating modes are in fact dynamically disallowed. (b) The allowed modes of the antiferromagnet result from the two sublattices canting towards one another away from the aligned state.

where Roman indices here denote the d spatial dimensions, and the sum is hereafter omitted in accordance with the Einstein summation convention. The constant ρ is the spin stiffness, a material constant that captures the resistance to spin deformations, in turn proportional to the strength of interaction between each magnetic site on the lattice. Since the terms $\vec{m}(\vec{r})^2$ are spatially and dynamically constant, these represent a physically irrelevant shift in the absolute value of the energy. Hence Eq. C.13 is the continuum equivalent of Eq. C.9.

Let us consider what happens if we attempt to describe the 2-sublattice classical antiferromagnet with a single staggered field

$$\vec{m} = \vec{m}_1 = -\vec{m}_2 . \quad (\text{C.14})$$

For a collinear ground state, locally perturbed away from the easy axis in a uniform, staggered way, there will be a restoring force seeking to realign the perturbed spins (see Fig.C.2a). Each pair of spins will experience a torque as a result of the restoring force, but if the spins are restricted by the condition Eq. C.14, then they cannot precess since their torques both have the same orientation. In this deadlocked situation, nothing happens, that is, the system is not dynamical.

If we instead relax the condition Eq. C.14, then we can instead envision perturbations described by a uniform, but not staggered field \vec{l} . A local configuration of a pair of spins might look like FigC.2b, in which we see that spins on each sublattice deviate away from the ground state towards one another, a behaviour known as canting.

We can then define the fluctuating canting field as

$$\vec{l} = \vec{m}_1 + \vec{m}_2 . \quad (\text{C.15})$$

The staggered magnetization field is defined in terms of the continuum fields on the two sublattices

$$\vec{m} = \frac{1}{2}(\vec{m}_1 - \vec{m}_2) , \quad (\text{C.16})$$

where the 2-sublattice fields can be reexpressed

$$\vec{m}_1 = \frac{\vec{l}}{2} + \vec{m} , \quad \vec{m}_2 = \frac{\vec{l}}{2} - \vec{m} . \quad (\text{C.17})$$

Notice that

$$|\vec{m}|^2 = |\vec{m}_1|^2 = |\vec{m}_2|^2 = 1 \implies \vec{m} \perp \vec{l} . \quad (\text{C.18a})$$

From this starting point, we can motivate the appropriate Lagrangian density. It will have geometric terms, of form motivated in the previous Section e.g. [257], and potential terms.

Let us consider first which terms contribute to the potential energy. There will be a term mediated by the spin stiffness of the spin field \vec{m} . In addition, since there is a fluctuation field \vec{l} , there must be a term which penalizes the fluctuations. This simplest such term that respects the symmetry of the Hamiltonian is $\mathcal{O}(|\vec{l}|^2)$. Furthermore, in more highly magnetizable materials (with larger susceptibility χ) these canting fluctuations occur at lower energy cost, therefore we can write

$$\mathcal{L}_U(\vec{m}, \vec{l}) = \frac{l^2}{2\chi} + \frac{\rho}{2} \partial_i \vec{m} \partial_i \vec{m} , \quad (\text{C.19})$$

There will also be geometric terms for each sublattice associated with a gauge field $A[\vec{m}]$, each of the gyroscopic form shown in the previous Section

$$\mathcal{L}_g = \vec{A}_1[\vec{m}_1] \partial_t \vec{m}_1 + \vec{A}_2[\vec{m}_2] \partial_t \vec{m}_2 , \quad (\text{C.20})$$

We will see that these two geometric terms in combination will give rise to a kinetic term $(\partial_t \vec{m})^2$, where for a system with a single sublattice, such as the ferromagnet, there would remain a term first order in the time derivative. Massaging the terms using Eq. C.17 and expanding to first order in \vec{l} leads to

$$\mathcal{L}_g = \vec{A}_1 \left[\frac{\vec{l}}{2} + \vec{m} \right] \partial_t \left(\frac{\vec{l}}{2} + \vec{m} \right) + \vec{A}_2 \left[\frac{\vec{l}}{2} - \vec{m} \right] \partial_t \left(\frac{\vec{l}}{2} - \vec{m} \right) , \quad (\text{C.21a})$$

$$= \left(\vec{A}(\vec{m}) + \frac{\partial A_j l_i}{\partial m_i} \frac{l_i}{2} \right) \left(\frac{\partial_t l_i}{2} + \partial_t \vec{m} \right) + \left(\vec{A}(\vec{m}) - \frac{\partial A_j l_i}{\partial m_i} \frac{l_i}{2} \right) \left(\frac{\partial_t l_i}{2} - \partial_t \vec{m} \right) , \quad (\text{C.21b})$$

$$= A_i \partial_t l_i + \frac{\partial A_j}{\partial m_i} l_i \partial_t m_j . \quad (\text{C.21c})$$

Notice that in the limit of vanishing canting \vec{l} , the geometric terms also vanish. The absence of geometric terms in the absence of canting removes the time derivative terms from the Lagrangian, and so also demonstrates that a Néel state without canting as described by Eq. (C.14) is not dynamical.

This expression can be more elegantly expressed after a little bit of work

$$\mathcal{L}_g = -\partial_t A_i l_i + \frac{\partial A_j}{\partial m_i} l_i \partial_t m_j, \quad (\text{C.22})$$

$$= -\frac{\partial A_i}{\partial m_j} \frac{\partial m_j}{\partial t} l_i + \frac{\partial A_j}{\partial m_i} l_i \partial_t m_j, \quad (\text{C.23})$$

$$= \left(\frac{\partial A_i}{\partial m_j} - \frac{\partial A_j}{\partial m_i} \right) \partial_t m_i l_j, \quad (\text{C.24})$$

$$= \epsilon_{ijk} \partial_t m_i l_j (\vec{\nabla}_m \times \vec{A})_k \quad (\text{C.25})$$

$$= s \epsilon_{ijk} l_i m_j \partial_t m_k, \quad (\text{C.26})$$

$$= s \vec{l} \cdot (\vec{m} \times \partial_t \vec{m}). \quad (\text{C.27})$$

Two things become obvious in this form: first we did not need to choose a gauge for the geometric field \vec{A} since the final result is gauge invariant. Secondly, if we consider the full Lagrangian density

$$\mathcal{L} = s \vec{l} \cdot (\vec{m} \times \partial_t \vec{m}) - \frac{\vec{l}^2}{2\chi} - \frac{\rho}{2} \partial_i \vec{m} \partial_i \vec{m}, \quad (\text{C.28})$$

we observe that $\partial_t \vec{l}$ does not feature, the implication being that \vec{l} does not have independent dynamical character from \vec{m} , and therefore we can look for a dependent expression for $\vec{l}(\vec{m}, \partial_t \vec{m})$. To do this, we extremize the action by saddle-point approximation, or equivalently consider the Euler-Lagrange equations for the canting field

$$\frac{\delta \mathcal{S}}{\delta \vec{l}} = 0 = \frac{\partial \mathcal{L}}{\partial \vec{l}} - \partial_t \frac{\partial \mathcal{L}}{\partial \dot{\vec{l}}} = \frac{\partial \mathcal{L}}{\partial \vec{l}}, \quad (\text{C.29a})$$

$$0 = s \vec{m} \times \partial_t \vec{m} - \frac{\vec{l}}{\chi}, \quad (\text{C.29b})$$

$$\vec{l} = \chi S (\vec{m} \times \partial_t \vec{m}). \quad (\text{C.29c})$$

Substituting the Lagrangian density into the action, we find

$$\mathcal{S} = \int dt dr^d \left[\frac{\chi s^2}{2} |\vec{m} \times \partial_t \vec{m}|^2 - \frac{\rho}{2} \partial_i \vec{m} \partial_i \vec{m} \right], \quad (\text{C.30})$$

and where since \vec{m} is unit normalized, then¹

$$|\vec{m} \times \partial_t \vec{m}|^2 = |\partial_t \vec{m}|^2 . \quad (\text{C.32})$$

Finally we obtain

$$\mathcal{S} = \int dt dr^d \left[\frac{1}{c^2} |\partial_t \vec{m}|^2 - \partial_i \vec{m} \partial_i \vec{m} \right] , \quad (\text{C.33a})$$

where the material properties define a wave speed

$$c^2 = \frac{\rho}{\chi S^2} . \quad (\text{C.34})$$

To describe the behaviour of the canting field, we can focus attention on the vector components orthogonal to \vec{m} . Without loss of generality, we can choose the ground state to be described by the constant vector

$$\vec{m}_0 = (1, 0, 0) , \quad (\text{C.35})$$

such that the fluctuations are captured by the field

$$\vec{l} = (l_x, l_y, 0) . \quad (\text{C.36})$$

From the Euler-Lagrange equations for the

$$\frac{\chi S^2}{\rho} \partial_t^2 \vec{l} - \sum_i \partial_i^2 \vec{l} = 0 , \quad (\text{C.37})$$

with wave solutions

$$\vec{l} = \vec{e} e^{\pm i(\vec{k}\vec{r} - \omega t)} . \quad (\text{C.38})$$

In this form, if we restrict $\vec{k} \parallel \vec{m}_0$ it is apparent that each component of the vector describes a propagating transverse, fluctuation. Also note that in this form, the fluctuations are not yet precessional, and describe a basis of oscillations in the y and z planes. We can straightforwardly transform this into a circularly polarized basis by taking

$$\epsilon_{\circlearrowleft} = \epsilon_x + i\epsilon_y , \quad \epsilon_{\circlearrowright} = \epsilon_x - i\epsilon_y . \quad (\text{C.39})$$

These wave solutions for the long wavelength behaviour of the antiferromagnet propagate according to the relativistic dispersion

$$\omega = v|\vec{k}| . \quad (\text{C.40})$$

In conclusion, the semiclassical hydrodynamic treatment leads to an action Eq. C.33a which predicts linearly dispersing excitations of a continuum field. Next, I will review

¹Recall that

$$(\vec{a} \times \vec{b}) \cdot (\vec{c} \times \vec{d}) = (\vec{a} \cdot \vec{c})(\vec{b} \cdot \vec{d}) - (\vec{b} \cdot \vec{c})(\vec{a} \cdot \vec{d}) \quad (\text{C.31})$$

a fully quantum mechanical treatment and show we recover this result.

Appendix D

Singlet, triplet and quintuplet for $s = 1$

Using the fundamental principles of spin angular momentum laid out in e.g. [78], I here reproduce the two-particle basis of spin states for the well known $s = \frac{1}{2}$ case and—for the unfamiliar reader—I subsequently derive the corresponding result for the $s = 1$ case.

Let us start by identifying the transformation properties of the total spin operator $\mathbf{S}^2 = (\mathbf{S}_1 + \mathbf{S}_2)^2$ on a generic two spin state described in terms of the angular momentum quantum numbers—obtained by z -projection— $|\alpha, \beta\rangle$

$$(\mathbf{S}_1 + \mathbf{S}_2)^2 |\alpha, \beta\rangle = (\mathbf{S}_1^2 + \mathbf{S}_2^2 + 2\mathbf{S}_1\mathbf{S}_2) |\alpha, \beta\rangle \quad (\text{D.1a})$$

$$= (\mathbf{S}_1^2 + \mathbf{S}_2^2 + 2S_1^z S_2^z) |\alpha, \beta\rangle + (S_1^+ S_2^- + S_1^- S_2^+) |\alpha, \beta\rangle \quad (\text{D.1b})$$

$$\begin{aligned} &= (s_1(s_1 + 1) + s_2(s_2 + 1) + 2s_1 s_2) |\alpha, \beta\rangle \\ &\quad + \hbar^2 \sqrt{s_1(s_1 + 1) - \alpha(\alpha + 1)} \sqrt{s_2(s_2 + 1) - \beta(\beta - 1)} |\alpha + 1, \beta - 1\rangle \\ &\quad + \hbar^2 \sqrt{s_1(s_1 + 1) - \alpha(\alpha - 1)} \sqrt{s_2(s_2 + 1) - \beta(\beta + 1)} |\alpha - 1, \beta + 1\rangle \end{aligned} \quad (\text{D.1c})$$

Notice how the final two terms will behave differently in terms of whether the individual spins are integer or half-integer valued.

Consider first $s_1 = s_2 = \frac{1}{2}$, with the following two cases.

Case 1: choosing $\alpha = \beta$

$$(\mathbf{S}_1 + \mathbf{S}_2)^2 |\alpha, \beta\rangle = \hbar^2 \left(\frac{3}{4} + \frac{3}{4} + 2\frac{1}{4} \right) |\alpha, \beta\rangle \quad (\text{D.2a})$$

$$= 2\hbar^2 |\alpha, \beta\rangle \equiv \hbar^2 s(s + 1) |\alpha, \beta\rangle \quad (\text{D.2b})$$

$$\implies s = 1. \quad (\text{D.2c})$$

Case 2: choosing $\alpha \neq \beta$

$$(\mathbf{S}_1 + \mathbf{S}_2)^2 |\alpha, \beta\rangle = \hbar^2 \left(\frac{3}{4} + \frac{3}{4} + 2\frac{1}{4} \right) |\alpha, \beta\rangle + \hbar^2 \left(\frac{3}{4} + \frac{1}{4} \right) |\beta, \alpha\rangle \quad (\text{D.3a})$$

$$= \hbar^2 (|\alpha, \beta\rangle + |\beta, \alpha\rangle) \quad (\text{D.3b})$$

Applying this result to the superpositions

$$\mathbf{S}^2 (|\alpha, \beta\rangle + |\beta, \alpha\rangle) = 2\hbar^2 (|\alpha, \beta\rangle + |\beta, \alpha\rangle) \quad (\text{D.4a})$$

$$\implies s = 1, \quad (\text{D.4b})$$

$$\mathbf{S}^2 (|\alpha, \beta\rangle - |\beta, \alpha\rangle) = \hbar^2 (|\alpha, \beta\rangle + |\beta, \alpha\rangle - |\alpha, \beta\rangle + |\beta, \alpha\rangle) = 0 \quad (\text{D.4c})$$

$$\implies s = 0, \quad (\text{D.4d})$$

Using $\alpha, \beta \in \uparrow, \downarrow$ allows us to then explicitly construct the eigenbasis Eq. (1.4) of the \mathbf{S}^2 operator in terms of the triplet and singlet with respective eigenvalues $s = 1$ and $s = 0$.

Next I repeat a similar procedure for $s = 1$, case by case, bearing in mind now that the magnetic basis includes a ladder of three states $\alpha, \beta \in 1, 0, -1$.

Case 1: choosing $\alpha = \beta \neq 0$

$$(\mathbf{S}_1 + \mathbf{S}_2)^2 |\alpha, \beta\rangle = \hbar^2(2 + 2 + 2) |\alpha, \beta\rangle \quad (\text{D.5a})$$

$$= 6\hbar^2 |\alpha, \beta\rangle \quad (\text{D.5b})$$

$$\implies s = 2. \quad (\text{D.5c})$$

Case 2: choosing $\alpha = \beta = 0$

$$(\mathbf{S}_1 + \mathbf{S}_2)^2 |0, 0\rangle = \hbar^2(2 + 2 + 0) |0, 0\rangle + 2\hbar^2 (|1, -1\rangle + |-1, 1\rangle) \quad (\text{D.6a})$$

$$= \hbar^2 (4 |0, 0\rangle + 2 |1, -1\rangle + 2 |-1, 1\rangle) \quad (\text{D.6b})$$

Case 3: choosing $\alpha = -\beta \neq 0$

$$(\mathbf{S}_1 + \mathbf{S}_2)^2 |\alpha, \beta\rangle = \hbar^2(2 + 2 - 2) |\alpha, \beta\rangle + \hbar^2 |0, 0\rangle \quad (\text{D.7a})$$

$$= 2\hbar^2 (|\alpha, \beta\rangle + |0, 0\rangle) \quad (\text{D.7b})$$

Combining Cases 2 and 3, we can identify respectively the symmetric and antisymmetric combinations

$$(\mathbf{S}_1 + \mathbf{S}_2)^2 (|1, -1\rangle + 2|0, 0\rangle + |-1, 1\rangle) = 6\hbar^2 (|1, -1\rangle + 2|0, 0\rangle + |-1, 1\rangle) \quad (\text{D.8a})$$

$$\implies s = 2, \quad (\text{D.8b})$$

$$(\mathbf{S}_1 + \mathbf{S}_2)^2 (|1, -1\rangle - |-1, 1\rangle) = 2\hbar^2 (|1, -1\rangle - |-1, 1\rangle) \quad (\text{D.8c})$$

$$\implies s = 1 \quad (\text{D.8d})$$

$$(\mathbf{S}_1 + \mathbf{S}_2)^2 (|1, -1\rangle - |0, 0\rangle + |-1, 1\rangle) = 0 \quad (\text{D.8e})$$

$$\implies s = 0. \quad (\text{D.8f})$$

Case 4: choosing $\alpha = \pm 1, \beta = 0$

$$(\mathbf{S}_1 + \mathbf{S}_2)^2 |\alpha, 0\rangle = \hbar^2(2 + 2 + 0) |\alpha, 0\rangle + \hbar^2 s(s + 1) |0, \alpha\rangle \quad (\text{D.9a})$$

$$= 2\hbar^2 (2 |\alpha, 0\rangle + |0, \alpha\rangle) \quad (\text{D.9b})$$

From which we can compose the symmetric and antisymmetric eigenvectors

$$(\mathbf{S}_1 + \mathbf{S}_2)^2 (|\alpha, 0\rangle + |0, \alpha\rangle) = 6\hbar^2 (|\alpha, 0\rangle + |0, \alpha\rangle) \quad (\text{D.10a})$$

$$\implies s = 2, \quad (\text{D.10b})$$

$$(\mathbf{S}_1 + \mathbf{S}_2)^2 (|\alpha, 0\rangle - |0, \alpha\rangle) = 2\hbar^2 (|\alpha, 0\rangle - |0, \alpha\rangle) \quad (\text{D.10c})$$

$$\implies s = 1. \quad (\text{D.10d})$$

again with $\alpha = \pm 1$.

Collecting these results, we can write the nine states of the two particle eigenbasis of the \mathbf{S}^2 operator in terms of the $s = 2$ quintuplet

$$|s = 2, m = 2\rangle = |1, 1\rangle \quad (\text{D.11a})$$

$$|s = 2, m = 1\rangle = \frac{1}{\sqrt{2}}(|1, 0\rangle + |0, 1\rangle) \quad (\text{D.11b})$$

$$|s = 2, m = 0\rangle = \frac{1}{\sqrt{6}}(|1, -1\rangle + 2|0, 0\rangle + |-1, 1\rangle) \quad (\text{D.11c})$$

$$|s = 2, m = -1\rangle = \frac{1}{\sqrt{2}}(|-1, 0\rangle + |0, -1\rangle) \quad (\text{D.11d})$$

$$|s = 2, m = -2\rangle = |-1, -1\rangle, \quad (\text{D.11e})$$

the triplet

$$|s = 1, m = 1\rangle = \frac{1}{\sqrt{2}}(|1, 0\rangle - |0, 1\rangle) \quad (\text{D.12a})$$

$$|s = 1, m = 0\rangle = \frac{1}{\sqrt{2}}(|1, -1\rangle - |-1, 1\rangle) \quad (\text{D.12b})$$

$$|s = 1, m = -1\rangle = \frac{1}{\sqrt{2}}(|-1, 0\rangle - |0, -1\rangle), \quad (\text{D.12c})$$

and the singlet

$$|s = 0, m = 0\rangle = \frac{1}{\sqrt{6}}(|1, -1\rangle - |0, 0\rangle + |-1, 1\rangle). \quad (\text{D.13})$$

Appendix E

Spin probability density

The representation of a general state can then be visualized in terms of the probability density surface, whose parametric form can be obtained by considering a given state

$$|d\rangle = d_x \left(\frac{i(|1\rangle - |\bar{1}\rangle)}{\sqrt{2}} \right) + d_y \left(\frac{(|1\rangle + |\bar{1}\rangle)}{\sqrt{2}} \right) - id_z |0\rangle , \quad (\text{E.1})$$

and evaluating the contours of constant probability density for the overlap of the general state

$$P = |\langle d|\Omega\rangle|^2 \quad (\text{E.2a})$$

$$= |d_x \left[\frac{(1 + \cos \theta)}{\sqrt{2}} e^{-i(\phi - \frac{\pi}{2})} \langle 1|1\rangle - \frac{(1 - \cos \theta)}{\sqrt{2}} e^{i(\phi - \frac{\pi}{2})} \langle \bar{1}|\bar{1}\rangle \right] \quad (\text{E.2b})$$

$$+ d_y \left[\frac{(1 + \cos \theta)}{\sqrt{2}} e^{-i\phi} \langle 1|1\rangle - \frac{(1 - \cos \theta)}{\sqrt{2}} e^{i\phi} \langle \bar{1}|\bar{1}\rangle \right] + d_z (-i) \frac{\sin \theta}{\sqrt{2}} \langle 0|0\rangle|^2 . \quad (\text{E.2c})$$

The contours corresponding to the constant probability density of the magnetic basis states are shown in Fig. 4.1.

Appendix F

Enter the A-matrix

The wave-like character of the quadrupolar excitations can be identified in the structure of the equations of motion, which can be more compactly expressed in the U(3) formalism derived in [11]. This formalism exploits the simplicity of the U(3) representation to provide an alternative numerically integrable for the equations of motion of the BBQ model. This is carried out in terms of the A operators

$$A_i^{\alpha\beta} = d^{*\alpha} d^\beta \quad (\text{F.1})$$

or explicitly as a projector on the time reversal invariant basis

$$A_i^{\alpha\beta} = |\alpha\rangle_i \langle\beta|_i \quad (\text{F.2})$$

such that the Hamiltonian then becomes

$$H_{BBQ} = \sum_{\langle ij \rangle} \left(J_1 A_i^{\alpha\beta} A_j^{\beta\alpha} + (J_2 - J_1) A_i^{\alpha\beta} A_j^{\alpha\beta} \right) \quad (\text{F.3})$$

The A matrices encode the antisymmetric dipole component and traceless symmetric quadrupole components in the following way

$$S^\alpha = -i\epsilon^{\alpha\beta\gamma} A^{\beta\gamma} \quad (\text{F.4})$$

$$Q^{\alpha\beta} = -A^{\alpha\beta} - A^{\beta\alpha} + \frac{2}{3}\delta^{\alpha\beta} \text{Tr}(\hat{A}) \quad (\text{F.5})$$

F.1 U(3) representation of the FQ phase and its excitations

A state with ferroquadrupolar order corresponds to a state where all sites are oriented along a specified d-vector.

In terms of A-matrices, this corresponds to a state with corresponding non-trivial

components. For director order along the z axis, this can be specified by

$$\hat{A}_0 = \begin{pmatrix} 0 & 0 & 0 \\ 0 & 0 & 0 \\ 0 & 0 & 1 \end{pmatrix} \quad (\text{F.6})$$

where the U(3) generators specified by the corresponding A-matrices can be applied to rotate the state in its state space RP^2 . However, not all such actions are non trivial. In particular, only the actions of the generators

$$A^{13} = |x\rangle \langle z| \quad (\text{F.7a})$$

$$A^{23} = |y\rangle \langle z|, \quad (\text{F.7b})$$

$$A^{31} = |z\rangle \langle x|, \quad (\text{F.7c})$$

$$A^{32} = |z\rangle \langle y|, \quad (\text{F.7d})$$

$$A^{33} = |z\rangle \langle z|, \quad (\text{F.7e})$$

are closed within the Hilbert space, with this last element acting as the identity.

A representation for the state rotations can be expressed then in terms of the generators in the following way

$$R^{\alpha\beta}(\phi) = e^{-i\phi A^{\alpha\beta}} \quad (\text{F.8})$$

which can be asymptotically expressed in the limit of infinitesimal rotations as

$$R^{\alpha\beta}(\phi) \sim \mathbf{1} + i\phi A^{\alpha\beta} \quad (\text{F.9})$$

and the rotated state is described by

$$\hat{A}_0 \rightarrow \hat{R}\hat{A}_0\hat{R}^\dagger \quad (\text{F.10})$$

An example of such a transformation is here provided for further insight. Consider $R^{13}(\phi)$, which from the generator

$$\hat{A}^{13}(\phi) = \begin{pmatrix} 0 & 0 & 1 \\ 0 & 0 & 0 \\ 0 & 0 & 0 \end{pmatrix} \quad (\text{F.11})$$

can be expressed as

$$\hat{R}^{13}(\phi) = \begin{pmatrix} 1 & 0 & \sin(\phi) \\ 0 & 1 & 0 \\ 0 & 0 & \cos(\phi) \end{pmatrix} \quad (\text{F.12})$$

this carries out a trace preserving rotation between the $|z\rangle$ and $|x\rangle$ state, resulting in the following state

$$\hat{A}'_0 = \begin{pmatrix} \sin^2(\phi) & 0 & \sin(\phi)\cos(\phi) \\ 0 & 0 & 0 \\ \sin(\phi)\cos(\phi) & 0 & \cos^2(\phi) \end{pmatrix} \quad (\text{F.13})$$

The A-matrix description here makes explicit the spin-2 nature of the quadrupole fluctuations about a given state. By virtue of the transformation property, performing a rotation through ϕ results in the off-diagonal symmetric components of the state being rotated through a phase 2ϕ . Specifically, we see in this case that the action

$$A^{13} |z\rangle = \cos(\phi) |z\rangle + \sin(\phi) |x\rangle \quad (\text{F.14})$$

results in the off-diagonal elements $|x\rangle\langle z|$ and $|z\rangle\langle x|$ being mixed with amplitude $\frac{1}{2} \sin(2\phi)$ that is periodic in increments of $\phi = \pi$. Rotations parametrized by real fields ϕ (as exemplified above) map states

$$|\alpha\rangle = \sum_i a_i |i\rangle \rightarrow |\beta\rangle = \sum_i b_i |i\rangle, \quad (\text{F.15})$$

which keeps the site degrees of freedom in the quadrupole channel. However, rotations parametrized by complex fields can result in magnetic states $|\bar{1}\rangle$ or $|1\rangle$ which are dipolar in nature.

We therefore write together all possible ground state fluctuations in terms of the A-matrix formalism from the full set of non-trivial generators, which makes explicit that a complete description requires that the fields ϕ be complex. In the limit of small fluctuations this gives

$$\hat{\phi} = \begin{pmatrix} |\phi^{1,3}|^2 & \phi^{1,3}\phi^{2,3} & i\phi^{1,3} \\ \phi^{*1,3}\phi^{*2,3} & |\phi^{2,3}|^2 & i\phi^{*2,3} \\ -i\phi^{*1,3} & -i\phi^{2,3} & -|\phi^{1,3}|^2 - |\phi^{2,3}|^2 \end{pmatrix} \quad (\text{F.16})$$

Observe that four degrees of freedom remain. Two of these will encode the dipolar degrees of freedom, and the remaining two the quadrupolar degrees of freedom.

The low energy quadrupolar degrees of freedom can be isolated from the corresponding definition and recast in the following form

$$\hat{Q} = \begin{pmatrix} \frac{2}{3} - 2|\phi^{1,3}|^2 & -\phi^{1,3}\phi^{2,3} - \phi^{*1,3}\phi^{*2,3} & -2i \text{Im} \phi^{1,3} \\ -\phi^{1,3}\phi^{2,3} - \phi^{*1,3}\phi^{*2,3} & \frac{2}{3} - 2|\phi^{2,3}|^2 & 2i \text{Im} \phi^{2,3} \\ -2i \text{Im} \phi^{1,3} & 2i \text{Im} \phi^{2,3} & -\frac{4}{3} + 2|\phi^{1,3}|^2 + 2|\phi^{2,3}|^2 \end{pmatrix} \quad (\text{F.17})$$

which to first order in the fields reduces to

$$\hat{Q} = \begin{pmatrix} 0 & 0 & -2i \text{Im} \phi^{1,3} \\ 0 & 0 & 2i \text{Im} \phi^{2,3} \\ -2i \text{Im} \phi^{1,3} & 2i \text{Im} \phi^{2,3} & 0 \end{pmatrix} \quad (\text{F.18})$$

expressed in terms of the two exclusively quadrupolar fluctuations. These are the degrees of freedom that we will look to map onto the polarizations of gravitational waves. The requirement that the fields be real is consistent with the finding of the next section.

F.2 Equations of motion

One may ask in this context if it is possible to express the wave equations corresponding to the dipolar and quadrupolar degrees of freedom in terms of the convenient A-matrix representation.

The Heisenberg equation of motion takes the following form

$$\partial_t A_i^{\alpha\beta} = -i[A_i^{\alpha\beta}, H] \quad (\text{F.19})$$

$$= -i \sum_{\delta} \left(J_1 (A_i^{\alpha\sigma} A_{i+\delta}^{\sigma\beta} - A_i^{\sigma\beta} A_{i+\delta}^{\alpha\sigma}) + (J_2 - J_1) (A_i^{\alpha\sigma} A_{i+\delta}^{\beta\sigma} - A_i^{\sigma\beta} A_{i+\delta}^{\sigma\alpha}) \right) \quad (\text{F.20})$$

We restrict attention to the ferroquadrupolar ordered state, for which it can be assumed $J_1 = 0, J_2 = -1$.

In the small fluctuation limit, assuming order along z, $A^{zz} \sim 1$. Therefore, we assume from preservation of the trace that $A^{xx} \sim 0, A^{yy} \sim 0$. Furthermore, for consistency we expect $\partial_t A^{xx} = \partial_t A^{yy} = \partial_t A^{zz} = 0$. The condition necessary for this is verified below

$$\partial_t A_i^{zz} = i \sum_{\delta} \left(A_i^{zx} A_{i+\delta}^{zx} - A_i^{xz} A_{i+\delta}^{xz} + A_i^{zy} A_{i+\delta}^{zy} - A_i^{yz} A_{i+\delta}^{yz} + A_i^{zz} A_{i+\delta}^{zz} - A_i^{zz} A_{i+\delta}^{zz} \right) \quad (\text{F.21})$$

$$= i \sum_{\delta} \left(A_i^{zx} A_{i+\delta}^{zx} - A_i^{xz} A_{i+\delta}^{xz} + A_i^{zy} A_{i+\delta}^{zy} - A_i^{yz} A_{i+\delta}^{yz} \right) \quad (\text{F.22})$$

$$\sim i \sum_{\delta} \left(-i(\phi_i^{*1,3} \phi_{i+\delta}^{*1,3} - \phi_i^{1,3} \phi_{i+\delta}^{1,3}) - i(\phi_i^{*2,3} \phi_{i+\delta}^{*2,3} - \phi_i^{2,3} \phi_{i+\delta}^{2,3}) \right) \quad (\text{F.23})$$

which vanishes if we can assume that the components of the fluctuation are symmetric $A^{\alpha\beta} = A^{\beta\alpha}$, implying that the fluctuations are purely real, that is $\phi^{1,3} = \phi^{*1,3}$ and $\phi^{2,3} = \phi^{*2,3}$.

Furthermore, if we employ the assumption of real, symmetric fluctuations and ignore terms $\mathcal{O}(A^3)$, then we find equations of motion for the off diagonal fluctuations of the form

$$\partial_t^2 A_i^{xz} = \nabla^2 A_i^{xz}, \quad (\text{F.24})$$

which are wave equations.

Appendix G

Discrete Fourier transform methods

For any periodic function $f(x)$, there exists a Fourier series decomposition $\tilde{f}(k)$ in terms of its frequency components.

For a periodic function f_x defined on a discrete space with N elements, one can write a similar decomposition, namely the discrete Fourier transform \tilde{f}_k . Despite the nomenclature, it is more accurate to think of the discrete Fourier transform (FT) as a Fourier series decomposition as it is ill defined for aperiodic functions.

Specifically, the discrete representation takes the form

$$\tilde{f}_k = \sum_{j=0}^{N-1} f_j e^{-i2\pi jk/N} \quad \text{for } j, k \in \mathbb{N}, \quad (\text{G.1})$$

with inverse transformation

$$f_j = \frac{1}{N} \sum_{k=0}^{N-1} \tilde{f}_k e^{-i2\pi jk/N}. \quad (\text{G.2})$$

In the language of linear algebra, we can rewrite this as

$$\begin{pmatrix} \tilde{f}_0 \\ \tilde{f}_1 \\ \vdots \\ \tilde{f}_N \end{pmatrix} = \begin{pmatrix} 1 & 1 & 1 & \dots & 1 \\ 1 & e^{i2\pi/N} & e^{i4\pi/N} & \dots & e^{-i2\pi/N} \\ 1 & e^{i4\pi/N} & e^{i8\pi/N} & \dots & e^{-i4\pi/N} \\ \vdots & \vdots & \vdots & \ddots & \vdots \\ 1 & e^{-i2\pi/N} & e^{-i4\pi/N} & \dots & e^{i2\pi/N} \end{pmatrix} \begin{pmatrix} f_0 \\ f_1 \\ \vdots \\ f_N \end{pmatrix} \quad (\text{G.3})$$

Notice that F_N is a symmetric and unitary matrix, that is $F_N^{jk} = F_N^{kj}$, and $\frac{1}{N} F_N^\dagger F_N = \mathbf{1}_N$

More compactly, for an N dimensional input vector f , its transform \tilde{f} can be written $\tilde{f}_k = F_N^{kj} f_j$. It is clear that there are N^2 operations involved in evaluating this matrix product and thus evaluating the discrete Fourier transform in this way is an $\mathcal{O}(N^2)$ algorithm.

The next natural question is, can we do better than $\mathcal{O}(N^2)$? As we shall see, the answer is yes if we use what is called the fast Fourier transform (FFT).

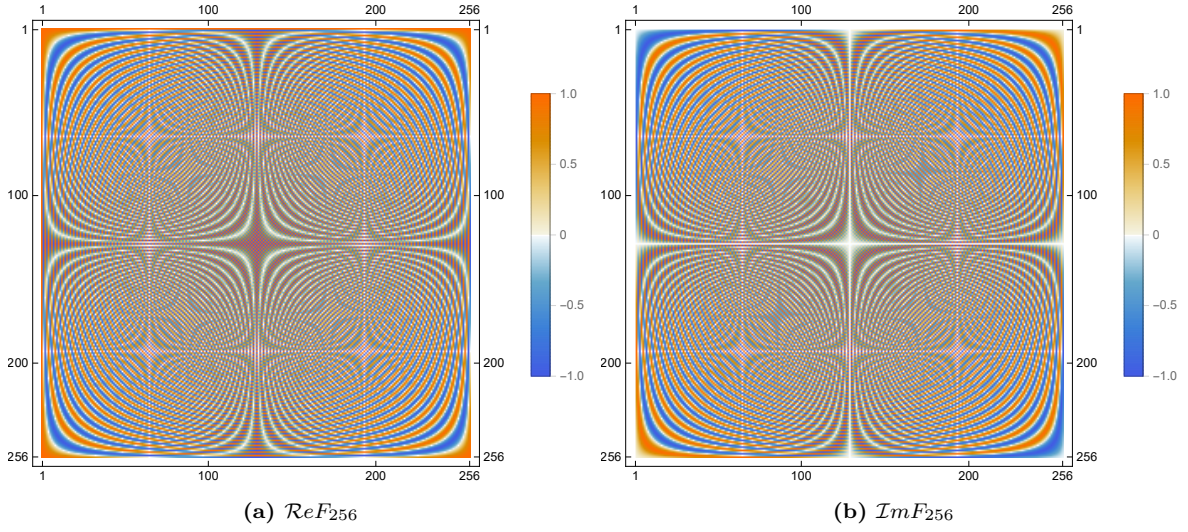


Figure G.1: Colour map of the matrix elements of F_{256}

The premise behind the FFT is that the elements of the matrix product $F_N f$ can be decomposed into matrices with blocks of size $\frac{N}{2}$, provided N is even. As an elementary example, consider the case of $N = 4$. The discrete Fourier transform looks like

$$\begin{pmatrix} \tilde{f}_0 \\ \tilde{f}_1 \\ \tilde{f}_2 \\ \tilde{f}_3 \end{pmatrix} = \begin{pmatrix} 1 & 1 & 1 & 1 \\ 1 & e^{i\pi/2} & e^{i\pi} & e^{-i\pi/2} \\ 1 & e^{i\pi} & e^{i2\pi} & e^{-i\pi} \\ 1 & e^{-i\pi/2} & e^{-i\pi} & e^{i\pi/2} \end{pmatrix} \begin{pmatrix} f_0 \\ f_1 \\ f_2 \\ f_3 \end{pmatrix} \quad (\text{G.4})$$

By permuting the elements of $F_N f$ to group the elements of f with even and odd indices, we can observe

$$\tilde{f} = F_4 f = \begin{pmatrix} 1 & 1 & 1 & 1 \\ 1 & e^{i\pi} & e^{i\pi/2} & e^{-i\pi/2} \\ 1 & e^{i2\pi} & e^{i\pi} & e^{-i\pi} \\ 1 & e^{-i\pi} & e^{-i\pi/2} & e^{i\pi/2} \end{pmatrix} \begin{pmatrix} f_0 \\ f_2 \\ f_1 \\ f_3 \end{pmatrix} \quad (\text{G.5})$$

$$= \begin{pmatrix} 1 & 0 & 1 & 0 \\ 0 & 1 & 0 & e^{i\pi/2} \\ 1 & 0 & -1 & 0 \\ 0 & 1 & 0 & -e^{i\pi/2} \end{pmatrix} \begin{pmatrix} 1 & 1 & 0 & 0 \\ 1 & e^{i\pi} & 0 & 0 \\ 0 & 0 & 1 & 1 \\ 0 & 0 & 1 & e^{i\pi} \end{pmatrix} \begin{pmatrix} 1 & 0 & 0 & 0 \\ 0 & 0 & 1 & 0 \\ 0 & 1 & 0 & 1 \\ 0 & 0 & 0 & 0 \end{pmatrix} \begin{pmatrix} f_0 \\ f_1 \\ f_2 \\ f_3 \end{pmatrix} \quad (\text{G.6})$$

where the decomposition on the right hand side has the following block structure

$$\tilde{f} = \begin{pmatrix} \mathbf{1}_2 & D_2 \\ \mathbf{1}_2 & -D_2 \end{pmatrix} \begin{pmatrix} F_2 & 0 \\ 0 & F_2 \end{pmatrix} P_4 f \quad (\text{G.7})$$

This decomposition makes use of the property $e^{i2\pi/\frac{N}{2}} = e^{i4\pi/N}$, which allows for elements of the smaller block $F_{\frac{N}{2}}$ to be used to reconstruct the elements of F_N . Gen-

eralizing to arbitrary even N , the transformation decomposes in the following way

$$\tilde{f} = \begin{pmatrix} \mathbf{1}_{\frac{N}{2}} & D_{\frac{N}{2}} \\ \mathbf{1}_{\frac{N}{2}} & -D_{\frac{N}{2}} \end{pmatrix} \begin{pmatrix} F_{\frac{N}{2}} & 0 \\ 0 & F_{\frac{N}{2}} \end{pmatrix} P_N f \quad (\text{G.8})$$

where the diagonal matrix $D_{\frac{N}{2}}$ is defined in terms of the fundamental element $e^{i2\pi/N}$ of the F_N matrix

$$D_{\frac{N}{2}} := \begin{pmatrix} 1 & 0 & 0 & \dots & 0 \\ 0 & e^{i2\pi/N} & 0 & \dots & 0 \\ 0 & 0 & e^{i4\pi/N} & \dots & 0 \\ \vdots & & & \ddots & \\ 0 & 0 & 0 & \dots & e^{i\pi} \end{pmatrix}, \quad (\text{G.9})$$

the blocks $F_{\frac{N}{2}}$ are defined in terms of the element $e^{i4\pi/N}$

$$F_{\frac{N}{2}} = \begin{pmatrix} 1 & 1 & 1 & \dots & 1 \\ 1 & e^{i4\pi/N} & e^{i8\pi/N} & \dots & e^{i4(N-1)\pi/N} \\ 1 & e^{i8\pi/N} & e^{i16\pi/N} & \dots & e^{i8(N-1)\pi/N} \\ \vdots & & & \ddots & \\ 1 & e^{-i4\pi/N} & e^{-i8\pi/N} & \dots & e^{i4\pi/N} \end{pmatrix} \quad (\text{G.10})$$

and P_N is the permutation matrix that maps f into $\begin{pmatrix} f_{\text{even}} \\ f_{\text{odd}} \end{pmatrix}$,

$$P_N \begin{pmatrix} f_0 \\ f_1 \\ f_2 \\ \vdots \\ f_N \end{pmatrix} = \begin{pmatrix} f_0 \\ f_2 \\ \vdots \\ f_1 \\ f_3 \\ \vdots \end{pmatrix} \quad (\text{G.11})$$

Notice that aside from cleanly reexpressing the Fourier transform operation in a block structure of sparse matrices, a single matrix decomposition of this kind doesn't by itself grant any real speed up. The power of the FFT comes from applying this decomposition iteratively, and thus is most efficient in cases where $N = 2^M$ for $M \in \mathbb{N}$.

To understand how such a procedure can be implemented iteratively, consider the next decomposition in the sequence for the example of $N = 4$. The matrix F_4 was decomposed into

$$F_4 = \begin{pmatrix} 1 & 0 & 1 & 0 \\ 0 & 1 & 0 & e^{i\pi/2} \\ 1 & 0 & -1 & 0 \\ 0 & 1 & 0 & -e^{i\pi/2} \end{pmatrix} \begin{pmatrix} 1 & 1 & 0 & 0 \\ 1 & e^{i\pi} & 0 & 0 \\ 0 & 0 & 1 & 1 \\ 0 & 0 & 1 & e^{i\pi} \end{pmatrix} = \begin{pmatrix} \mathbf{1}_2 & D_2 \\ \mathbf{1}_2 & -D_2 \end{pmatrix} \begin{pmatrix} F_2 & 0 \\ 0 & F_2 \end{pmatrix} \quad (\text{G.12})$$

where the second matrix now contains the F_2 matrices. Applying the same decompo-

sition to each F_2 matrix within this second matrix, and using the fact that $D_1 = 1$, $F_1 = 1$ we see

$$\begin{pmatrix} F_2 & 0 \\ 0 & F_2 \end{pmatrix} = \begin{pmatrix} \mathbb{1}_1 & D_1 & | & 0 & 0 \\ \mathbb{1}_1 & -D_1 & | & 0 & 0 \\ \hline 0 & 0 & | & \mathbb{1}_1 & D_1 \\ 0 & 0 & | & \mathbb{1}_1 & -D_1 \end{pmatrix} \begin{pmatrix} F_1 & 0 & | & 0 & 0 \\ 0 & F_1 & | & 0 & 0 \\ \hline 0 & 0 & | & F_1 & 0 \\ 0 & 0 & | & 0 & F_1 \end{pmatrix} \quad (\text{G.13})$$

$$\begin{pmatrix} 1 & 1 & 0 & 0 \\ 1 & e^{i\pi} & 0 & 0 \\ 0 & 0 & 1 & 1 \\ 0 & 0 & 1 & e^{i\pi} \end{pmatrix} = \begin{pmatrix} 1 & 1 & 0 & 0 \\ 1 & e^{i\pi} & 0 & 0 \\ 0 & 0 & 1 & 1 \\ 0 & 0 & 1 & e^{i\pi} \end{pmatrix} \begin{pmatrix} 1 & 0 & 0 & 0 \\ 0 & 1 & 0 & 0 \\ 0 & 0 & 1 & 0 \\ 0 & 0 & 0 & 1 \end{pmatrix} \quad (\text{G.14})$$

In this case, further iteration does not simplify the results any further. However, for larger N , this procedure is the key behind the speed up associated to the fast Fourier transform. To see this, consider the number of operations involved in Eq.G.8.

$$\tilde{f} = \begin{pmatrix} \mathbb{1}_{\frac{N}{2}} & D_{\frac{N}{2}} \\ \mathbb{1}_{\frac{N}{2}} & -D_{\frac{N}{2}} \\ \underbrace{\hspace{2cm}}_{\mathcal{O}(\frac{N}{2})} \end{pmatrix} \begin{pmatrix} F_{\frac{N}{2}} & 0 \\ 0 & \underbrace{F_{\frac{N}{2}}}_{\mathcal{O}(\frac{N}{2})^2} \end{pmatrix} P_N f \quad (\text{G.15})$$

$$= \underbrace{\begin{pmatrix} \mathbb{1}_{\frac{N}{2}} & D_{\frac{N}{2}} \\ \mathbb{1}_{\frac{N}{2}} & -D_{\frac{N}{2}} \end{pmatrix}}_{\mathcal{O}(N)} \underbrace{\begin{pmatrix} \mathbb{1}_{\frac{N}{4}} & D_{\frac{N}{4}} & | & 0 & 0 \\ \mathbb{1}_{\frac{N}{4}} & -D_{\frac{N}{4}} & | & 0 & 0 \\ \hline 0 & 0 & | & \mathbb{1}_{\frac{N}{4}} & D_{\frac{N}{4}} \\ 0 & 0 & | & \mathbb{1}_{\frac{N}{4}} & -D_{\frac{N}{4}} \end{pmatrix}}_{\mathcal{O}(N)} \begin{pmatrix} F_{\frac{N}{4}} & 0 & 0 & 0 \\ 0 & F_{\frac{N}{4}} & 0 & 0 \\ 0 & 0 & F_{\frac{N}{4}} & 0 \\ 0 & 0 & 0 & \underbrace{F_{\frac{N}{4}}}_{\mathcal{O}(\frac{N}{4})^2} \end{pmatrix} P_N f \quad (\text{G.16})$$

The matrix composed of F_N subblocks is the only place where the number of non-trivial elements (and thus operations) is of order $\mathcal{O}(N)^2$. However, through iterative application of the matrix decomposition, this matrix can be reduced to the identity $\mathbb{1}_N$ matrix as we shown in the $N = 4$ example.

By requiring that $N = 2^M$, the matrix F_N can be decomposed into M matrices with $\mathcal{O}(N)$ scaling.

This means in total, the number of operations carried out is $\mathcal{O}(M)\mathcal{O}(N) = \mathcal{O}(N \log_2 N)$.